ATOMIC WEAPONS ESTABLISHMENT

AWE REPORT NO. O 26/88

P-wave Seismograms Recorded at Yellowknife, Canada from Underground Nuclear Explosions in Nevada USA (UK UNCLASSIFIED)

T G A Gillbanks
P D Marshall
R C Stewart

Recommended for issue by,

A Douglas, Superintendent

Approved by,

B L Elphick, Head of Division

CONTENTS

SUMMARY

This report contains an analysis of P-wave seismograms recorded at the Yellowknife (YKA) seismometer array from 135 nuclear explosions at the Nevada Test Site (NTS). Three types of seismogram are presented for each explosion: the short period (SP), the broad band (BB) Wiener filtered seismogram and the BB seismogram corrected for anelastic attenuation using a t* of 0.5 s; t* being the ratio of travel time to specific quality factor Q. The first arrival on the t* corrected seismogram is, it is hoped, an approximation of the P pulse radiated from the source region.

For each explosion, estimates are given of the P-wave magnitude, the rise time and duration of the initial P pulse and Ψ_∞, the long term level of the reduced displacement potential. From the measurements of Ψ_∞ the seismic moment M_0 is determined for those explosions for which M_0 is also available from surface wave data and the results are compared and found to be in good agreement. The relationship between $\log_{10} \Psi_\infty$ and the yield of explosions Y in kton in saturated rock and is estimated to be:

$$\log_{10} \Psi_\infty \approx \log_{10} Y + 1.8$$

1. INTRODUCTION

Lyman et al (1) describe a method of deconvolving short-period (SP) P seismograms from explosions to obtain estimates of the radiated ground displacement close to the source; the deconvolved seismograms being broad-band (BB) estimates of ground displacement corrected for anelastic attenuation. On such seismograms individual source pulses can often be identified and estimates made of such properties as rise time (τ), pulse duration (D) and pulse area. From the pulse area, estimates can be obtained of Ψ_∞ the long-term level of the reduced displacement potential, and of M_0, the seismic moment. The estimates can be used to investigate the seismic source functions of explosions, their scaling laws and the relation of the seismic size of the explosion (Ψ_∞, moment and magnitude) and explosion yield.

Lyman et al (1) show the results of deconvolving the SP P seismograms from 39 Nevada Test Site (NTS) explosions recorded at Eskdalemuir (EKA) Scotland. Here we present the results of applying the deconvolution method of Lyman et al (1) to the SP recordings of 135 NTS explosions from the seismometer array at Yellowknife (YKA) Canada. The NTS-EKA distance is 71.5° so that all the main arrivals - P, the surface reflections and any other arrivals originating in the vicinity of the source-follow, in effect, the same single ray path to EKA. Consequently only one filter operator is required to correct the P seismograms for the effects of anelastic attenuation. The NTS-YKA distance however is about

25^o and at this distance the discontinuities in the P-wave speed in the Upper Mantle at depths of around 200, 400 and 650 km mean that there are several P ray paths between source and receiver. In general different operators are required to correct for the anelastic attenuation on each path. Here however, the main interest is in the first P arrival and it is the operator for the path followed by this arrival that is applied to correct for anelastic attenuation.

The explosions analysed in the report were conducted in four distinct area of the NTS: Pahute Mesa (26 explosions); Yucca Flats (94 explosions); Rainier Mesa (14 explosions); and Climax Stock (one explosion, PILE DRIVER. A list of the explosions together with epicentral details is given in table 1 and their locations are shown in figure 1.

For the analysis, those measurements from the deconvolved seismograms which are related to source size, are plotted against yield where this has been published. In the absence of a published yield the maximum-likelihood estimate of the body-wave magnitude (m_b) determined from many stations located world-wide has been used as a measure of source size.

The purpose of the report is:

(a) to provide a catalogue of YKA seismograms from NTS explosions;

(b) to investigate the relationship of $\Psi\infty$, D and τ with yield and magnitude;

(c) to complement the catalogue of EKA seismograms published by Lyman et al (1).

2. DATA AND PROCESSING METHODS

The SP array at YKA has 19 seismometers. The 19 individual seismometer channels are recorded in analogue form on magnetic tape. Full details of the recording system are given by Mowat & Burch (2). A diagram of the array is given in figure 2. The ambient noise level at the site is low so the array recording system is operated at high magnification. This however means that because of the limited dynamic range of the analogue system the array channels saturate at amplitudes of about 115 nm for signals of around 1 Hz. For some years however, a broad-band instrument with response flat to velocity in the range 0.1 to 5 Hz (VBB) has been operated at low gain at YKA and some of the signals that saturate on the array are not saturated on the VBB. If available, recordings from this instrument are used when the array records are saturated, to derive the deconvolved seismograms. Before the installation of the VBB, a low gain SP channel was operated at YKA.

All the usable YKA seismograms of NTS explosions up to 31 July 1985 are presented here. Most of the seismograms are array recordings. Of the signals that are overloaded on the array, three - RUMMY, PEPATO and HEARTS - are available on the VBB channel and these are used here. The signals from some of the other explosions that are overloaded on the array are available on the SP strong motion channel but for some periods the calibration of this channel is uncertain and so these recordings are usually of little use. However for one explosion - PILE DRIVER - the calibration of the channel is thought to be well known and for this explosion the strong motion recording is used. For processing, the analogue signals have been digitised at 20 samples/s.

Although much of the analogue data has been stored for many years the quality of most of the signals is good. Drop-outs are few and the analogue tape noise is low enough to allow satisfactory processing after digitisation of most of the signals. However for some of the low amplitude signals, analogue system noise can be a problem particularly on the deconvolved seismograms as noted in section 4.

For each explosion three seismograms are shown: the SP, the BB and the BB signal corrected for attenuation, that is the deconvolved seismogram. Where array recordings are available the BB seismograms are derived from the SP array sum. The array sum is formed by time shifting the individual channels to correct for differences in the arrival time of the initial P signal at each seismometer and the shifted signals are then summed. As the apparent speed across the array of the later arrivals will in general be different from that of the initial P they will be suppressed somewhat relative to P.

The BB recordings are obtained from the SP by passing the seismogram through a filter with a response as a function of frequency of $|a_2(\omega)|/a_1(\omega)$, where $a_1(\omega)$ is the SP instrument response and $a_2(\omega)$ the BB instrument response. By using $|a_2(\omega)|$ rather than $a_2(\omega)$, phase shifts due to the instrument are removed and the resultant recordings are effectively "phaseless" seismograms. The advantage of phaseless seismograms is that they show the source pulse with less instrument distortion than those recorded on conventional SP and BB systems (Stewart & Douglas (3)). (For those explosions where the P signals are only available as VBB recordings SP and BB seismograms are obtained from the VBB by a similar method to that described above for obtaining BB seismograms from the SP). BB seismograms have a much lower signal-to-noise ratio than SP (or VBB) seismograms. To attenuate the noise the BB seismograms are passed through a Wiener frequency filter; the filter being designed using the spectrum of the noise ahead of the signal and a theoretical signal spectrum. The use of the Wiener filter produces a least squares estimate of the BB ground displacement (Douglas and Young (4)).

The Wiener filtered BB seismograms are estimates of ground displacement at the recording station. To obtain the seismograms corrected for attenuation the BB seismograms (before Wiener filtering) are passed through a filter with response $b(\omega)^{-1}$ where $b(\omega)$ is the response as a function of frequency of an attenuation operator. Here we use the operator of Carpenter (5) where $|b(\omega)|$ is defined as $\exp(-\omega t^*/2)$ and the phase spectrum is specified using the theory of Futterman (6) t^* being the ratio of travel time to Q the specific quality factor. The attenuation corrected BB seismogram - referred to here as the deconvolved seismogram - is then Wiener filtered to improve the signal-to-noise ratio.

To correct for attenuation it is necessary to assume a value for t^*. A test was made of a range of t^* values between 0.1 s and 0.7 s and it was found that a value of 0.5 s seems appropriate for the NTS-YKA path. This is also the value predicted using the method of Marshall et al (7) and assuming that between NTS and YKA half of the ray path is in the upper mantle beneath the ancient, geologically stable Canadian shield. Each deconvolved seismogram presented here has been corrected for anelastic attenuation using a t* of 0.5 s. For the NTS-EKA path Lyman et al (1) use a value of 0.35 s for t* indicating that the anelastic loss on this path is less than between YKA and NTS; the reason for this being presumably that much of the ray path to EKA lies in the lower (higher Q) mantle but to YKA the rays remain in the low Q upper mantle.

3. MEASUREMENTS

In total, four different amplitude and three different period measurements (figure 3a) are made on each SP P-wave. The amplitudes measured are: A_{oa}, the height of the first positive peak; A_{ab}, the height of the first peak to the first trough; A_{bc}, the height of the first trough to second peak; and A_{max}, the maximum peak-to-peak amplitude in the first few cycles. The periods measured were: T_{od}, the time between the onset and the second crossing of the base-line; T_{bc}, the time between the trough and peak used to determine the A_{bc} amplitude; and T_{p2}, the time between the trough and peak used to determine the A_{max} amplitude. Log_{10} (A/T) is calculated in four ways:

$$\log_{10}(A/T)_{oa} = \log_{10}(A_{oa}/T_{od})$$

$$\log_{10}(A/T)_{ab} = \log_{10}(A_{ab}/2T_{od})$$

$$\log_{10}(A/T)_{bc} = \log_{10}(A_{bc}/4T_{bc})$$

$$\log_{10}(A/T)_{max} = \log_{10}(A_{max}/4T_{p2})$$

The amplitudes and periods are given in table 2 and $\log_{10}(A/T)$ in table 3.

The deconvolved seismogram is used to provide estimates of τ, D and Ψ_∞. The manner in which these measurements are made is illustrated in figure 3b. The pulse rise-time, τ, is obtained by dividing the maximum gradient of the leading edge by the peak pulse amplitude (Stewart (8)). The pulse duration, D, is taken as the time from the onset of the pulse to the time when the pulse returns to the same amplitude level. If the pulse does not return to the same amplitude level then the time at which the pulse ends and a second pulse begins is taken (see, for example, the BB recording of MINT LEAF shown in figure 33). Those pulses which do not return to the same level are indicated with an asterisk in table 4.

To obtain estimates of Ψ_∞ the area under the pulse is measured by integrating the pulse from its onset to the end of the pulse indicated by D its duration. The pulse area is corrected for the effects of geometrical spreading using the appropriate values from Carpenter (9) and for amplification at the free surface at the receiver, assumed to be a factor of 2. The Ψ_∞ estimates should not be affected by the amount of attenuation along the transmission path (Douglas (10)) but it is usually best to estimate Ψ_∞ from attenuation corrected seismograms since the measurement is made on a P-pulse of short duration with the minimum contamination with noise or interference from later arrivals.

4. SEISMOGRAMS

The P-wave seismograms from the 135 explosions are given in figures 10-144. Three seismograms are given in each figure and unless indicated are: (a) the SP array sum, (b) the Wiener filtered phaseless BB seismogram and (c) seismogram (b) corrected for the effects of attenuation over the path between NTS and YKA assuming a t* value of 0.5 s.

For small magnitude explosions ($m_b \leqslant 4\frac{1}{2}$) where the signal-to-noise ratio is small the process of correcting for t* amplifies the high frequency tape noise. The effect of this can be seen in a number of the seismograms presented here, for example, the processed seismograms for the explosions REDMUD and TENAJA (figures 64 and 104 respectively).

The seismograms from explosions in each area of the NTS appear to be rather similar but they do differ in fine detail. For example, the seismograms for explosions in the Yucca flat area are characterised by a high frequency pulse which arrives shortly after the initial P pulse. The variation of amplitude of this secondary arrival appears to be a function of the location of the explosion. It is a large amplitude arrival for explosions in the most southerly position of Yucca (see PICCALILLI, figure 26) and a small amplitude arrival for explosions in north Yucca (see CALABASH, figure 25). However in this report only the main features of the seismogram are analysed.

The waveform of the seismogram is determined primarily by the nature of the transmission path between NTS and YKA. The upper mantle velocity models of Archambeau, Flinn and Lambert, (11) and Helmberger and Wiggins, (12) both indicate multiple arrivals at distances around $\Delta \approx 25^{\circ}$ the NTS-YKA distance: a direct P arrival followed within a second or two by a reflection from the 660 km discontinuity and an arrival some 10 s or more later from the 430 km discontinuity. The specific model of Helmberger and Wiggins (12) designated Model HWNE appears to explain the YKA record rather better than the Archambeau et al (11) model which predicts a large amplitude arrival from the 430 km discontinuity and this is not observe on the YKA seismograms. Helmberger and Wiggins (12) show a seismogram recorded at Edgewood, Missouri (EDMI) at a distance of 24.82° from the NTS explosion CORDUROY which looks very similar to the YKA seismograms from NTS explosions (figure 4). It is presumed, on the evidence of Helmberger and Wiggins (12) that the YKA seismograms show a directed arrival followed by a reflection from the 600 km discontinuity. Some YKA seismograms do appear to have discrete later arrivals which may be associated with the 430 and 200 km discontinuities.

An additional factor which influences the appearance of a P-wave seismogram is the free surface reflection (pP) from the surface above the shot point. The free surface reflection is often difficult to identify in SP seismograms from explosions at shallow depths of burial. The normal procedure is to identify a pulse of opposite polarity to the P onset and assume that this is the pP arrival. pP should be most clearly observed on the BB record corrected for the effects of attenuation: seismogram (c) in the illustrations of the waveforms. Examination of these seismograms reveals a large negative arrival which appears some 2 s after the P onset. This negative pulse is too late to be pP and is presumed to be the arrival of the wave reflected at the 660 km discontinuity. In the synthetic seismograms published by Helberger and Wiggins for a delta source and the HWNE earth model this reflected arrival recorded at $\Delta = 25^{o}$ appears to be a Hilbert transform of the P-pulse. Such a transformation could give rise to the appearance of a negative initial arrival. Following the negative arrival in the BB recordings is a large amplitude positive pulse the arrival time of which may be a function of source depth. However to exploit any evidence of source depth within the seismograms or even explain much of the fine detail in the YKA seismogram requires a comprehensive study which is beyond the scope of this report.

5. RESULTS

5.1 Magnitudes

The body wave magnitude m_b of a seismic disturbance is defined as (Gutenberg and Richter (13))

$$m_b = \log_{10} (A/T) + B (\Delta)$$

where A is the maximum amplitude in the first few cycles of the P wave (measured in nanometres) and T the period (seconds) of the cycle on which the amplitude is measured. $B(\Delta)$ is a distance normalising term. However at sensitive stations equipped with limited dynamic range recording systems large magnitude sources saturate the system and it is useful to be able to make an estimate of the magnitude of the explosion using some other, unsaturated, part of the wavetrain. To investigate the variation in amplitude of particular cycles within the P wave as a function of a global magnitude, measurements (described in section 3) were made and plotted against the maximum-likelihood magnitude for each explosion. The results are shown in figures 5a to 5d with least square lines through the data. The equations of the lines are:

$$\log_{10}(A/T)_{oa} = (1.20 \pm 0.08)m_b - (5.48 \pm 0.40) \qquad r = 0.93$$

$$\log_{10}(A/T)_{ab} = (1.11 \pm 0.06)m_b - (4.72 \pm 0.31) \qquad r = 0.95$$

$$\log_{10}(A/T)_{bc} = (1.04 \pm 0.7)m_b - (4.20 \pm 0.35) \qquad r = 0.93$$

$$\log_{10}(A/T)_{max} = (1.28 \pm 0.09)m_b - (4.94 \pm 0.49) \qquad r = 0.92$$

where r is the correlation coefficient and the error terms are $\pm\ 1\sigma$. Given these results it is possible to make a reasonable estimate of the magnitude of the source using any one of the four amplitude measurements.

5.2 Source size estimates

Rise time, duration and $\Psi\infty$ are all related to the size of the source. To investigate their relation with source size the observations are plotted against the maximum likelihood magnitude. Figure 6 shows $\log_{10} \Psi\infty$ as a function of m_b. The best least squares line through the data is

$$\log_{10} \Psi\infty = (1.22 \pm 0.07)m_b - (3.16 \pm 0.38) \qquad r = 0.95$$

The high correlation coefficient indicates that $\Psi\infty$ is likely to be a good estimator of source size, a result which is in agreement with the conclusions of Lyman et al (1).

The rise time and duration of a source pulse should be inversely proportional to the corner frequency of its spectrum. How these factors vary with source size should indicate the scaling law appropriate for the explosions at the NTS. However, unlike Ψ_∞ both τ and D are affected by the value to t* used to correct for attenuation over the path. Estimating D has the added problem that pP may arrive before the end of the P pulse which will consequently be truncated and give a duration which is too short. If the t* value used is not correct then the relationship between τ and source size will be incorrect and it would be difficult to compare results from one test site with those from another. This is not a problem if the test site - recording station remains the same, for in this situation the relationship between τ and source size for explosions in different source media can be investigated but caution should be exercised in applying the results from one test site to another.

The relationship between τ, D and Ψ_∞ for explosions at NTS recorded at YKA are illustrated in figures 7a and 7b. The equations of the best least squares line through the data are found to be:

$$\log_{10}\tau = (0.15 \pm 0.04)\log_{10} \Psi_\infty -(1.26 \pm 0.15) \qquad r = 0.52$$

and

$$\log_{10}D = (0.21 \pm 0.03)\log_{10} \Psi_\infty -(0.90 \pm 0.11) \qquad r = 0.77$$

From the slopes of these equations it can be s een that the corner frequency of the source function is roughly proportional to $Y^{-1/5}$ where Y is the yield in kton. Lyman et al (1) found τ proportional to $Y^{-1/3}$for explosions at NTS recorded at Eskdalemuir. The result determined here is in agreement with the theoretical model of Murphy (14) and the assumption of Bache et al (15) that a theoretical scaling of $Y^{-1/3}$ together with the effects of the scaled depth of burial gives a scaling factor of $Y^{-1/5}$. The difference between the results obtained here ($\alpha\ Y^{-1/5}$) and Lyman et al (1) ($\alpha\ Y^{-1/3}$) for NTS explosions may be due to errors in the values of t* used or to the different magnitude range of the explosions used in each study. Lyman et al (1) used explosions in the magnitude range 5½ to 6½ whereas this study uses explosions in the magnitude range 4½ to 5¾ and it is possible that the scaling laws are not constant over the magnitude range 4¾ to 6½.

The scaling laws for explosions at NTS determined here and by Lyman et al (1) are quite different form those determined by Stewart (16) for explosions at the Soviet test site at Shagan River, E Kazakhstan. Stewart (6) found that for the Soviet test site τ is proportional to $Y^{-1/10}$. The relationship between τ, D and yield warrants further research; it may be that it is possible to identify the source medium using τ or D and such information could lead to an improvement in seismological methods of yield determination of nuclear tests.

5.2.1 Ψ_∞ and yield

The yield of seven of the explosions analysed in this report have been published, [NVO(17), Springer and Kinnaman (18), (19)] and are given in table 5. The estimates of Ψ_∞ for these explosions and for those of known yield used by Lyman et al (1) are combined to estimate the relationship between Ψ_∞ and yield in kton for explosions in fully saturated rocks at NTS (figure 8). The results indicate that

$$\mathrm{Log}_{10}\ \Psi_\infty \simeq \log_{10} Y + 1.8$$

where Ψ_∞ is in cubic metres and Y is in kton. Stimpson (20) gives the relationship between Ψ_∞ and Y for explosions in granite at the French nuclear test site in S Algeria as

$$\mathrm{Log}_{10}\ \Psi_\infty \simeq \log_{10} Y + 2.0$$

The Ψ_∞ for the PILE DRIVER explosion (in granite at NTS) is 6590 m^3 which, using Stimpson's results gives a yield of 66 kton which is in close agreement with the announced yield of 62 kton. More observations of Ψ_∞ are required before definitive statements can be made on the relationship between yield and Ψ_∞ for other materials.

5.2.2 Surface wave magnitude M_s and Ψ_∞

The surface wave magnitude M_s determined using the Marshall and Basham (21) formula applied to data from American stations is available for a number of the NTS explosions analysed in this report (Marshall, personal communication) and it is well established that M_s is a useful measure of source size and hence of the yield of explosions (Marshall et al (22), Bache (23)). The explosions for which both M_s and Ψ_∞ are available are plotted in figure 9. The best least squares line through the data is:

$$\mathrm{Log}_{10}\ \Psi_\infty = (0.96 \pm 0.13)M_s - (0.18 \pm 0.52) \qquad r = 0.91$$

This clear linear relationship is not a surprising result in that theoretically M_s should be directly related to Ψ_∞. It is, however reassuring that the results, obtained from surface waves for M_s and body waves for Ψ_∞ are in such close agreement.

5.2.3 Seismic moment M_o and Ψ_∞

The seismic moment of an explosive source is defined as $M_o = 4\pi\rho V^2 \Psi_\infty$ where ρ is the density and V the P-wave speed of the source medium. Appendix A describes in detail the method used to calculate moment for explosions studied in this report. Four estimates of moment for a number of NTS explosions are given in table 6. Two of the moment estimates are determined from surface waves recorded in the far field; those given by Stevens (24) are designated $M_o^{(1)}$ and those by Given and Mellman (25) are designated $M_o^{(3)}$. Two estimates of moment using Ψ_∞ estimated for explosions studied in this report and for which moment estimates derived from surface waves are available are given in table 6.

The two moment estimates are designated $M_o^{(2)}$ and $M_o^{(4)}$. $M_o^{(2)}$ is calculated using the ρ and V values published by Ramspott and Howard (26) and are for the material at the explosion point. Whether this is a strictly valid procedure is questionable: a more realistic approach might be to use the ρ and V values at the elastic radius, at a point directly below the shot point for rays which emerge to be recorded at teleseismic distances. For convenience the values assumed for estimation of $M_o^{(4)}$ are the same as found at YKA, ie, ρ = 2.67 g cm^{-3} and V = 5.64 km s^{-1}. These are reasonable values for ρ and V that may be expected at a depth > 2 km beneath NTS (Stevens (24)).

A comparison between the moment determined from surface waves and those calculated here for explosions which are common to the two or three studies are given in table 6. In general the agreement is good between the moment determined for surface waves and $M_0^{(4)}$. However estimates of $M_0^{(2)}$ which uses ρ and V at the explosion point appear to be too low when compared to moments determined from surface waves.

Using the values of $M_0^{(4)}$ it is possible to relate moment to the yield values given in table 5. For the PILE DRIVER explosion in granite:

$$\text{Log}_{10}M_o \approx \log_{10} Y + 14.06$$

and for the four explosions detonated below the water table:

$$\text{Log}_{10}M_o \approx \log_{10} Y + 13.74$$

6. CONCLUSIONS

The main purpose of the report is to publish the SP and deconvolved seismograms from the YKA seismometer array of explosions at the NTS. An analysis of the data has been made and the main conclusions are

(1) The best estimate of the source magnitude is obtained using $\log_{10}(A/T)_{bc}$ which is derived from the maximum peak-peak amplitude within the first 2-3 cycles of the onset of the P-wave. It is found that

$$\log_{10}(A/T)_{bc} = (1.04 \pm 0.07)m_b - (4.20 \pm 0.35)$$

where m_b is the maximum likelihood estimate of the source magnitude. The distance correction factor plus station correction for the NTS-YKA path is thus about 4.2. As the Gutenberg and Richter (13) distance correction factor for $\Delta = 25^\circ$ is 3.5 the implied station correction for YKA is 0.7, that is the amplitude recorded at the station is about a factor of five below average.

(2) The relationship between $\Psi\infty$ and the yield of explosions detonated below the water table is

$$\log_{10} \Psi\infty \approx \log_{10} Y(\text{kton}) + 1.8.$$

(3) The relationship between $\Psi\infty$ derived from the deconvolved seismograms and global average estimates of M_0 is

$$\log_{10} \Psi\infty \approx M_s - 0.20.$$

(4) Seismic moments derived from the deconvolved P seismograms and from surface waves are in good agreement if the P wave moments are computed using a density and P-wave speed more

appropriate to the values at the elastic radius beneath the source instead of the values at the explosion point.

(5) The relationship between M_0 and yield in kton is found to be

$$\log_{10} M_0 \approx \log_{10} Y + 14.06$$

for the PILE DRIVER explosion and

$$\log_{10} M_0 \approx \log_{10} Y + 13.74$$

for explosions at NTS detonated below the water table.

7. ACKNOWLEDGEMENTS

We would like to express our appreciation to the staff at the Yellowknife array for their dedication and conscientious work over many years. Their work has made available a large volume of high quality recordings on which this work is based. The co-operation of the staff of the Canadian Department of Energy and Mines, Ottawa is also acknowledged. The authors would also like to thank Professor A Douglas for a critical review of this report and to Miss Jean Farthing for assistance in running some of the computer programs used to prepare this report.

REFERENCES

1. N S Lyman, A Douglas, P D Marshall, J B Young: "P Seismograms Recorded at Eskdalemuir, Scotland from Explosions in Nevada, USA." AWRE Report O 10/86, HMSO, London. (1986)

2. M W H Mowat, R F Burch: "Handbook for the Stations which Provide Seismograms to the Blacknest Seismological Centre, United Kingdom." AWRE Blacknest Tech Report 44/47/29 Blacknest, Brimpton, RG7 4RS, UK. (1977).

3. R C Stewart, A Douglas: "Seismograms from Phaseless Seismographs." Geophys J R Astr Soc, 72, 517-521. (1983).

4. A Douglas, J B Young: "The Estimation of Seismic Body Wave Signals in the Presence of Oceanic Microseisms." AWRE Report O 14/81, HMSO, London. (1981).

5. E W Carpenter: "Absorption of Elastic Waves - an Operator for a Constant Q Mechanism." AWRE Report O 43/66, HMSO, London. (1966).

6. W I Futterman: "Dispersive Body Waves." J Geophys Res, 67, 5279-5291.(1962).

7. P D Marshall, D L Springer, H C Rodean: "Magnitude Corrections for Attenuation in the Upper Mantle." Geophys J R Astr Soc, 5, 609-638. (1979)

8. R C Stewart: "Q and the Rise and Fall of a Seismic Pulse". Geophys J R Astr Soc, 76, 793-805. (1984)

9. E W Carpenter: "A Quantitative Evaluation of a Teleseismic Explosion Records". Proc Roy Soc, A, 290, 396-407. (1966a).

10. A Douglas: "Differences in Upper Mantle Attenuation Between the Nevada and Shagan River Test Sites: Can the Effects be Seen in P-Wave Seismograms?" Bull Seism Soc Am, 77, 270-276 (1987).

11. C B Archambeau, E A Flinn, D G Lambert: "Fine Structure of the Upper Mantle". J Geophys Res, 74, 5825-5866. (1969).

12. D Helmberger, R A Wiggins "Upper Mantle Structure of Midwestern United States". J Geophys Res 76, 3229-3245. (1971)

13. B Gutenberg, C F Richter: "Magnitude and Energy of Earthquakes". Annali Geofis, 9, 1-15. (1956).

14. J R Murphy: "Seismic Source Functions and Magnitude Determinations for Underground Nuclear Detonations". Bull Seism Soc Am, 67, 1, 135-158. (1977).

15. T C Bache, P D Marshall, J B Young: "Q and its Effect on Short Period P Waves from Explosions in Central Asia." AWRE Report O 17/84, HMSO, London. (1984).

16. R C Stewart: "P-wave Seismograms from Underground Explosions at the Shagan River Test Site Recorded at Four Arrays". AWE Report O 4/88, HMSO, London. (1988).

17. NVO: "Announced United States Nuclear Tests". NVO-209 (Rev 5). Office of Public Affairs, DOE, Nevada Operations Office, Las Vegas, US." (1985).

18. D L Springer, R L Kinnaman: "Seismic source summary for US Underground Nuclear Explosions, 1961-1970." BSSA, 61, (4) 1073-1098. (1971).

19. D L Springer, R L Kinnaman: "Seismic Source Summary for US Underground Nuclear Explosions 1971-1973." BSSA, 65, (2) 343-349. (1975).

20. I G Stimpson: "Source Parameters of Explosions in Granite at the French Test Site in Algeria." AWE Report O 11/88, HMSO, London. (1988).

21. P D Marshall, P W Basham: "Discrimination between Earthquakes and Underground Explosions Employing an improved M_S Scale." Geophys Res J and R Astr Soc, 28, 431-458. (1972).

22. P D Marshall, A Douglas, J A Hudson: "Surface Waves from Underground Nuclear Explosions." Nature. 234, 8-9. (1971).

23. T C Bache: "Estimating the yield of Underground Nuclear Explosions." Bull Seism Soc Am, 72, (6) 5131-5168. (1982).

24. J L Stevens: "Estimation o Scalar Moments from Explosion-Generated Waves." Bull Seism Soc Am 76, 123-152. (1986)

25. J W Given, G R Mellman: "Source Parameters for Nuclear Explosions at NTS and Shagan River from observations of Rayleigh and Love Waves." Presented at at DARPA/AFGL Seismic Res Symp, USAF Academy, Colorado Springs, May 6-8 1985. (1985).

26. L D Ramspott, N W Howard: "Average Properties of Nuclear Test areas and media at the USERDA Nevada Site." UCRL-51948, LLNL, Livermore, CA, USA. (1975).

27. A Douglas, P D Marshall, J B Young: "The P-waves from the Amchitka Island Explosions." Geophys J R Astr Soc, 90, 107-117. (1987).

28. H A Hasegawa: "Analysis of Seismic Signals from Underground Nuclear Explosions originating in our Geological Environments." Geophys J Roy Astr Soc, 24, 365-381. (1971).

APPENDIX A

MOMENT AND Ψ_∞

If A_o is the area of the P pulse on a deconvolved seismogram then it has been usual to assume (see, for example, Douglas et al (27) that a rough estimate of the long term level of the reduced displacement potential is given by

$$\Psi_\infty = [2G(\Delta)]^{-1}A_o$$

where $G(\Delta)$ is the geometrical factor for P waves propagating to distance Δ. However this implies that $\rho_1 V_1 \approx \rho_o V_o$ where ρ_1 and V_1 are the density and P-wave speed respectively of the source material and $\rho_o V_o$ the density and P-wave speed at the recording station. If $\rho_1 V_1 \neq \rho_o V_o$ then from Carpenter (9) a better estimator of the long term level is given by

$$\Psi_\infty \text{ corr} = [2G(\Delta)]^{-1} \left[\frac{\rho_o V_o}{\rho_1 V_1}\right]^{1/2} A_o$$

That is, $$\Psi_\infty \text{ corr} = \left[\frac{\rho_o V_o}{\rho_1 V_1}\right]^{1/2} \Psi_\infty$$

It is Ψ_∞ that is listed in table 4 in this report. However in computing moment M_o, Ψ_∞ corr has been used. For the YKA receiver the values of ρ_o and V_o are 2.67 g.cm^{-3} and 5.64 km s^{-1} respectively (Hasegawa, 28). To calculate $M^{(2)}$ in table 6 the density and P-wave speed at the explosion point reported by Ramspott and Howard (28) are used:

	ρ_1 g.cm^{-3}	V_1 km.s^{-1}	$\left[\frac{\rho_o V_o}{\rho_1 V_1}\right]^{1/2}$
Climas Stock (Granite)	2.7	5.7	0.99
Yucca: above water table (D)	1.8	1.8	2.16
below water table (W)	1.9	2.4	1.82
Pahute Mesa: below water table* (W)	2.2	3.4	1.42
Rainier Mesa	1.9	2.5	1.78

To calculate $M^{(4)}$ the values of ρ and V below the explosion point are assumed to be the same as ρ and V at Yellowknife which means $\left[\frac{\rho_o V_o}{\rho_1 V_1}\right]^{1/2} = 1$ and Ψ_∞ (as given in table 4) = Ψ_∞ corr.

*Note the depth to the water table varies between 274 and 715 m at the Pahute Mesa site (Springer and Kinnaman, (8, 19), thus it is difficult to estimate from the depth of emplacement whether the shot is above or below the water table.

LIST OF TABLES

Table 1

	Date	Name	Origin Time	Lat˜N	Long˜W	mb	Depth	Test Area
1	660527	Discus Thrower	20 00 00.0	37.178	116.098	4.77	337m	Yucca Flats
2	660602	Piledriver	15 30 00.1	37.227	116.056	5.61	463m	Climax Stock
3	670510	Mickey	13 40 00.0	37.078	115.995	4.75	500m	Yucca Flats
4	670523	Scotch	14 00 00.0	37.275	116.370	5.66	977m	Pahute Mesa
5	670526	Knickerbocker	15 00 01.5	37.248	116.480	5.32	631m	Pahute Mesa
6	680906	Noggin	14 00 00.1	37.136	116.047	5.56	582m	Yucca Flats
7	680917	Stoddard	14 00 00.0	37.120	116.127	4.79	468m	Yucca Flats
8	681208	Schooner	16 00 00.1	37.343	116.566	4.69	107m	Pahute Mesa
9	690115	Wineskin	19 30 00.0	37.209	116.225	5.22	518m	Rainier Mesa
10	690130	Vise	15 00 00.0	37.053	116.029	4.87	454m	Yucca Flats
11	690321	Coffer	14 30 00.0	37.133	116.087	4.81	465m	Yucca Flats
12	690430	Thistle	17 00 00.0	37.090	116.006	5.22	560m	Yucca Flats
13	690527	Torrido	14 15 00.0	37.075	115.995	4.87	515m	Yucca Flats
14	690716	Hutch	14 55 00.0	37.140	116.087	5.50	549m	Yucca Flats
15	691008	Pipkin	14 30 00.1	37.257	116.441	5.49	617m	Pahute Mesa
16	691029	Calabash	22 10 51.4	37.143	116.064	5.60	625m	Yucca Flats
17	691121	Piccalilli	14 52 00.0	37.031	116.002	4.74	394m	Yucca Flats
18	691205	Diesel Train	17 00 00.0	37.180	116.211	4.85	419m	Rainier Mesa
19	691217	Grape A	15 00 00.0	37.084	116.002	5.37	551m	Yucca Flats
20	691217	Lovage	15 15 00.0	37.006	116.023	4.66	378m	Yucca Flats
21	691218	Terrine	19 00 00.0	37.120	116.035	5.05	457m	Yucca Flats
22	700204	Grape B	17 00 00.0	37.099	116.027	5.59	554m	Yucca Flats
23	700323	Shaper	23 05 00.0	37.086	116.021	5.49	561m	Yucca Flats
24	700505	Mint Leaf	15 30 00.2	37.217	116.184	4.85	405m	Rainier Mesa
25	700526	Flask	15 00 00.1	37.113	116.062	5.55	531m	Yucca Flats
26	701014	Tijeras	14 30 00.0	37.071	116.005	5.53	561m	Yucca Flats
27	710623	Laguna	15 30 00.0	37.022	116.023	4.71	455m	Yucca Flats
28	710818	Algodones	14 00 00.0	37.057	116.036	5.33	528m	Yucca Flats
29	711214	Chaenactis	21 09 59.2	37.124	116.096	4.53	331m	Yucca Flats
30	720519	Monero	17 00 00.0	37.064	116.002	4.56	537m	Yucca Flats
31	720720	Diamond Sculls	17 16 00.2	37.215	116.183	4.87	424m	Rainier Mesa
32	720921	Oscuro	15 30 00.2	37.082	116.037	5.67	560m	Yucca Flats
33	721221	Flax	20 15 00.2	37.140	116.083	4.93	436m	Yucca Flats
34	730308	Miera	16 10 00.2	37.103	116.027	5.32	569m	Yucca Flats
35	730425	Angus	22 25 00.0	37.005	116.028	4.58	453m	Yucca Flats
36	730426	Starwort	17 15 00.2	37.123	116.059	5.56	564m	Yucca Flats
37	730605	Dido Queen	17 00 00.2	37.185	116.215	4.97	391m	Rainier Mesa
38	730621		17 44 59.3	37.090	116.001	5.37		Yucca Flats
39	730628	Portulaca	19 15 12.4	37.148	116.086	4.89	466m	Yucca Flats
40	731012	Husky Ace	17 00 00.8	37.200	116.203	4.66	413m	Rainier Mesa
41	740227	Latir	17 00 00.1	37.104	116.053	5.63	641m	Yucca Flats
42	740523	Fallon	13 38 29.7	37.093	116.123	4.80	466m	Yucca Flats
43	740619	Ming Blade	16 00 00.2	37.201	116.190	4.83	389m	Rainier Mesa
44	740710	Escabosa	16 00 00.1	37.068	116.032	5.73	640m	Yucca Flats
45	740830	Portmanteau	15 00 00.2	37.152	116.083	5.76	655m	Yucca Flats
46	740926	Stanyan	15 05 00.2	37.133	116.068	5.52	572m	Yucca Flats
47	750228	Topgallant	15 15 00.0	37.106	116.056	5.68	713m	Yucca Flats
48	750307	Cabrillo	15 00 00.0	37.134	116.084	5.57	600m	Yucca Flats
49	750405	Dining Car	19 45 00.0	37.188	116.214	4.88	305m	Rainier Mesa
50	750430	Obar	15 00 00.0	37.109	116.029	5.08	569m	Yucca Flats
51	750603	Mizzen	14 40 00.1	37.094	116.036	5.64	637m	Yucca Flats

Table 1 contd

Date	Name	Origin Time	Lat˜N	Long˜W	mb	Depth	Test Area
52 760204	Esrom	14 40 00.2	37.107	116.037	5.67	655m	Yucca Flats
53 760204	Keelson	14 20 00.1	37.069	116.030	5.67	640m	Yucca Flats
54 760512	Mighty Epic	19 50 00.2	37.209	116.212	4.79		Rainier Mesa
55 761208	Redmud	14 49 30.1	37.079	116.002	4.76	427m	Yucca Flats
56 761228	Rudder	18 00 00.1	37.100	116.036	5.47	640m	Yucca Flats
57 770405	Marsilly	15 00 00.2	37.120	116.062	5.72	690m	Yucca Flats
58 770427	Bulkhead	15 00 00.1	37.095	116.028	5.38	594m	Yucca Flats
59 770525	Crewline	17 00 00.1	37.094	116.045	5.36	564m	Yucca Flats
60 770804	Strake	16 40 00.1	37.087	116.007	5.18	518m	Yucca Flats
61 770819	Scantling	17 55 00.1	37.111	116.055	5.67	701m	Yucca Flats
62 770927	Coulommiers	14 00 00.2	37.151	116.068	4.87	530m	Yucca Flats
63 771117	Seamount	19 30 00.1	37.021	116.025	4.71	372m	Yucca Flats
64 780223	Reblochlon	17 00 00.2	37.125	116.064	5.74	658m	Yucca Flats
65 780323	Iceberg	16 30 00.2	37.102	116.051	5.72	640m	Yucca Flats
66 780411	Backbeach	17 45 00.1	37.233	116.367	5.55	672m	Pahute Mesa
67 780712	Lowball	17 00 00.1	37.079	116.044	5.67	564m	Yucca Flats
68 780831	Panir	14 00 00.2	37.275	116.357	5.67	681m	Pahute Mesa
69 780913	Diablo Hawk	15 15 00.2	37.209	116.211	4.73	388m	Rainier Mesa
70 780927	Draughts	17 00 00.0	37.080	116.050	5.10	442m	Yucca Flats
71 780927	Rummy	17 20 00.0	37.070	116.019	5.86	640m	Yucca Flats
72 781118	Quargel	19 00 00.0	37.126	116.084	5.33	542m	Yucca Flats
73 781216	Farm	15 30 00.2	37.273	116.410	5.63	689m	Pahute Mesa
74 790208	Quinella	20 00 00.1	37.102	116.055	5.60	579m	Yucca Flats
75 790215	Kloster	18 05 00.2	37.152	116.072	4.97	536m	Yucca Flats
76 790611	Pepato	14 00 00.2	37.290	116.455	5.57	681m	Pahute Mesa
77 790628	Fajy	14 44 00.2	37.142	116.088	5.23	536m	Yucca Flats
78 790808	Offshore	15 00 00.1	37.015	116.008	4.82	396m	Yucca Flats
79 790829	Nessel	15 08 00.2	37.121	116.066	4.94	464m	Yucca Flats
80 790906	Hearts	15 00 00.1	37.088	116.053	5.89	640m	Yucca Flats
81 790926	Sheepshead	15 00 00.1	37.229	116.364	5.65	640m	Pahute Mesa
82 800403	Liptauer	14 00 00.1	37.150	116.082	4.90	417m	Yucca Flats
83 800416	Pyramid	20 00 00.1	37.101	116.031	5.42	579m	Yucca Flats
84 800426	Colwick	17 00 00.1	37.248	116.422	5.55	633m	Pahute Mesa
85 800612	Kash	17 15 00.1	37.282	116.454	5.67	645m	Pahute Mesa
86 800725	Tafi	19 05 00.1	37.256	116.477	5.57	680m	Pahute Mesa
87 801031	Miners Iron	18 00 00.1	37.211	116.205	4.93	390m	Rainier Mesa
88 801217	Serpa	15 10 00.1	37.325	116.312	5.29	573m	Pahute Mesa
89 810115	Baseball	20 25 00.1	37.097	116.057	5.73	564m	Yucca Flats
90 810529	Aligote	16 00 00.1	37.102	116.004	4.37	320m	Yucca Flats
91 810606	Harzer	18 00 00.1	37.303	116.326	5.63	637m	Pahute Mesa
92 811001	Paliza	19 00 00.1	37.082	116.009	5.12	472m	Yucca Flats
93 811112	Rousanne	15 00 00.1	37.108	116.049	5.46	518m	Yucca Flats
94 820212	Molbo	14 55 00.1	37.224	116.463	5.41	638m	Pahute Mesa
95 820417	Tenaja	18 00 00.1	37.017	116.010	4.46	357m	Yucca Flats
96 820507	Bouschet	18 17 00.1	37.069	116.045	5.73	564m	Yucca Flats
97 820624	Nebbiolo	14 15 0.1	37.236	116.370	5.64	640m	Pahute Mesa
98 820729	Monterey	20 05 00.1	37.102	116.075	4.46	400m	Yucca Flats
99 820805	Atrisco	14 00 00.1	37.084	116.007	5.74	640m	Yucca Flats
100 820923	D.A + H.L	16 00 00.1	37.212	116.207	4.98	409m	Rainier Mesa
101 820923	Frisco	17 00 00.1	37.175	116.088	4.85	451m	Yucca Flats
102 821112	Seyval	19 17 00.1	37.024	116.032	4.55	366m	Yucca Flats

Table 1 contd

	Date	Name	Origin Time	Lat°N	Long°W	mb	Depth	Test Area
103	821210	Manteca	15 20 00.1	37.030	116.072	4.74	413m	Yucca Flats
104	830326	Cabra	20 20 00.1	37.301	116.460	5.28	543m	Pahute Mesa
105	830414	Turquoise	19 05 00.1	37.073	116.046	5.74	533m	Yucca Flats
106	830505	Crowdie	15 20 00.1	37.012	116.089	4.44	390m	Yucca Flats
107	830526	Fahada	15 00 00.1	37.103	116.006	4.65	384m	Yucca Flats
108	830609	Danablu	17 10 00.1	37.158	116.089	4.52	320m	Yucca Flats
109	830803	Laban	13 33 00.1	37.119	116.089	4.21	326m	Yucca Flats
110	830811	Sabado	14 00 00.1	36.998	116.003	4.39	320m	Yucca Flats
111	830901	Chancellor	14 00 00.1	37.273	116.355	5.45	625m	Pahute Mesa
112	831216	Romano	18 30 00.1	37.140	116.072	5.14	515m	Yucca Flats
113	840215	Midas Myth/M.	17 00 00.1	37.221	116.181	5.08		Rainier Mesa
114	840501	Mundo	19 00 00.1	37.106	116.022	5.47	567m	Yucca Flats
115	840531	Caprock	13 04 00.1	37.103	116.048	5.74	600m	Yucca Flats
116	840620	Duoro	15 15 00.1	37.000	116.043	4.78	381m	Yucca Flats
117	840725	Kappeli	15 30 00.1	37.268	116.411	5.39	640m	Pahute Mesa
118	840802	Correo	15 00 00.1	37.017	116.008	4.67	355m	Yucca Flats
119	841215	Tierra	14 45 00.1	37.281	116.305	5.45	640m	Pahute Mesa
120	850315	Vaughn	16 31 00.1	37.058	116.045	4.80	427m	Yucca Flats
121	850323	Cottage	18 30 00.1	37.180	116.089	5.30	515m	Yucca Flats
122	850406	Misty Rain	23 15 00.1	37.201	116.207	4.80		Rainier Mesa
123	850502	Towanda	15 20 00.1	37.253	116.325	5.70	661m	Pahute Mesa
124	850612	Salut	15 15 00.1	37.248	116.489	5.50	608m	Pahute Mesa
125	850626	Maribo	18 03 00.1	37.124	116.122	4.30	381m	Yucca Flats
126	850927	Ponil	14 15 00.1	37.090	116.002	4.60	366m	Yucca Flats
127	851016	Roquefort	21 35 00.1	37.110	116.121	4.60	415m	Yucca Flats
128	851205	Kinibito	15 00 00.1	37.053	116.045	5.70	600m	Yucca Flats
129	851228	Goldstone	19 01 00.1	37.238	116.473	5.30	500m	Pahute Mesa
130	860322	Glencoe	16 15 00.1	37.083	116.066	5.10	600m	Yucca Flats
131	860410	Mighty Oak	14 08 30.1	37.218	116.183	4.90	400m	Rainier Mesa
132	860422	Jefferson	14 30 00.1	37.264	116.440	5.30	600m	Pahute Mesa
133	860625	Darwin	20 27 45.1	37.265	116.499	5.50	500m	Pahute Mesa
134	860717	Cybar	21 00 00.1	37.279	116.356	5.70	600m	Pahute Mesa
135	860724	Cornucopia	15 05 00.1	37.143	116.071	4.50	400m	Yucca Flats

Table 2

=======

	Date	Name	Amplitudes (mμ)				Period (s)			
	Date	Name	Aoa	Aab	Abc	Amax	Tod	Tbc	Tp2	
1	660527	Discus Thrower	3.20	8.62	15.09	23.40	0.82	0.42	0.74	*
2	660602	Piledriver	93.40	169.63	390.73	724.29	0.74	0.25	0.25	
3	670510	Mickey	2.46	14.05	17.57	44.50	0.74	0.37	0.63	
4	670523	Scotch	23.77	104.01	177.71	222.86	0.85	0.42	0.26	
5	670526	Knickerbocker	10.87	42.76	51.46	137.70	0.80	0.42	0.61	
6	680906	Noggin	17.13	67.44	77.07	162.71	0.85	0.40	0.82	
7	680917	Stoddard	1.74	9.51	14.58	23.47	0.85	0.42	0.46	
8	681208	Schooner	3.81	21.56	38.05	48.20	0.76	0.32	0.42	
9	690115	Wineskin	3.85	12.72	15.60	26.62	0.83	0.44	0.38	
10	690130	Vise	3.12	14.76	19.75	39.50	0.76	0.25	0.79	*
11	690321	Coffer	1.11	9.61	19.60	25.96	0.74	0.42	0.38	
12	690430	Thistle	9.08	34.29	42.92	86.30	0.74	0.25	0.85	
13	690527	Torrido	4.97	17.64	28.57	45.65	0.89	0.64	0.68	
14	690716	Hutch	12.66	47.80	82.93	120.29	1.02	0.47	0.49	
15	691008	Pipkin	18.61	71.81	105.33	186.19	0.80	0.61	0.42	
16	691029	Calabash	22.41	87.44	100.90	213.00	0.85	0.42	0.85	
17	691121	Piccalilli	4.63	17.73	24.98	51.66	0.68	0.23	0.34	
18	691205	Diesel Train	3.43	13.16	20.38	43.50	0.74	0.46	0.55	*
19	691217	Grape A	14.28	61.60	78.40	106.40	0.85	0.58	0.81	
20	691217	Lovage	3.58	12.79	22.17	27.79	0.67	0.23	0.23	
21	691218	Terrine	8.06	23.67	32.57	63.80	0.89	0.23	1.04	*
22	700204	Grape B	23.97	79.89	89.29	178.57	0.84	0.25	0.76	*
23	700323	Shaper	15.60	55.03	62.43	148.29	0.82	0.32	0.76	*
24	700505	Mint Leaf	5.21	19.54	30.22	49.50	0.82	0.42	0.59	*
25	700526	Flask	14.77	54.17	67.96	187.14	0.95	0.63	0.82	
26	701014	Tijeras	26.15	92.67	117.77	194.57	0.88	0.63	1.05	
27	710623	Laguna	4.23	17.27	27.78	45.90	0.63	0.23	0.82	*
28	710818	Algodones	10.31	41.26	59.32	98.00	0.85	0.32	0.42	
29	711214	Chaenactis	2.73	7.50	13.10	20.45	0.68	0.23	0.23	
30	720519	Monero	1.70	6.24	11.30	21.57	0.74	0.21	0.68	*
31	720720	Diamond Sculls	4.33	13.55	19.04	28.60	0.85	0.42	0.61	*
32	720921	Oscuro	20.66	73.86	78.51	196.29	0.85	0.34	0.89	
33	721221	Flax	3.88	13.50	21.65	32.82	0.83	0.44	0.34	
34	730308	Miera	10.21	49.78	56.41	97.00	0.85	0.37	0.85	
35	730425	Angus	1.57	7.87	11.45	24.34	0.64	0.34	0.21	
36	730426	Starwort	12.99	46.77	64.96	164.57	0.85	0.40	0.85	*
37	730605	Dido Queen	3.77	12.59	20.45	40.90	0.81	0.61	0.64	*
38	730621		13.11	43.73	51.93	103.86	0.87	0.37	0.79	*
39	730628	Portulaca	2.73	11.57	23.38	31.40	0.83	0.42	0.42	
40	731012	Husky Ace	2.65	6.78	12.58	20.12	0.64	0.55	0.61	*
41	740227	Latir	21.54	83.04	110.37	199.71	0.85	0.49	0.85	*
42	740523	Fallon	1.42	6.64	14.00	17.91	0.85	0.42	0.38	
43	740619	Ming Blade	4.59	15.32	22.97	29.10	0.74	0.42	1.00	*
44	740710	Escabosa	21.00	77.64	77.64	241.86	0.85	0.27	0.63	
45	740830	Portmanteau	36.47	101.83	131.30	231.00	1.01	0.42	0.89	*
46	740926	Stanyan	13.36	40.49	51.63	153.86	0.85	0.37	0.89	*
47	750228	Topgallant	25.51	85.72	109.71	193.90	0.91	0.38	0.84	*
48	750307	Cabrillo	14.98	46.82	71.78	118.60	0.91	0.44	0.86	*
49	750405	Dining Car	3.05	13.21	18.79	38.60	0.89	0.55	0.78	*
50	750430	Obar	5.71	21.56	30.57	48.20	0.85	0.38	0.85	*
51	750603	Mizzen	23.46	78.20	87.25	156.40	0.89	0.25	0.51	

Table 2 contd

	Date	Name	Amplitudes (mμ) Aoa	Aab	Abc	Amax	Period (s) Tod	Tbc	Tp2	
52	760204	Esrom	26.03	82.91	99.33	152.20	0.95	0.27	0.85	*
53	760204	Keelson	17.31	64.28	71.70	187.90	0.85	0.36	0.59	
54	760512	Mighty Epic	3.49	11.01	11.92	26.49	0.85	0.44	0.68	*
55	761208	Redmud	2.55	6.08	8.36	15.79	0.85	0.40	0.82	*
56	761228	Rudder	19.42	64.74	81.24	123.00	0.89	0.32	0.85	*
57	770405	Marsilly	20.62	72.17	103.11	195.90	0.89	0.30	0.85	
58	770427	Bulkhead	14.30	49.66	59.80	98.80	0.89	0.25	0.85	*
59	770525	Crewline	10.95	40.51	54.30	83.20	0.88	0.32	0.84	*
60	770804	Strake	6.32	25.26	28.04	48.00	0.86	0.38	0.82	*
61	770819	Scantling	22.14	70.86	93.01	168.30	0.99	0.36	1.01	*
62	770927	Coulommiers	4.65	13.96	20.83	42.10	0.85	0.38	0.87	*
63	771117	Seamount	3.11	7.56	9.78	15.57	0.74	0.36	0.40	
64	780223	Reblochlon	21.47	76.23	92.33	204.00	0.96	0.34	1.02	
65	780323	Iceberg	22.32	79.05	102.30	176.70	0.88	0.38	0.84	*
66	780411	Backbeach	13.63	52.14	77.70	126.43	0.89	0.63	0.63	
67	780712	Lowball	15.43	73.17	94.53	150.30	0.87	0.37	0.89	
68	780831	Panir	17.13	64.22	107.04	162.70	0.95	0.42	0.90	*
69	780913	Diablo Hawk	3.55	10.39	12.57	18.58	0.63	0.44	0.30	
70	780927	Draughts	3.77	20.76	32.08	71.70	0.82	0.63	0.68	
71	780927	Rummy	29.37	132.16	190.89	279.00	0.83	0.42	0.64	*
72	781118	Quargel	5.69	25.36	39.96	58.40	0.89	0.48	1.02	
73	781216	Farm	17.12	68.55	110.32	158.52	0.89	0.44	0.63	
74	790208	Quinella	16.98	63.71	80.70	161.40	0.89	0.34	0.85	*
75	790215	Kloster	4.34	14.09	21.68	41.20	0.88	0.47	0.85	*
76	790611	Pepato	17.29	74.92	132.55	219.00	0.76	0.44	0.64	
77	790628	Fajy	6.44	22.19	41.52	54.40	0.88	0.46	0.63	
78	790808	Offshore	2.84	15.16	19.14	36.00	0.77	0.32	0.81	*
79	790829	Nessel	2.08	10.98	14.97	31.60	0.86	0.37	0.46	
80	790906	Hearts	28.95	124.47	177.30	275.00	0.95	0.42	0.64	
81	790926	Sheepshead	12.89	55.87	94.54	163.30	0.84	0.54	0.40	
82	800403	Liptauer	2.52	9.16	18.53	27.40	0.89	0.44	0.42	
83	800416	Pyramid	13.67	50.58	59.61	103.90	0.89	0.29	0.84	*
84	800426	Colwick	16.73	55.78	76.22	131.26	0.89	0.47	0.53	
85	800612	Kash	19.94	66.47	106.34	252.57	0.85	0.59	0.47	
86	800725	Tafi	17.39	80.53	104.27	220.14	0.83	0.62	0.47	
87	801031	Miners Iron	5.26	15.47	21.66	29.40	0.89	0.47	1.04	*
88	801217	Serpa	6.12	20.39	39.36	69.95	0.84	0.53	0.52	
89	810115	Baseball	16.32	69.68	82.62	151.30	0.89	0.34	0.80	
90	810529	Aligote	0.56	2.39	2.82	5.35	0.85	0.32	0.42	*
91	810606	Harzer	16.16	51.71	81.60	153.50	0.89	0.49	0.85	*
92	811001	Paliza	8.1	18.9	20.25	51.30	0.84	0.36	0.79	*
93	811112	Rousanne	9.38	39.39	53.15	118.80	0.91	0.38	0.95	*
94	820212	Molbo	8.94	31.69	44.97	97.10	0.89	0.47	0.64	
95	820417	Tenaja	1.42	6.72	7.66	15.13	0.68	0.21	0.63	*
96	820507	Bouschet	27.80	115.87	162.21	207.71	0.85	0.32	0.40	
97	820624	Nebbiolo	16.51	61.89	101.10	155.98	0.89	0.44	0.68	
98	820729	Monterey				9.98			0.32	*
99	820805	Atrisco	36.47	116.72	126.44	184.80	0.95	0.63	0.85	
100	820923	Diamond Ace + Huron Landing	3.01	15.80	18.82	28.60	0.65	0.42	0.89	*

Table 2 contd

	Date	Name	Aoa	Aab	Abc	Amax	Tod	Tbc	Tp2	
			Amplitudes (mµ)				Period (s)			
101	820923	Frisco				31.0	0.85		0.37	
102	821112	Seyval	0.25	3.83	5.57	9.40	0.65	0.36	0.63	
103	821210	Manteca	1.29	6.20	12.50	16.16	0.95	0.36	0.65	*
104	830326	Cabra	11.13	37.85	66.79	112.80	0.85	0.42	0.42	
105	830414	Turquoise	20.78	82.21	113.15	175.50	0.89	0.25	0.42	
106	830505	Crowdie	1.18	2.44	5.96	7.88	0.85	0.44	0.53	
107	830526	Fahada	0.75	5.75	7.12	13.01	0.85	0.27	0.53	
108	830609	Danablu	1.08	3.98	8.97	12.30	0.67	0.57	0.34	
109	830803	Laban	0.54	0.90	2.74	5.78	0.53	0.38	0.53	
110	830811	Sabado	0.23	1.03	3.30	6.22	0.42	0.40	0.59	
111	830901	Chancellor	7.41	34.06	60.48	93.80	0.87	0.53	0.86	*
112	831216	Romano	4.22	15.63	19.43	53.50	0.85	0.41	0.46	
113	840215	Midas Myth/Milagro	5.44	16.52	26.64	40.50	0.85	0.46	0.44	
114	840501	Mundo	13.53	47.75	53.05	100.80	0.89	0.63	0.68	
115	840531	Caprock	26.16	88.05	109.19	191.20	0.89	0.25	0.89	*
116	840620	Duoro	2.31	9.28	12.79	21.90	0.72	0.37	0.64	*
117	840725	Kappeli	10.65	39.48	59.74	98.70	0.88	0.44	0.42	
118	840802	Correo	1.23	7.37	11.25	15.55	0.68	0.30	0.63	*
119	841215	Tierra	13.69	41.98	58.10	115.60	0.84	0.42	0.38	
120	850315	Vaughn	1.29	12.30	15.02	21.20	0.79	0.26	0.61	
121	850323	Cottage	15.40	42.62	69.40	84.80	0.89	0.42	0.65	*
122	850406	Misty Rain	2.72	10.53	15.71	34.50	0.65	0.49	0.32	
123	850502	Towanda	15.37	55.89	93.16	177.00	0.95	0.44	0.93	*
124	850612	Salut	11.12	39.46	57.75	136.30	0.89	0.44	0.58	
125	850626	Maribo				12.02			0.49	
126	850927	Ponil	1.50	5.24	5.99	14.23	1.06	0.25	0.59	
127	851016	Roquefort	0.36	5.86	6.90	17.13	0.85	0.40	0.64	*
128	851205	Kinibito	14.32	73.82	105.58	170.00	0.83	0.37	1.06	*
129	851228	Goldstone	7.50	26.40	34.00	76.00	0.89	0.44	0.42	
130	860322	Glencoe	9.28	33.27	58.80	58.80	0.87	0.38	0.38	
131	860410	Mighty Oak	6.96	23.52	35.59	57.87	0.79	0.55	0.64	*
132	860422	Jefferson	11.51	38.11	57.55	91.44	0.85	0.47	0.59	
133	860625	Darwin	14.81	59.74	97.75	187.60	0.84	0.42	0.48	
134	860717	Cybar	15.50	53.75	84.75	157.10	0.89	0.44	0.87	
135	860724	Cornucopia	1.13	4.24	8.22	14.26	0.69	0.42	0.53	

Table 3

	Date	Name	log(A/T)oa	log(A/T)ab	log(A/T)bc	log(A/T)max
1	660527	Discus Thrower	0.441	0.570	0.819	1.319
2	660602	Piledriver	1.888	1.846	2.190	2.458
3	670510	Mickey	0.308	0.764	0.861	1.478
4	670523	Scotch	1.320	1.660	1.890	1.946
5	670526	Knickerbocker	0.967	1.260	1.352	1.947
6	680906	Noggin	1.178	1.472	1.516	2.245
7	680917	Stoddard	0.185	0.621	0.804	1.037
8	681208	Schooner	0.502	0.954	1.183	1.323
9	690115	Wineskin	0.524	0.742	0.846	1.046
10	690130	Vise	0.415	0.789	0.894	1.600
11	690321	Coffer	-0.037	0.599	0.932	1.035
12	690430	Thistle	0.876	1.152	1.231	2.000
13	690527	Torrido	0.653	0.902	1.297	1.544
14	690716	Hutch	1.111	1.387	1.593	1.771
15	691008	Pipkin	1.200	1.486	1.831	1.910
16	691029	Calabash	1.295	1.585	1.644	2.393
17	691121	Piccalilli	0.574	0.856	0.997	1.320
18	691205	Diesel Train	0.453	0.736	0.976	1.384
19	691217	Grape A	1.099	1.433	1.671	2.051
20	691217	Lovage	0.461	0.713	0.945	1.043
21	691218	Terrine	0.863	1.030	1.112	2.046
22	700204	Grape B	1.321	1.543	1.549	2.223
23	700323	Shaper	1.129	1.375	1.398	2.142
24	700505	Mint Leaf	0.652	0.925	1.120	1.482
25	700526	Flask	1.148	1.412	1.662	2.306
26	701014	Tijeras	1.371	1.619	1.901	2.539
27	710623	Laguna	0.530	0.839	1.043	1.696
28	710818	Algodones	0.957	1.259	1.376	1.631
29	711214	Chaenactis	0.344	0.482	0.716	0.910
30	720519	Monero	0.148	0.412	0.653	1.219
31	720720	Diamond Sculls	0.581	0.775	0.920	1.265
32	720921	Oscuro	1.259	1.511	1.502	2.397
33	721221	Flax	0.527	0.768	0.988	1.123
34	730308	Miera	0.953	1.340	1.368	2.051
35	730425	Angus	0.100	0.499	0.666	0.987
36	730426	Starwort	1.058	1.313	1.442	2.281
37	730605	Dido Queen	0.509	0.732	1.119	1.453
38	730621		1.068	1.290	1.332	2.019
39	730628	Portulaca	0.374	0.701	1.009	1.137
40	731012	Husky Ace	0.327	0.434	0.846	1.112
41	740227	Latir	1.277	1.562	1.733	2.365
42	740523	Fallon	0.096	0.465	0.786	0.873
43	740619	Ming Blade	0.579	0.802	1.001	1.670
44	740710	Escabosa	1.266	1.533	1.488	2.214
45	740830	Portmanteau	1.566	1.711	1.758	2.468
46	740926	Stanyan	1.070	1.250	1.329	2.291
47	750228	Topgallant	1.371	1.596	1.661	2.342
48	750307	Cabrillo	1.139	1.333	1.509	2.149
49	750405	Dining Car	0.441	0.777	1.020	1.579
50	750430	Obar	0.701	0.977	1.106	1.747
51	750603	Mizzen	1.327	1.549	1.539	1.902

Table 3 contd

	Date	Name	log(A/T)oa	log(A/T)ab	log(A/T)bc	log(A/T)max
52	760204	Esrom	1.395	1.597	1.595	2.247
53	760204	Keelson	1.182	1.451	1.468	2.061
54	760512	Mighty Epic	0.487	0.685	0.729	1.308
55	761208	Redmud	0.351	0.427	0.552	1.232
56	761228	Rudder	1.245	1.467	1.513	2.154
57	770405	Marsilly	1.271	1.514	1.613	2.356
58	770427	Bulkhead	1.112	1.352	1.375	2.059
59	770525	Crewline	0.993	1.260	1.338	1.974
60	770804	Strake	0.748	1.049	1.068	1.715
61	770819	Scantling	1.341	1.545	1.581	2.441
62	770927	Coulommiers	0.612	0.788	0.939	1.709
63	771117	Seamount	0.410	0.495	0.603	0.822
64	780223	Reblochlon	1.315	1.564	1.573	2.533
65	780323	Iceberg	1.302	1.550	1.630	2.302
66	780411	Backbeach	1.091	1.373	1.720	1.932
67	780712	Lowball	1.139	1.514	1.592	2.281
68	780831	Panir	1.213	1.486	1.670	2.325
69	780913	Diablo Hawk	0.453	0.619	0.752	0.869
70	780927	Draughts	0.512	0.952	1.336	1.740
71	780927	Rummy	1.406	1.758	1.921	2.287
72	781118	Quargel	0.712	1.060	1.284	1.990
73	781216	Farm	1.190	1.492	1.695	2.030
74	790208	Quinella	1.187	1.460	1.514	2.272
75	790215	Kloster	0.591	0.801	1.010	1.679
76	790611	Pepato	1.159	1.495	1.775	2.181
77	790628	Fajy	0.762	0.999	1.285	1.566
78	790808	Offshore	0.377	0.803	0.885	1.580
79	790829	Nessel	0.265	0.687	0.792	1.166
80	790906	Hearts	1.441	1.773	1.889	2.280
81	790926	Sheepshead	1.051	1.387	1.712	1.842
82	800403	Liptauer	0.358	0.618	0.920	1.078
83	800416	Pyramid	1.093	1.360	1.375	2.071
84	800426	Colwick	1.180	1.402	1.556	1.845
85	800612	Kash	1.244	1.466	1.814	2.077
86	800725	Tafi	1.179	1.543	1.837	2.017
87	801031	Miners Iron	0.678	0.845	1.010	1.709
88	801217	Serpa	0.728	0.950	1.322	1.562
89	810115	Baseball	1.170	1.499	1.524	2.193
90	810529	Aligote	-0.308	0.022	0.053	0.368
91	810606	Harzer	1.165	1.369	1.602	2.251
92	811001	Paliza	0.850	0.917	0.919	1.713
93	811112	Rousanne	0.936	1.258	1.346	2.236
94	820212	Molbo	0.908	1.157	1.327	1.828
95	820417	Tenaja	0.061	0.435	0.485	1.010
96	820507	Bouschet	1.388	1.707	1.813	1.946
97	820624	Nebbiolo	1.175	1.448	1.657	2.078
98	820729	Monterey				0.602
99	820805	Atrisco	1.541	1.745	1.932	2.331
100	820923	D.A + H.L	0.384	0.803	0.915	1.560
101	820923	Frisco				1.108
102	821112	Seyval	-0.697	0.187	0.359	0.803

Table 3 contd

	Date	Name	log(A/T)oa	log(A/T)ab	log(A/T)bc	log(A/T)max
103	821210	Manteca	0.090	0.470	0.710	1.060
104	830326	Cabra	0.991	1.221	1.465	1.692
105	830414	Turquoise	1.275	1.571	1.652	1.884
106	830505	Crowdie	0.016	0.030	0.428	0.623
107	830526	Fahada	-0.181	0.403	0.451	0.841
108	830609	Danablu	-0.060	0.206	0.719	0.697
109	830803	Laban	-0.368	-0.448	0.058	0.488
110	830811	Sabado	-0.737	-0.387	0.148	0.581
111	830901	Chancellor	0.820	1.182	1.508	2.047
112	831216	Romano	0.569	0.837	0.923	1.395
113	840215	Midas Myth/M.	0.680	0.861	1.092	1.260
114	840501	Mundo	1.088	1.335	1.555	1.888
115	840531	Caprock	1.375	1.601	1.636	2.385
116	840620	Duoro	0.278	0.580	0.723	1.181
117	840725	Kappeli	0.981	1.249	1.429	1.634
118	840802	Correo	-0.002	0.475	0.651	1.022
119	841215	Tierra	1.078	1.263	1.404	1.683
120	850315	Vaughn	0.039	0.717	0.775	1.135
121	850323	Cottage	1.144	1.286	1.481	1.780
122	850406	Misty Rain	0.340	0.626	0.887	1.141
123	850502	Towanda	1.166	1.425	1.622	2.390
124	850612	Salut	1.003	1.252	1.414	1.911
125	850626	Maribo				0.770
126	850927	Ponil	0.204	0.446	0.376	0.940
127	851016	Roquefort	-0.500	0.411	0.468	1.075
128	851205	Kinibito	1.094	1.505	1.640	2.488
129	851228	Goldstone	0.832	1.078	1.184	1.521
130	860322	Glencoe	0.918	1.171	1.390	1.390
131	860410	Mighty Oak	0.771	0.998	1.297	1.603
132	860422	Jefferson	1.005	1.224	1.434	1.748
133	860625	Darwin	1.112	1.416	1.630	1.955
134	860717	Cybar	1.147	1.386	1.581	2.281
135	860724	Cornucopia	-0.037	0.236	0.555	0.881

Table 4

=======

	Date	Name	mb	ψ_∞	τ	D	
1	660527	Discus Thrower	4.77	447	0.10	0.45	
2	660602	Piledriver	5.61	6590	0.10	0.24	
3	670510	Mickey	4.75	975	0.11	0.55	*
4	670523	Scotch	5.66	7093	0.16	0.67	
5	670526	Knickerbocker	5.32	1763	0.20	0.53	
6	680906	Noggin	5.56	4202	0.11	0.50	*
7	680917	Stoddard	4.79	613	0.12	0.62	
8	681208	Schooner	4.69	721	0.10	0.41	
9	690115	Wineskin	5.22	2499	0.17	0.65	*
10	690130	Vise	4.87	682	0.14	0.52	
11	690321	Coffer	4.81	465	0.15	0.45	*
12	690430	Thistle	5.22	2025	0.14	0.62	
13	690527	Torrido	4.87	1155	0.11	0.54	
14	690716	Hutch	5.50	4370	0.17	0.84	
15	691008	Pipkin	5.49	4022	0.18	0.60	*
16	691029	Calabash	5.60	5594	0.11	0.55	*
17	691121	Piccalilli	4.74	456	0.13	0.42	
18	691205	Diesel Train	4.85	638	0.20	0.59	
19	691217	Grape A	5.37	4118	0.21	0.69	
20	691217	Lovage	4.66	278	0.09	0.28	
21	691218	Terrine	5.05	1231	0.12	0.54	
22	700204	Grape B	5.59	5604	0.13	0.60	*
23	700323	Shaper	5.49	4440	0.16	0.80	*
24	700505	Mint Leaf	4.85	1170	0.17	0.65	*
25	700526	Flask	5.55	6313	0.20	0.90	*
26	701014	Tijeras	5.53	7547	0.17	0.75	*
27	710623	Laguna	4.71	776	0.16	0.53	
28	710818	Algodones	5.33	2398	0.14	0.69	
29	711214	Chaenactis	4.53	691	0.18	0.65	*
30	720519	Monero	4.56	334	0.19	0.50	*
31	720720	Diamond Sculls	4.87	685	0.14	0.60	*
32	720921	Oscuro	5.67	5792	0.17	0.85	*
33	721221	Flax	4.93	566	0.16	0.45	*
34	730308	Miera	5.32	3732	0.24	0.70	*
35	730425	Angus	4.58	313	0.10	0.25	*
36	730426	Starwort	5.56	4453	0.17	0.90	
37	730605	Dido Queen	4.97	604	0.13	0.55	*
38	730621		5.37	3107	0.18	0.69	
39	730628	Portulaca	4.89	560	0.16	0.63	
40	731012	Husky Ace	4.66				
41	740227	Latir	5.63	6583	0.20	0.75	*
42	740523	Fallon	4.80	486	0.13	0.67	
43	740619	Ming Blade	4.83	634	0.19	0.48	
44	740710	Escabosa	5.73	5309	0.22	0.70	
45	740830	Portmanteau	5.76	12367	0.19	1.05	*
46	740926	Stanyan	5.52	2546	0.11	0.61	*
47	750228	Topgallant	5.68	7502	0.25	0.80	*
48	750307	Cabrillo	5.57	4354	0.15	0.87	
49	750405	Dining Car	4.88	587	0.17	0.435	
50	750430	Obar	5.08	1720	0.16	0.75	*
51	750603	Mizzen	5.64	6867	0.18	0.75	*

Table 4 contd

	Date	Name	mb	Ψ_∞	γ	D	
52	760204	Esrom	5.67	7063	0.20	0.75	*
53	760204	Keelson	5.67	4977	0.28	0.70	*
54	760512	Mighty Epic	4.79	490	0.15	0.45	*
55	761208	Redmud	4.76				
56	761228	Rudder	5.47	5309	0.23	0.70	*
57	770405	Marsilly	5.72	7084	0.20	0.90	*
58	770427	Bulkhead	5.38	3379	0.19	0.68	
59	770525	Crewline	5.36	2707	0.18	0.72	
60	770804	Strake	5.18	2001	0.16	0.65	*
61	770819	Scantling	5.67	6697	0.25	0.90	*
62	770927	Coulommiers	4.87	444	0.11	0.30	*
63	771117	Seamount	4.71				
64	780223	Reblochlon	5.74	7085	0.18	0.70	*
65	780323	Iceberg	5.72	7514	0.25	0.80	*
66	780411	Backbeach	5.55	2630	0.23	0.695	
67	780712	Lowball	5.67	5234	0.24	0.745	
68	780831	Panir	5.67	4876	0.25	0.76	
69	780913	Diablo Hawk	4.73	485	0.17	0.42	
70	780927	Draughts	5.10	1418	0.22	0.65	*
71	780927	Rummy	5.86	7344	0.14	0.58	
72	781118	Quargel	5.33	2441	0.27	0.86	
73	781216	Farm	5.63	4449	0.27	0.77	
74	790208	Quinella	5.60	5063	0.24	0.90	*
75	790215	Kloster	4.97	736	0.13	0.35	*
76	790611	Pepato	5.57	2588	0.11	0.47	
77	790628	Fajy	5.23	1367	0.12	0.65	
78	790808	Offshore	4.82	595	0.22	0.49	
79	790829	Nessel	4.94	854	0.23	0.69	
80	790906	Hearts	5.89	7467	0.23	0.67	
81	790926	Sheepshead	5.65	2786	0.16	0.55	
82	800403	Liptauer	4.90	536	0.13	0.50	*
83	800416	Pyramid	5.42	3920	0.17	0.70	
84	800426	Colwick	5.55	3587	0.22	0.83	
85	800612	Kash	5.67	5656	0.19	0.86	
86	800725	Tafi	5.57	6271	0.19	0.70	*
87	801031	Miners Iron	4.93	629	0.12	0.40	
88	801217	Serpa	5.29	1244	0.27	0.55	*
89	810115	Baseball	5.73	5521	0.24	0.80	*
90	810529	Aligote	4.37				
91	810606	Harzer	5.63	4248	0.21	0.85	
92	811001	Paliza	5.12	492	0.10	0.41	
93	811112	Rousanne	5.46	2580	0.13	0.65	
94	820212	Molbo	5.41	1693	0.24	0.65	*
95	820417	Tenaja	4.46				
96	820507	Bouschet	5.73	6000	0.19	0.62	
97	820624	Nebbiolo	5.64	3505	0.20	0.72	
98	820729	Monterey	4.46				
99	820805	Atrisco	5.74	10495	0.21	0.75	*
00	820923	D.A + H.L	4.98	863	0.20	0.50	*
01	820923	Frisco	4.85				

Table 4 contd

	Date	Name	mb	Ψ_∞	γ	D	
102	821112	Seyval	4.55				
103	821210	Manteca	4.74				
104	830326	Cabra	5.28	1413	0.15	0.47	
105	830414	Turquoise	5.74	5478	0.22	0.69	
106	830505	Crowdie	4.44				
107	830526	Fahada	4.65				
108	830609	Danablu	4.52	252	0.13	0.57	
109	830803	Laban	4.21				
110	830811	Sabado	4.39				
111	830901	Chancellor	5.45	3176	0.20	0.92	
112	831216	Romano	5.14	818	0.17	0.45	*
113	840215	Midas Myth/M.	5.08	630	0.13	0.48	
114	840501	Mundo	5.47	4041	0.18	0.75	*
115	840531	Caprock	5.74	7097	0.24	0.90	
116	840620	Duoro	4.78	492	0.23	0.69	
117	840725	Kappeli	5.39	1818	0.22	0.58	
118	840802	Correo	4.67	258	0.11	0.39	
119	841215	Tierra	5.45	2276	0.22	0.55	*
120	850315	Vaughn	4.8				
121	850323	Cottage	5.3	3522	0.16	0.75	*
122	850406	Misty Rain	4.8	323	0.11	0.40	
123	850502	Towanda	5.7	5260	0.23	0.93	
124	850612	Salut	5.5	2450	0.23	0.61	
125	850626	Maribo	4.3				
126	850927	Ponil	4.6	321	0.11	0.55	*
127	851016	Roquefort	4.6				
128	851205	Kinibito	5.7	4482	0.18	0.73	
129	851228	Goldstone	5.3	1778	0.18	0.55	*
130	860322	Glencoe	5.1	1220	0.16	0.40	*
131	860410	Mighty Oak	4.9	510	0.11	0.35	*
132	860422	Jefferson	5.3	2506	0.20	0.50	*
133	860625	Darwin	5.5	4009	0.20	0.68	
134	860717	Cybar	5.7	5259	0.20	1.02	
135	860724	Cornucopia	4.5				

TABLE 5

ANNOUNCED YIELDS OF NTS EXPLOSIONS

Discus Thrower (Dry)	22 kton
Schooner (Dry)	30 kton
Starwort	90 kton
Calabash	110 kton
Flask	105 kton
Scotch	155 kton
Piledriver (Granite)	62 kton

TABLE 6

SEISMIC MOMENT M_o (NM)

			$\log_{10}M_o$ (1) (LR)	$\log_{10}M_o$ (2) (SP)	$\log_{10}M_o$ (3) (LR)	$\log_{10}M_o$ (4) (SP)
(a)	Yucca Flats					
	Noggin	(D)	16.05	14.82	15.90	15.65
	Calabash	(W)	-	15.15	15.69	15.78
	Flask	(D)	-	15.00	15.41	15.83
	Tijeras	(W)	16.01	15.28	15.88	15.91
	Oscuro	(W)	15.99	15.16	15.93	15.79
	Starwort	(W)	-	15.05	15.49	15.68
	Escabosa	(W)	16.14	15.13	16.04	15.76
	Portmanteau	(W)	16.08	15.49	15.83	16.12
	Top Gallant	(W)	15.83	15.28	15.70	15.91
	Mizzen	(W)	16.02	15.24	15.93	15.87
	Esrom	(W)	-	15.25	15.92	15.88
	Keelson	(W)	-	15.10	15.83	15.73
	Marsilly	(W)	16.01	15.25	15.58	15.88
	Scantling	(W)	-	15.23	15.90	15.86
	Iceberg	(W)	16.15	15.28	15.89	15.91
	Lowball	(W)	15.96	15.12	15.68	15.75
	Rummy	(W)	16.12	15.27	16.00	15.90
	Hearts	(W)	16.12	15.27	16.03	15.90
(b)	Pahute Mesa					
	Scotch	(W)	16.46	15.51	16.29	15.88
	Panir	(W)	15.97	15.35	15.79	15.72
	Farm	(W)	15.89	15.31	15.81	15.68
	Pepato	(W)	16.07	15.07	15.99	15.44
	Kash	(W)	16.16	15.41	16.00	15.78
	Tafi	(W)	16.10	15.46	15.99	15.83
(c)	Climax Stock					
	Piledriver		-	15.86	-	15.85

(1) M_o determined by Stevens (26).

(2) M_o derived from YKA SP: working point velocity and density.

(3) M_o derived by Given and Mellman (27).

(4) M_o derived from YKA SP: deep structure velocity and density, assumed to be same as YKA values ie $V = 5.64\ km.s^{-1}$ and $\rho = 2.67\ grm.cm^{-3}$.

<u>LIST OF FIGURES</u>

Figures 10-144 are P wave seismograms for each explosion listed in table 1. Three seismograms are shown

(a) Short period array-sum.

(b) Wiener filtered, phaseless broad-band.

(c) Seismogram (b) corrected for anelastic attenuation assuming $t* = 0.5$ s.

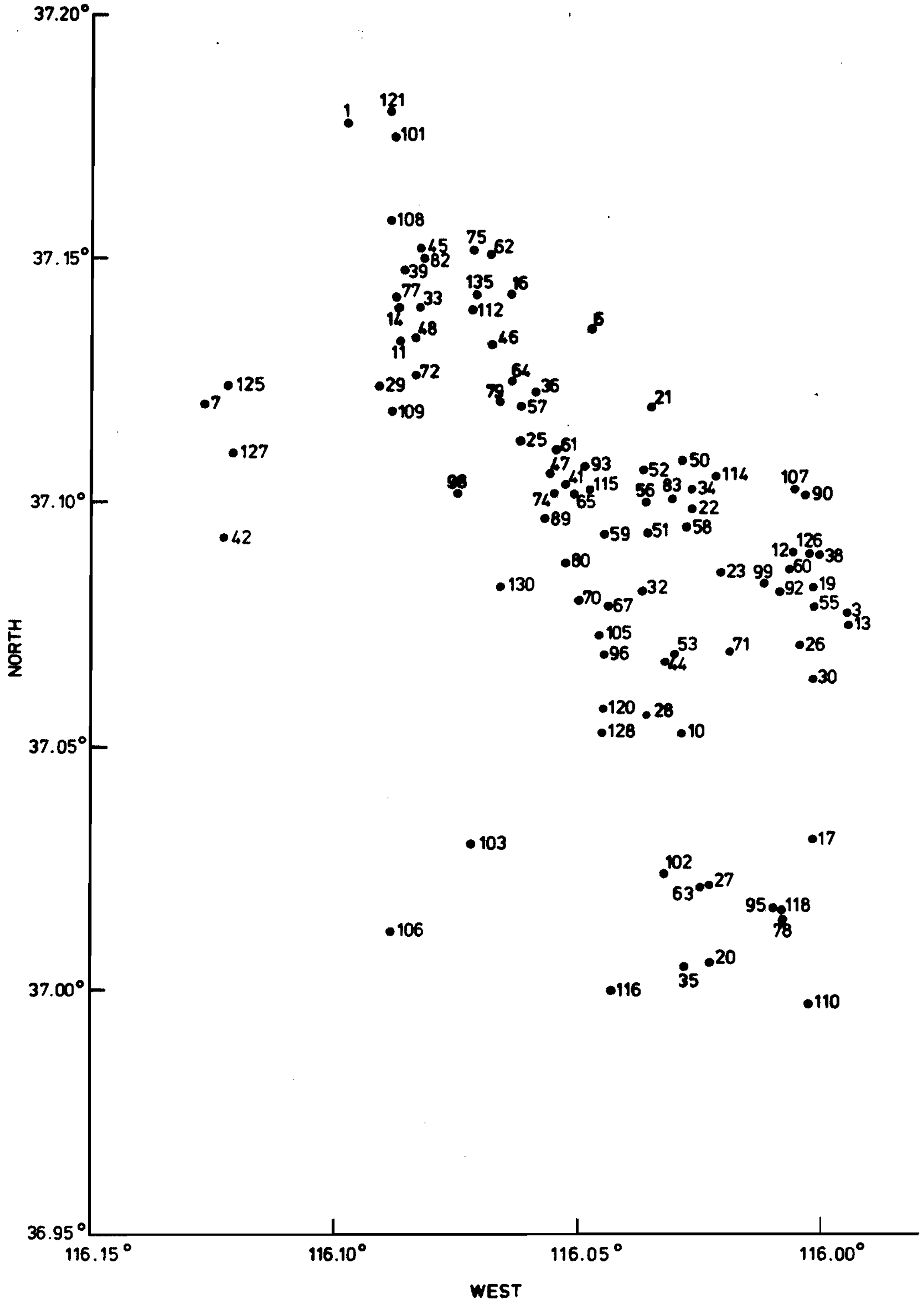

FIGURE 1A. LOCATION OF EXPLOSIONS DETONATED IN THE YUCCA FLAT AREAS OF NTS. (The numbers refer to explosions listed in table 1).

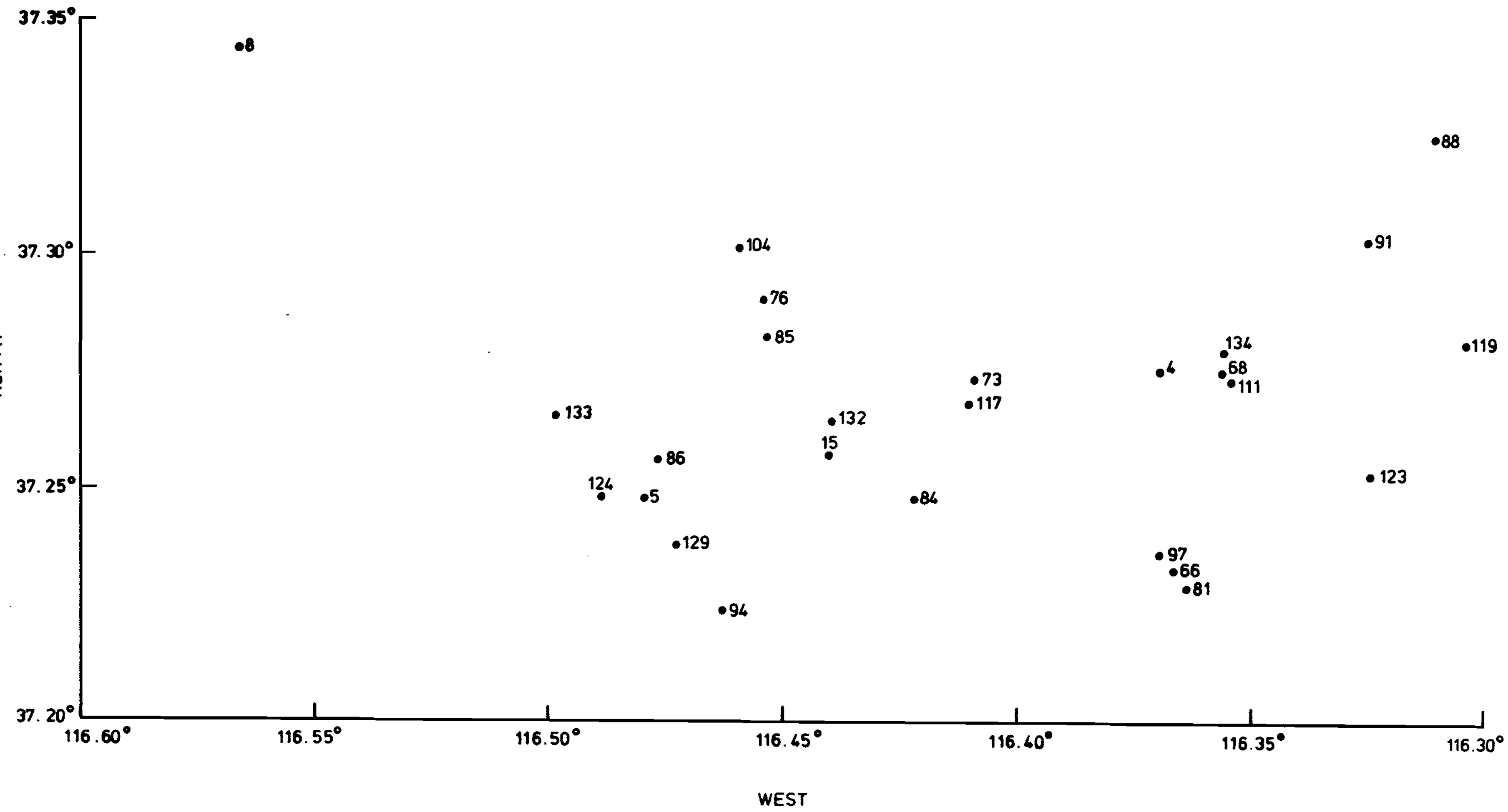

FIGURE 1B: LOCATION OF EXPLOSIONS DETONATED IN THE PAHUTE MESA AREA OF NTS. (The numbers refer to the explosions listed in table 1).

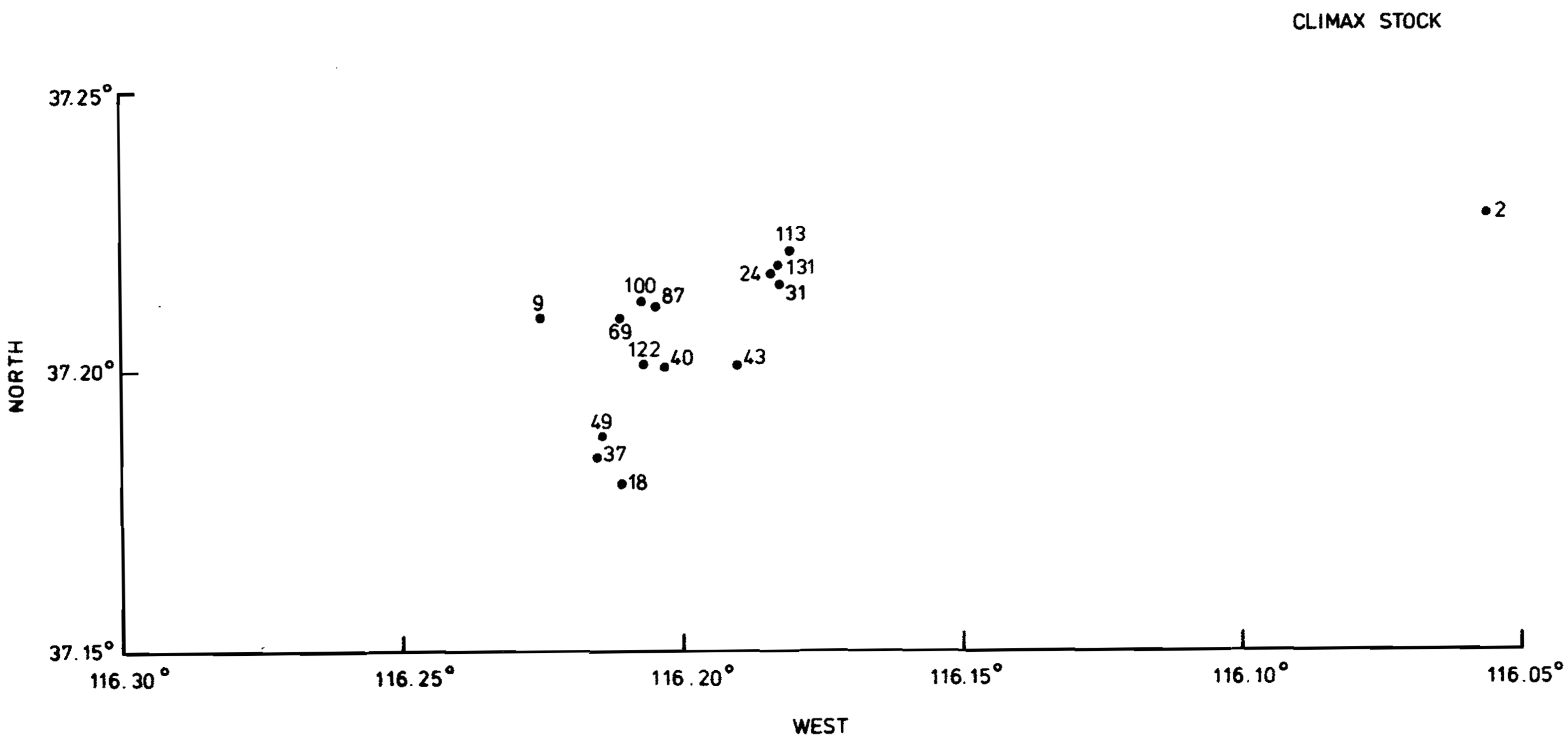

FIGURE 1C: LOCATION OF EXPLOSIONS DETONATED IN THE RAINIER MESA AREA OF NTS. (The numbers refer to explosions listed in table 1).

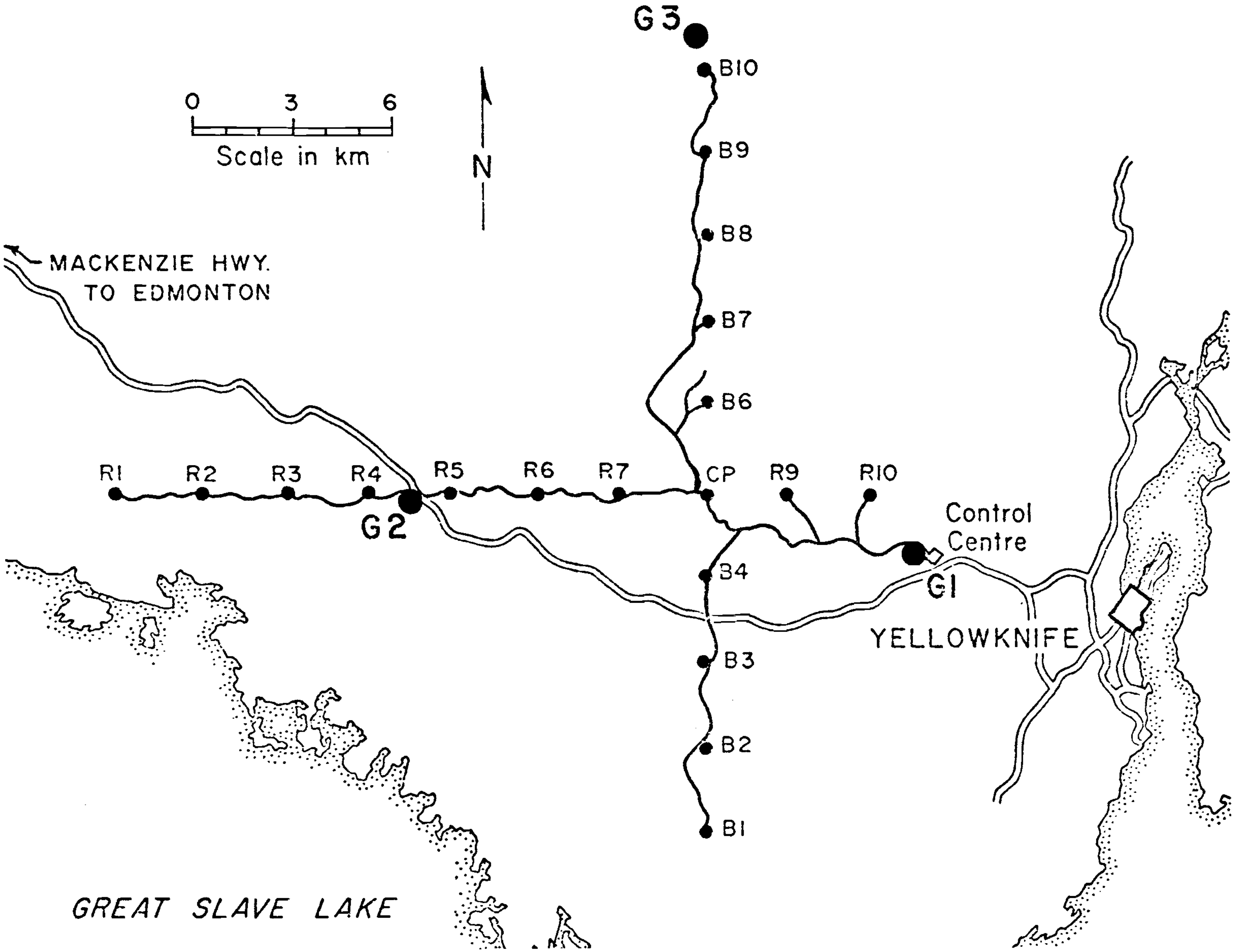

FIGURE 2: THE YELLOWKNIFE SHORT PERIOD SEISMOMETER ARRAY.

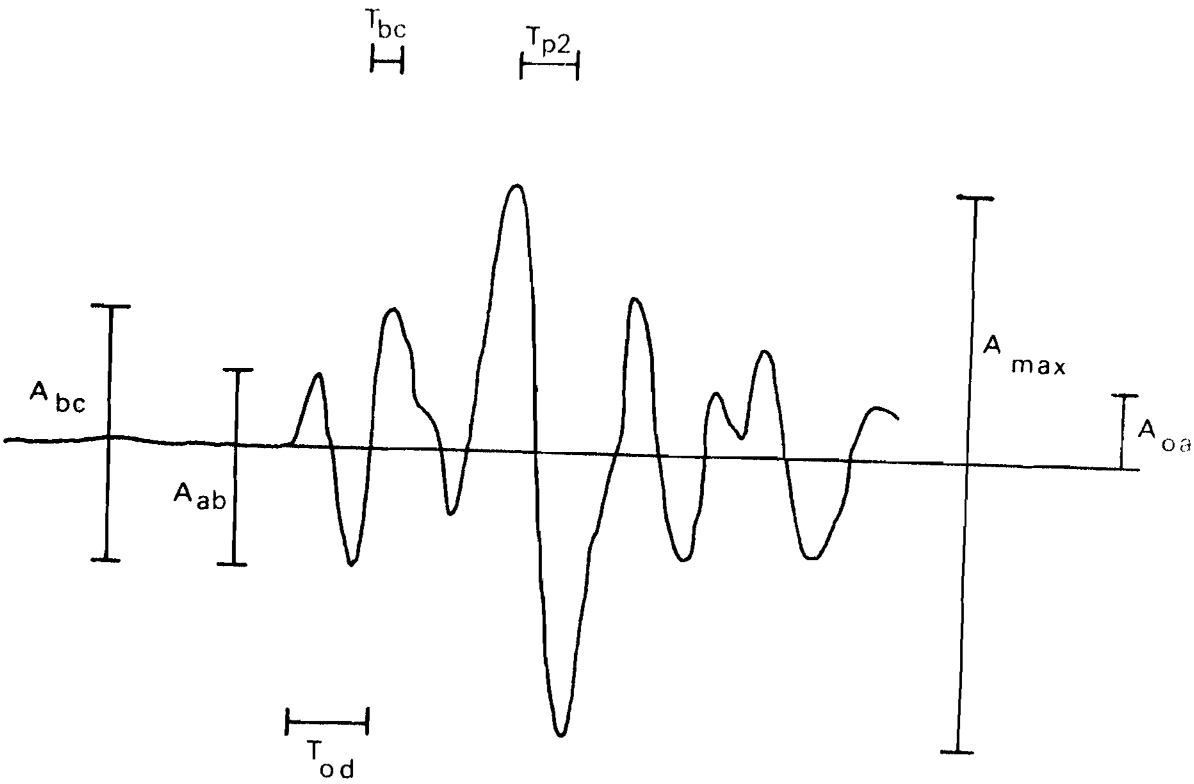

FIGURE 3A: MEASUREMENTS MADE ON SHORT PERIOD SEISMOGRAMS.

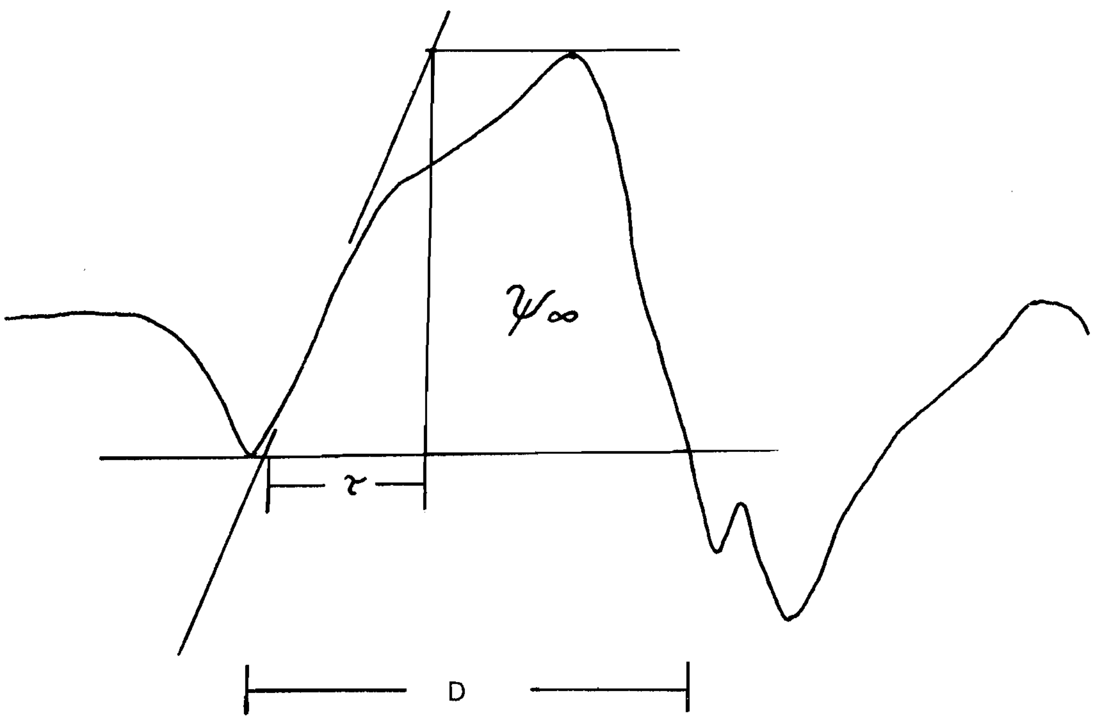

FIGURE 3B: MEASUREMENTS MADE ON BROAD BAND SEISMOGRAMS, Ψ_∞ THE PULSE AREA, τ THE PULSE RISE TIME AND D THE PULSE DURATION.

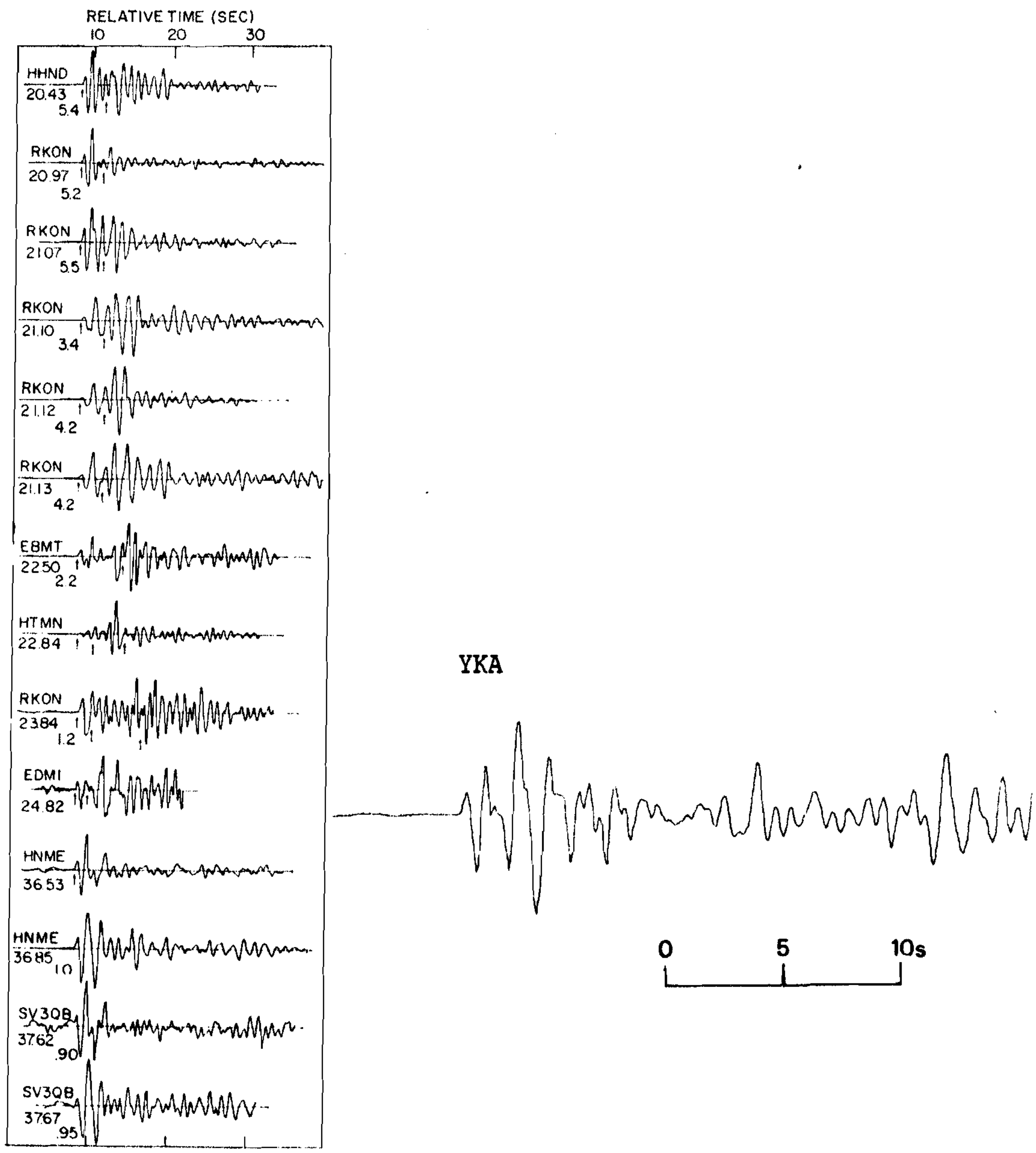

FIGURE 4: EFFECT OF UPPER MANTLE STRUCTURE ON P WAVE SEISMOGRAMS. Taken from Helmberger and Wiggins (12.). The YKA seismogram from LATIR is used to illustrate the similarity between the YKA recording and that recorded from CORDROY at EDMI.

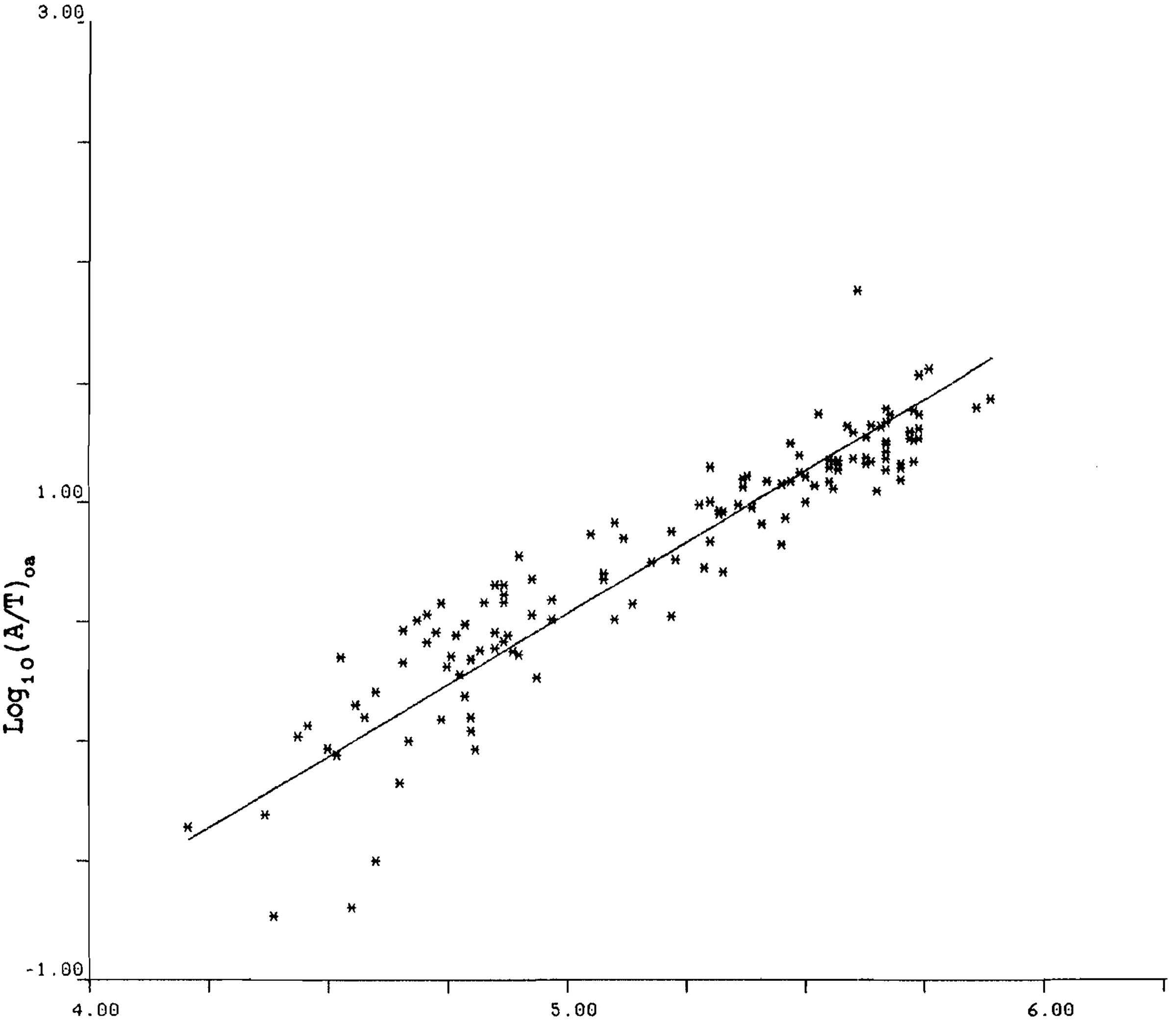

FIGURE 5A: $LOG_{10}(A/T)_{oa}$ VERSUS MAXIMUM-LIKELIHOOD MAGNITUDE m_b.

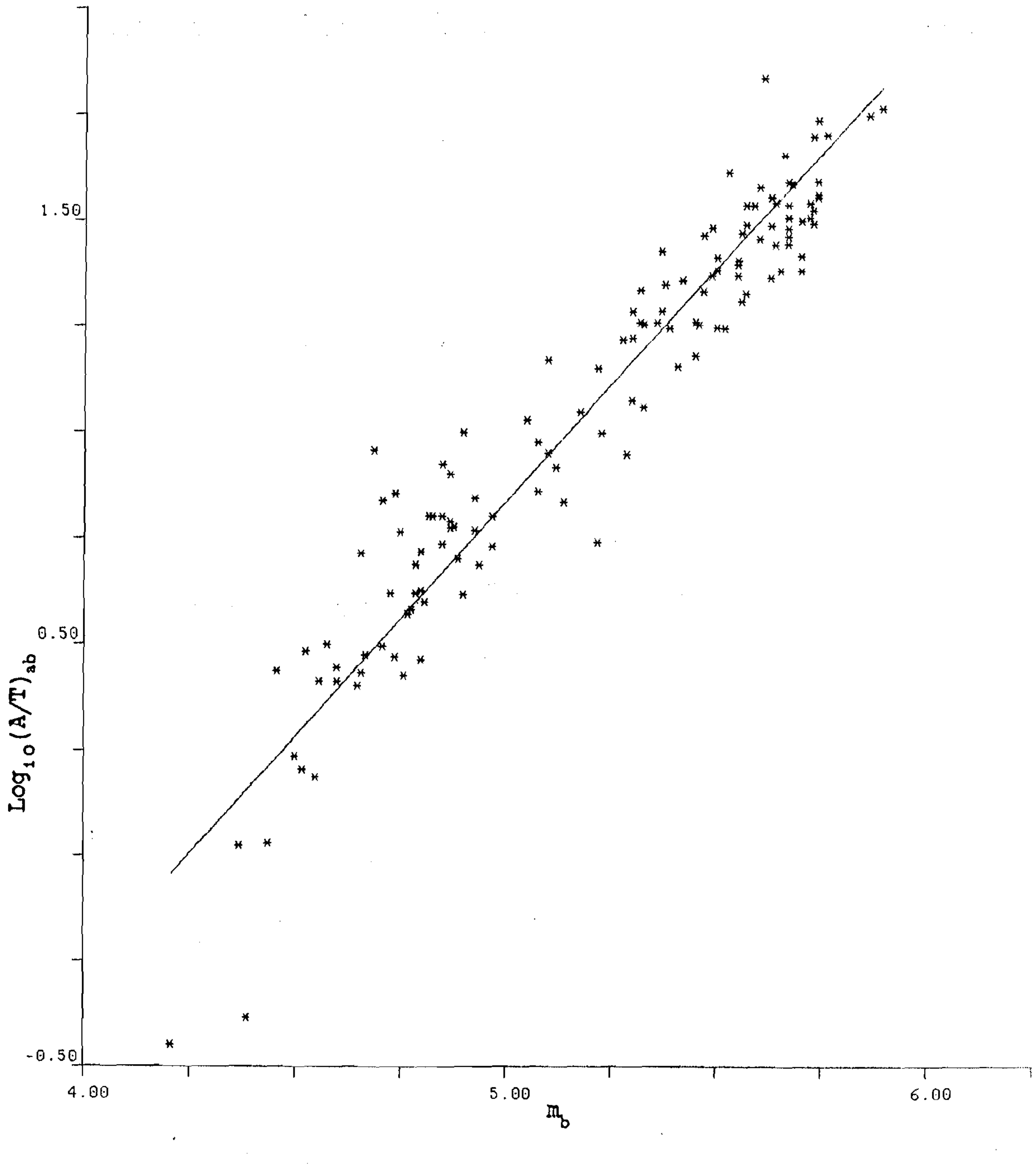

FIGURE 5B: $LOG_{10}(A/T)_{ab}$ VERSUS MAXIMUM-LIKELIHOOD MAGNITUDE m_b.

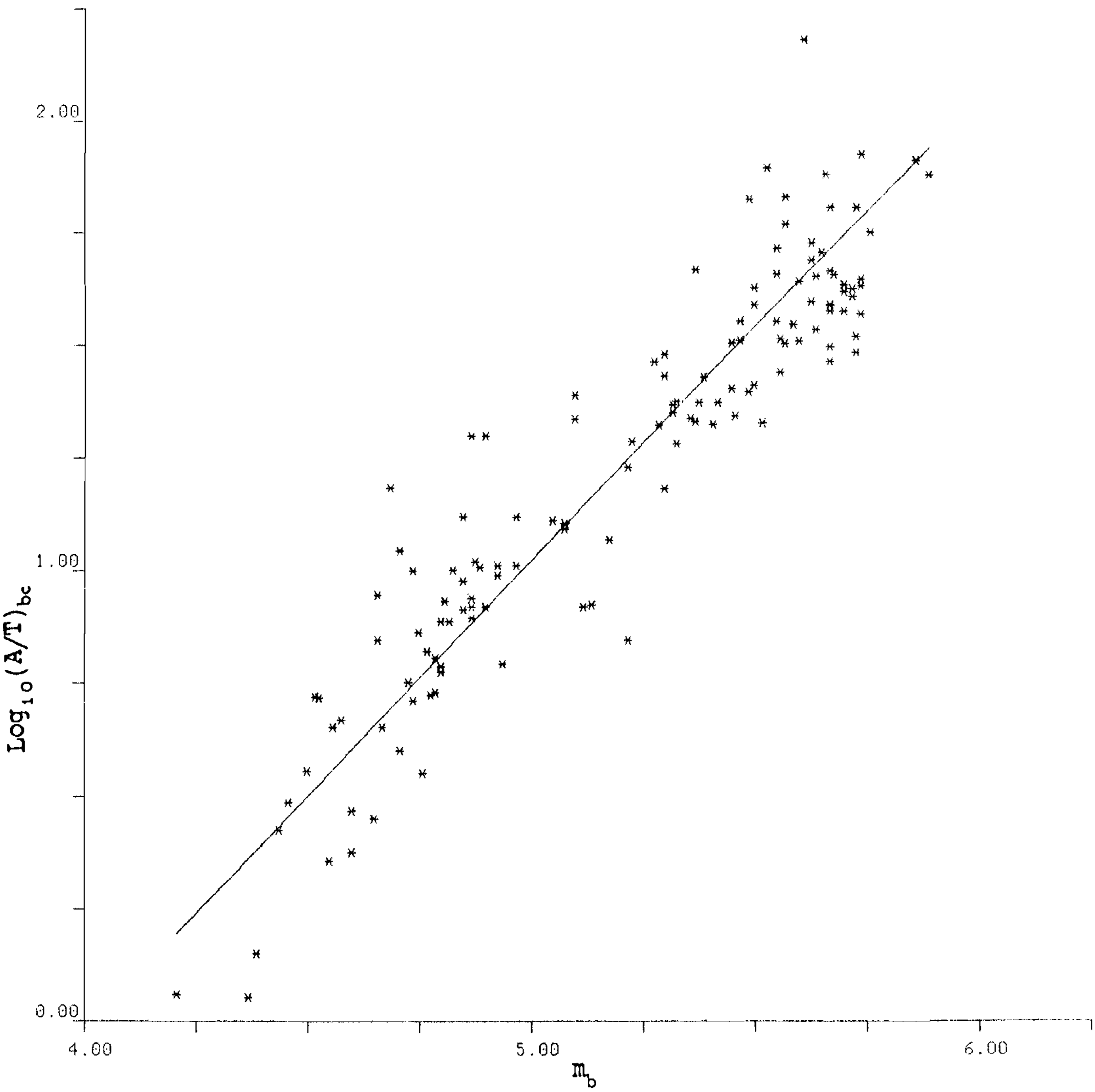

FIGURE 5C: $LOG_{10}(A/T)_{bc}$ VERSUS MAXIMUM-LIKELIHOOD MAGNITUDE m_b.

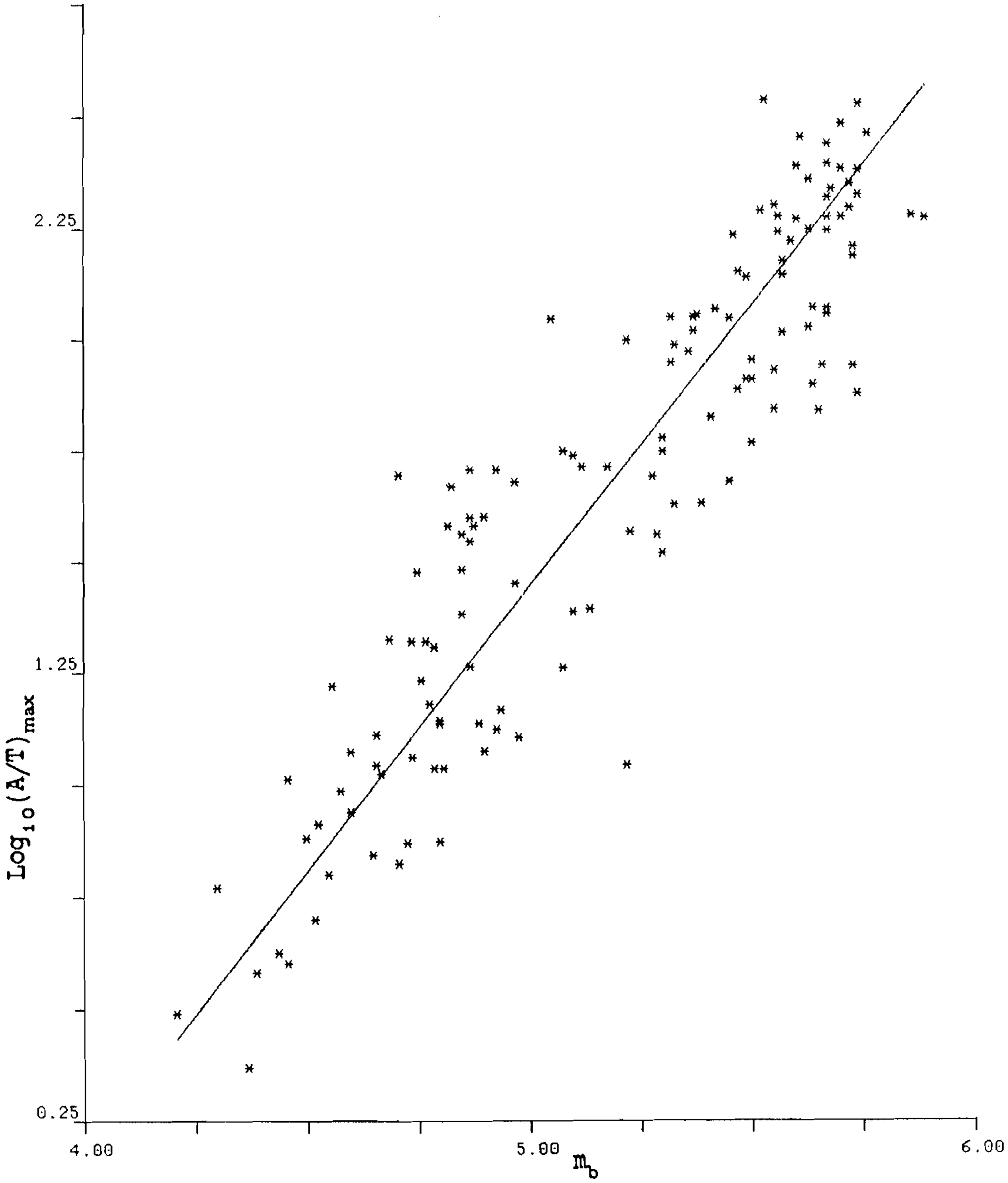

FIGURE 5D: $LOG_{10}(A/T)_{max}$ VERSUS MAXIMUM-LIKELIHOOD MAGNITUDE m_b.

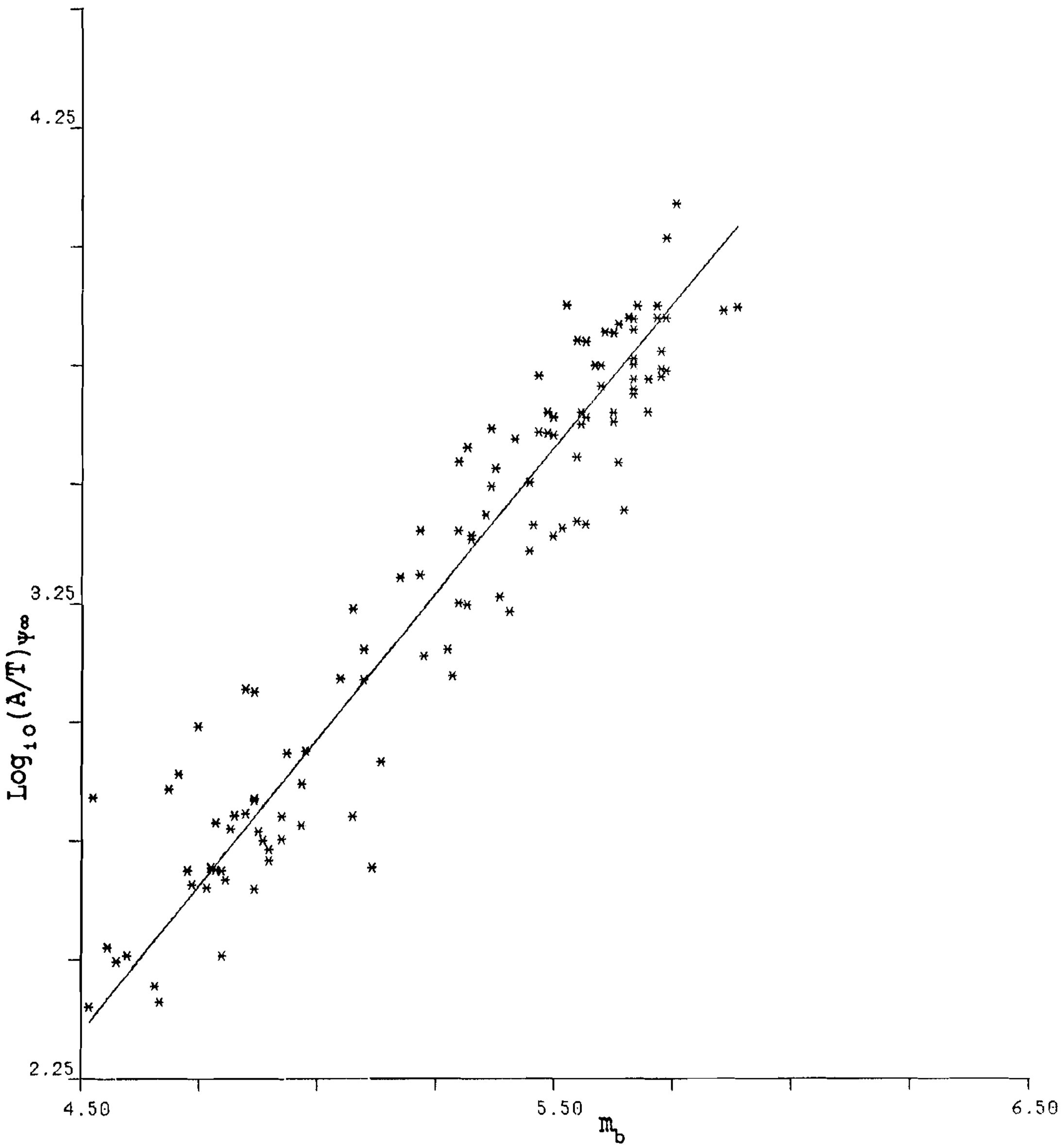

FIGURE 6: $LOG_{10}(A/T)_{\psi\infty}$ VERSUS MAXIMUM-LIKELIHOOD MAGNITUDE m_b.

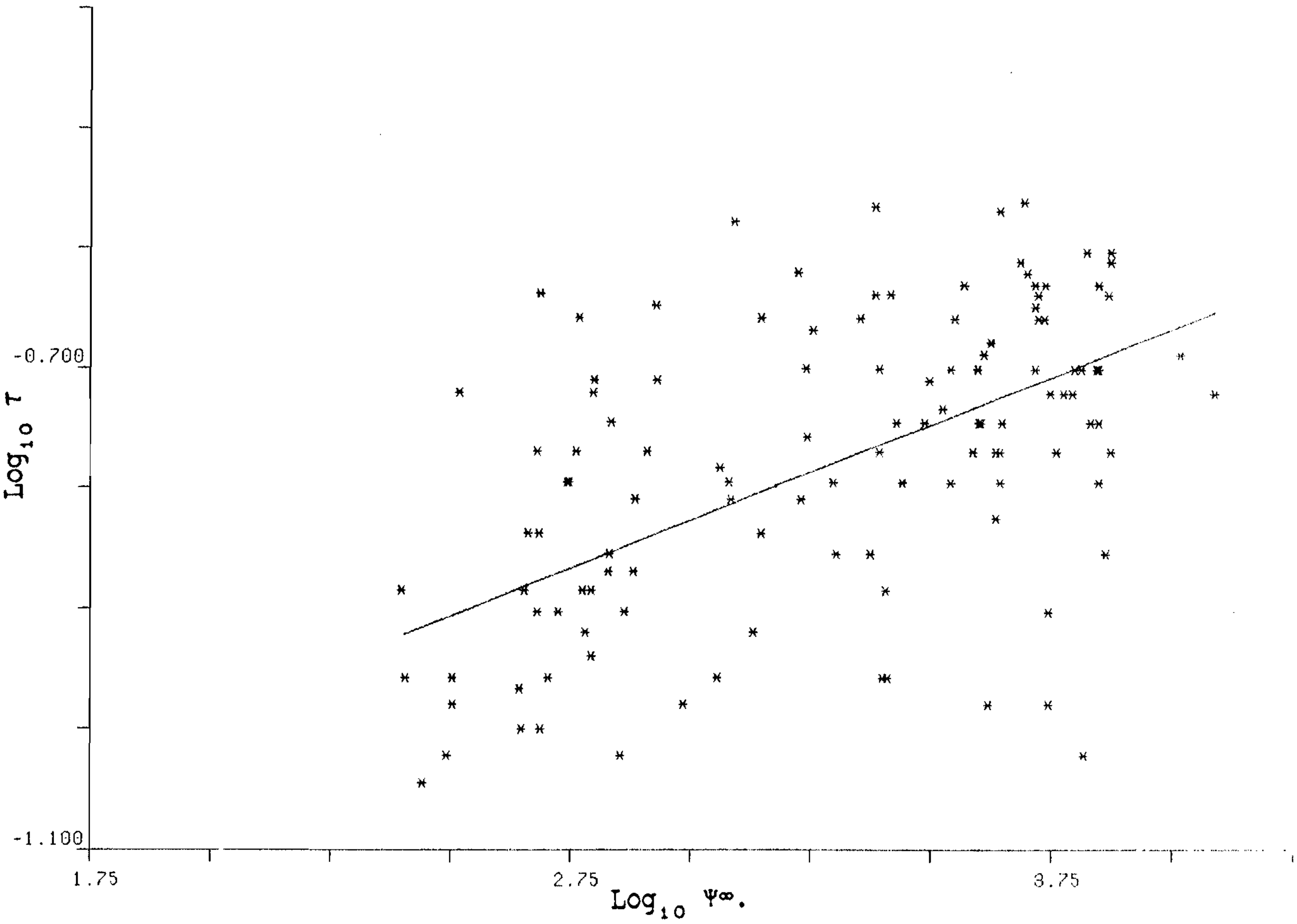

FIGURE 7A: LOG_{10} τ VERSUS LOG_{10} $\Psi\infty$.

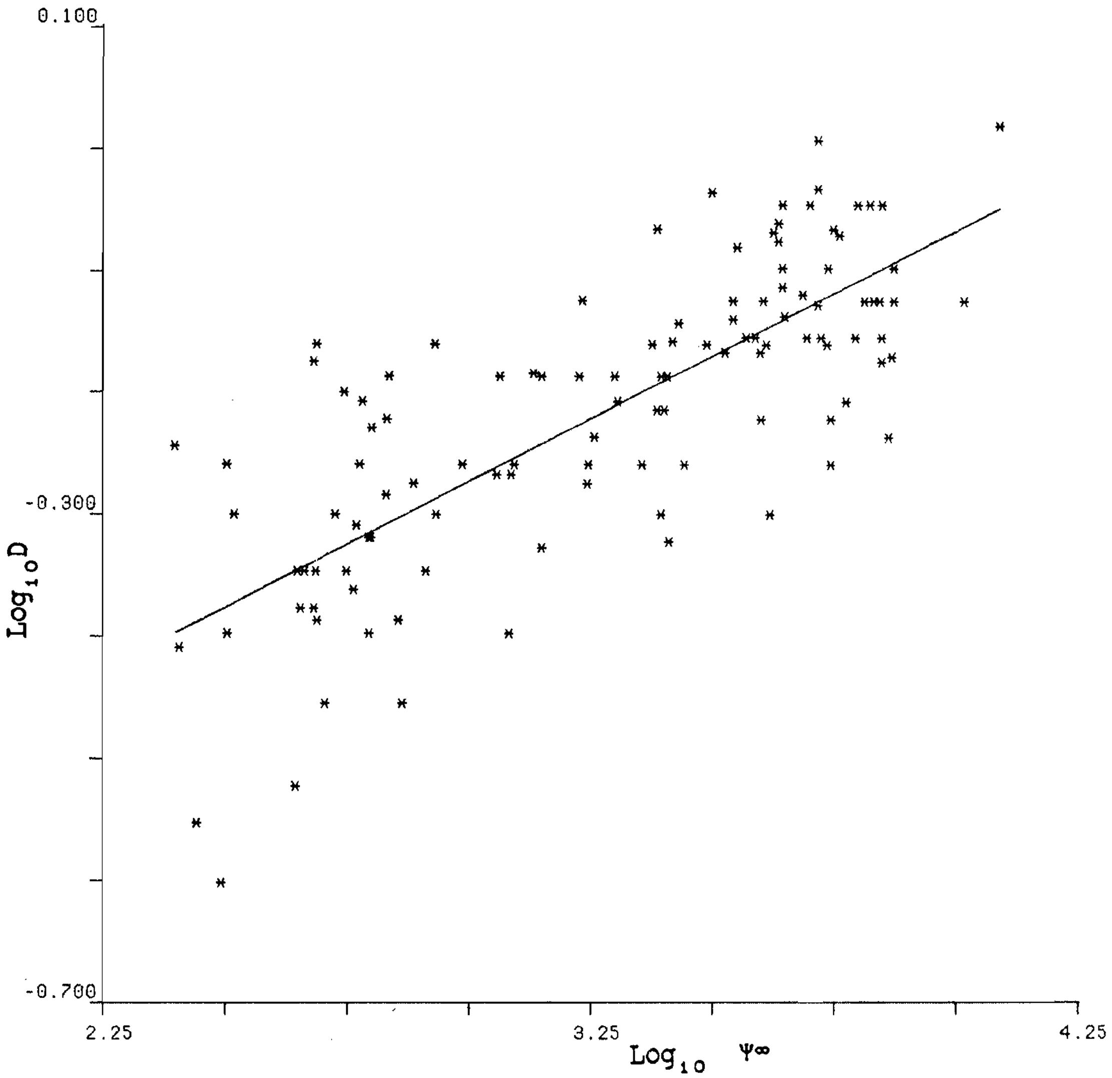

FIGURE 7B: $LOG_{10}D$ VERSUS $LOG_{10}\ \Psi\infty$

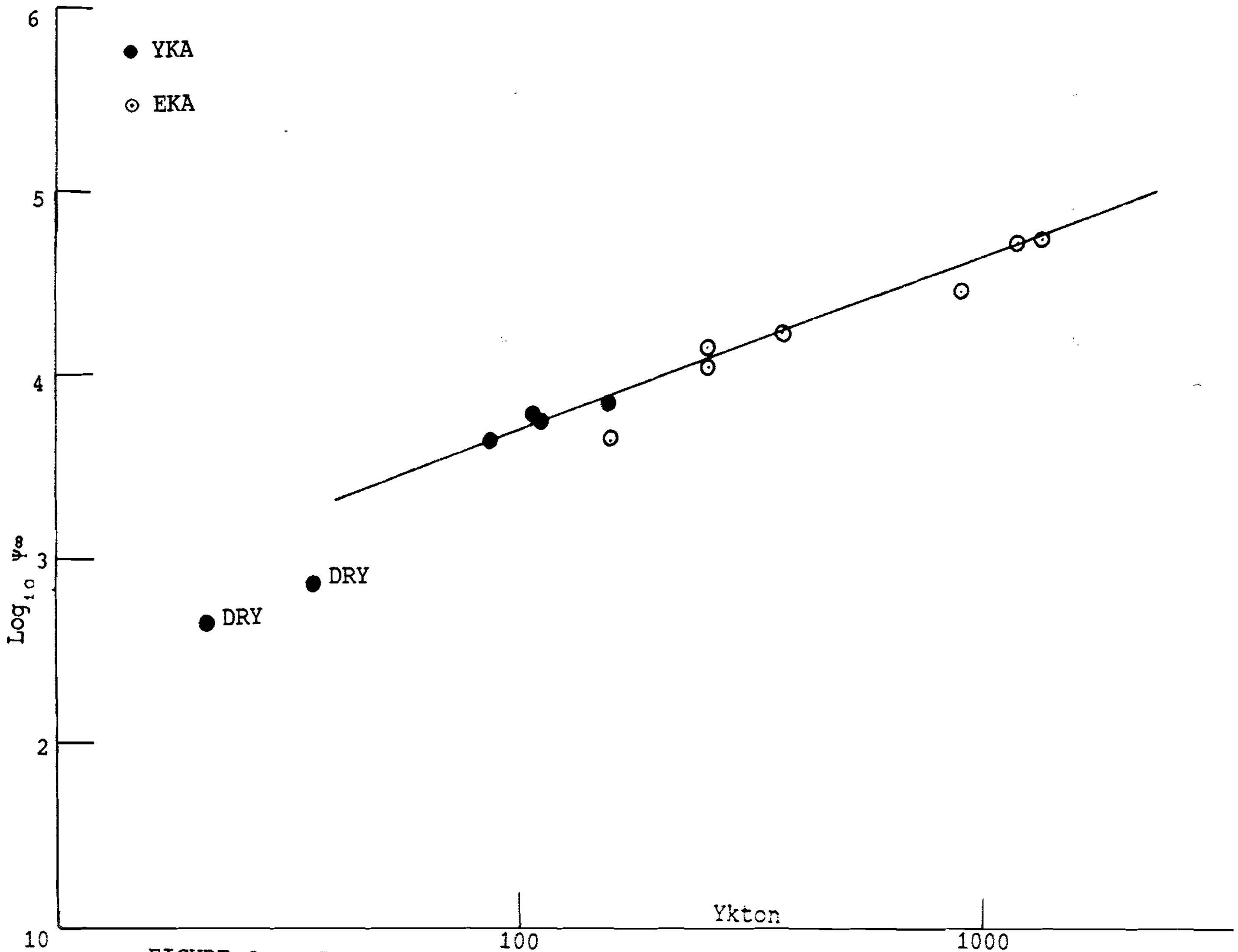

FIGURE 8: $LOG_{10}\ \Psi_\infty$ VERSUS YIELD (Y KTON) FOR EXPLOSIONS OF KNOWN YIELD IN TUFF AND RHYOLITE AT NTS.

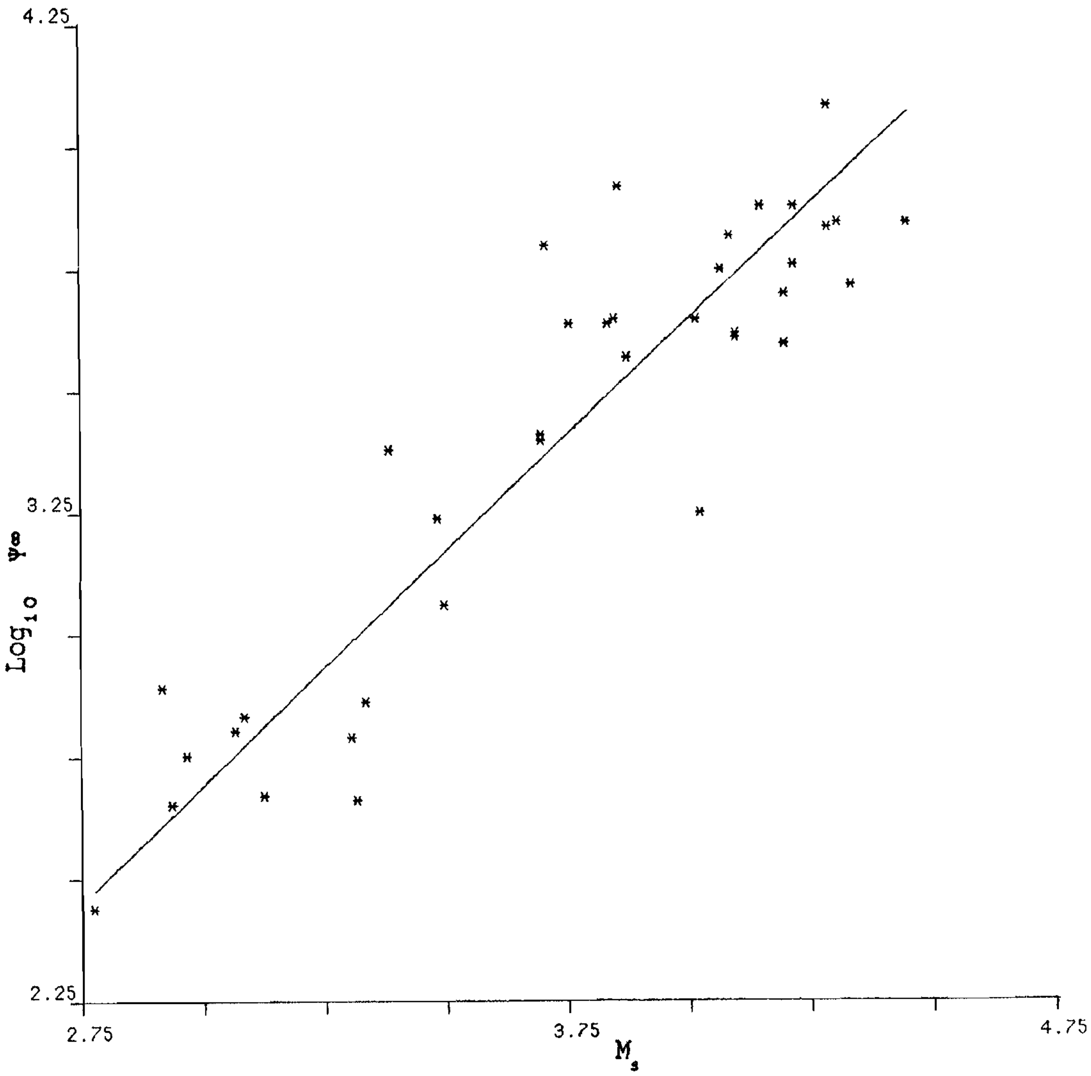

FIGURE 9: SURFACE WAVE M_S VERSUS $LOG_{10}\ \Psi\infty$

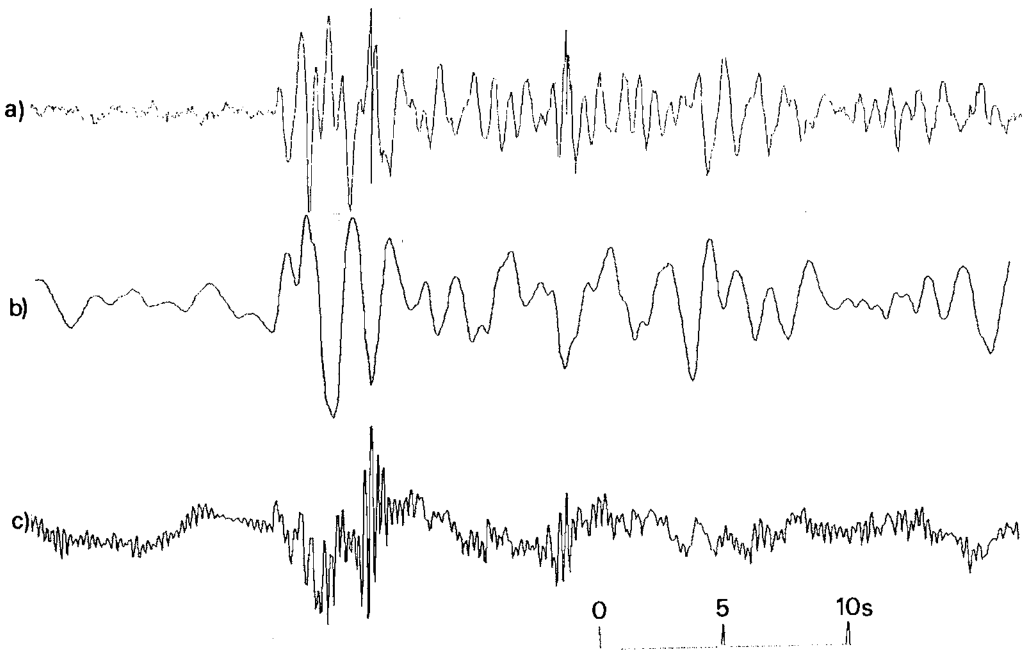

Figure 10. P seismograms recorded at Yellowknife, Canada from N.T.S explosion DISCUS THROWER.

(a) Short-period array-sum seismogram.
(b) Wiener filtered phaseless broad-band seismogram.
(c) Seismogram (b) corrected for anelastic attenuation assuming t*=0.5s.

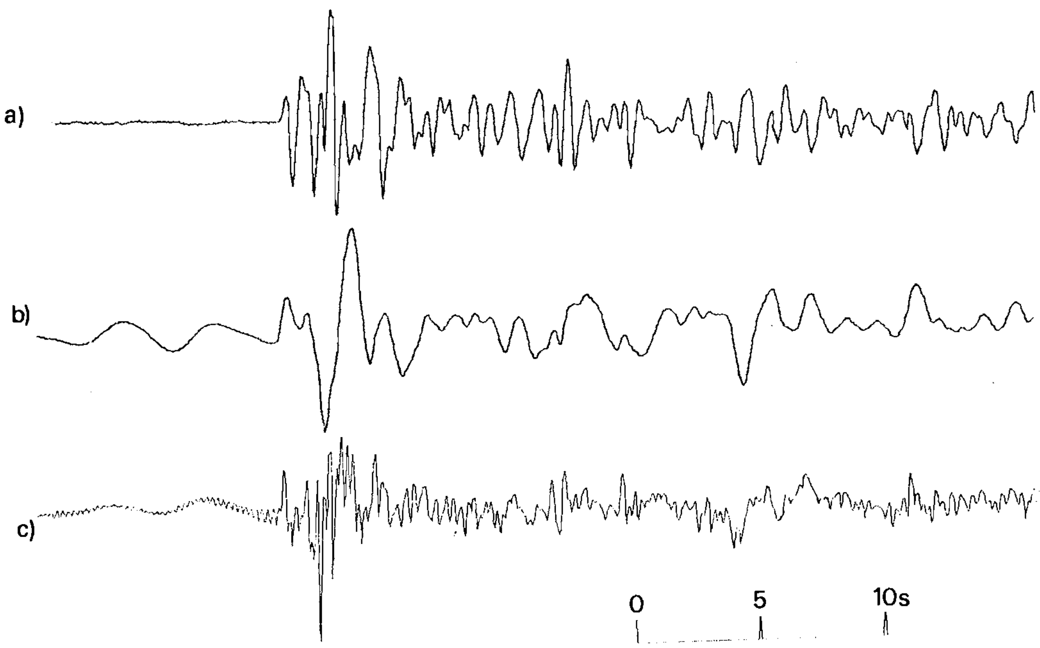

Figure 11. P seismograms recorded at Yellowknife, Canada from N.T.S explosion PILEDRIVER.

(a) Short-period array-sum seismogram.
(b) Wiener filtered phaseless broad-band seismogram.
(c) Seismogram (b) corrected for anelastic attenuation assuming t*=0.5s.

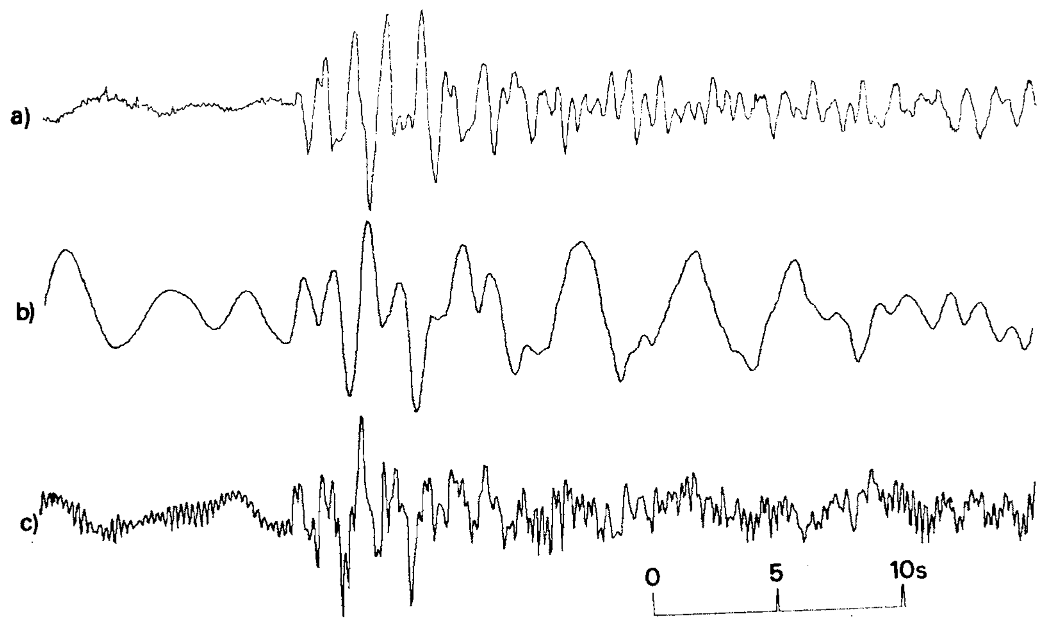

Figure 12. P seismograms recorded at Yellowknife,Canada from N.T.S explosion MICKEY.

(a) Short-period array-sum seismogram.
(b) Wiener filtered phaseless broad-band seismogram.
(c) Seismogram (b) corrected for anelastic attenuation assuming t*=0.5s.

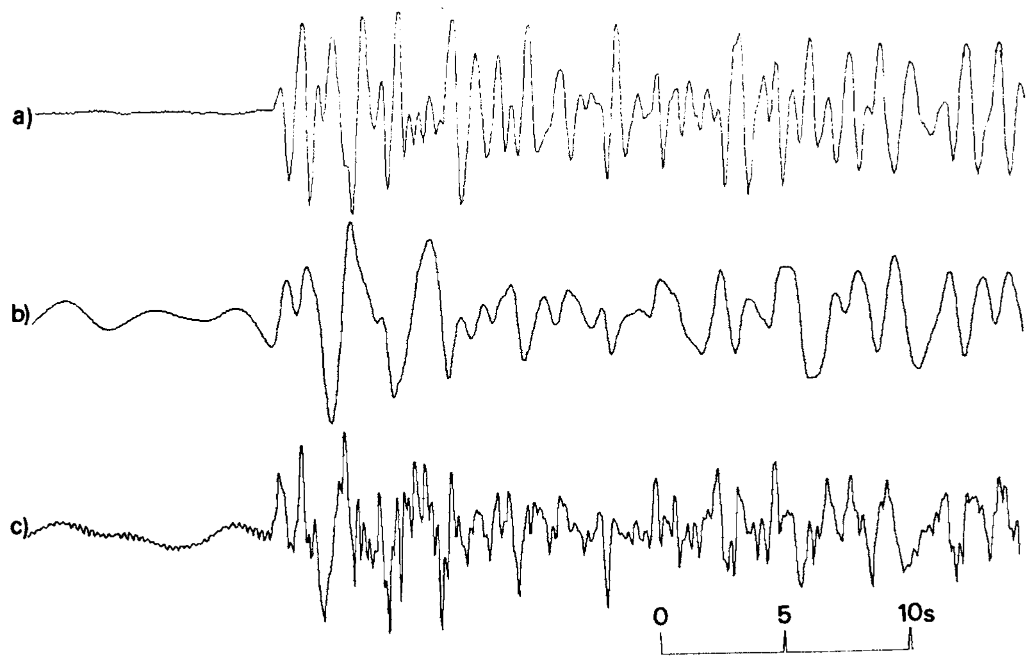

Figure 13. P seismograms recorded at Yellowknife,Canada from N.T.S explosion SCOTCH.

(a) Short-period array-sum seismogram.
(b) Wiener filtered phaseless broad-ba`d seismogram.
(c) Seismogram (b) corrected for anela. ic attenuation assuming t*=0.5s.

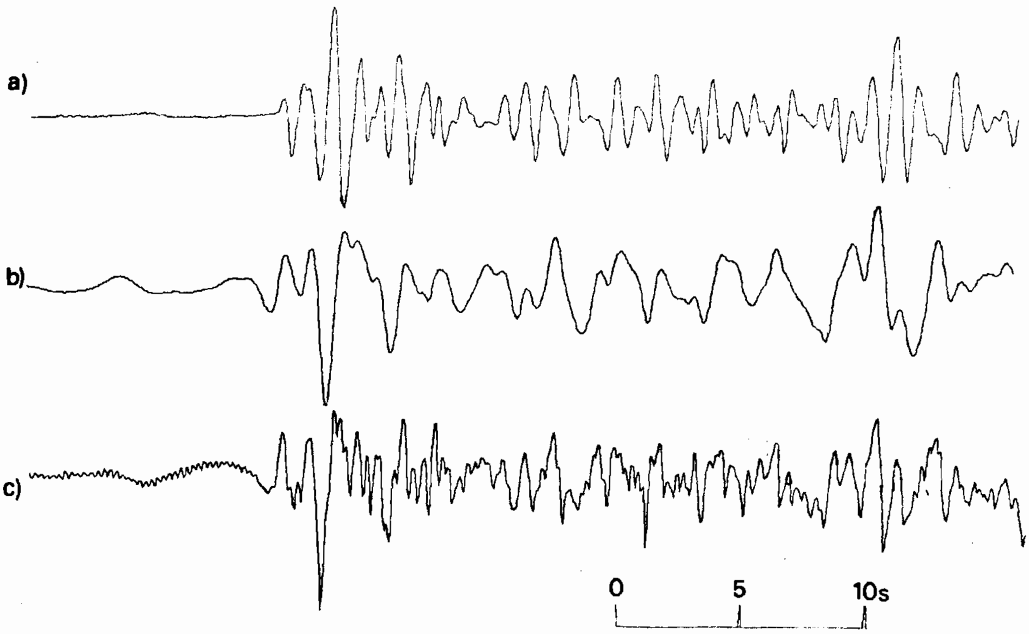

Figure 14. P seismograms recorded at Yellowknife,Canada from N.T.S explosion KNICKERBOCKER.

(a) Short-period array-sum seismogram.
(b) Wiener filtered phaseless broad-band seismogram.
(c) Seismogram (b) corrected for anelastic attenuation assuming t*=0.5s.

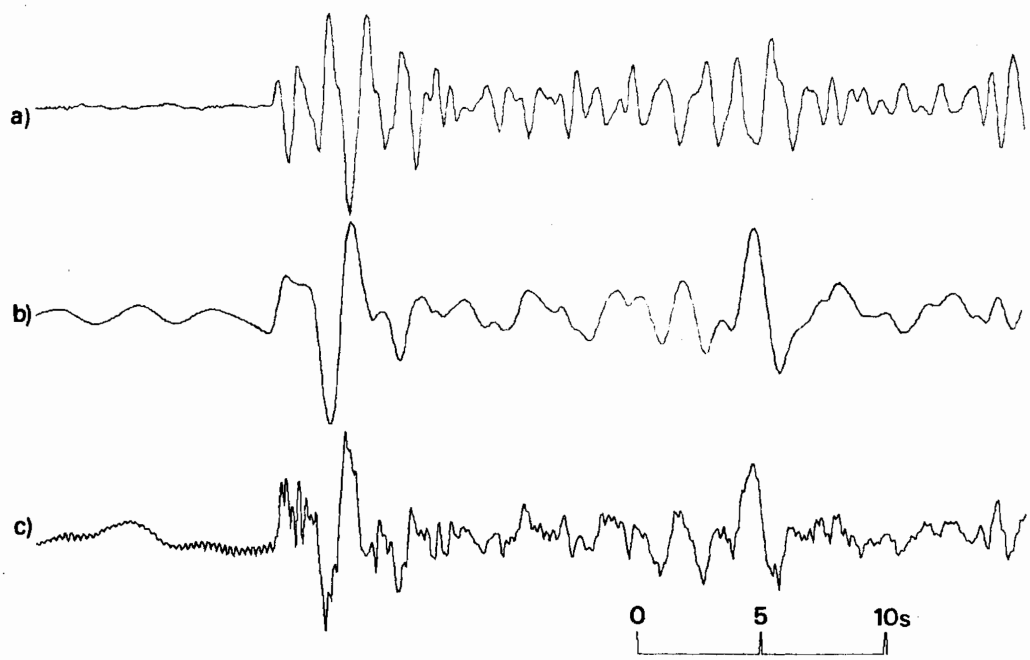

Figure 15. P seismograms recorded at Yellowknife,Canada from N.T.S explosion NOGGIN.

(a) Short-period array-sum seismogram.
(b) Wiener filtered phaseless broad-band seismogram.
(c) Seismogram (b) corrected for anelastic attenuation assuming t*=0.5s.

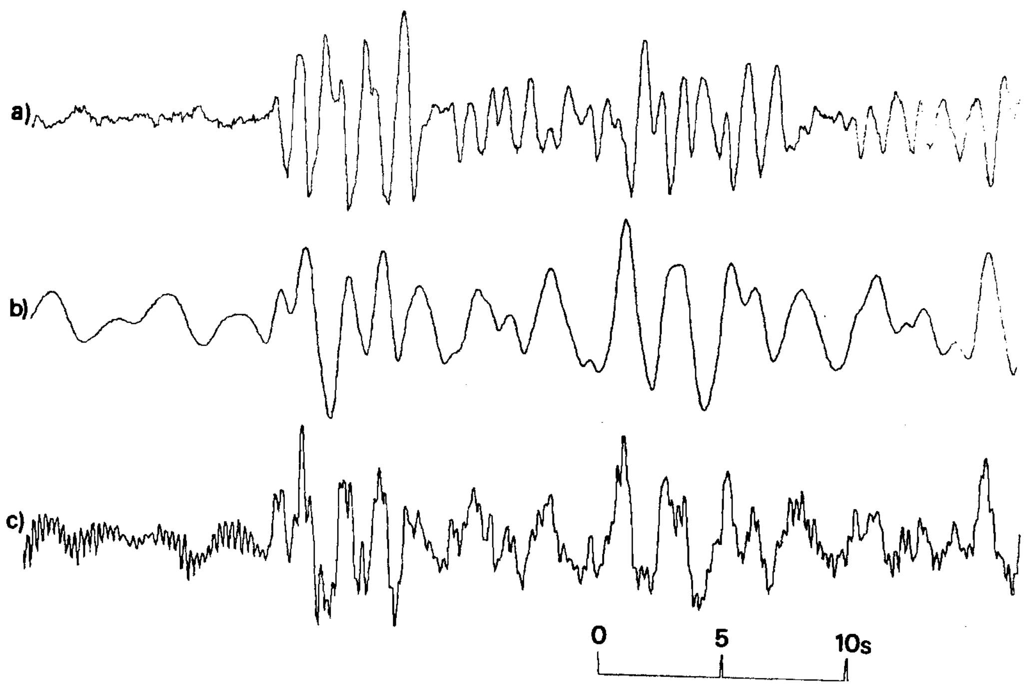

Figure 16. P seismograms recorded at Yellowknife, Canada from N.T.S explosion STODDARD.

(a) Short-period array-sum seismogram.
(b) Wiener filtered phaseless broad-band seismogram.
(c) Seismogram (b) corrected for anelastic attenuation assuming t*=0.5s.

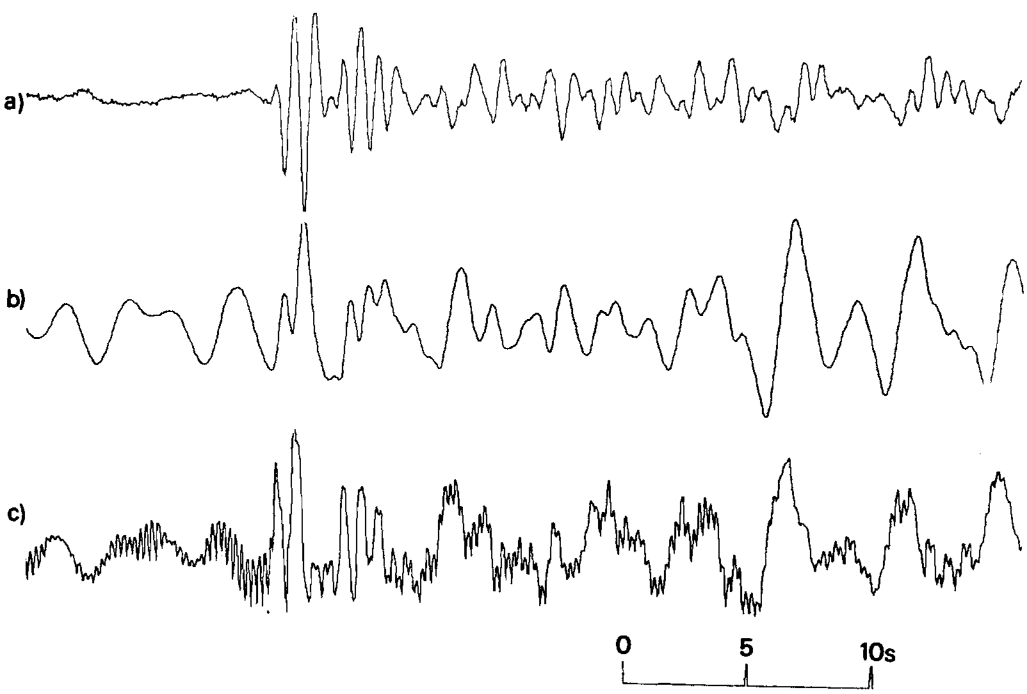

Figure 17. P seismograms recorded at Yellowknife, Canada from N.T.S explosion SCHOONER.

(a) Short-period array-sum seismogram.
(b) Wiener filtered phaseless broad-band seismogram.
(c) Seismogram (b) corrected for anelastic attenuation assuming t*=0.5s.

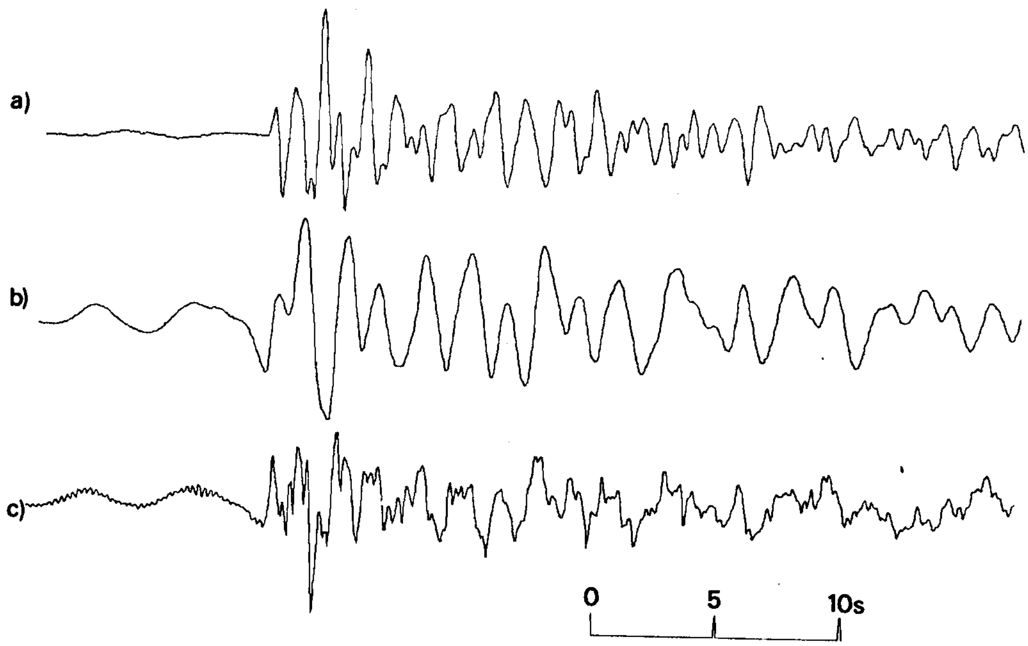

Figure 18. P seismograms recorded at Yellowknife, Canada from N.T.S explosion WINESKIN.

(a) Short-period array-sum seismogram.
(b) Wiener filtered phaseless broad-band seismogram.
(c) Seismogram (b) corrected for anelastic attenuation assuming t*=0.5s.

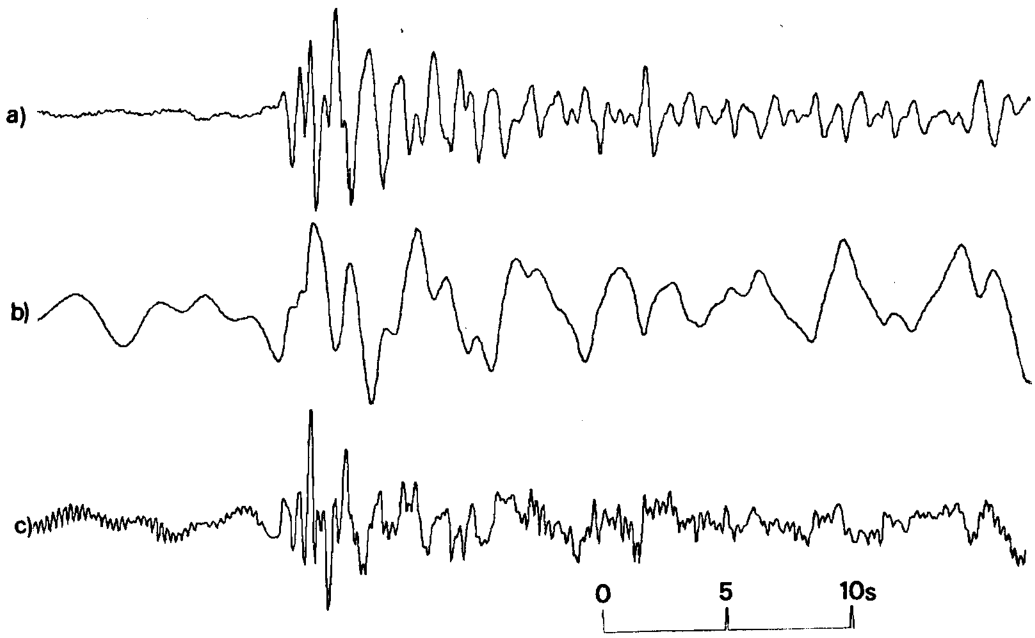

Figure 19. P seismograms recorded at Yellowknife, Canada from N.T.S explosion VISE.

(a) Short-period array-sum seismogram.
(b) Wiener filtered phaseless broad-band seismogram.
(c) Seismogram (b) corrected for anelastic attenuation assuming t*=0.5s.

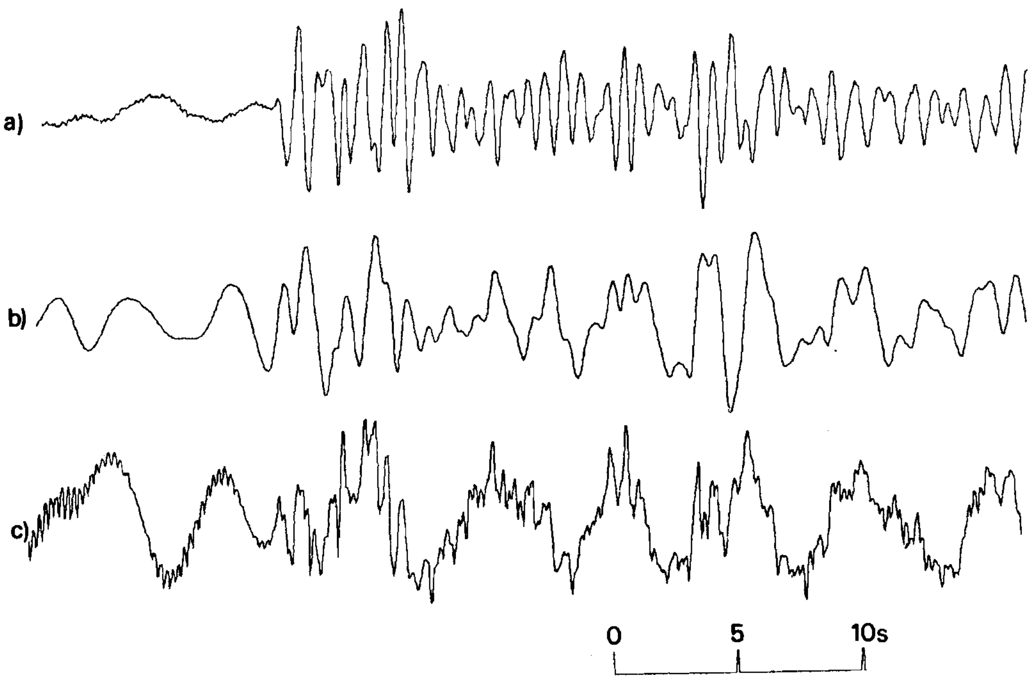

Figure 20. P seismograms recorded at Yellowknife, Canada from N.T.S explosion COFFER.

(a) Short-period array-sum seismogram.
(b) Wiener filtered phaseless broad-band seismogram.
(c) Seismogram (b) corrected for anelastic attenuation assuming t*=0.5s.

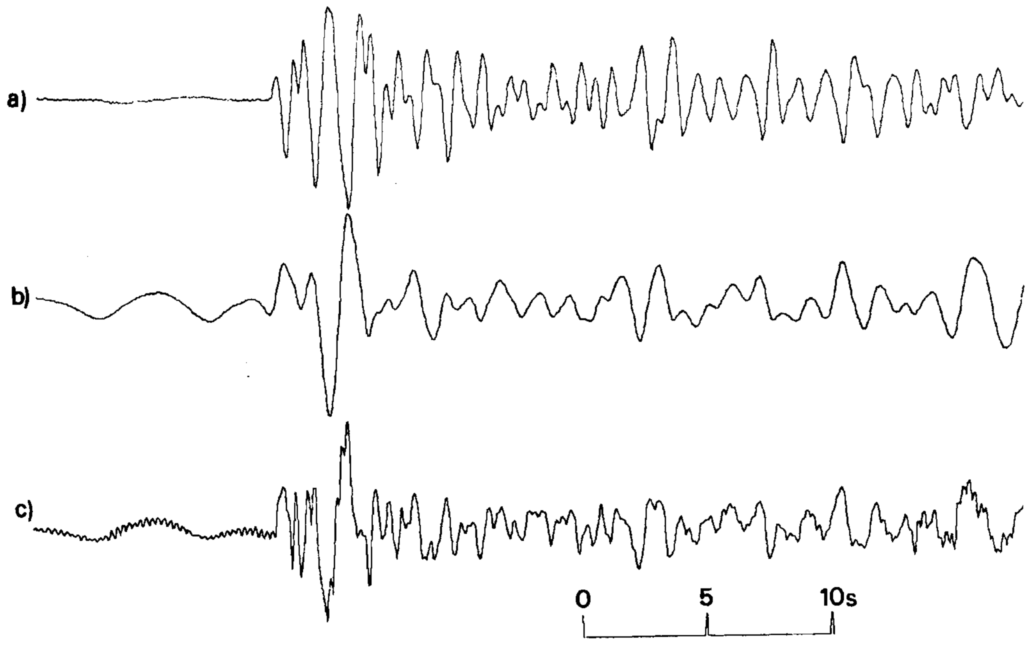

Figure 21. P seismograms recorded at Yellowknife, Canada from N.T.S explosion THISTLE.

(a) Short-period array-sum seismogram.
(b) Wiener filtered phaseless broad-band seismogram.
(c) Seismogram (b) corrected for anelastic attenuation assuming t*=0.5s.

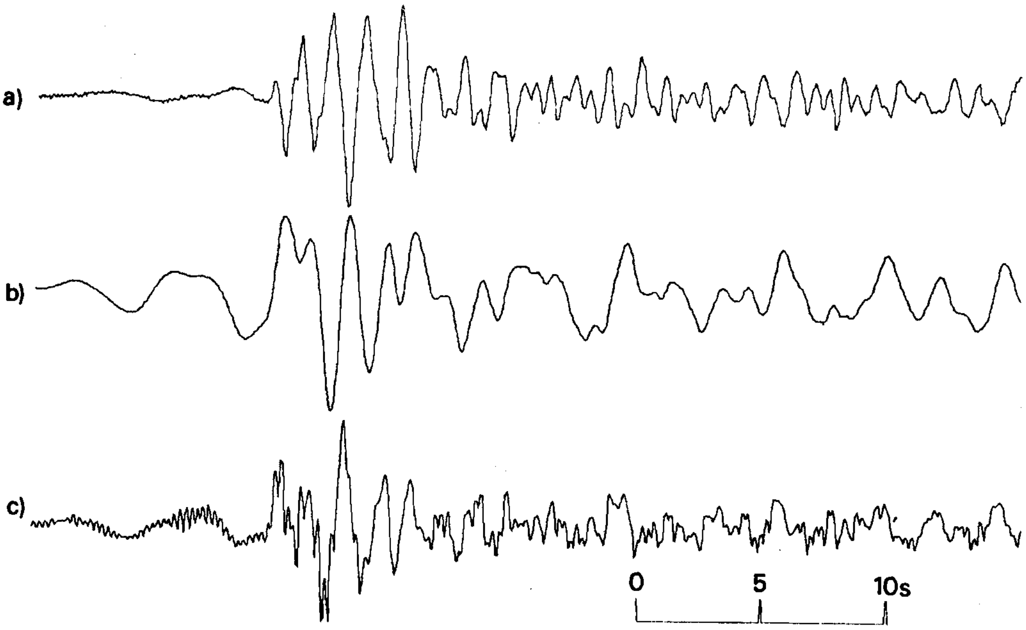

Figure 22. P seismograms recorded at Yellowknife,Canada from N.T.S explosion TORRIDO.

(a) Short-period array-sum seismogram.
(b) Wiener filtered phaseless broad-band seismogram.
(c) Seismogram (b) corrected for anelastic attenuation assuming t*=0.5s.

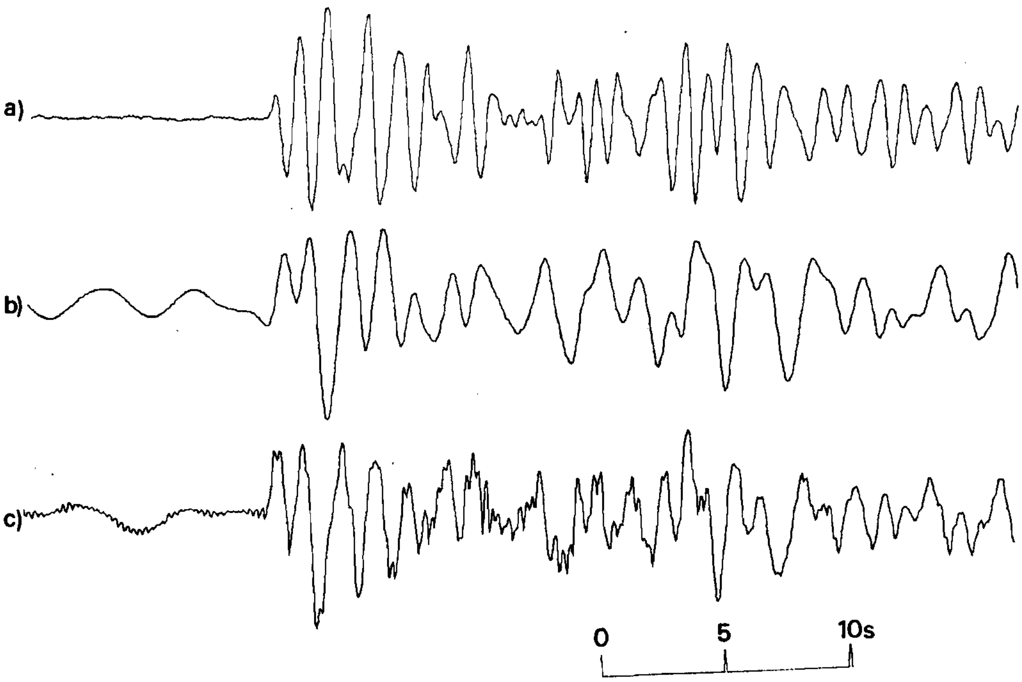

Figure 23. P seismograms recorded at Yellowknife,Canada from N.T.S explosion HUTCH.

(a) Short-period array-sum seismogram.
(b) Wiener filtered phaseless broad-band seismogram.
(c) Seismogram (b) corrected for anelastic attenuation assuming t*=0.5s.

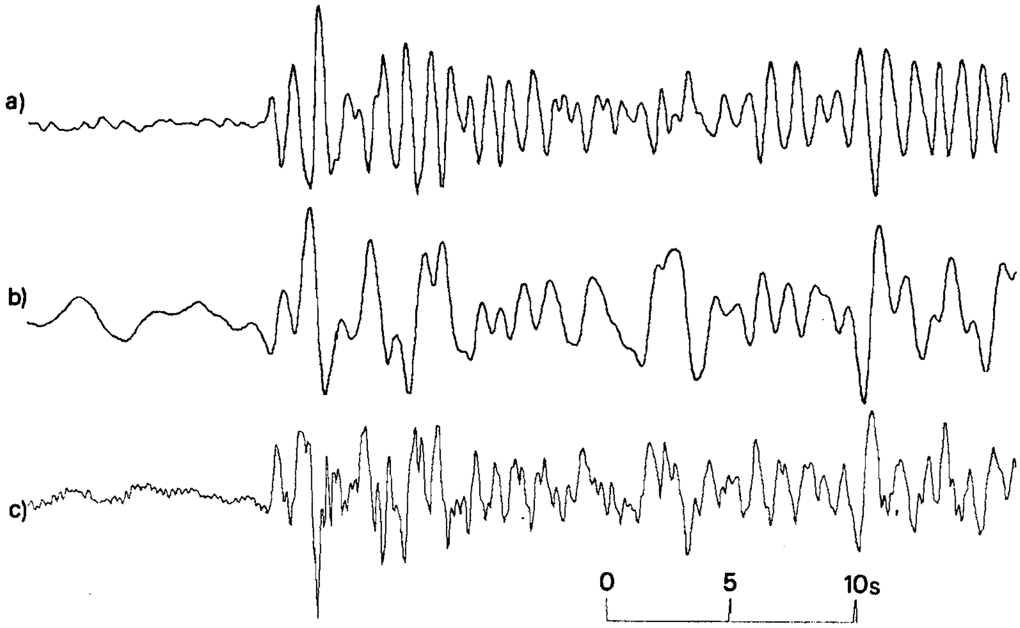

Figure 24. P seismograms recorded at Yellowknife,Canada from N.T.S explosion PIPKIN.

(a) Short-period array-sum seismogram.
(b) Wiener filtered phaseless broad-band seismogram.
(c) Seismogram (b) corrected for anelastic attenuation assuming t*=0.5s.

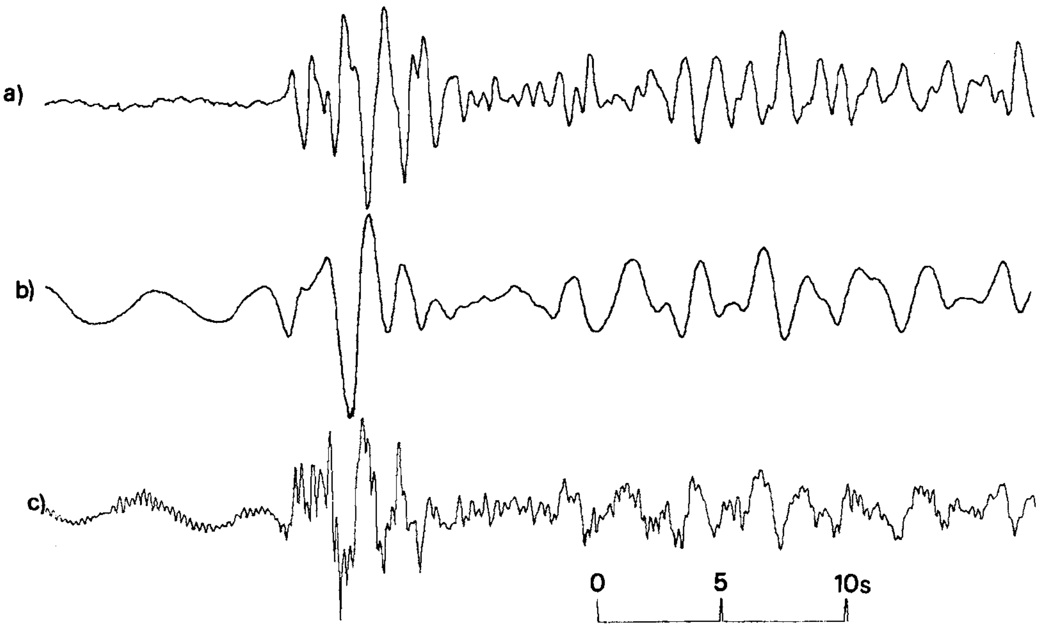

Figure 25. P seismograms recorded at Yellowknife,Canada from N.T.S explosion CALABASH.

(a) Short-period array-sum seismogram.
(b) Wiener filtered phaseless broad-band seismogram.
(c) Seismogram (b) corrected for anelastic attenuation assuming t*=0.5s.

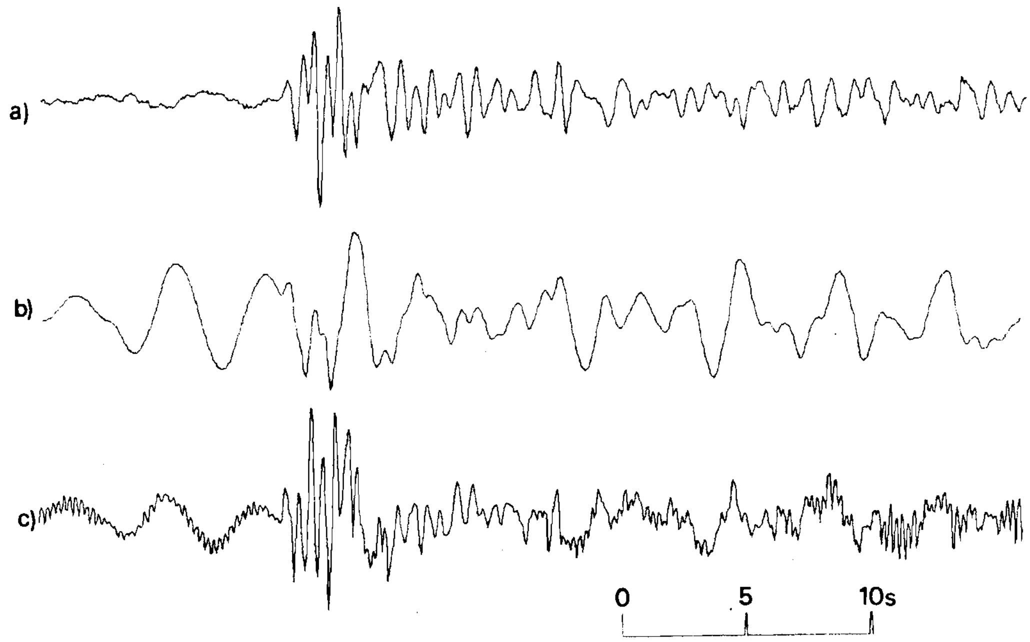

Figure 26. P seismograms recorded at Yellowknife,Canada from N.T.S explosion PICCALILLI.

(a) Short-period array-sum seismogram.
(b) Wiener filtered phaseless broad-band seismogram.
(c) Seismogram (b) corrected for anelastic attenuation assuming t*=0.5s.

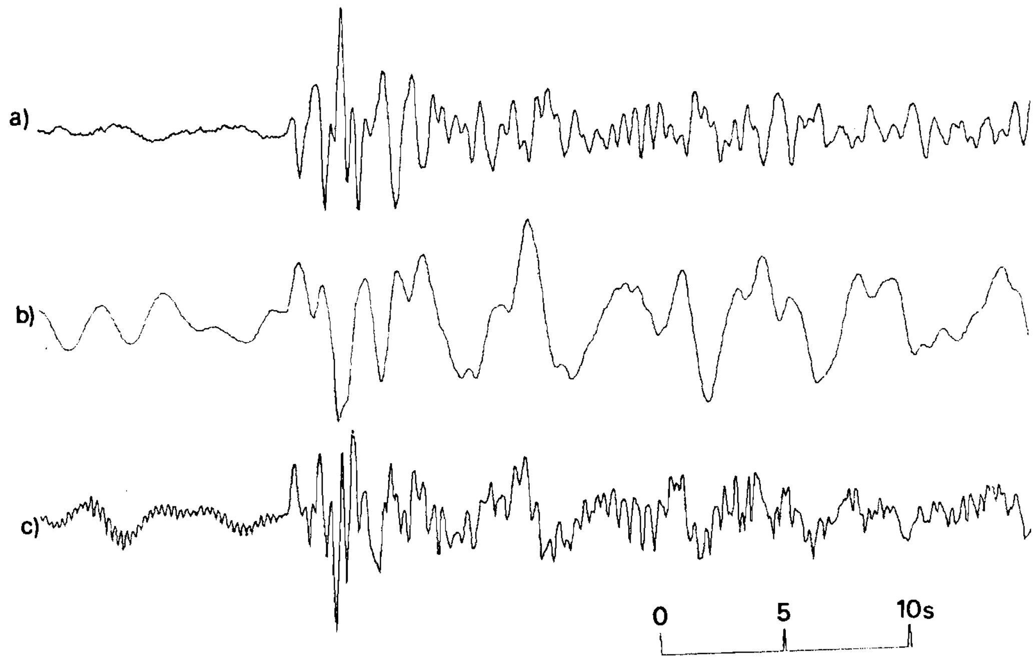

Figure 27. P seismograms recorded at Yellowknife,Canada from N.T.S explosion DIESEL TRAIN.

(a) Short-period array-sum seismogram.
(b) Wiener filtered phaseless broad-band seismogram.
(c) Seismogram (b) corrected for anelastic attenuation assuming t*=0.5s.

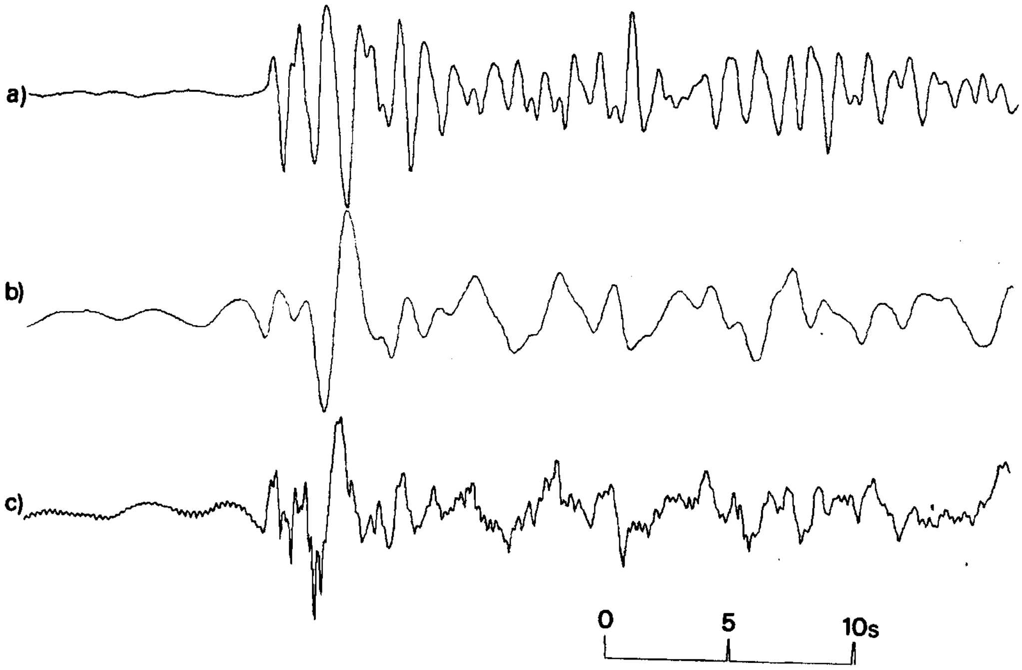

Figure 28. P seismograms recorded at Yellowknife, Canada from N.T.S explosion GRAPE A.

(a) Short-period array-sum seismogram.
(b) Wiener filtered phaseless broad-band seismogram.
(c) Seismogram (b) corrected for anelastic attenuation assuming $t^*=0.5s$.

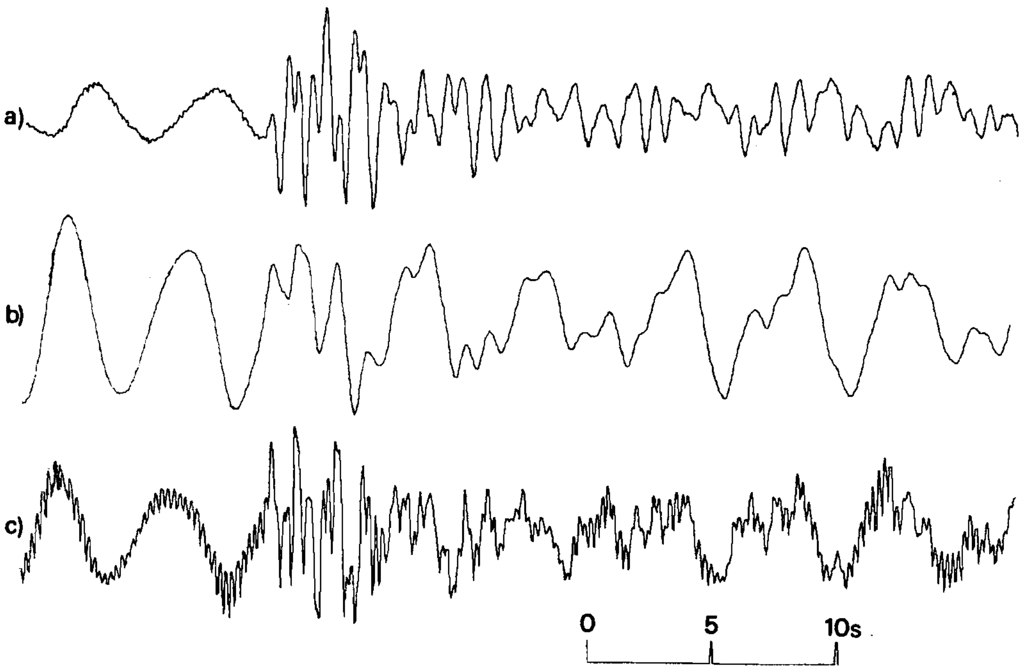

Figure 29. P seismograms recorded at Yellowknife, Canada from N.T.S explosion LOVAGE.

(a) Short-period array-sum seismogram.
(b) Wiener filtered phaseless broad-band seismogram.
(c) Seismogram (b) corrected for anelastic attenuation assuming $t^*=0.5s$.

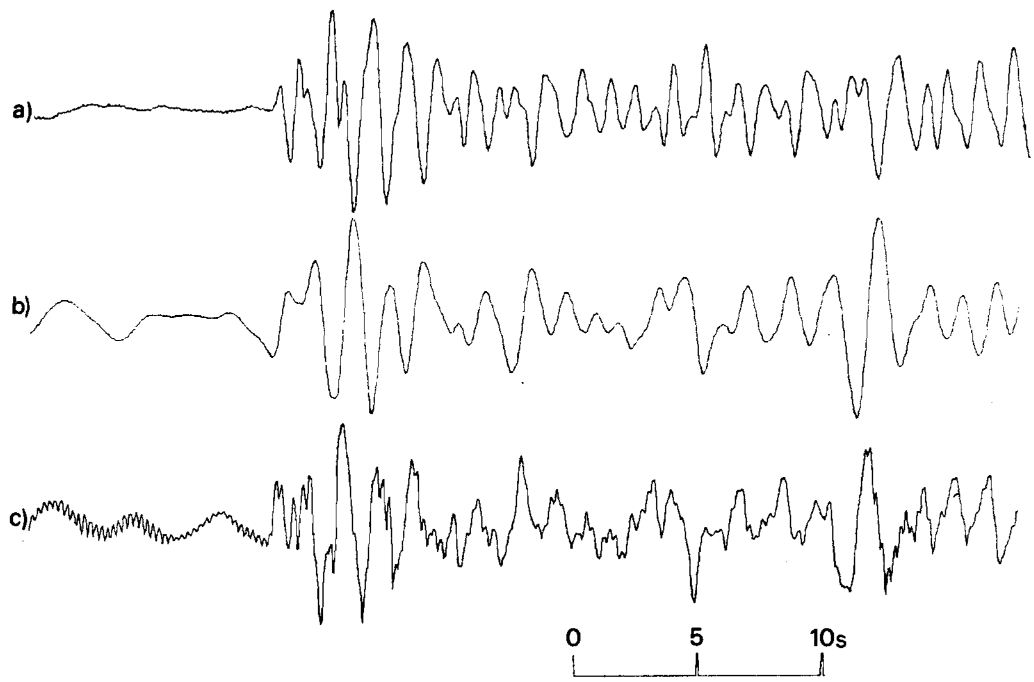

Figure 30 P seismograms recorded at Yellowknife,Canada from N.T.S explosion TERRINE.

(a) Short-period array-sum seismogram.
(b) Wiener filtered phaseless broad-band seismogram.
(c) Seismogram (b) corrected for anelastic attenuation assuming t*=0.5s.

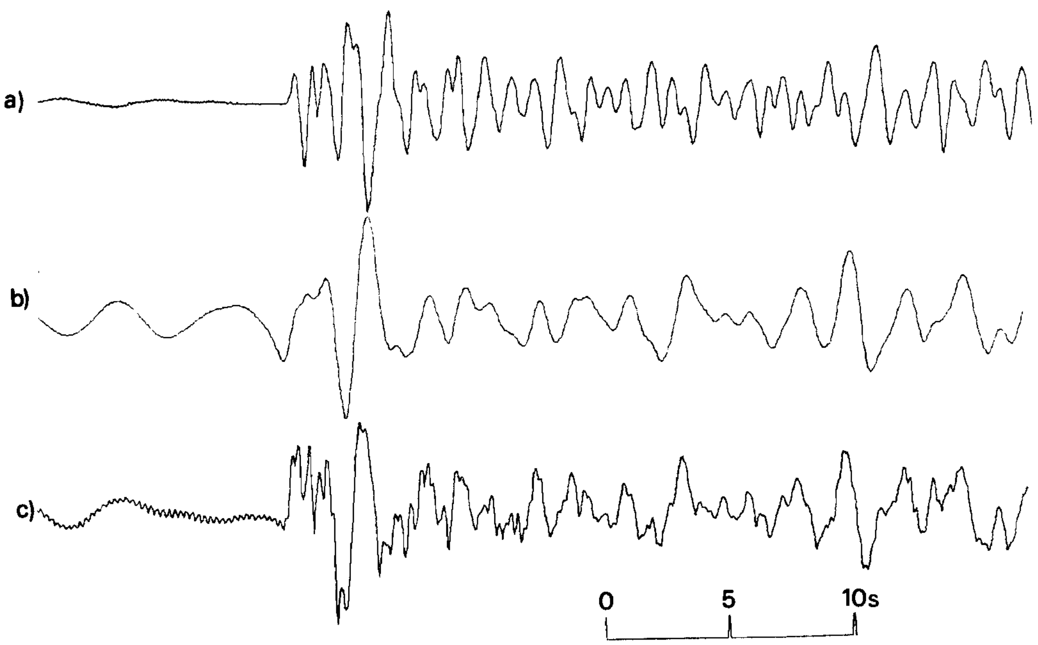

Figure 31. P seismograms recorded at Yellowknife,Canada from N.T.S explosion GRAPE B.

(a) Short-period array-sum seismogram.
(b) Wiener filtered phaseless broad-band seismogram.
(c) Seismogram (b) corrected for anelastic attenuation assuming t*=0.5s.

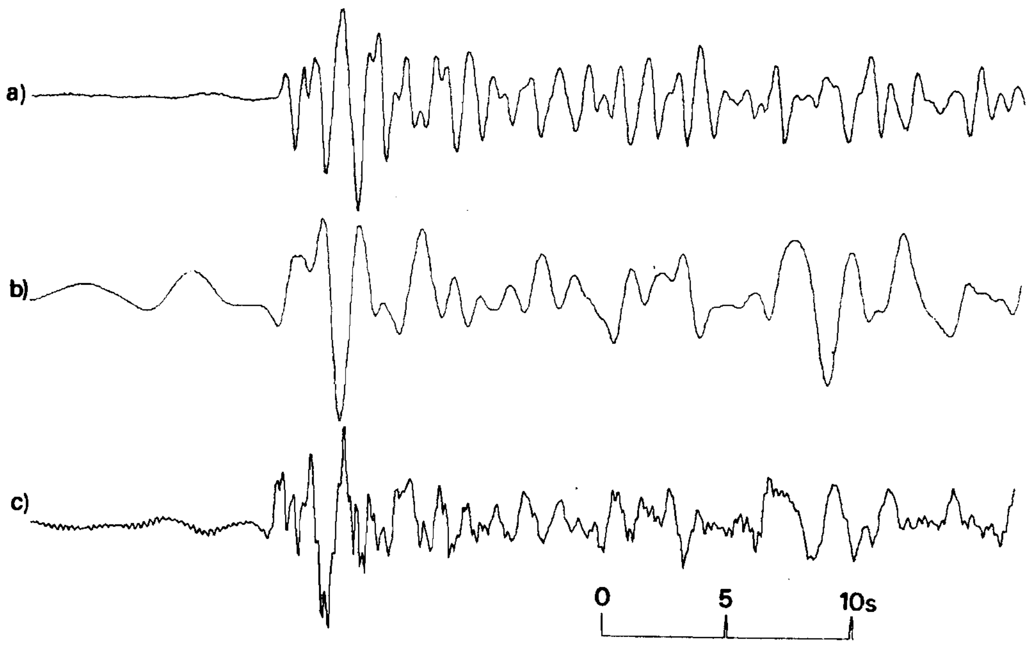

Figure 32. P seismograms recorded at Yellowknife, Canada from N.T.S explosion SHAPER.

(a) Short-period array-sum seismogram.
(b) Wiener filtered phaseless broad-band seismogram.
(c) Seismogram (b) corrected for anelastic attenuation assuming t*=0.5s.

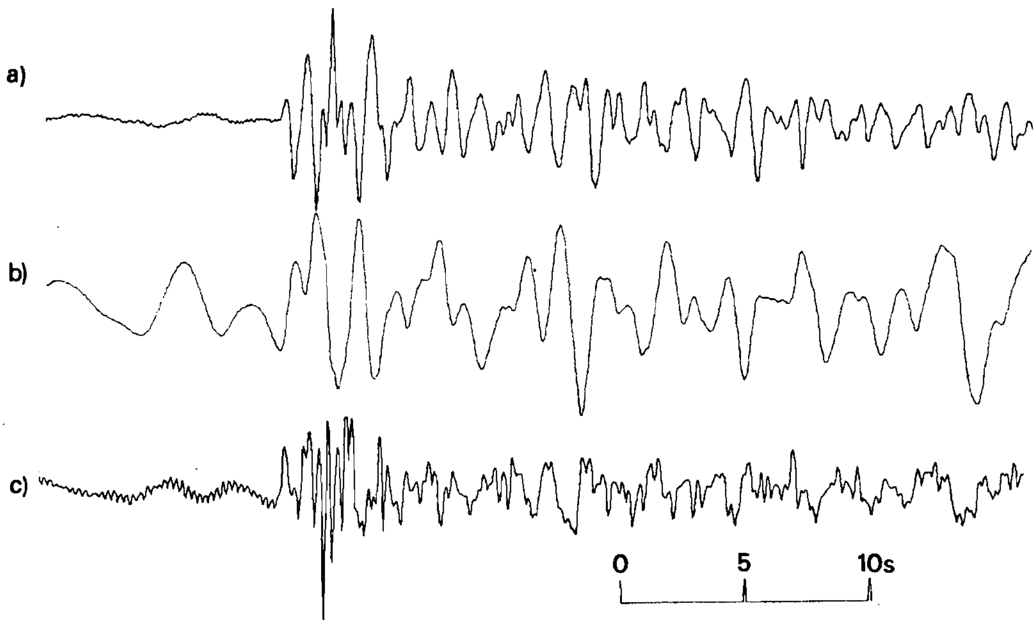

Figure 33. P seismograms recorded at Yellowknife, Canada from N.T.S explosion MINT LEAF.

(a) Short-period array-sum seismogram.
(b) Wiener filtered phaseless broad-band seismogram.
(c) Seismogram (b) corrected for anelastic attenuation assuming t*=0.5s.

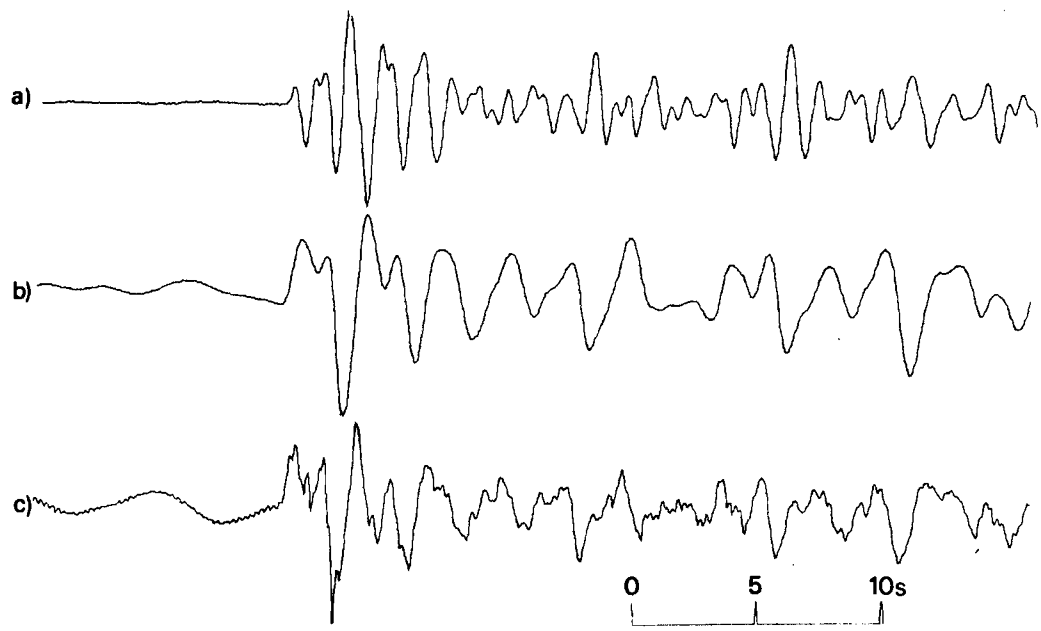

Figure 34. P seismograms recorded at Yellowknife,Canada from N.T.S explosion FLASK.

(a) Short-period array-sum seismogram.
(b) Wiener filtered phaseless broad-band seismogram.
(c) Seismogram (b) corrected for anelastic attenuation assuming t*=0.5s.

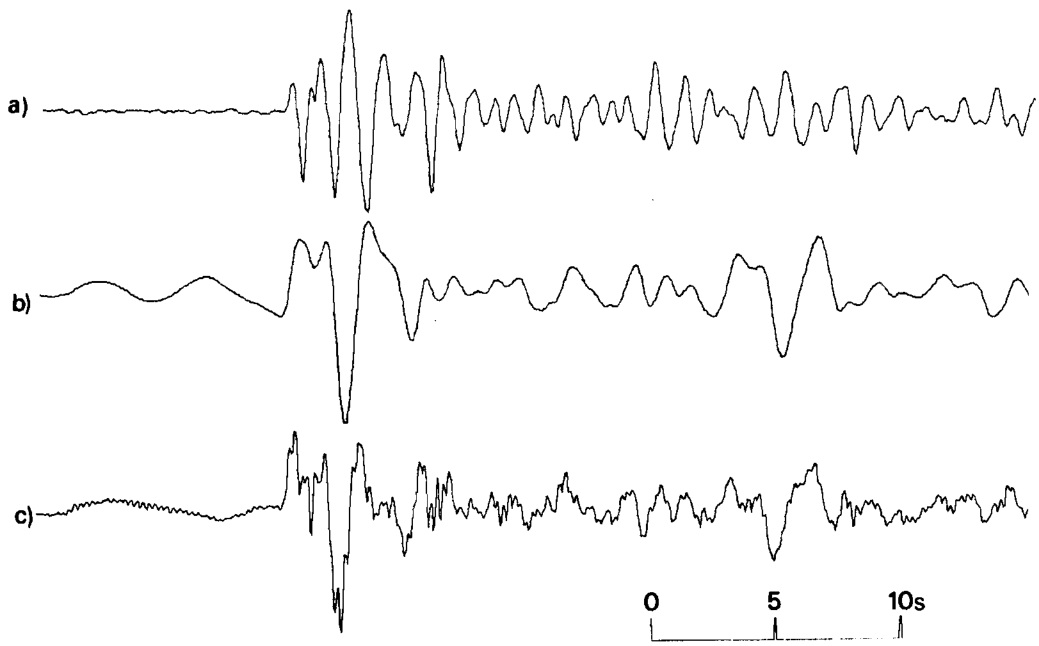

Figure 35. P seismograms recorded at Yellowknife,Canada from N.T.S explosion TIJERAS.

(a) Short-period array-sum seismogram.
(b) Wiener filtered phaseless broad-band seismogram.
(c) Seismogram (b) corrected for anelastic attenuation assuming t*=0.5s.

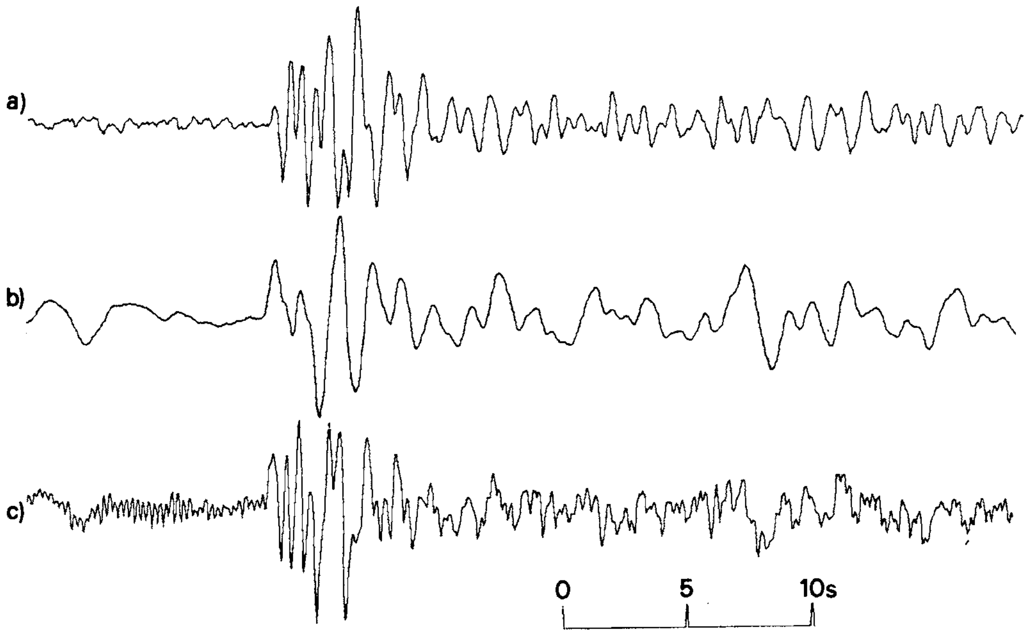

Figure 36. P seismograms recorded at Yellowknife, Canada from N.T.S explosion LAGUNA.

(a) Short-period array-sum seismogram.
(b) Wiener filtered phaseless broad-band seismogram.
(c) Seismogram (b) corrected for anelastic attenuation assuming t*=0.5s.

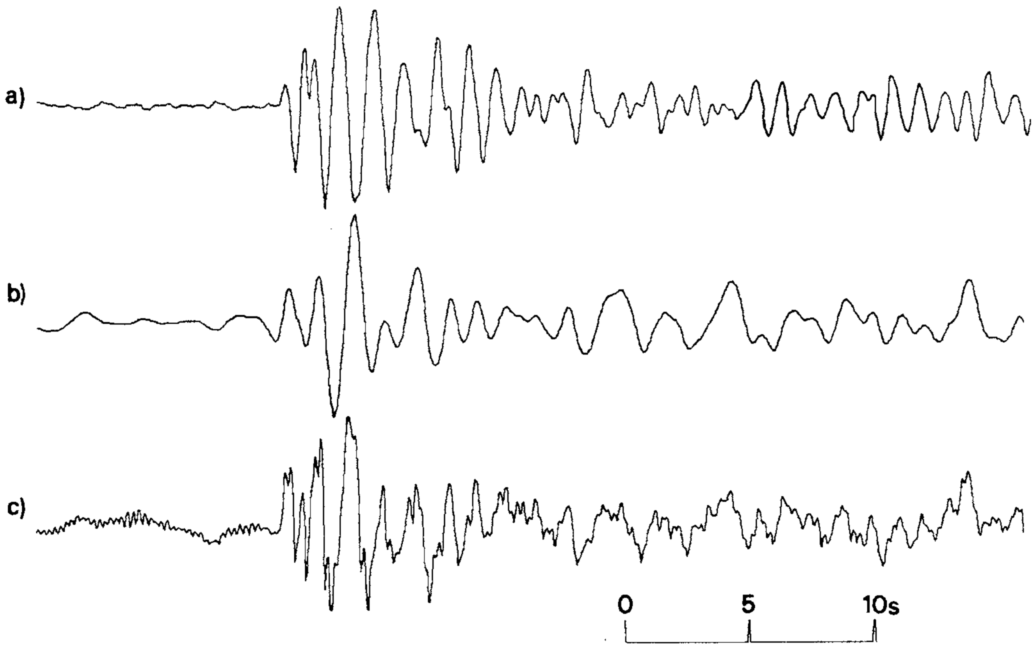

Figure 37. P seismograms recorded at Yellowknife, Canada from N.T.S explosion ALGODONES.

(a) Short-period array-sum seismogram.
(b) Wiener filtered phaseless broad-band seismogram.
(c) Seismogram (b) corrected for anelastic attenuation assuming t*=0.5s.

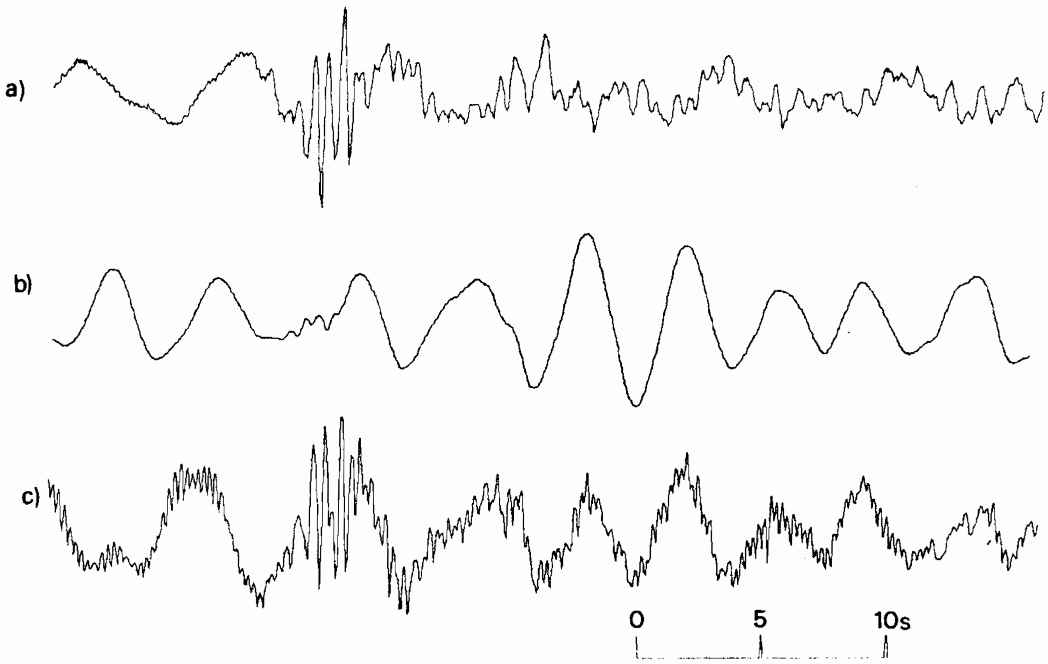

Figure 38. P seismograms recorded at Yellowknife, Canada from N.T.S explosion CHAENACTIS.

(a) Short-period array-sum seismogram.
(b) Wiener filtered phaseless broad-band seismogram.
(c) Seismogram (b) corrected for anelastic attenuation assuming t*=0.5s.

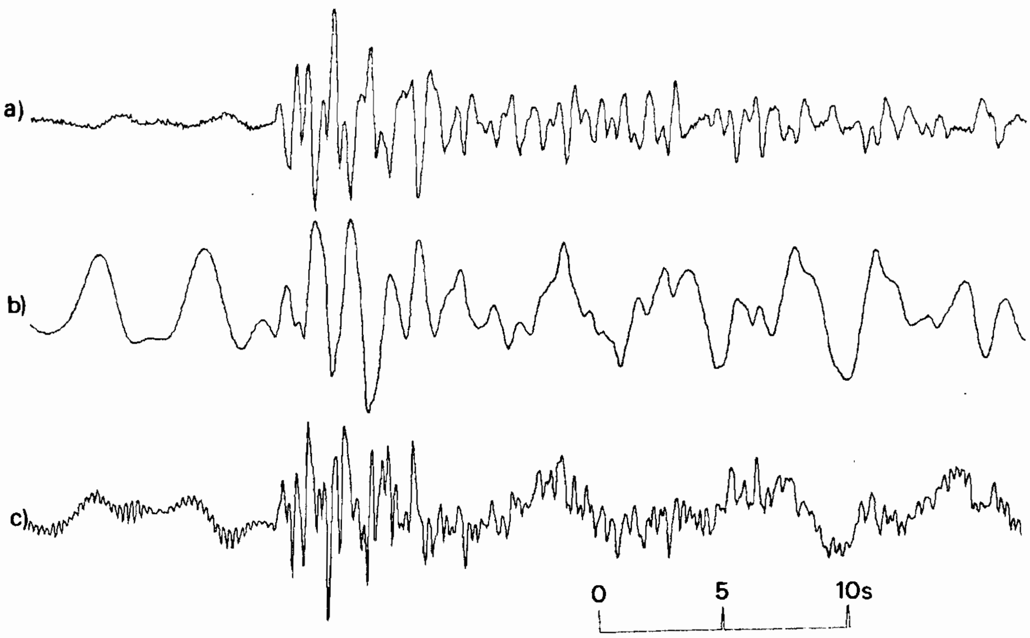

Figure 39. P seismograms recorded at Yellowknife, Canada from N.T.S explosion MONERO.

(a) Short-period array-sum seismogram.
(b) Wiener filtered phaseless broad-band seismogram.
(c) Seismogram (b) corrected for anelastic attenuation assuming t*=0.5s.

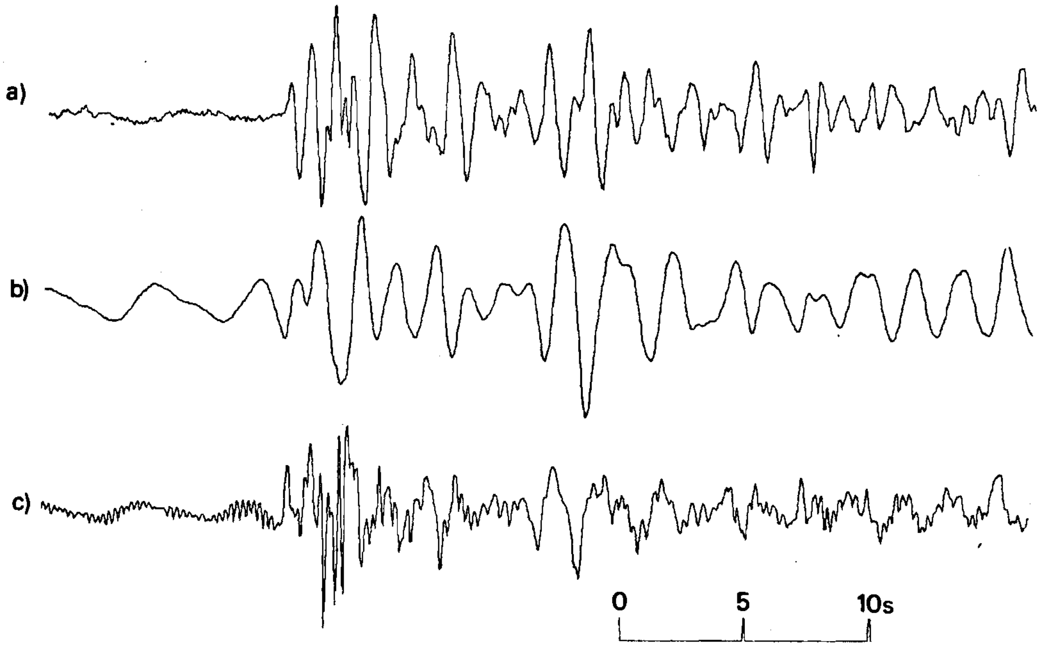

Figure 40. P seismograms recorded at Yellowknife,Canada from N.T.S explosion DIAMOND SCULLS.

(a) Short-period array-sum seismogram.
(b) Wiener filtered phaseless broad-band seismogram.
(c) Seismogram (b) corrected for anelastic attenuation assuming t*=0.5s.

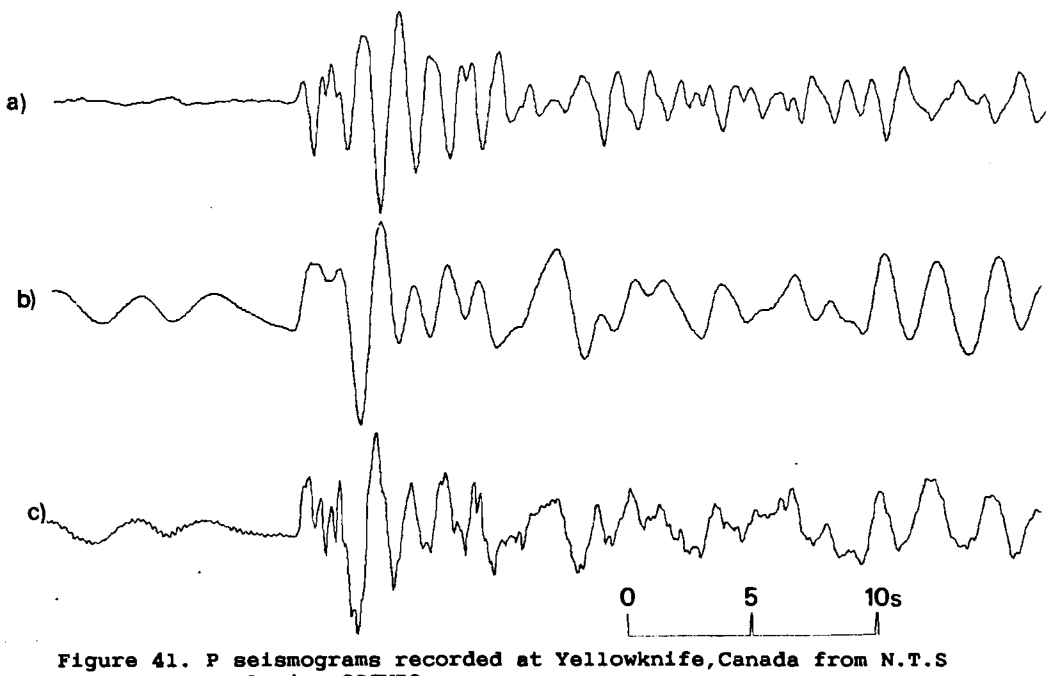

Figure 41. P seismograms recorded at Yellowknife,Canada from N.T.S explosion OSCURO.

(a) Short-period array-sum seismogram.
(b) Wiener filtered phaseless broad-band seismogram.
(c) Seismogram (b) corrected for anelastic attenuation assuming t*=0.5s.

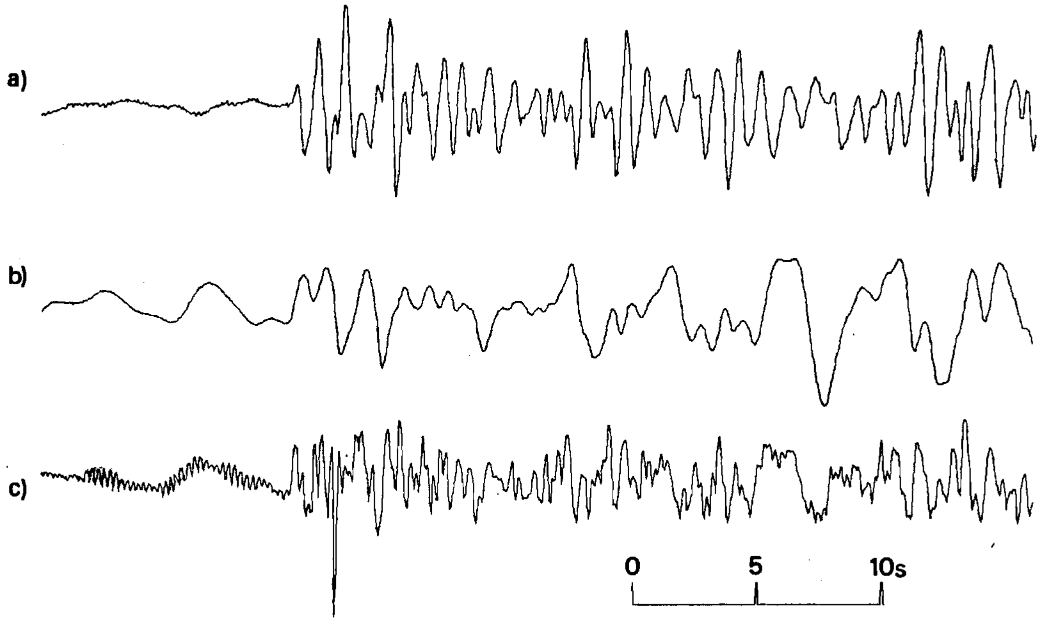

Figure 42. P seismograms recorded at Yellowknife, Canada from N.T.S explosion FLAX.

(a) Short-period array-sum seismogram.
(b) Wiener filtered phaseless broad-band seismogram.
(c) Seismogram (b) corrected for anelastic attenuation assuming t*=0.5s.

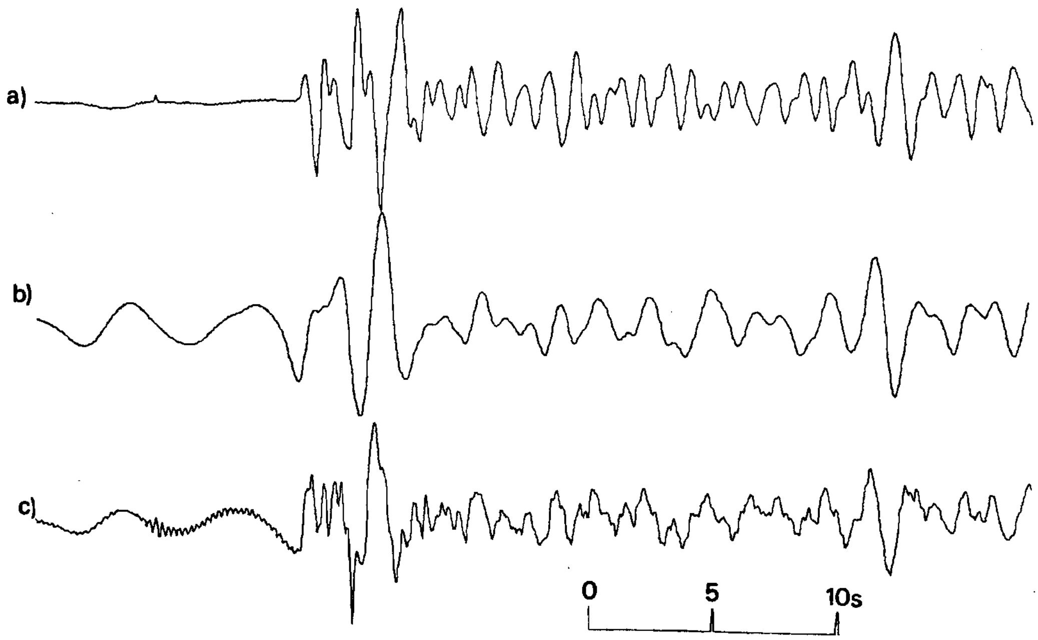

Figure 43. P seismograms recorded at Yellowknife, Canada from N.T.S explosion MIERA.

(a) Short-period array-sum seismogram.
(b) Wiener filtered phaseless broad-band seismogram.
(c) Seismogram (b) corrected for anelastic attenuation assuming t*=0.5s.

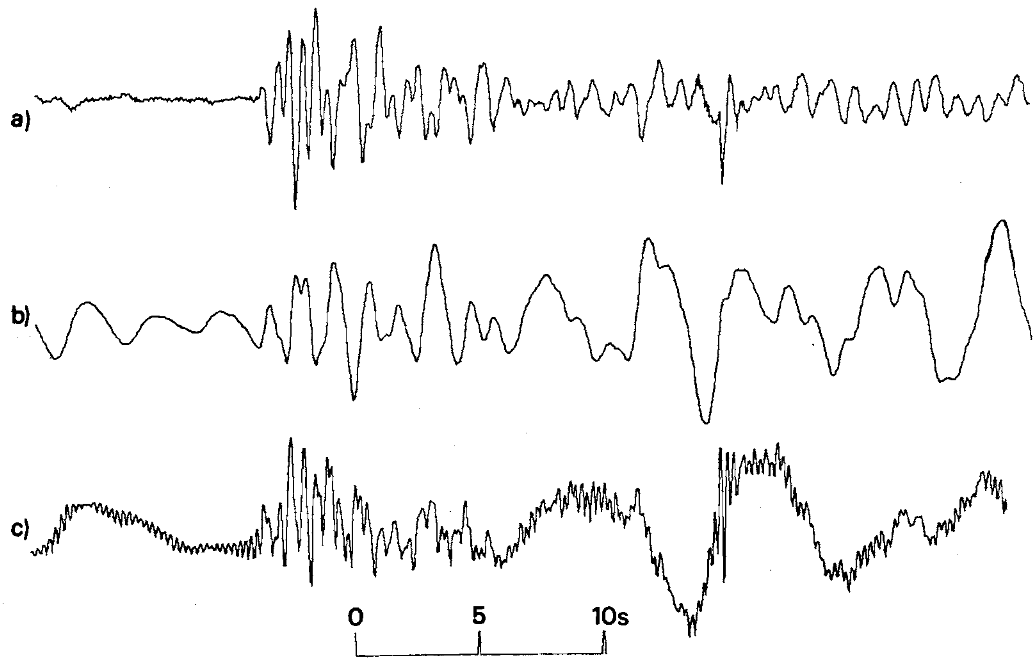

Figure 44. P seismograms recorded at Yellowknife,Canada from N.T.S explosion ANGUS.

(a) Short-period array-sum seismogram.
(b) Wiener filtered phaseless broad-band seismogram.
(c) Seismogram (b) corrected for anelastic attenuation assuming t*=0.5s.

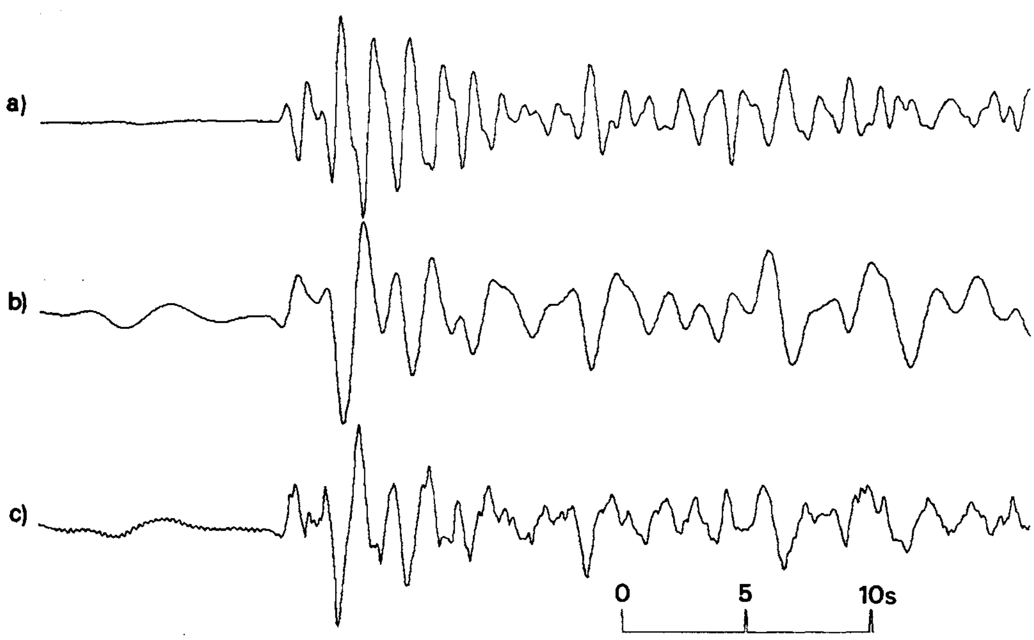

Figure 45. P seismograms recorded at Yellowknife,Canada from N.T.S explosion STARWORT.

(a) Short-period array-sum seismogram.
(b) Wiener filtered phaseless broad-band seismogram.
(c) Seismogram (b) corrected for anelastic attenuation assuming t*=0.5s.

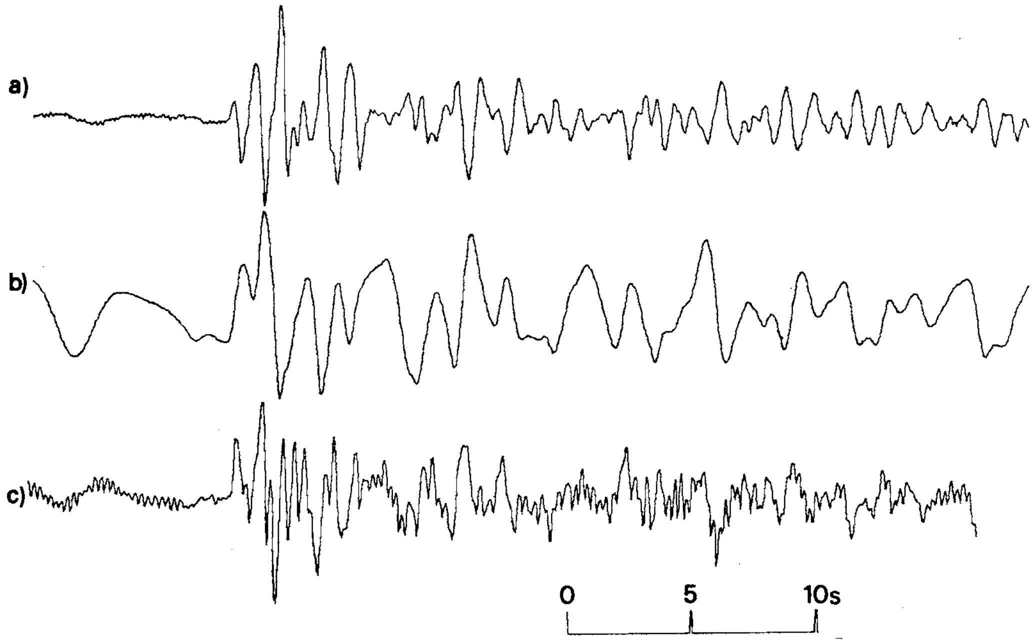

Figure 46. P seismograms recorded at Yellowknife, Canada from N.T.S explosion DIDO QUEEN.

(a) Short-period array-sum seismogram.
(b) Wiener filtered phaseless broad-band seismogram.
(c) Seismogram (b) corrected for anelastic attenuation assuming t*=0.5s.

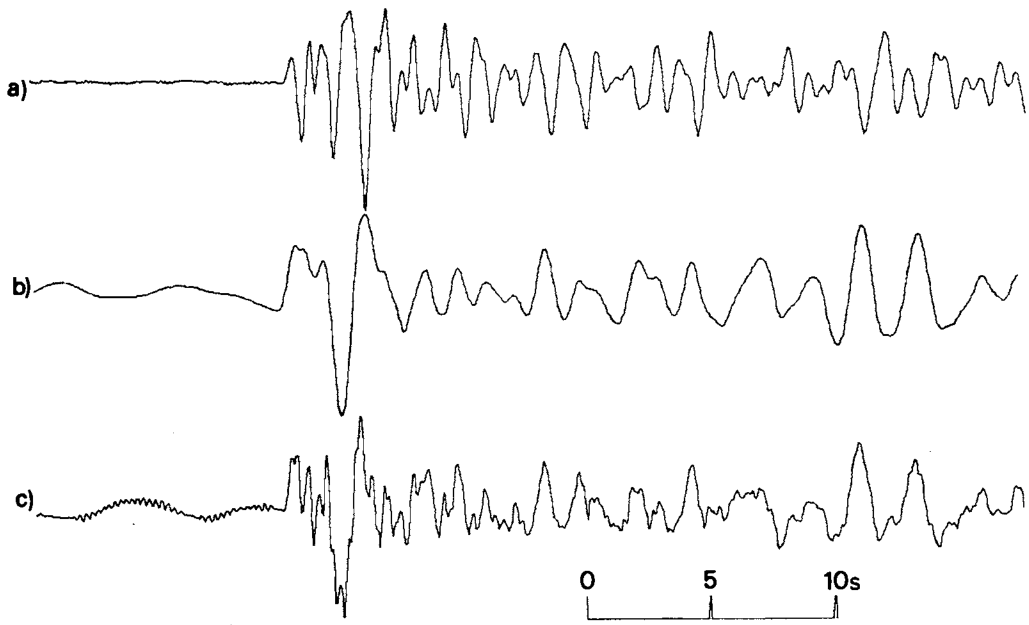

Figure 47. P seismograms recorded at Yellowknife, Canada from N.T.S explosion

(a) Short-period array-sum seismogram.
(b) Wiener filtered phaseless broad-band seismogram.
(c) Seismogram (b) corrected for anelastic attenuation assuming t*=0.5s.

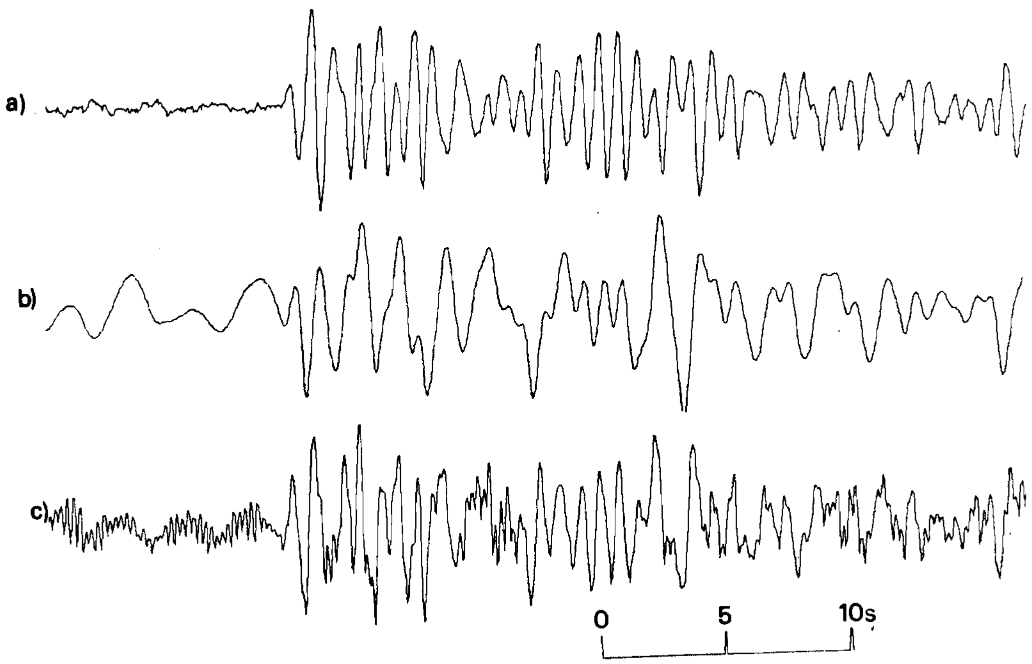

Figure 48. P seismograms recorded at Yellowknife, Canada from N.T.S explosion PORTULACA.

(a) Short-period array-sum seismogram.
(b) Wiener filtered phaseless broad-band seismogram.
(c) Seismogram (b) corrected for anelastic attenuation assuming t*=0.5s.

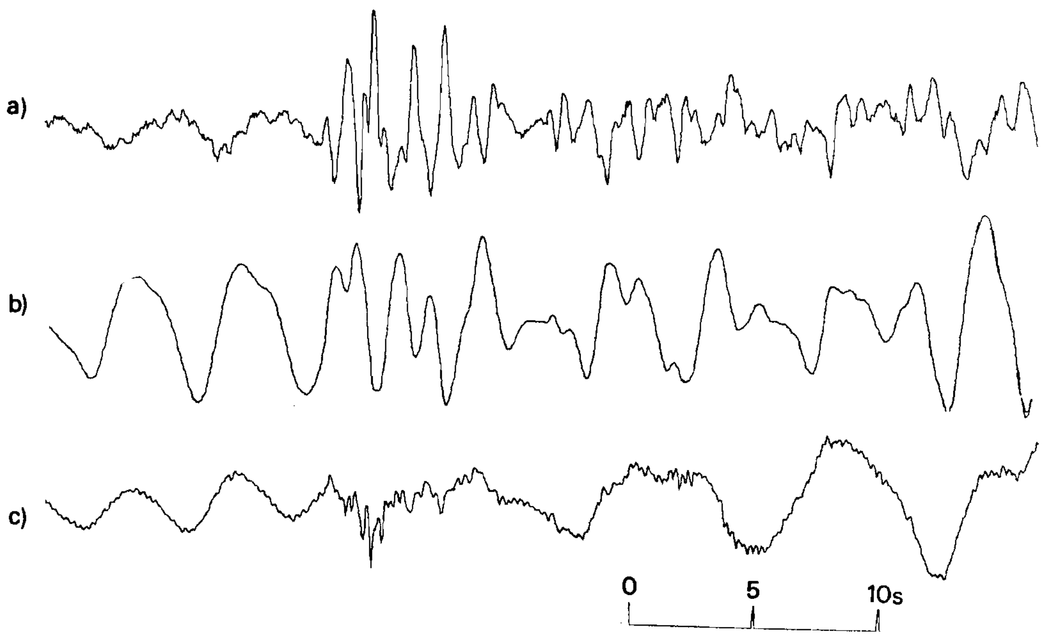

Figure 49. P seismograms recorded at Yellowknife, Canada from N.T.S explosion HUSKY ACE.

(a) Short-period array-sum seismogram.
(b) Wiener filtered phaseless broad-band seismogram.
(c) Seismogram (b) corrected for anelastic attenuation assuming t*=0.5s.

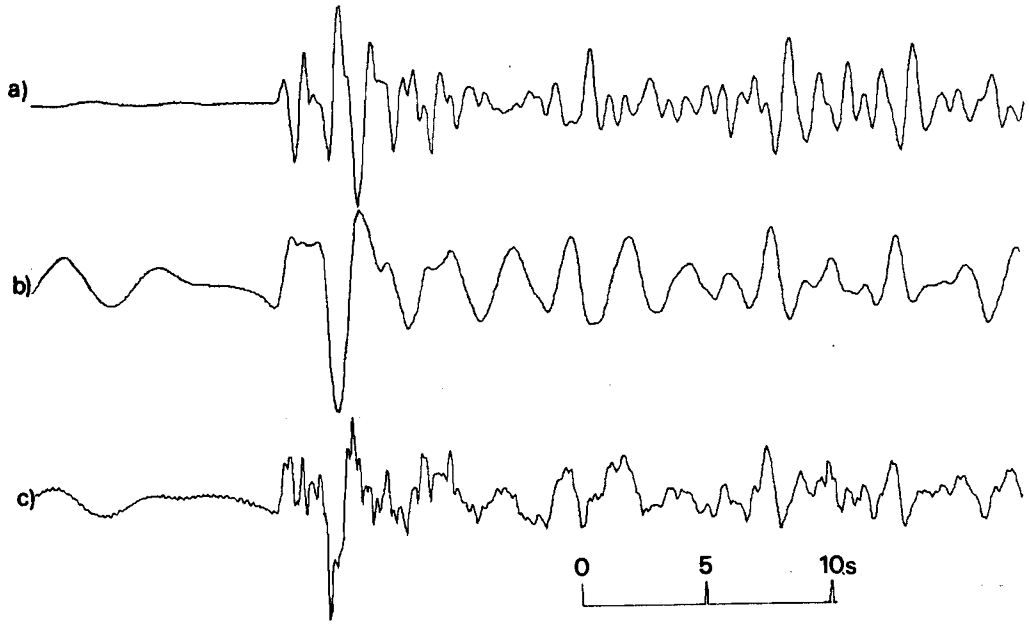

Figure 50. P seismograms recorded at Yellowknife,Canada from N.T.S explosion LATIR.

(a) Short-period array-sum seismogram.
(b) Wiener filtered phaseless broad-band seismogram.
(c) Seismogram (b) corrected for anelastic attenuation assuming t*=0.5s.

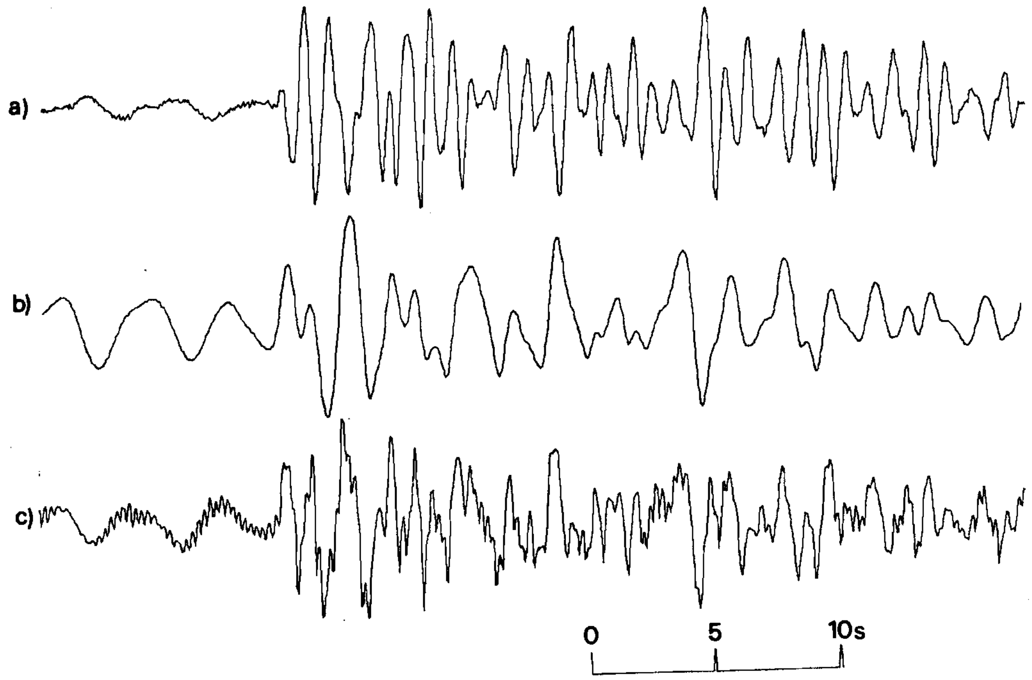

Figure 51. P seismograms recorded at Yellowknife,Canada from N.T.S explosion FALLON.

(a) Short-period array-sum seismogram.
(b) Wiener filtered phaseless broad-band seismogram.
(c) Seismogram (b) corrected for anelastic attenuation assuming t*=0.5s.

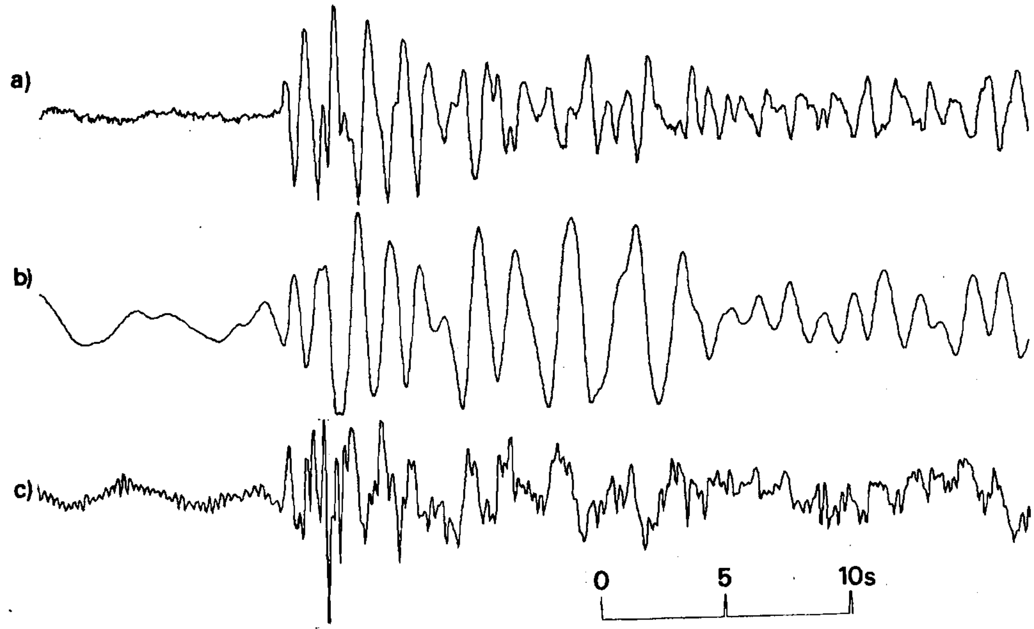

Figure 52. P seismograms recorded at Yellowknife, Canada from N.T.S explosion MING BLADE.

(a) Short-period array-sum seismogram.
(b) Wiener filtered phaseless broad-band seismogram.
(c) Seismogram (b) corrected for anelastic attenuation assuming $t^*=0.5s$.

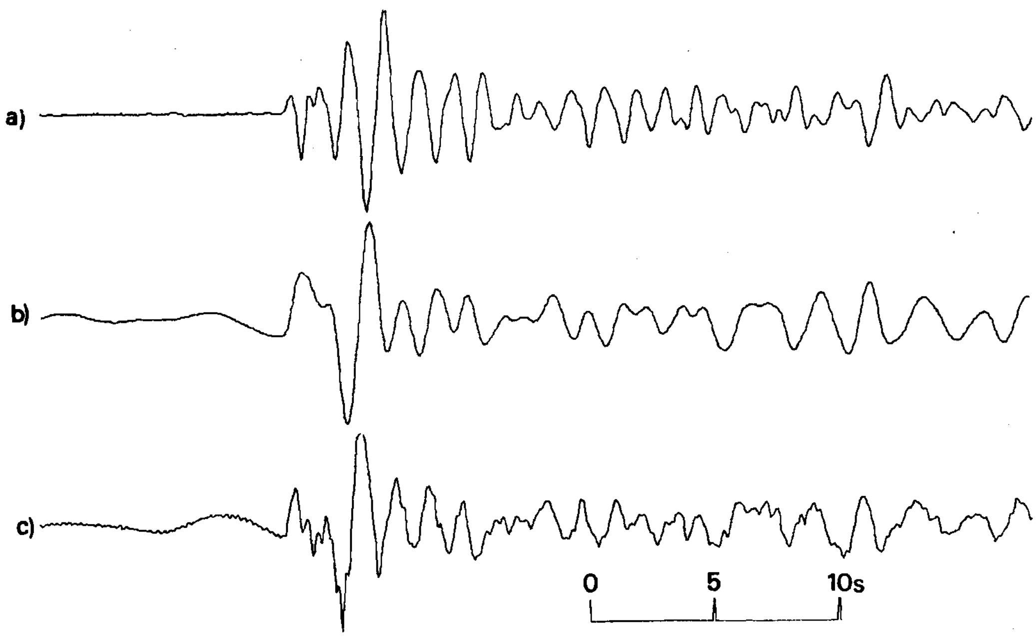

Figure 53. P seismograms recorded at Yellowknife, Canada from N.T.S explosion ESCABOSA.

(a) Short-period array-sum seismogram.
(b) Wiener filtered phaseless broad-band seismogram.
(c) Seismogram (b) corrected for anelastic attenuation assuming $t^*=0.5s$.

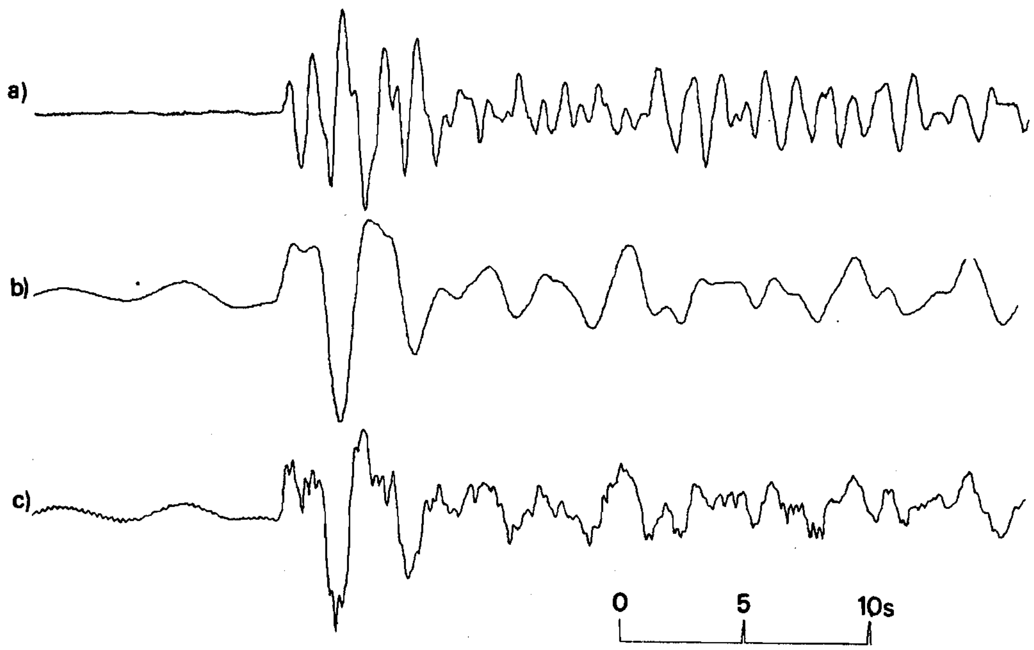

Figure 54. P seismograms recorded at Yellowknife, Canada from N.T.S explosion PORTMANTEAU.

(a) Short-period array-sum seismogram.
(b) Wiener filtered phaseless broad-band seismogram.
(c) Seismogram (b) corrected for anelastic attenuation assuming t*=0.5s.

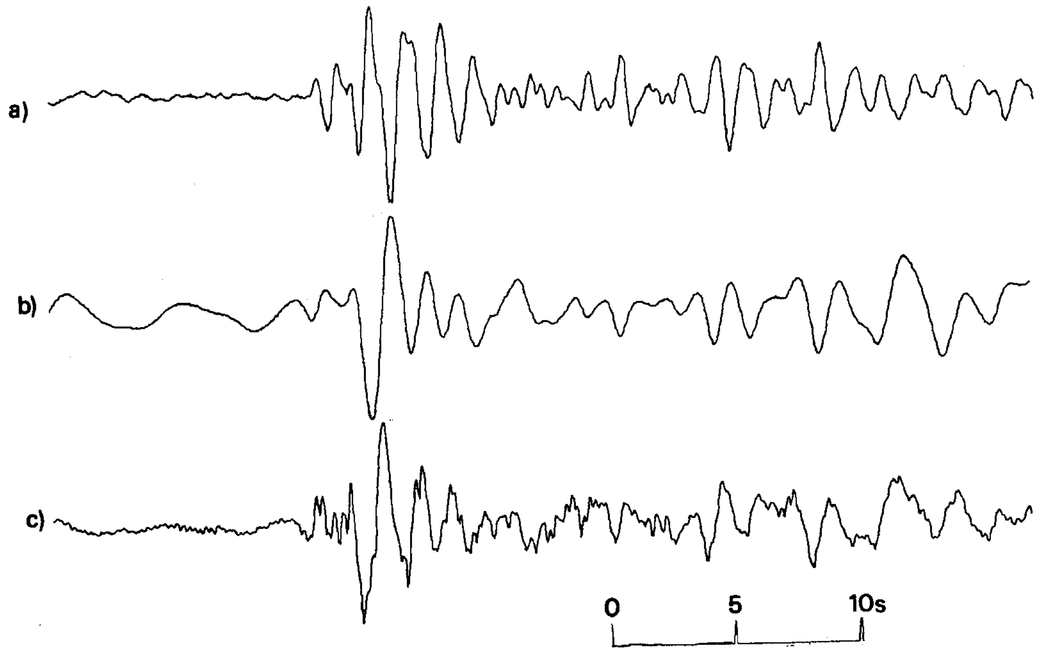

Figure 55. P seismograms recorded at Yellowknife, Canada from N.T.S explosion STANYAN.

(a) Short-period array-sum seismogram.
(b) Wiener filtered phaseless broad-band seismogram.
(c) Seismogram (b) corrected for anelastic attenuation assuming t*=0.5s.

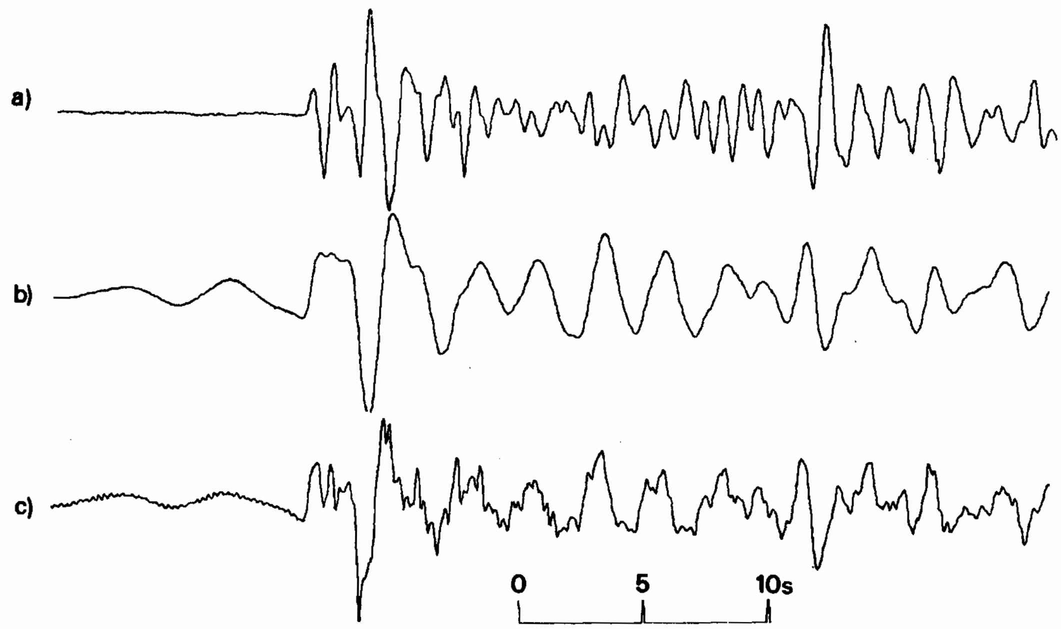

Figure 56. P seismograms recorded at Yellowknife,Canada from N.T.S explosion TOPGALLANT.

(a) Short-period array-sum seismogram.
(b) Wiener filtered phaseless broad-band seismogram.
(c) Seismogram (b) corrected for anelastic attenuation assuming t*=0.5s.

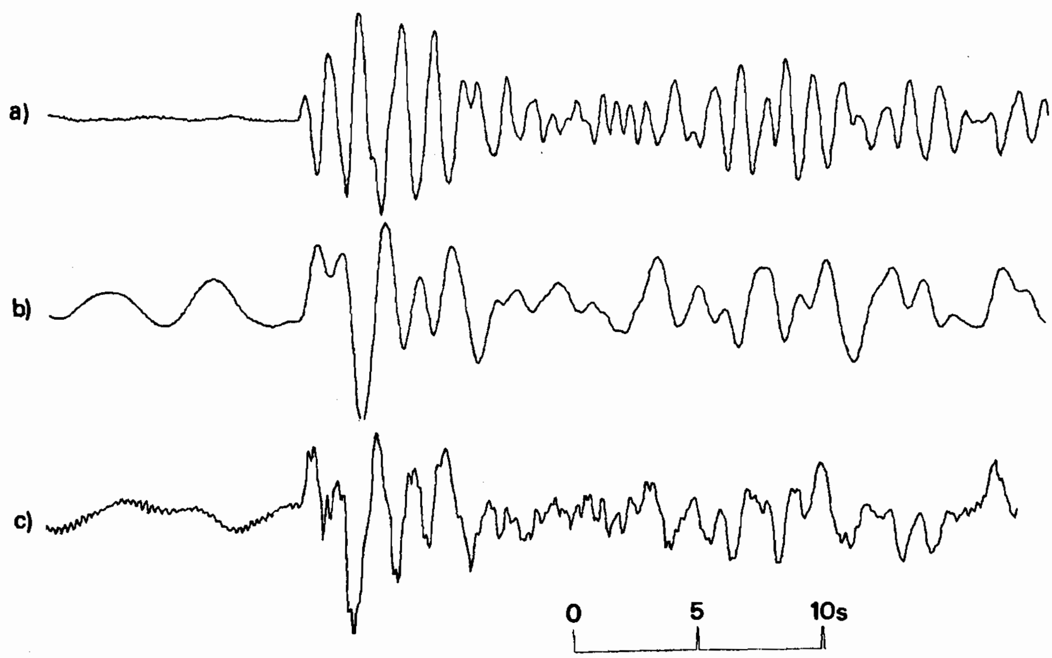

Figure 57. P seismograms recorded at Yellowknife,Canada from N.T.S explosion CABRILLO.

(a) Short-period array-sum seismogram.
(b) Wiener filtered phaseless broad-band seismogram.
(c) Seismogram (b) corrected for anelastic attenuation assuming t*=0.5s.

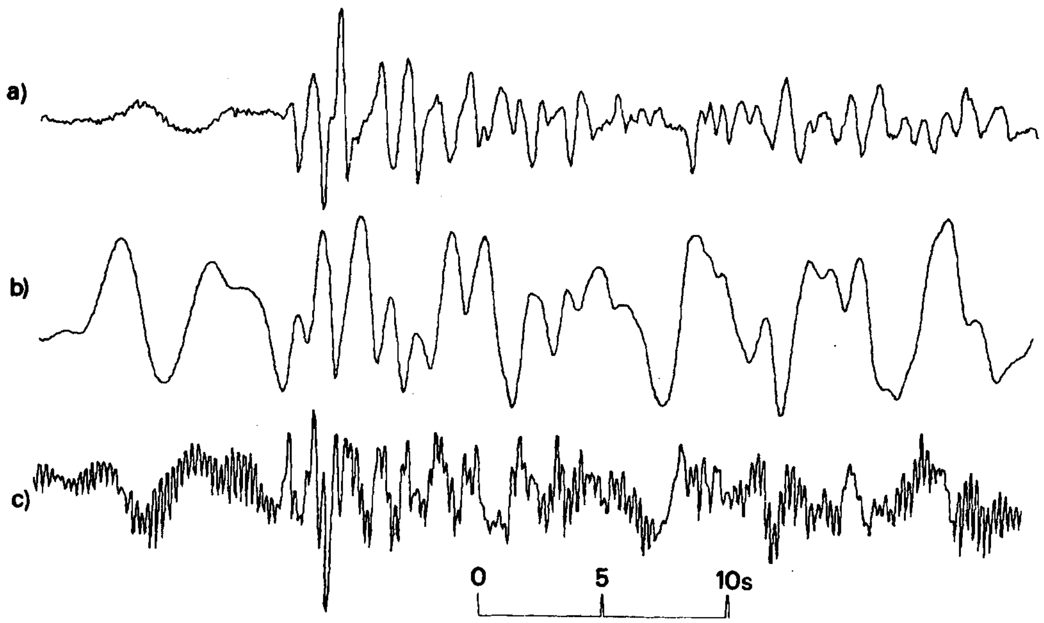

Figure 58. P seismograms recorded at Yellowknife,Canada from N.T.S explosion DINING CAR.

(a) Short-period array-sum seismogrem.
(b) Wiener filtered phaseless broad-band seismogram.
(c) Seismogram (b) corrected for anelastic attenuation assuming t*=0.5s.

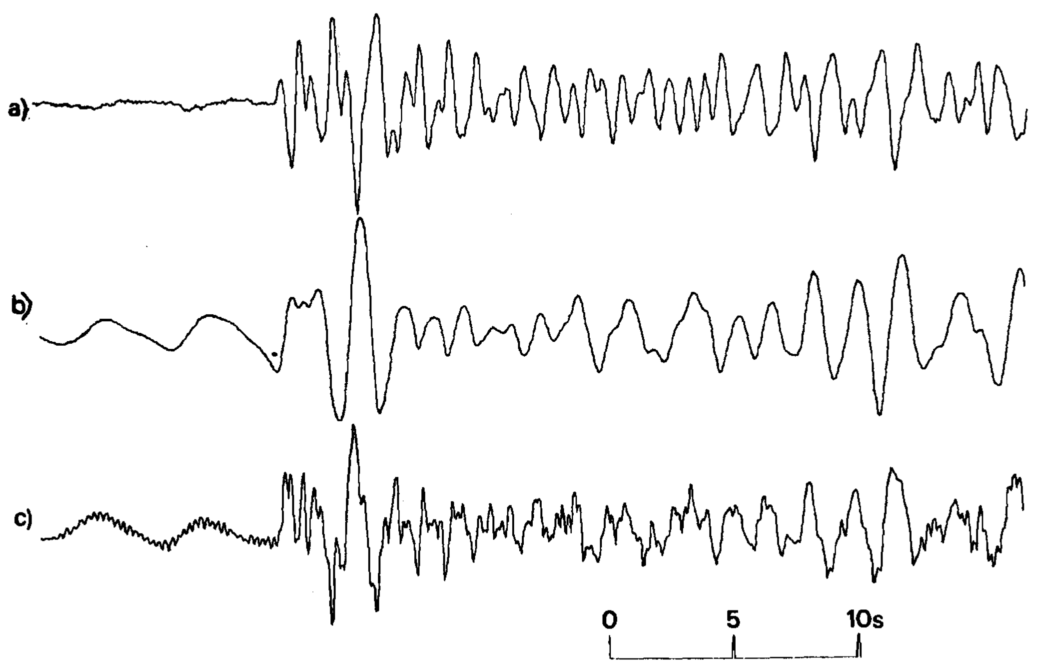

Figure 59. P seismograms recorded at Yellowknife,Canada from N.T.S explosion OBAR.

(a) Short-period array-sum seismogram.
(b) Wiener filtered phaseless broad-band seismogram.
(c) Seismogram (b) corrected for anelastic attenuation assuming t*=0.5s.

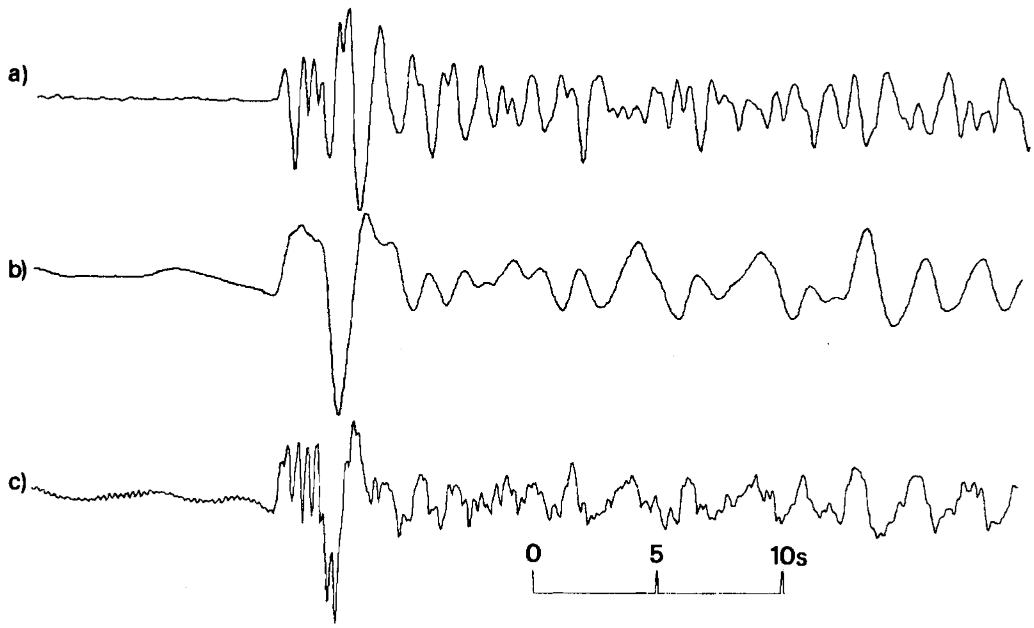

Figure 60. P seismograms recorded at Yellowknife, Canada from N.T.S explosion MIZZEN.

(a) Short-period array-sum seismogram.
(b) Wiener filtered phaseless broad-band seismogram.
(c) Seismogram (b) corrected for anelastic attenuation assuming t*=0.5s.

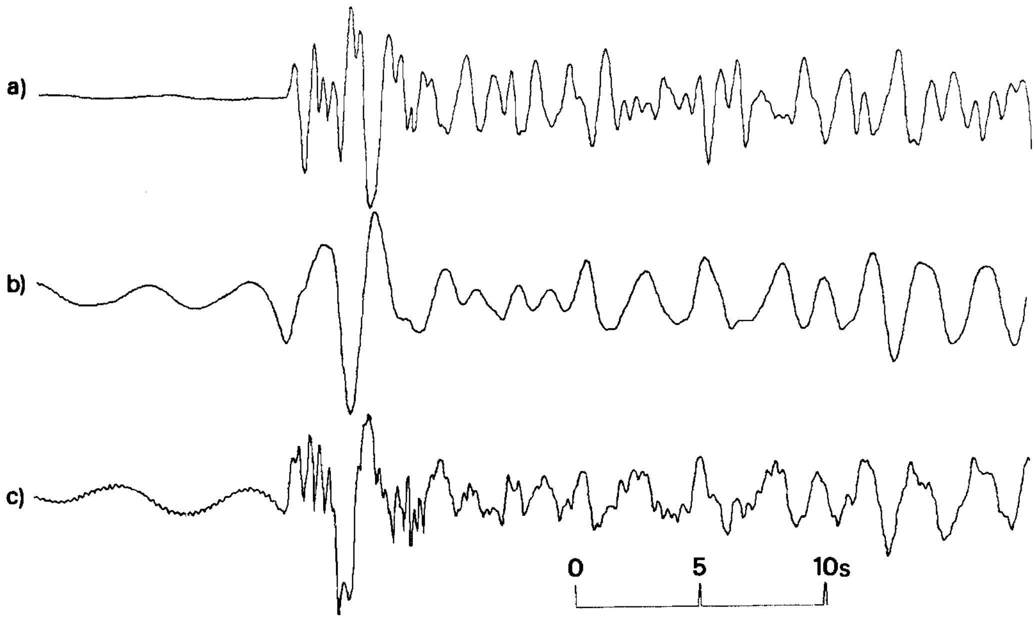

Figure 61. P seismograms recorded at Yellowknife, Canada from N.T.S explosion ESROM.

(a) Short-period array-sum seismogram.
(b) Wiener filtered phaseless broad-band seismogram.
(c) Seismogram (b) corrected for anelastic attenuation assuming t*=0.5s.

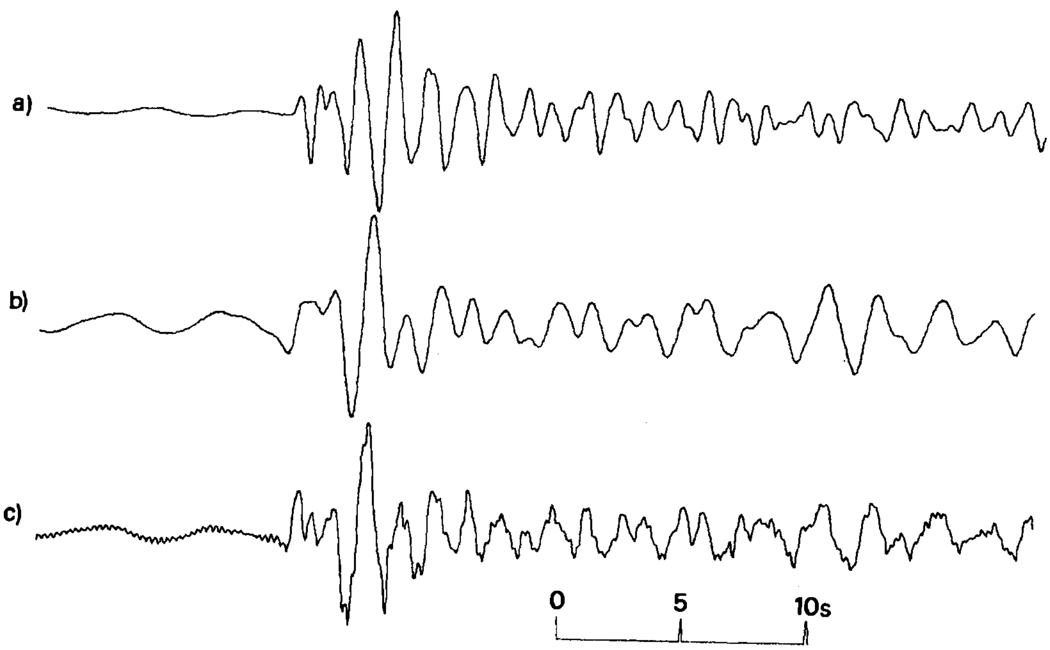

Figure 62. P seismograms recorded at Yellowknife,Canada from N.T.S explosion KEELSON.

(a) Short-period array-sum seismogram.
(b) Wiener filtered phaseless broad-band seismogram.
(c) Seismogram (b) corrected for anelastic attenuation assuming t*=0.5s.

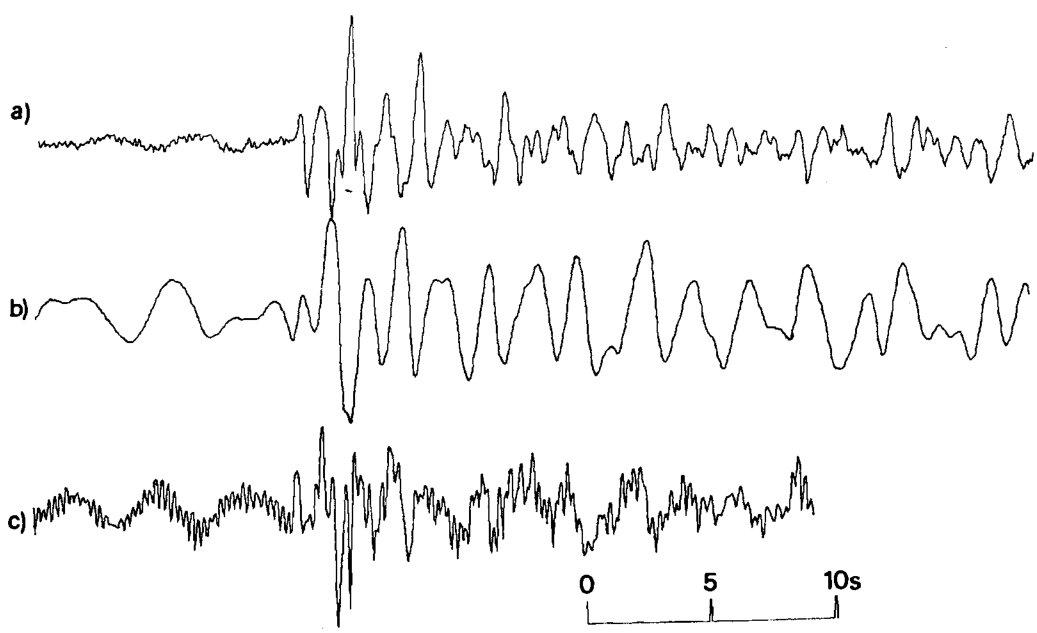

Figure 63. P seismograms recorded at Yellowknife,Canada from N.T.S explosion MIGHTY EPIC.

(a) Short-period array-sum seismogram.
(b) Wiener filtered phaseless broad-band seismogram.
(c) Seismogram (b) corrected for anelastic attenuation assuming t*=0.5s.

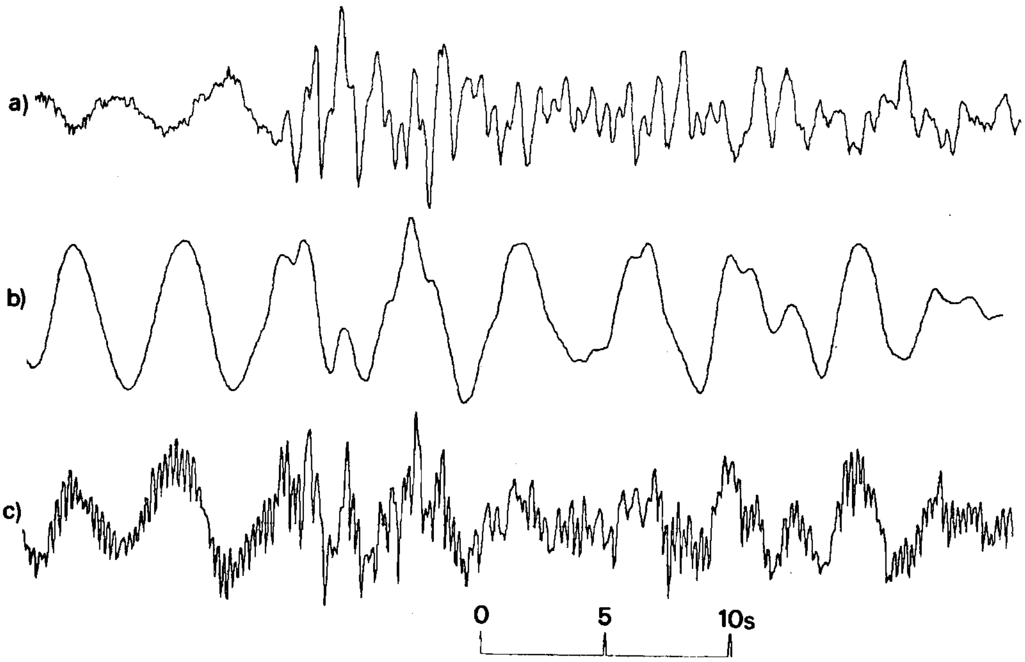

Figure 64. P seismograms recorded at Yellowknife,Canada from N.T.S explosion REDMUD.

(a) Short-period array-sum seismogram.
(b) Wiener filtered phaseless broad-band seismogram.
(c) Seismogram (b) corrected for anelastic attenuation assuming t*=0.5s.

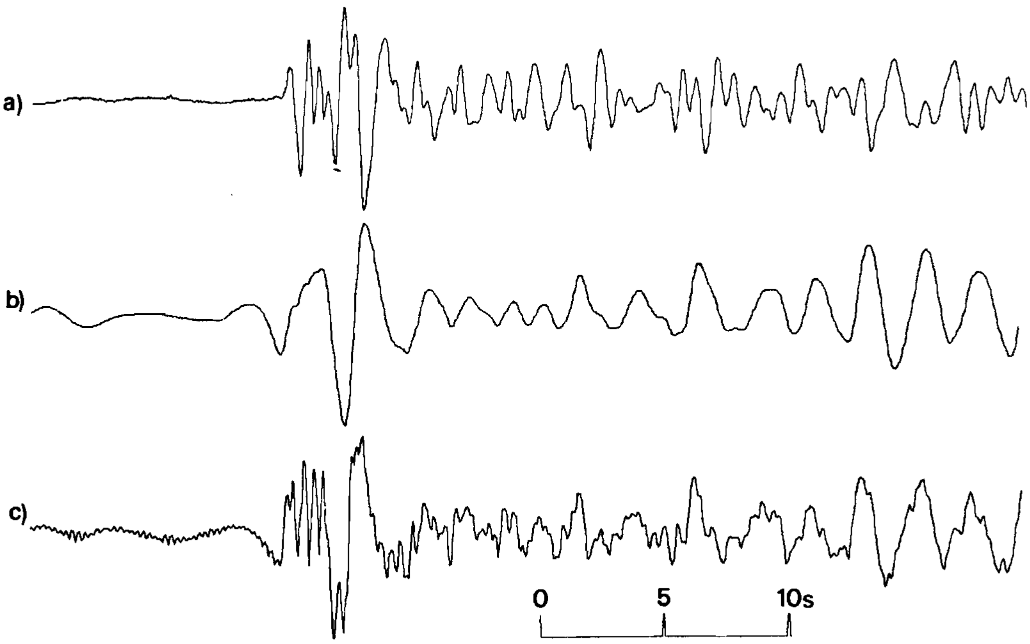

Figure 65. P seismograms recorded at Yellowknife,Canada from N.T.S explosion RUDDER.

(a) Short-period array-sum seismogram.
(b) Wiener filtered phaseless broad-band seismogram.
(c) Seismogram (b) corrected for anelastic attenuation assuming t*=0.5s.

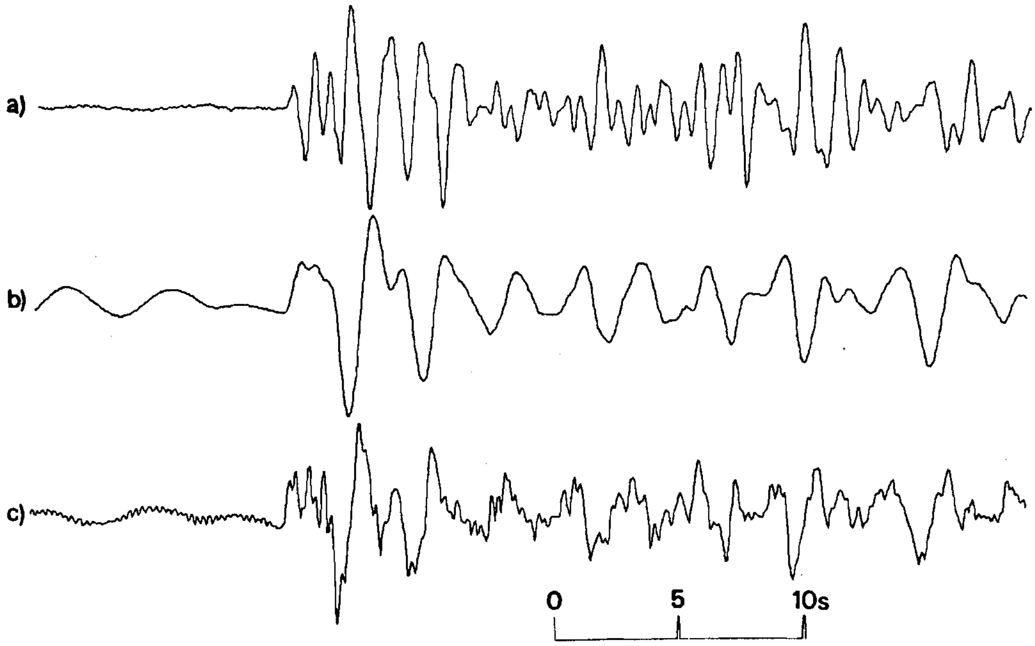

Figure 66. P seismograms recorded at Yellowknife,Canada from N.T.S explosion MARSILLY.

(a) Short-period array-sum seismogram.
(b) Wiener filtered phaseless broad-band seismogram.
(c) Seismogram (b) corrected for anelastic attenuation assuming t*=0.5s.

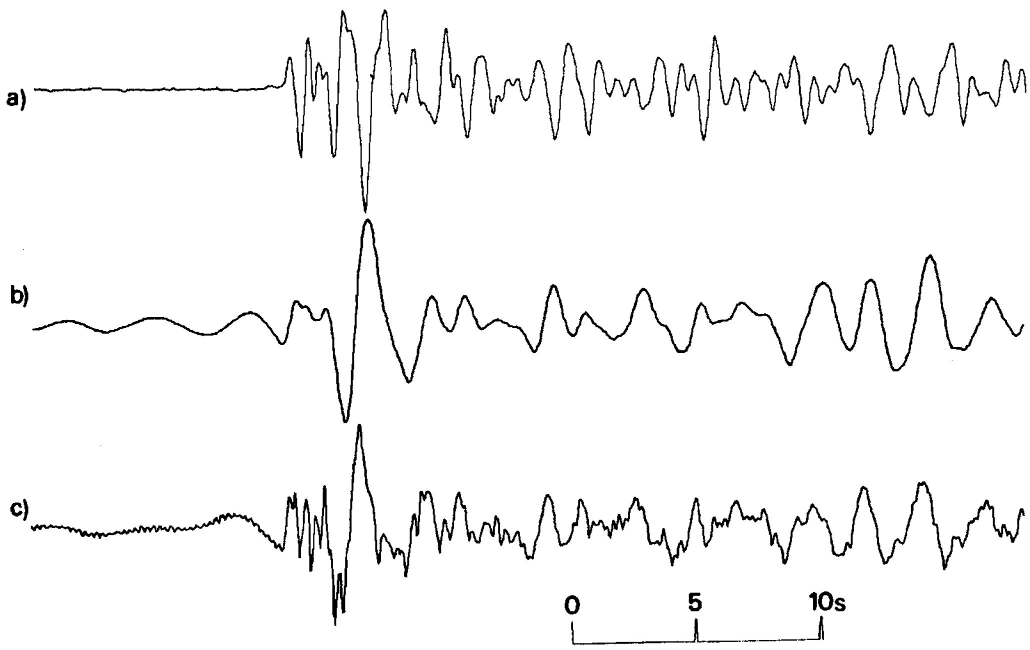

Figure 67. P seismograms recorded at Yellowknife,Canada from N.T.S explosion BULKHEAD.

(a) Short-period array-sum seismogram.
(b) Wiener filtered phaseless broad-band seismogram.
(c) Seismogram (b) corrected for anelastic attenuation assuming t*=0.5s.

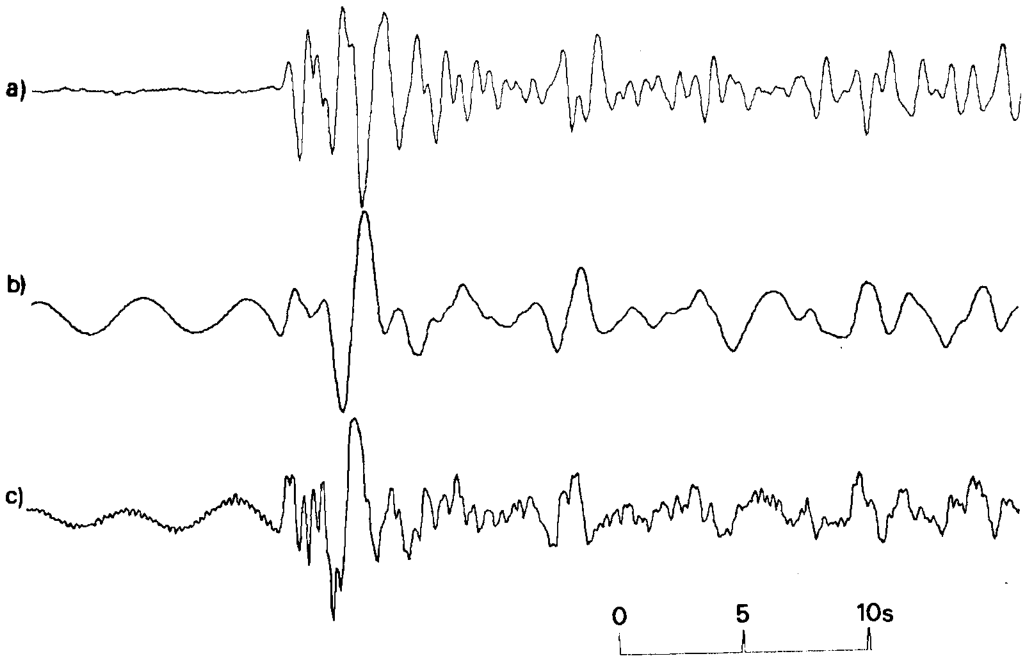

Figure 68. P seismograms recorded at Yellowknife,Canada from N.T.S explosion CREWLINE.

(a) Short-period array-sum seismogram.
(b) Wiener filtered phaseless broad-band seismogram.
(c) Seismogram (b) corrected for anelastic attenuation assuming t*=0.5s.

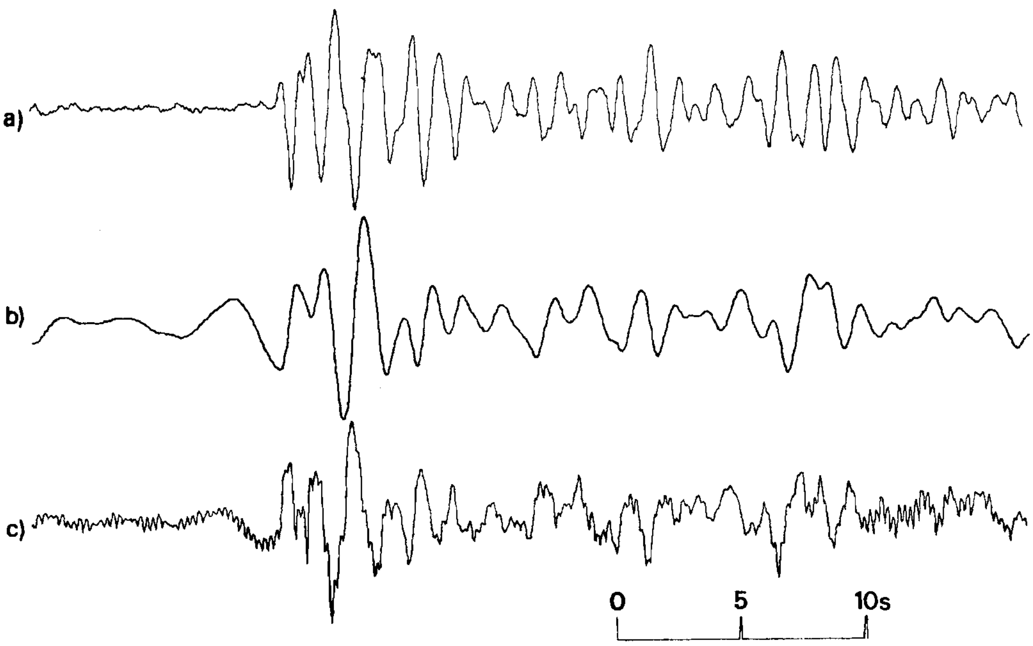

Figure 69. P seismograms recorded at Yellowknife,Canada from N.T.S explosion STRAKE.

(a) Short-period array-sum seismogram.
(b) Wiener filtered phaseless broad-band seismogram.
(c) Seismogram (b) corrected for anelastic attenuation assuming t*=0.5s.

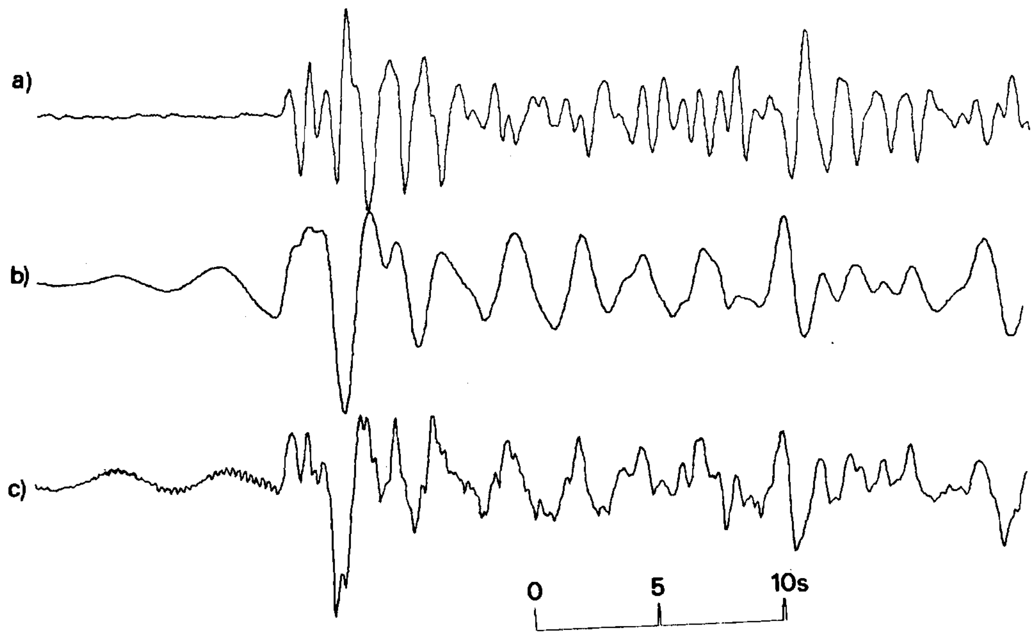

Figure 70. P seismograms recorded at Yellowknife, Canada from N.T.S explosion SCANTLING.

(a) Short-period array-sum seismogram.
(b) Wiener filtered phaseless broad-band seismogram.
(c) Seismogram (b) corrected for anelastic attenuation assuming t*=0.5s.

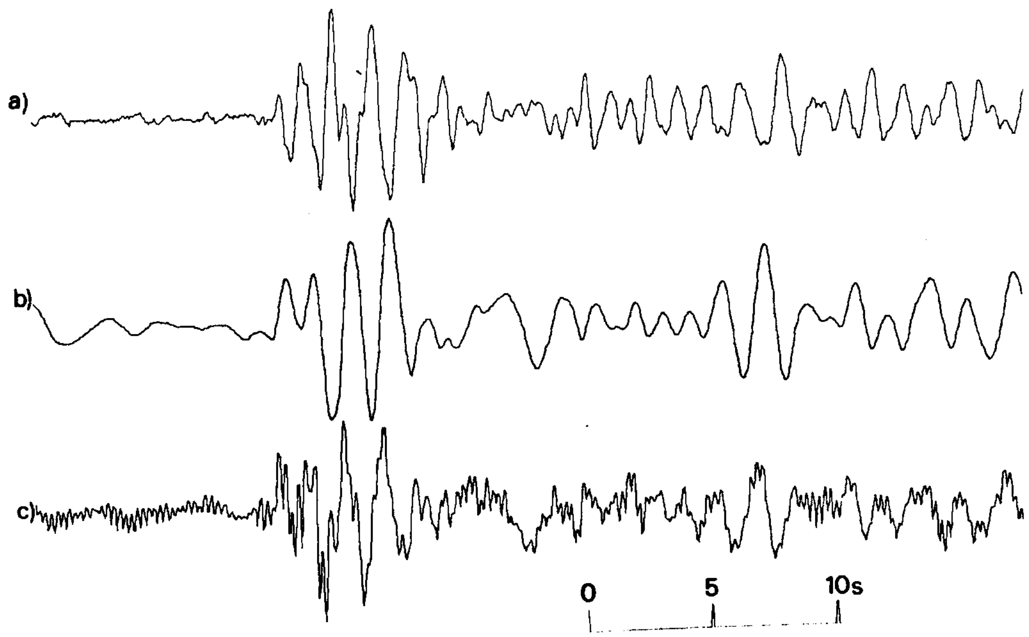

Figure 71. P seismograms recorded at Yellowknife, Canada from N.T.S explosion COULOMNIERS.

(a) Short-period array-sum seismogram.
(b) Wiener filtered phaseless broad-band seismogram.
(c) Seismogram (b) corrected for anelastic attenuation assuming t*=0.5s.

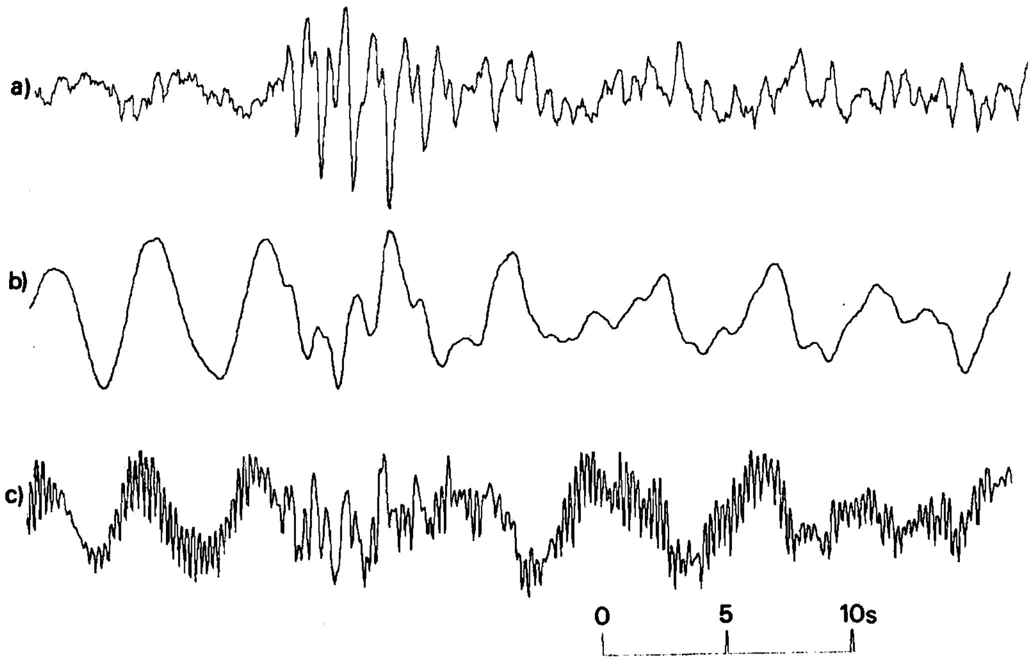

Figure 72. P seismograms recorded at Yellowknife,Canada from N.T.S explosion SEAMOUNT.

(a) Short-period array-sum seismogram.
(b) Wiener filtered phaseless broad-band seismogram.
(c) Seismogram (b) corrected for anelastic attenuation assuming t*=0.5s.

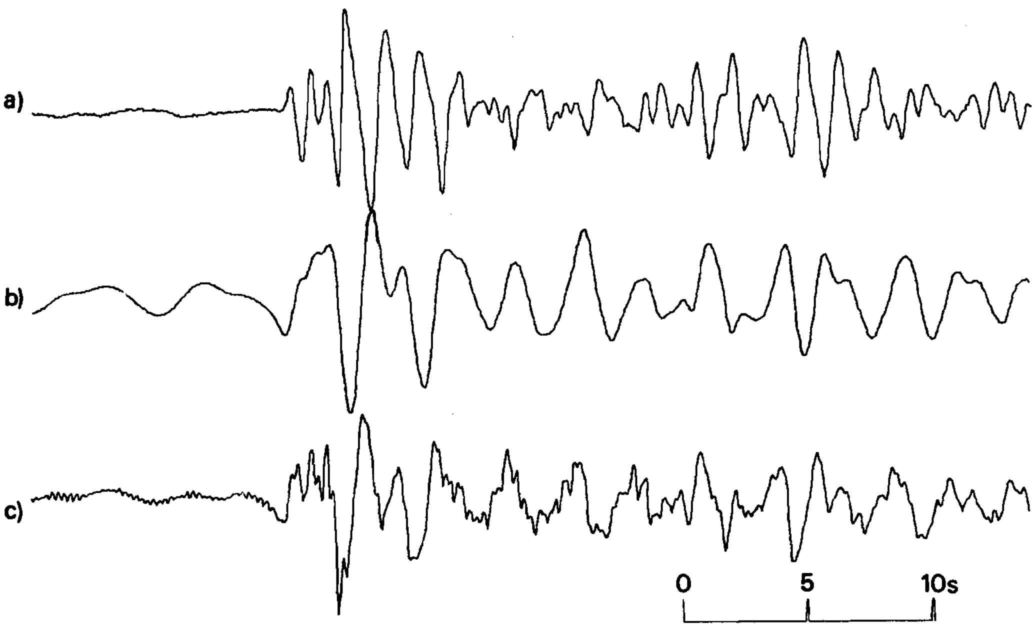

Figure 73. P seismograms recorded at Yellowknife,Canada from N.T.S explosion REBLOCHLON.

(a) Short-period array-sum seismogram.
(b) Wiener filtered phaseless broad-band seismogram.
(c) Seismogram (b) corrected for anelastic attenuation assuming t*=0.5s.

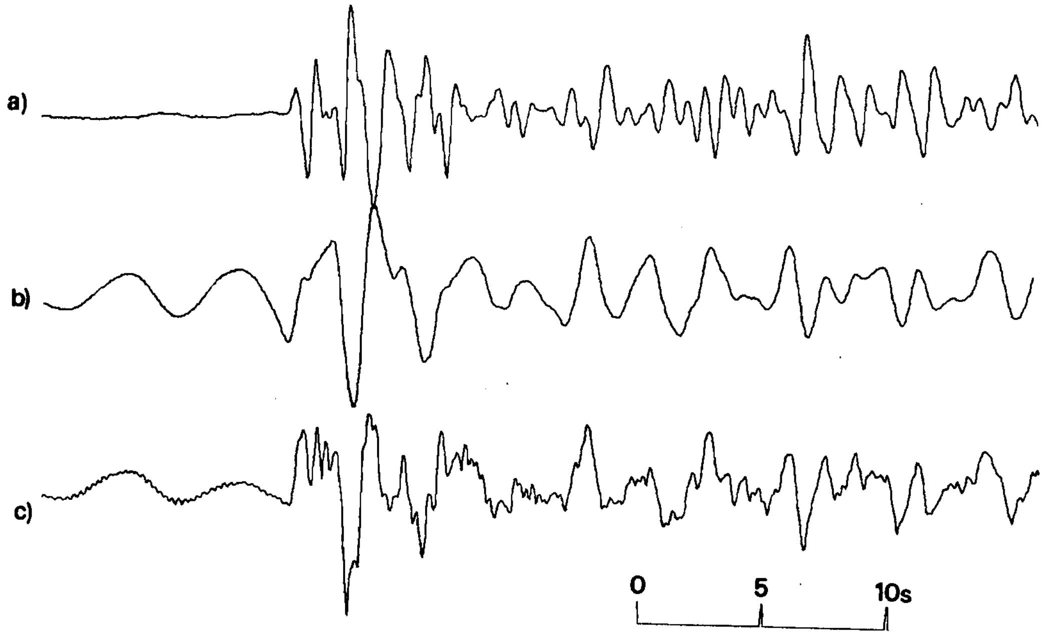

Figure 74. P seismograms recorded at Yellowknife,Canada from N.T.S explosion ICEBERG.

(a) Short-period array-sum seismogram.
(b) Wiener filtered phaseless broad-band seismogram.
(c) Seismogram (b) corrected for anelastic attenuation assuming t*=0.5s.

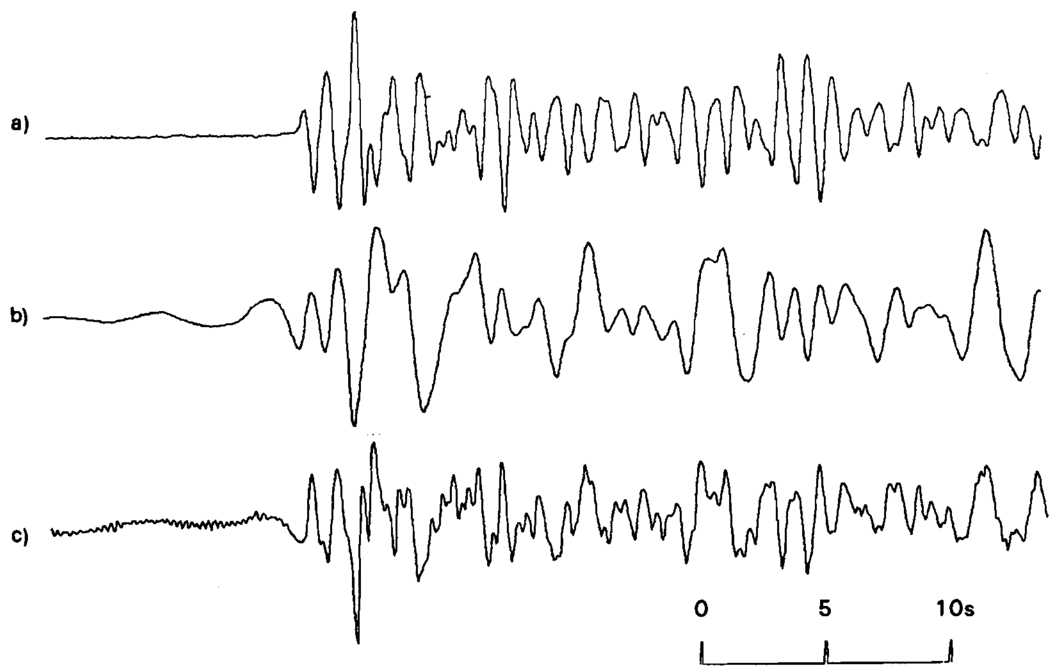

Figure 75. P seismograms recorded at Yellowknife,Canada from N.T.S explosion BACKBEACH.

(a) Short-period array-sum seismogram.
(b) Wiener filtered phaseless broad-band seismogram.
(c) Seismogram (b) corrected for anelastic attenuation assuming t*=0.5s.

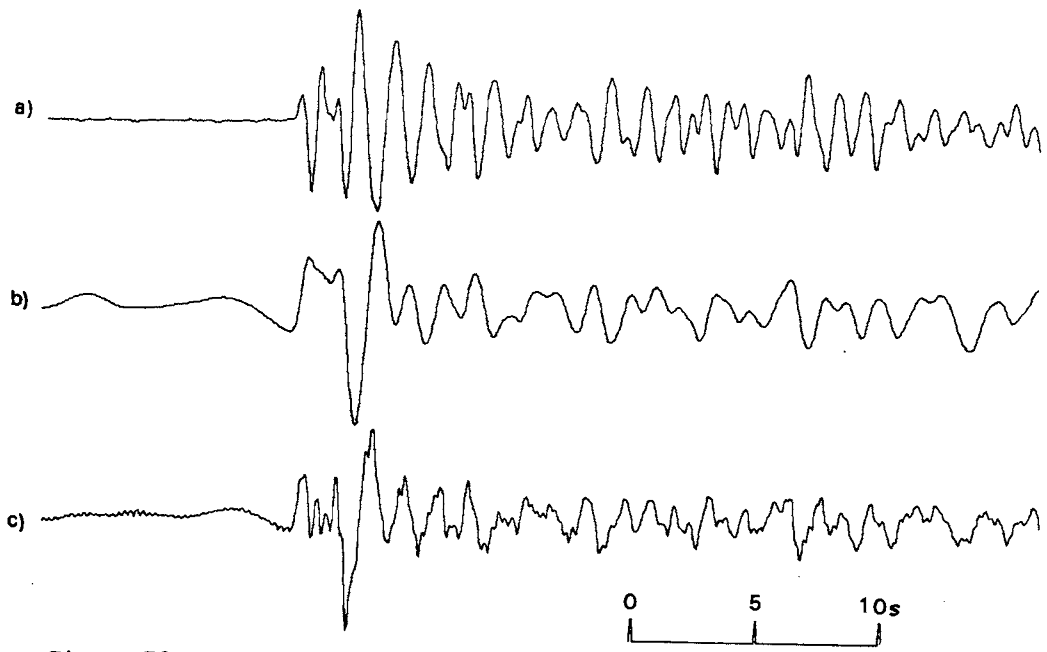

Figure 76. P seismograms recorded at Yellowknife, Canada from N.T.S explosion LOWBALL.

(a) Short-period array-sum seismogram.
(b) Wiener filtered phaseless broad-band seismogram.
(c) Seismogram (b) corrected for anelastic attenuation assuming t*=0.5s.

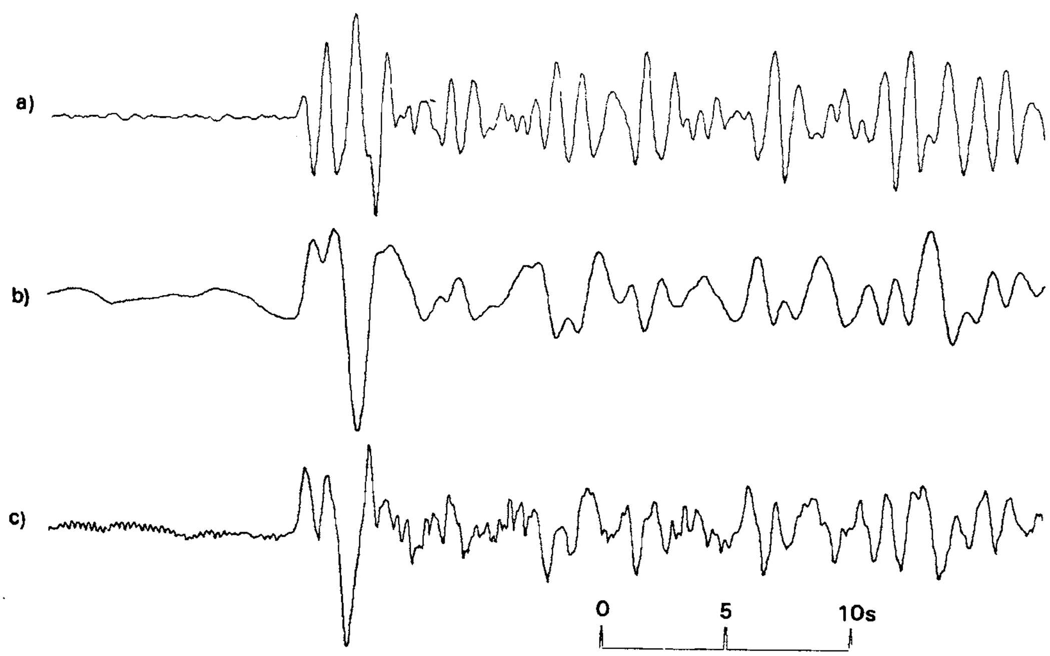

Figure 77. P seismograms recorded at Yellowknife, Canada from N.T.S explosion PANIR.

(a) Short-period array-sum seismogram.
(b) Wiener filtered phaseless broad-band seismogram.
(c) Seismogram (b) corrected for anelastic attenuation assuming t*=0.5s.

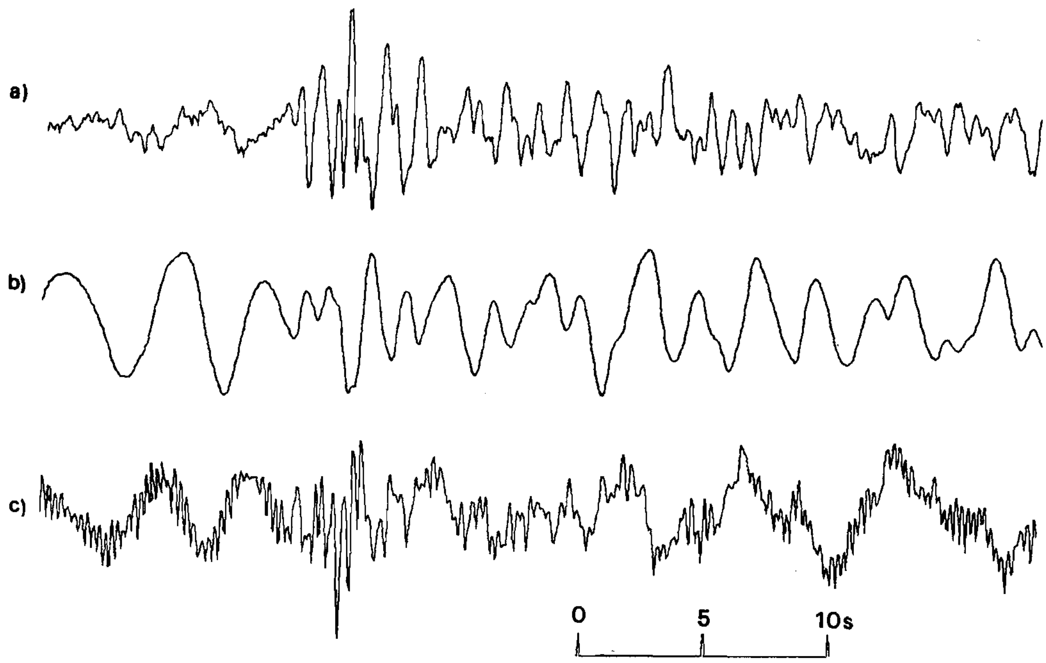

Figure 78. P seismograms recorded at Yellowknife,Canada from N.T.S explosion DIABLO HAWK.

(a) Short-period array-sum seismogram.
(b) Wiener filtered phaseless broad-band seismogram.
(c) Seismogram (b) corrected for anelastic attenuation assuming t*=0.5s.

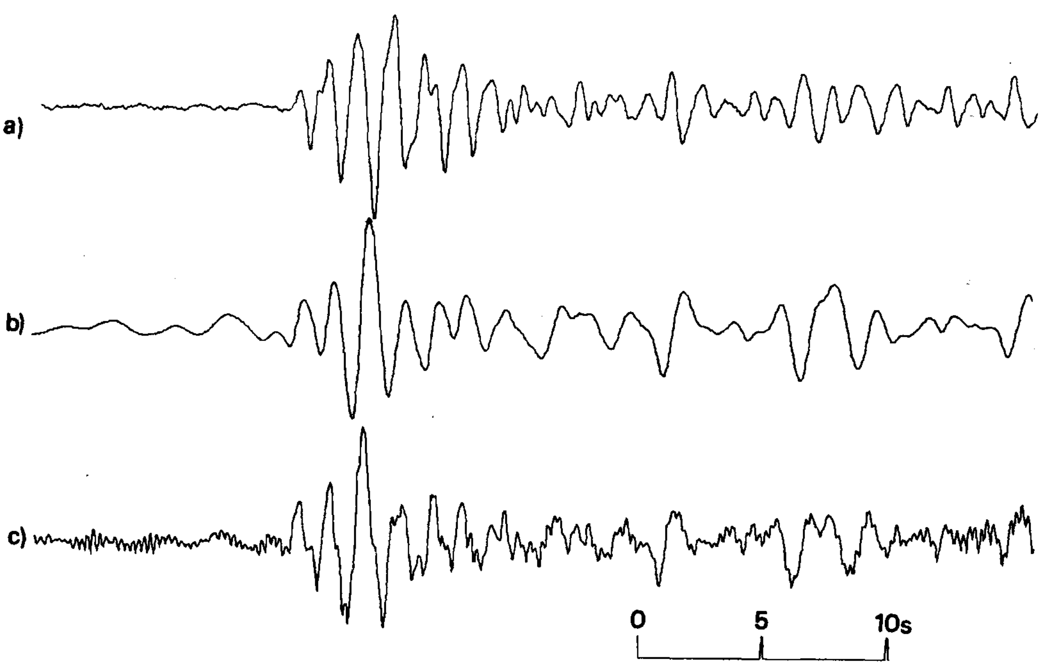

Figure 79. P seismograms recorded at Yellowknife,Canada from N.T.S explosion DRAUGHTS.

(a) Short-period array-sum seismogram.
(b) Wiener filtered phaseless broad-band seismogram.
(c) Seismogram (b) corrected for anelastic attenuation assuming t*=0.5s.

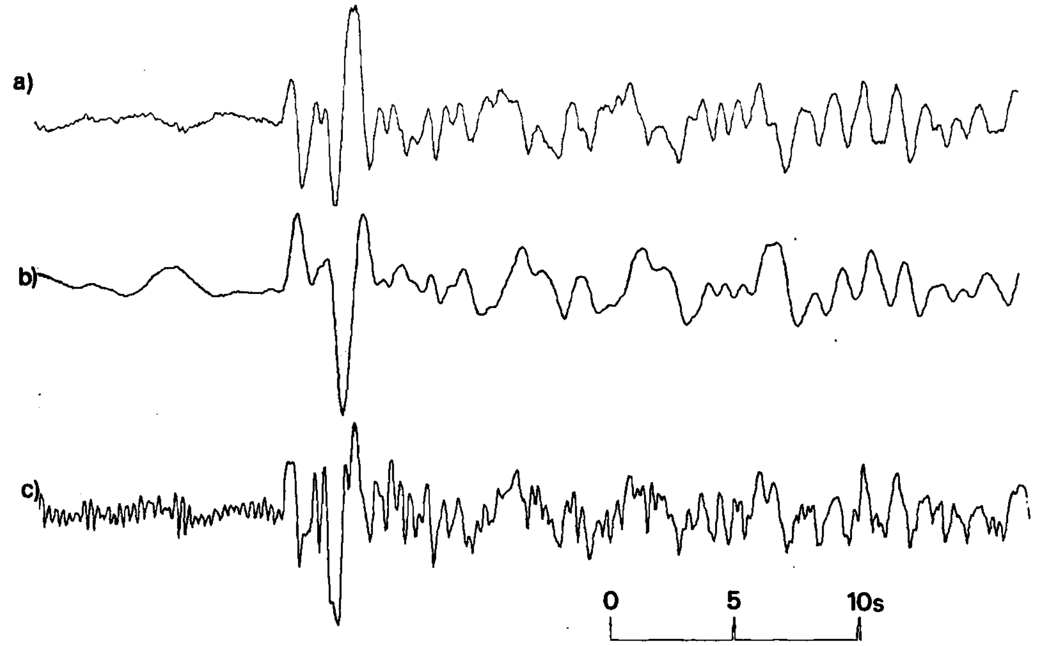

Figure 80. P seismograms recorded at Yellowknife,Canada from N.T.S explosion RUMMY.

(a) Short-period array-sum seismogram.
(b) Wiener filtered phaseless broad-band seismogram.
(c) Seismogram (b) corrected for anelastic attenuation assuming t*=0.5s.

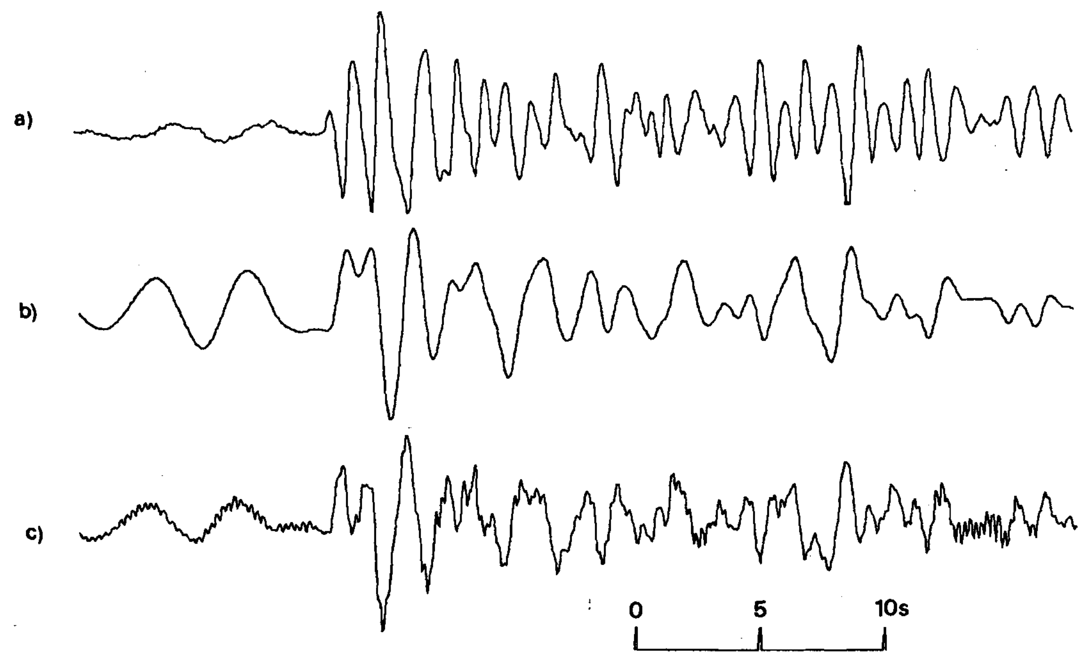

Figure 81. P seismograms recorded at Yellowknife,Canada from N.T.S explosion QUARGEL.

(a) Short-period array-sum seismogram.
(b) Wiener filtered phaseless broad-band seismogram.
(c) Seismogram (b) corrected for anelastic attenuation assuming t*=0.5s.

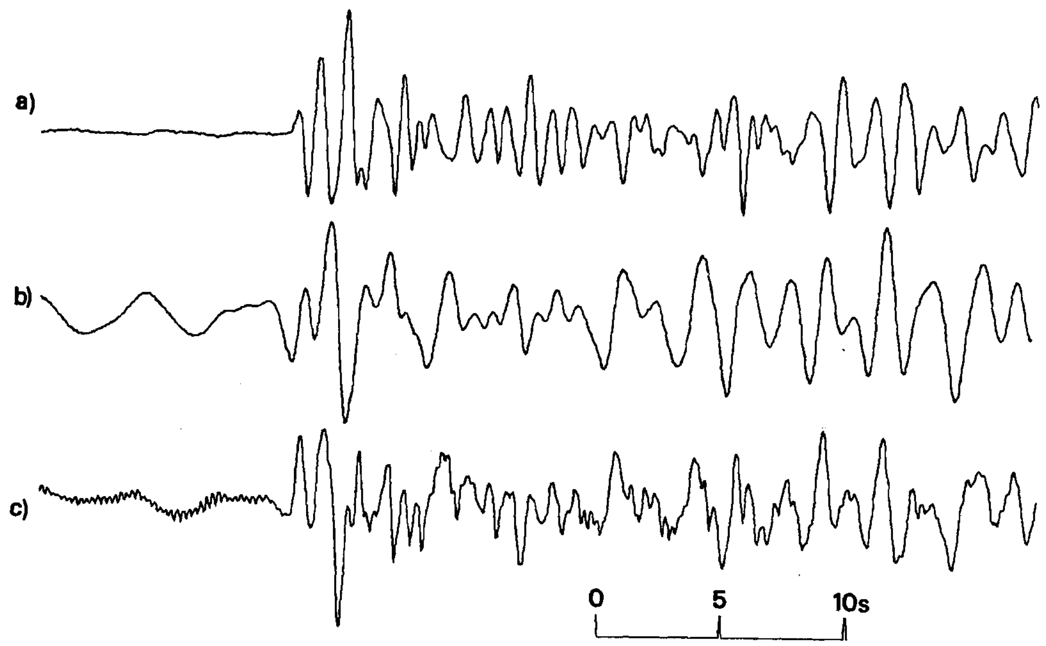

Figure 82. P seismograms recorded at Yellowknife,Canada from N.T.S explosion FARM.

(a) Short-period array-sum seismogram.
(b) Wiener filtered phaseless broad-band seismogram.
(c) Seismogram (b) corrected for anelastic attenuation assuming t*=0.5s.

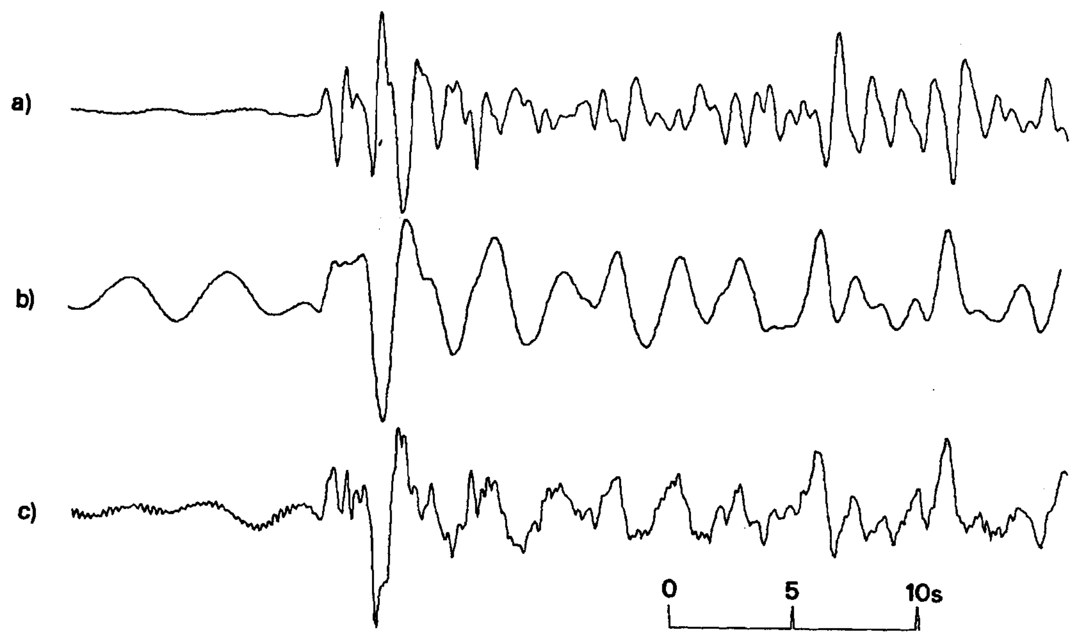

Figure 83. P seismograms recorded at Yellowknife,Canada from N.T.S explosion QUINELLA.

(a) Short-period array-sum seismogram.
(b) Wiener filtered phaseless broad-band seismogram.
(c) Seismogram (b) corrected for anelastic attenuation assuming t*=0.5s.

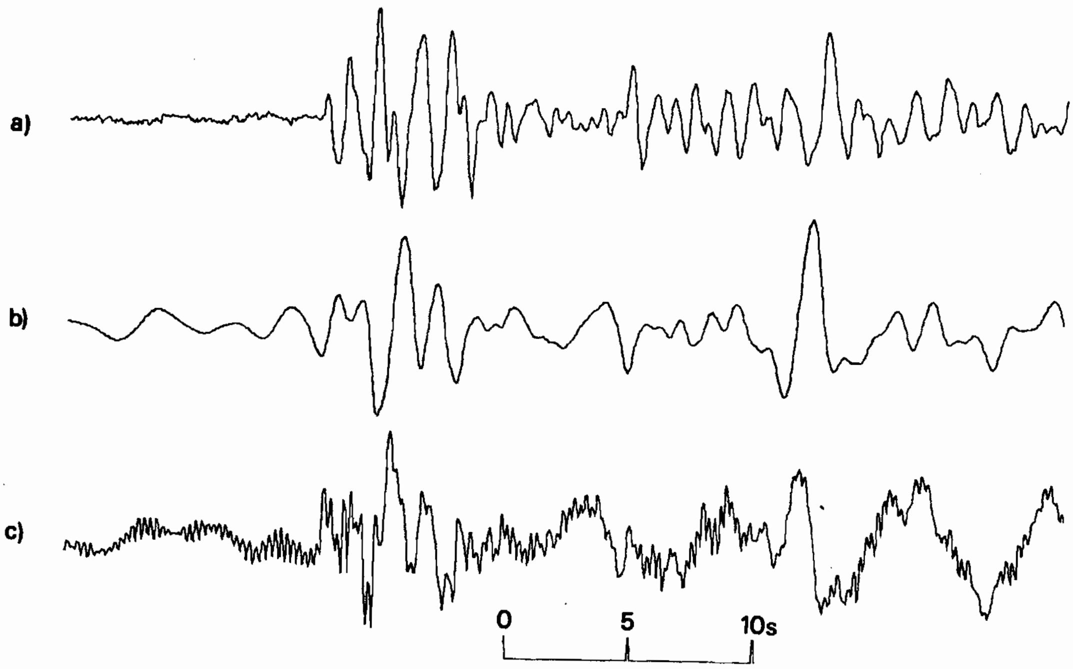

Figure 84. P seismograms recorded at Yellowknife,Canada from N.T.S explosion KLOSTER.

(a) Short-period array-sum seismogram.
(b) Wiener filtered phaseless broad-band seismogram.
(c) Seismogram (b) corrected for anelastic attenuation assuming t*=0.5s.

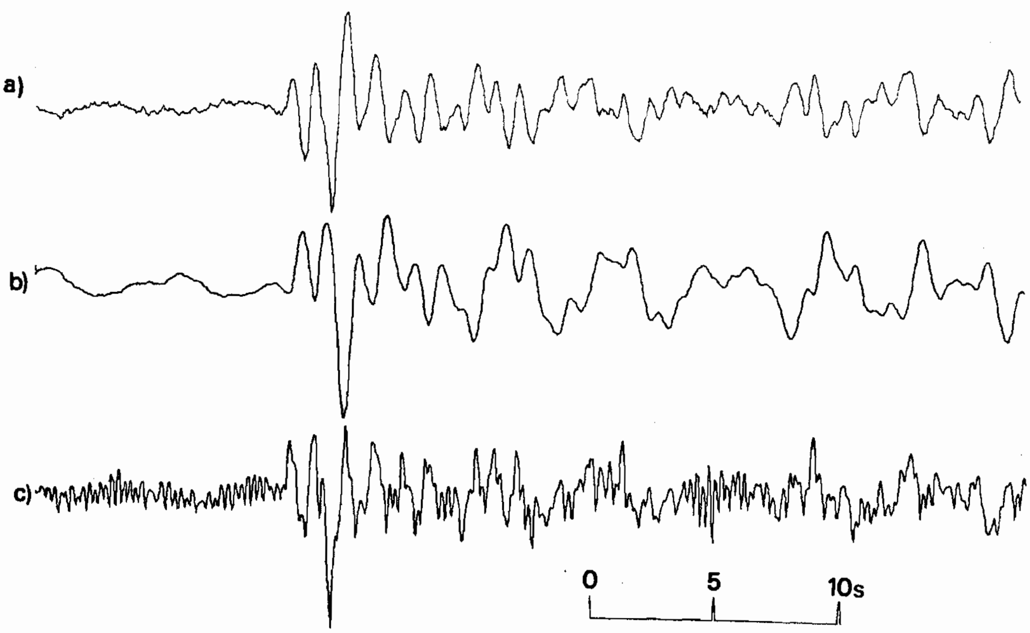

Figure 85. P seismograms recorded at Yellowknife,Canada from N.T.S explosion PEPATO.

(a) Short-period array-sum seismogram.
(b) Wiener filtered phaseless broad-band seismogram.
(c) Seismogram (b) corrected for anelastic attenuation assuming t*=0.5s.

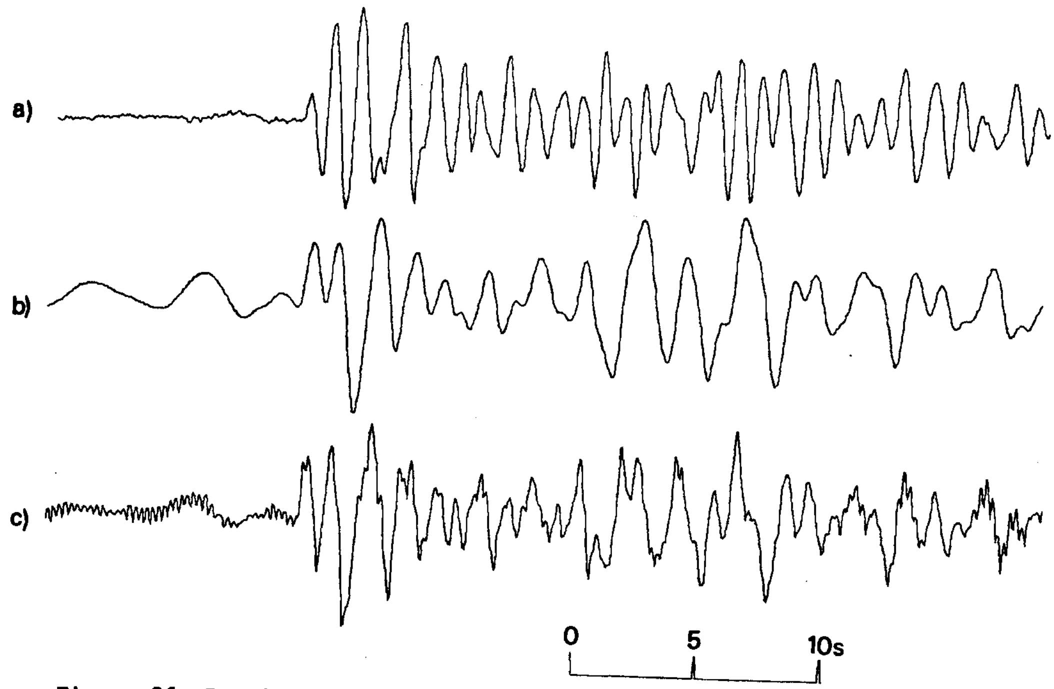

Figure 86. P seismograms recorded at Yellowknife, Canada from N.T.S explosion FAJY.

(a) Short-period array-sum seismogram.
(b) Wiener filtered phaseless broad-band seismogram.
(c) Seismogram (b) corrected for anelastic attenuation assuming t*=0.5s.

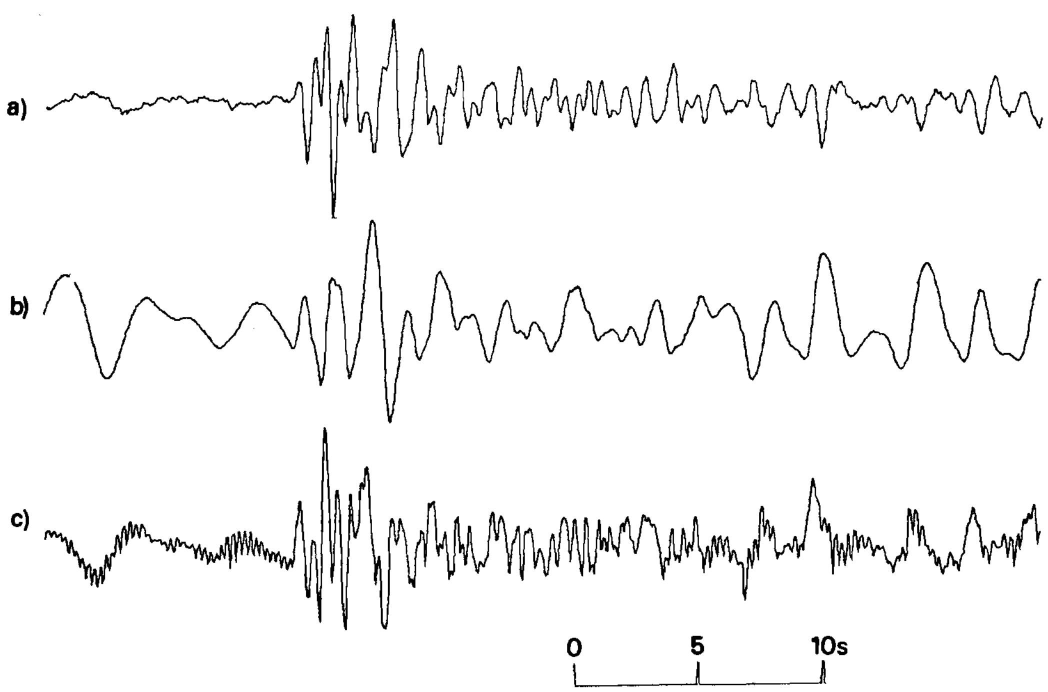

Figure 87. P seismograms recorded at Yellowknife, Canada from N.T.S explosion OFFSHORE.

(a) Short-period array-sum seismogram.
(b) Wiener filtered phaseless broad-band seismogram.
(c) Seismogram (b) corrected for anelastic attenuation assuming t*=0.5s.

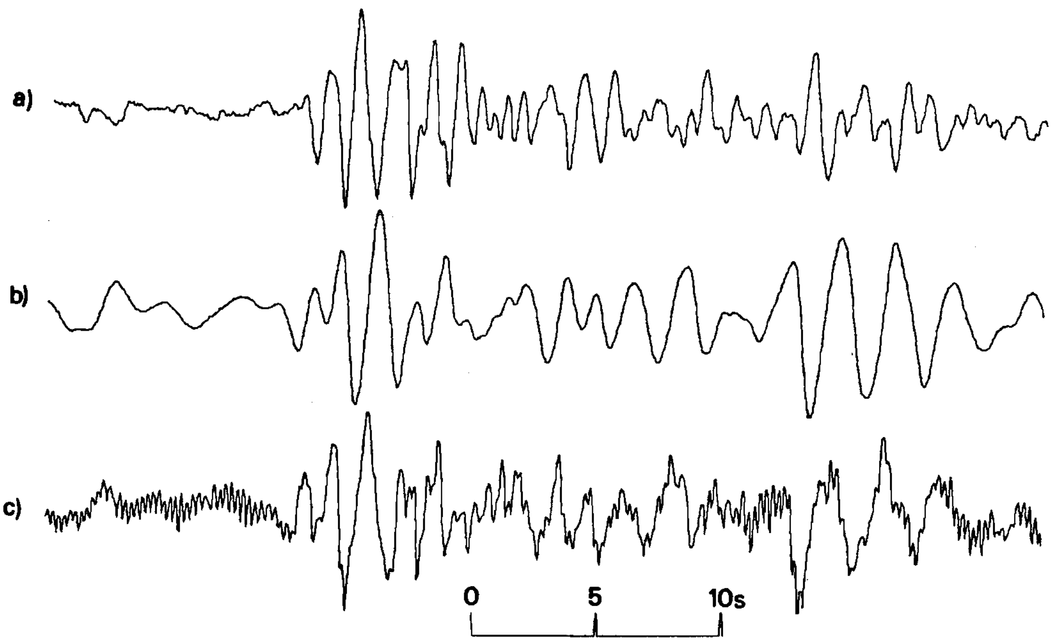

Figure 88. P seismograms recorded at Yellowknife,Canada from N.T.S explosion NESSEL.

(a) Short-period array-sum seismogram.
(b) Wiener filtered phaseless broad-band seismogram.
(c) Seismogram (b) corrected for anelastic attenuation assuming t*=0.5s.

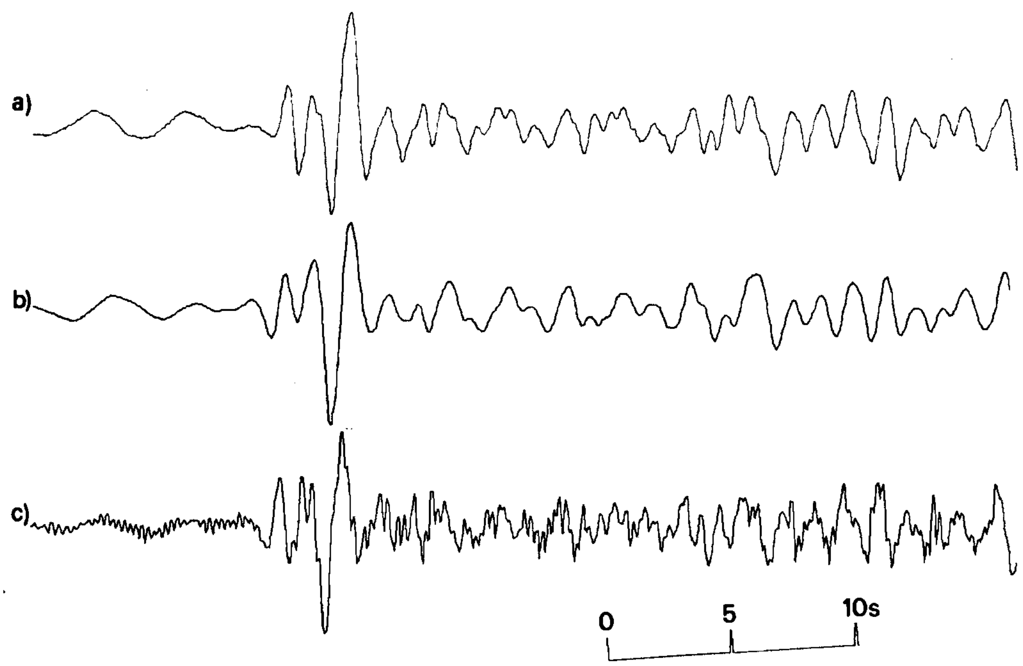

Figure 89. P seismograms recorded at Yellowknife,Canada from N.T.S explosion HEARTS.

(a) Short-period array-sum seismogram.
(b) Wiener filtered phaseless broad-band seismogram.
(c) Seismogram (b) corrected for anelastic attenuation assuming t*=0.5s.

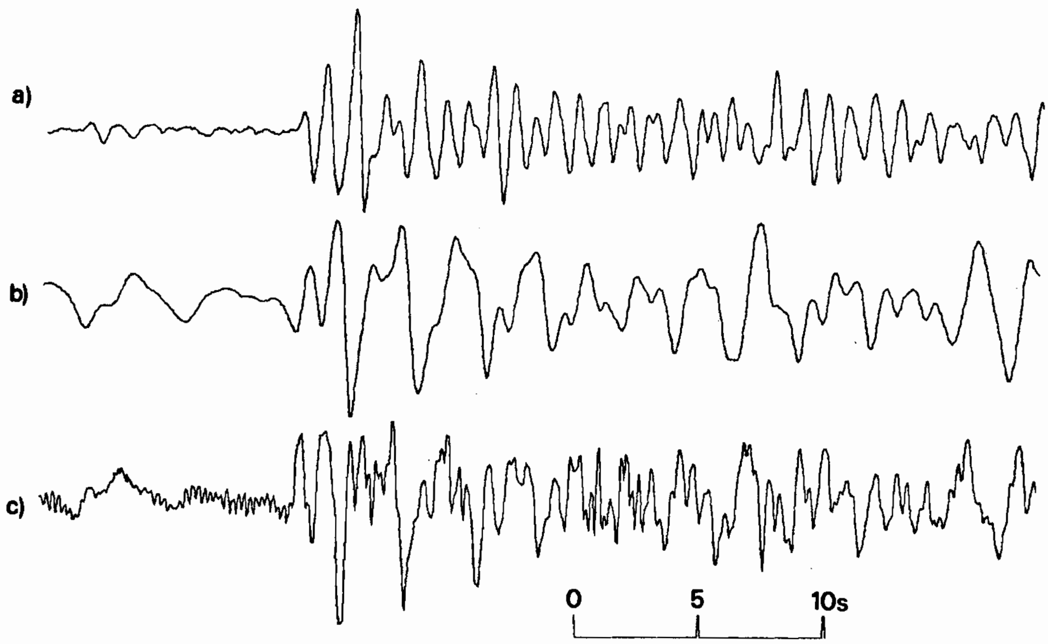

Figure 90. P seismograms recorded at Yellowknife,Canada from N.T.S explosion SHEEPSHEAD.

(a) Short-period array-sum seismogram.
(b) Wiener filtered phaseless broad-band seismogram.
(c) Seismogram (b) corrected for anelastic attenuation assuming t*=0.5s.

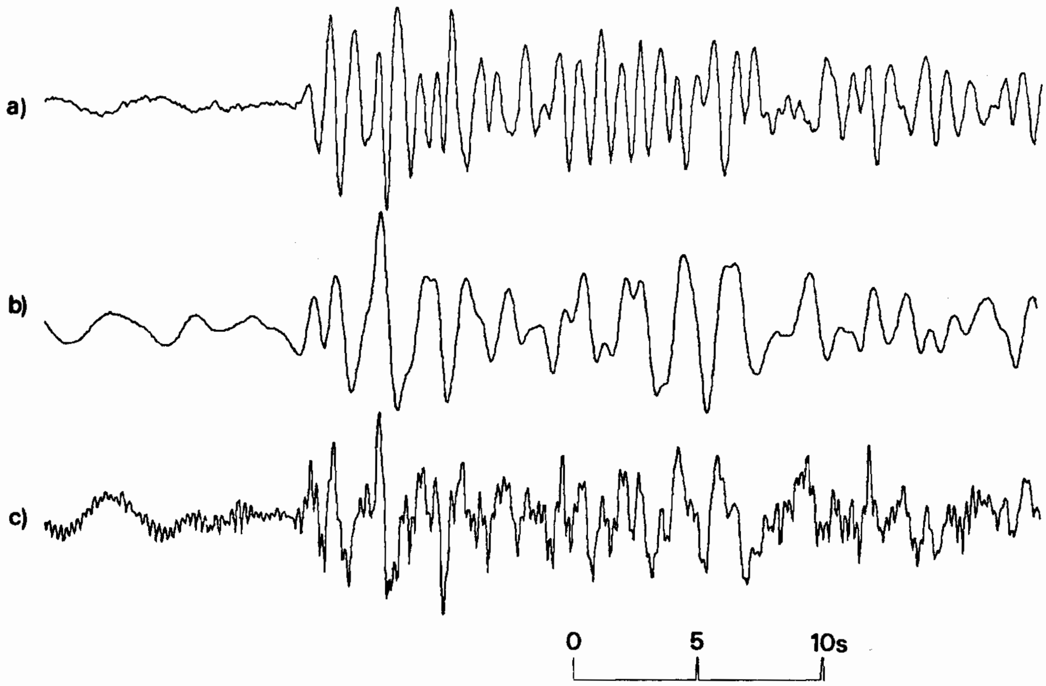

Figure 91. P seismograms recorded at Yellowknife,Canada from N.T.S explosion LIPTAUER.

(a) Short-period array-sum seismogram.
(b) Wiener filtered phaseless broad-band seismogram.
(c) Seismogram (b) corrected for anelastic attenuation assuming t*=0.5s.

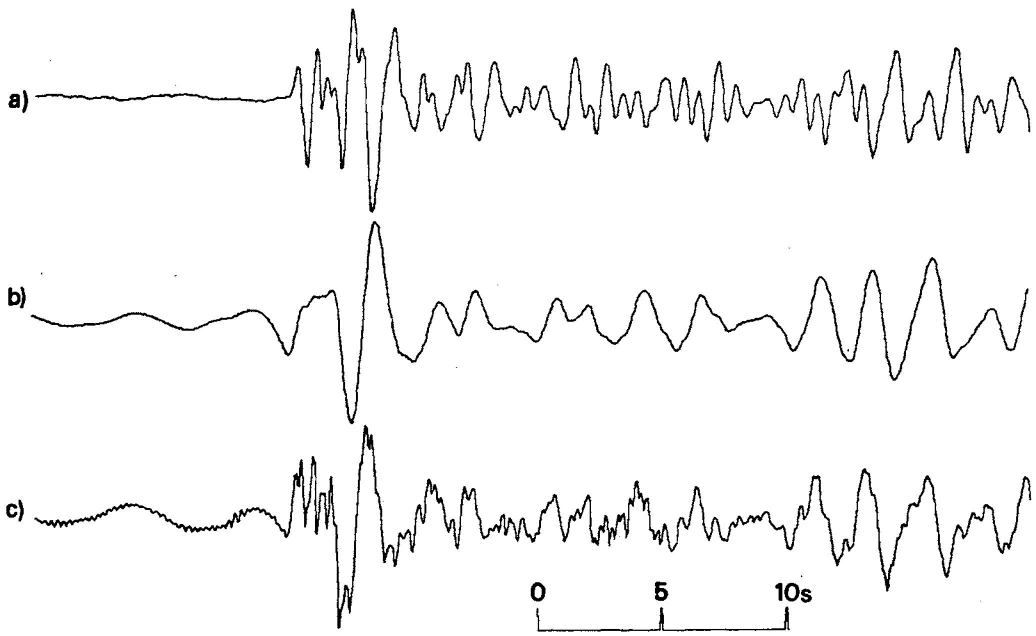

Figure 92. P seismograms recorded at Yellowknife,Canada from N.T.S explosion PYRAMID.

(a) Short-period array-sum seismogram.
(b) Wiener filtered phaseless broad-band seismogram.
(c) Seismogram (b) corrected for anelastic attenuation assuming t*=0.5s.

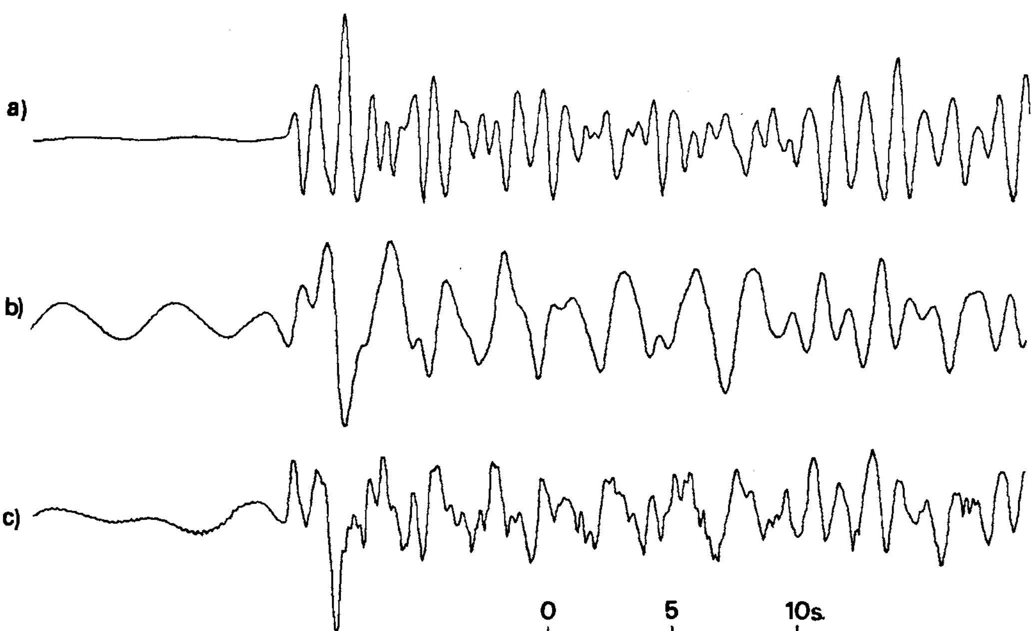

Figure 93. P seismograms recorded at Yellowknife,Canada from N.T.S explosion COLWICK.

(a) Short-period array-sum seismogram.
(b) Wiener filtered phaseless broad-band seismogram.
(c) Seismogram (b) corrected for anelastic attenuation assuming t*=0.5s.

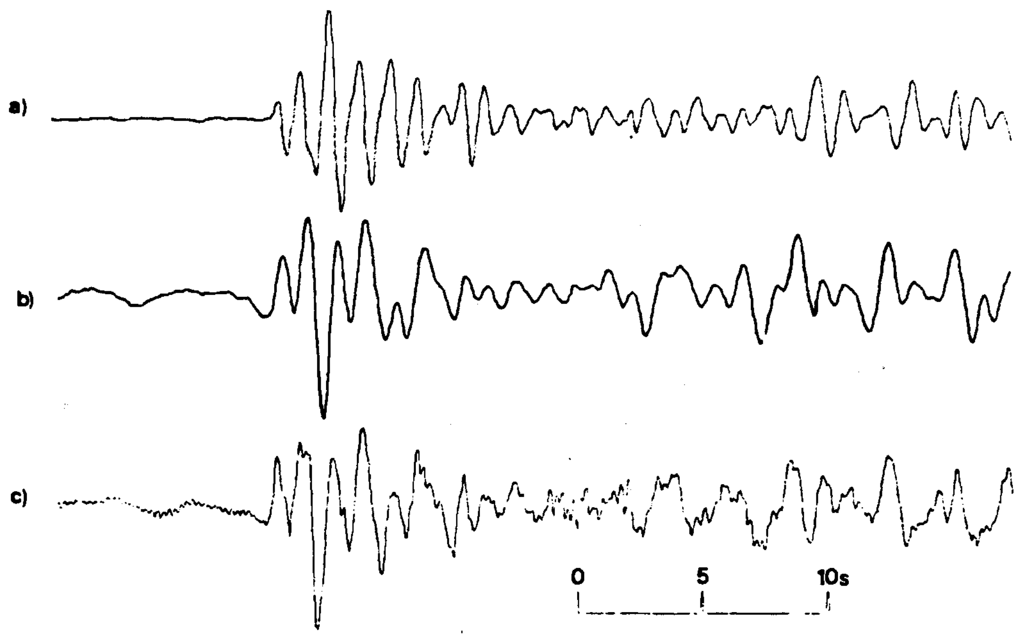

Figure 94. P seismograms recorded at Yellowknife, Canada from N.T.S. explosion KASH.

(a) Short-period array-sum seismogram.
(b) Wiener filtered phaseless broad-band seismogram.
(c) Seismogram (b) corrected for anelastic attenuation assuming $t^*=0.5s$.

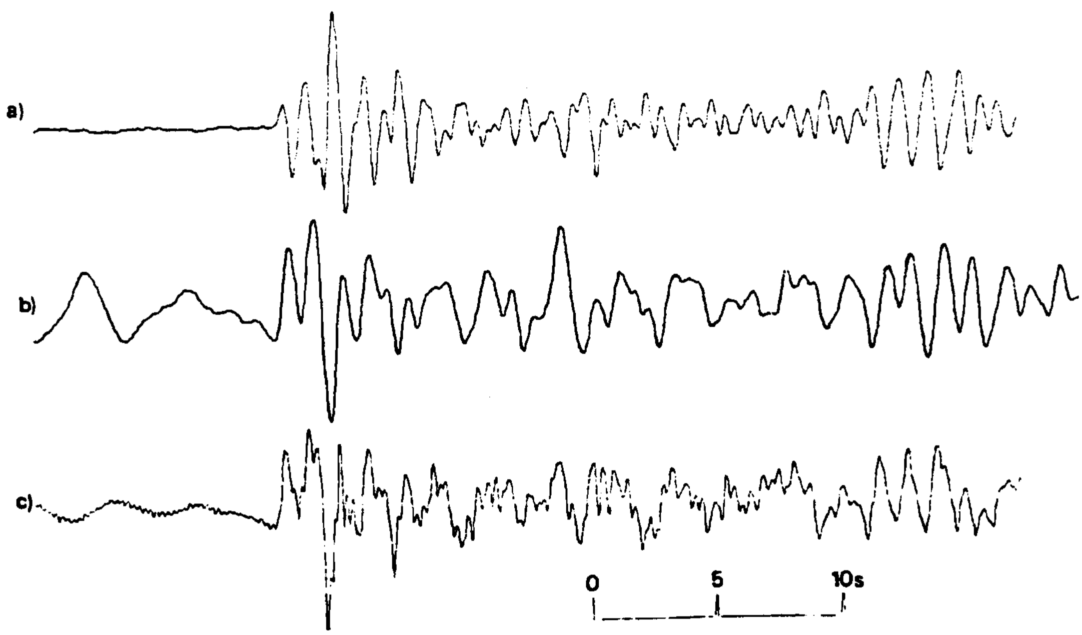

Figure 95. P seismograms recorded at Yellowknife, Canada from N.T.S. explosion TAFI.

(a) Short-period array-sum seismogram.
(b) Wiener filtered phaseless broad-band seismogram.
(c) Seismogram (b) corrected for anelastic attenuation assuming $t^*=0.5s$.

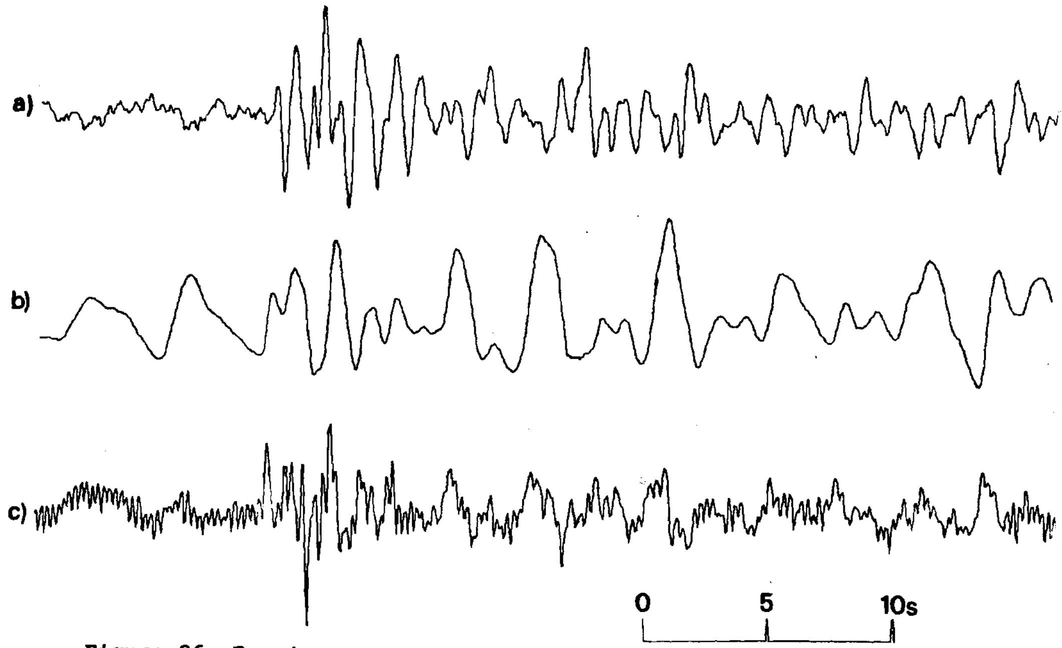

Figure 96. P seismograms recorded at Yellowknife,Canada from N.T.S. explosion MINERS IRON.

(a) Short-period array-sum seismogram.
(b) Wiener filtered phaseless broad-band seismogram.
(c) Seismogram (b) corrected for anelastic attenuation assuming t*=0.5s.

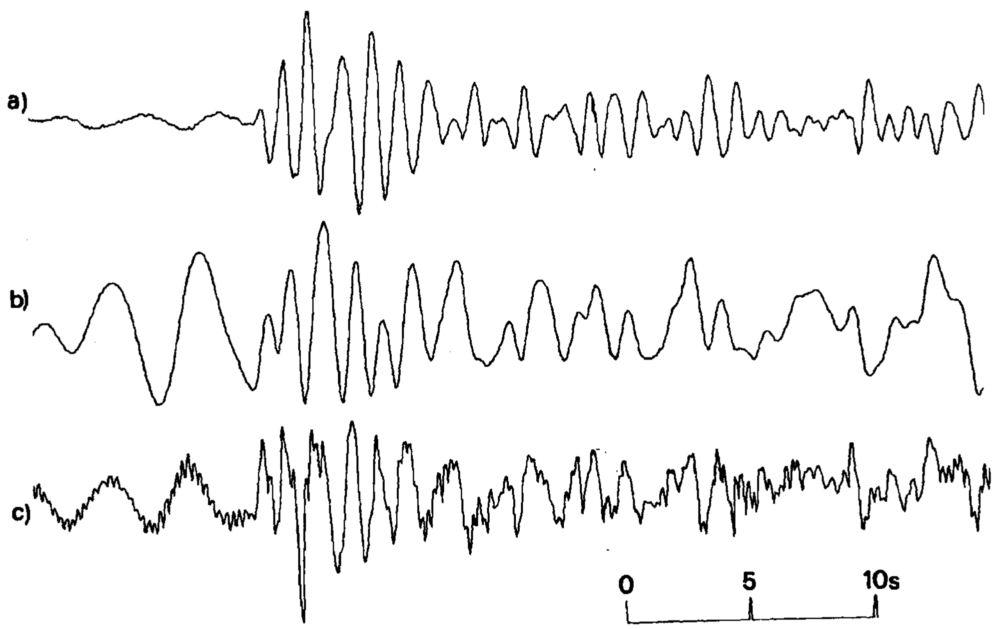

Figure 97. P seismograms recorded at Yellowknife,Canada from N.T.S. explosion SERPA.

(a) Short-period array-sum seismogram.
(b) Wiener filtered phaseless broad-band seismogram.
(c) Seismogram (b) corrected for anelastic attenuation assuming t*=0.5s.

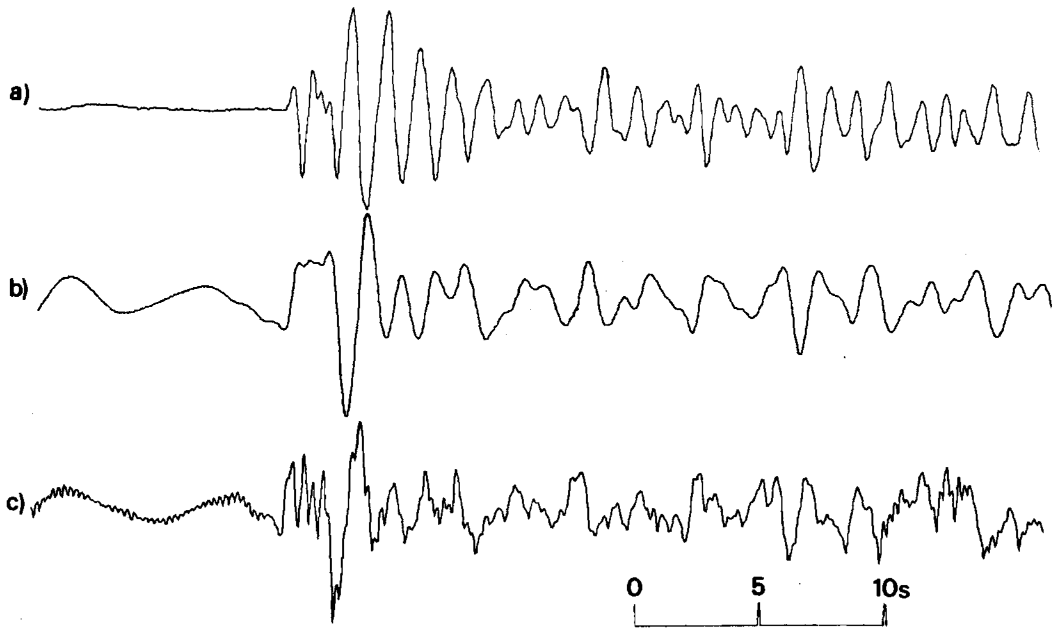

Figure 98. P seismograms recorded at Yellowknife,Canada from N.T.S. explosion BASEBALL.

(a) Short-period array-sum seismogram.
(b) Wiener filtered phaseless broad-band seismogram.
(c) Seismogram (b) corrected for anelastic attenuation assuming t*=0.5s.

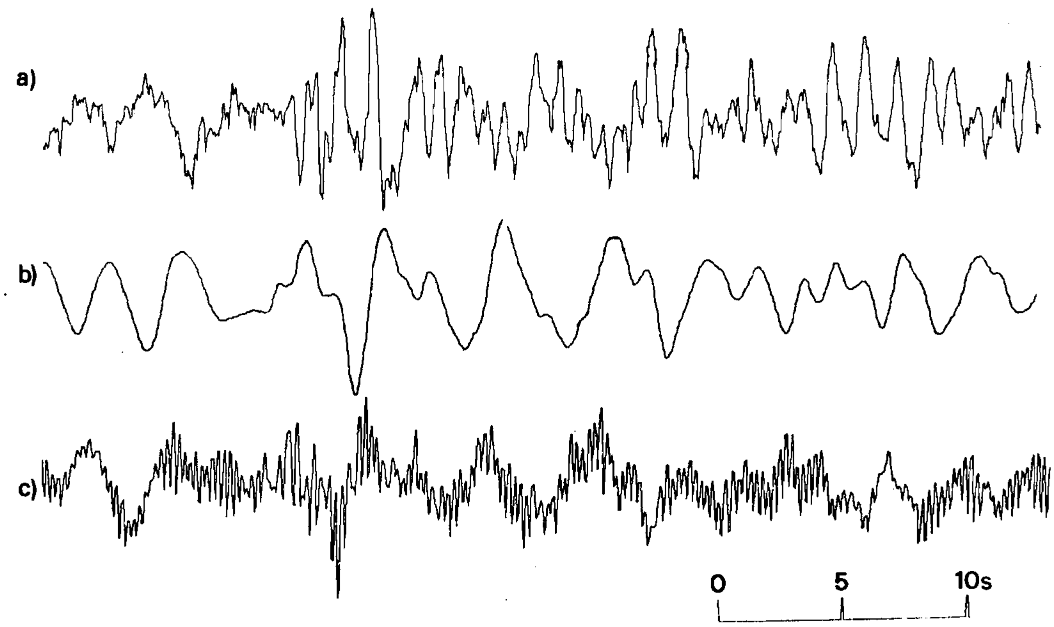

Figure 99. P seismograms recorded at Yellowknife,Canada from N.T.S. explosion ALIGOTE.

(a) Short-period array-sum seismogram.
(b) Wiener filtered phaseless broad-band seismogram.
(c) Seismogram (b) corrected for anelastic attenuation assuming t*=0.5s.

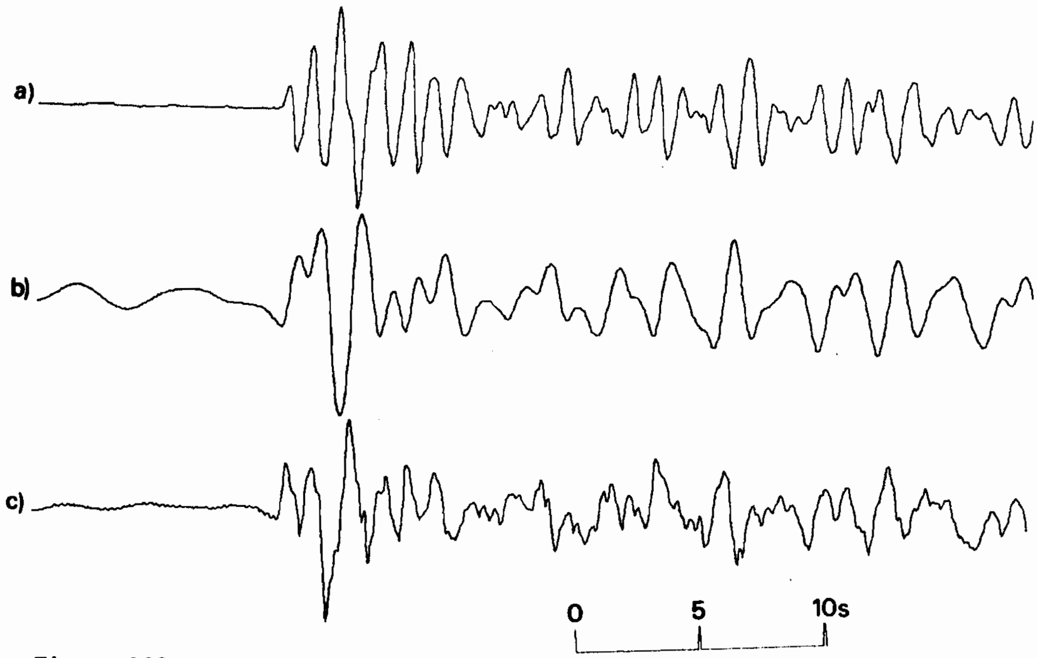

Figure 100. P seismograms recorded at Yellowknife, Canada from N.T.S. explosion HARZER.

(a) Short-period array-sum seismogram.
(b) Wiener filtered phaseless broad-band seismogram.
(c) Seismogram (b) corrected for anelastic attenuation assuming $t^*=0.5s$.

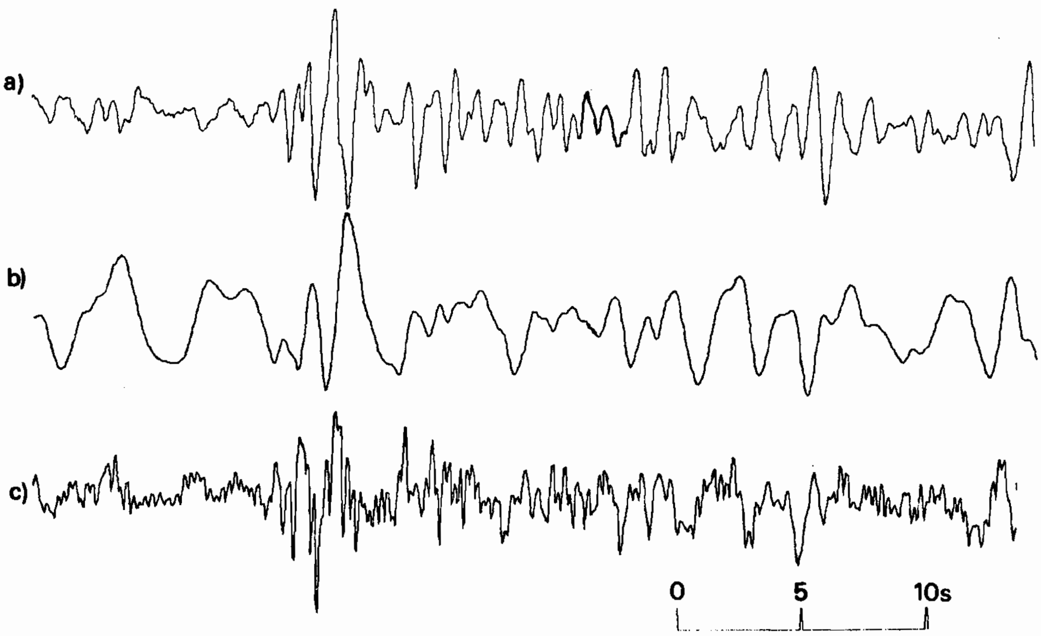

Figure 101. P seismograms recorded at Yellowknife, Canada from N.T.S. explosions PALIZA.

(a) Short-period array-sum seismogram.
(b) Wiener filtered phaseless broad-band seismogram.
(c) Seismogram (b) corrected for anelastic attenuation assuming $t^*=0.5s$.

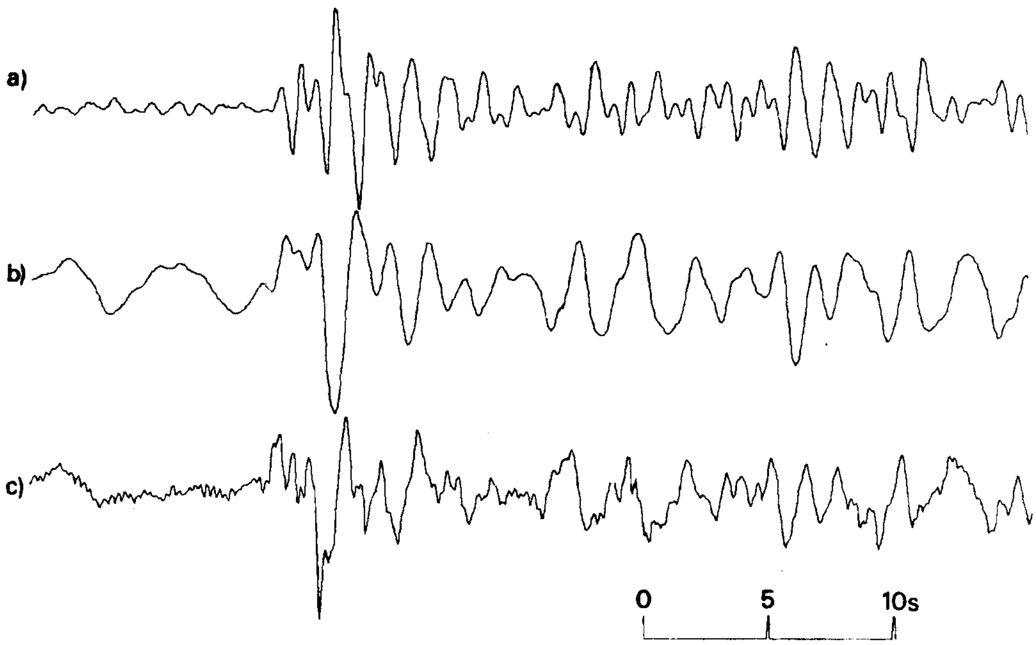

Figure 102. P seismograms recorded at Yellowknife,Canada from N.T.S. explosion ROUSANNE.

(a) Short-period array-sum seismogram.
(b) Wiener filtered phaseless broad-band seismogram.
(c) Seismogram (b) corrected for anelastic attenuation assuming t*=0.5s.

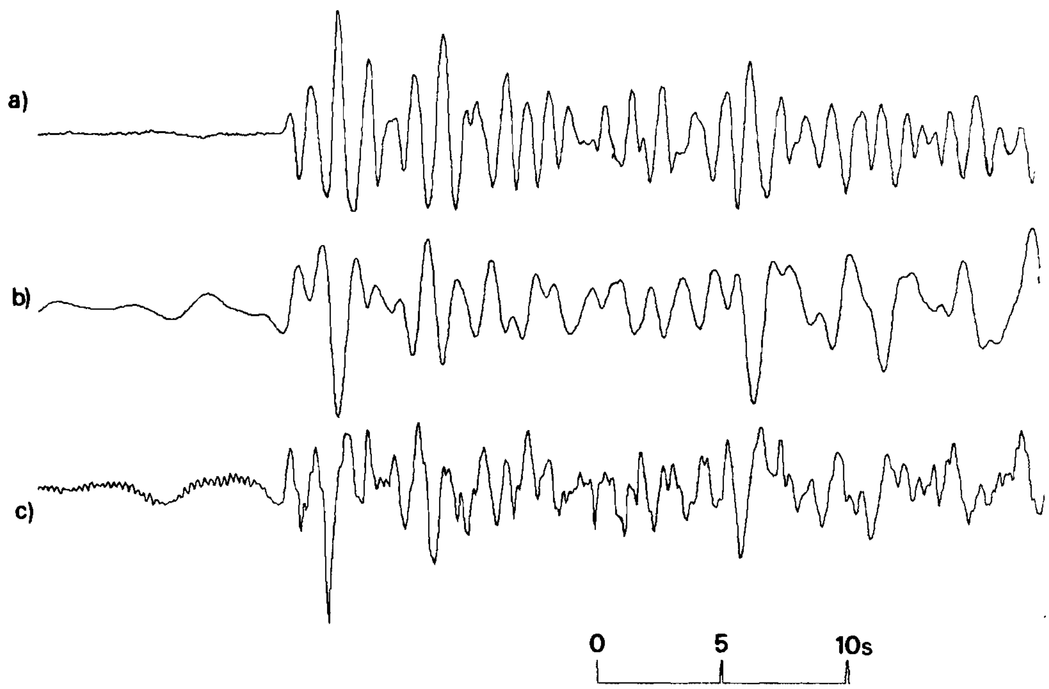

Figure 103. P seismograms recorded at Yellowknife,Canada from N.T.S. explosion MOLBO.

(a) Short-period array-sum seismogram.
(b) Wiener filtered phaseless broad-band seismogram.
(c) Seismogram (b) corrected for anelastic attenuation assuming t*=0.5s.

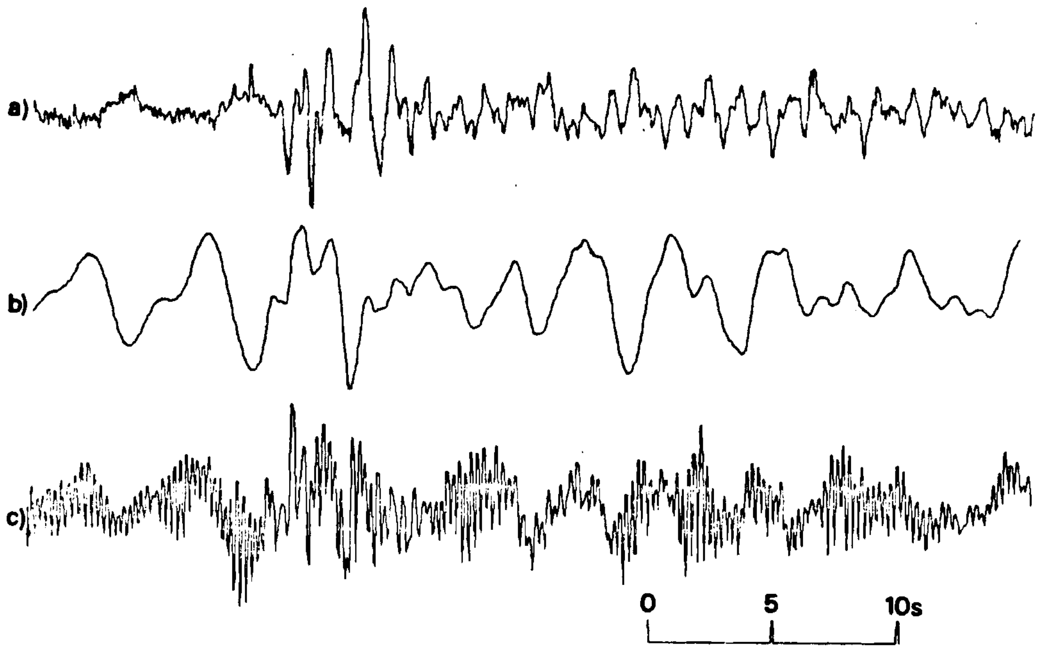

Figure 104. P seismograms recorded at Yellowknife, Canada from N.T.S. explosion TENAJA.

(a) Short-period array-sum seismogram.
(b) Wiener filtered phaseless broad-band seismogram.
(c) Seismogram (b) corrected for anelastic attenuation assuming t*=0.5s.

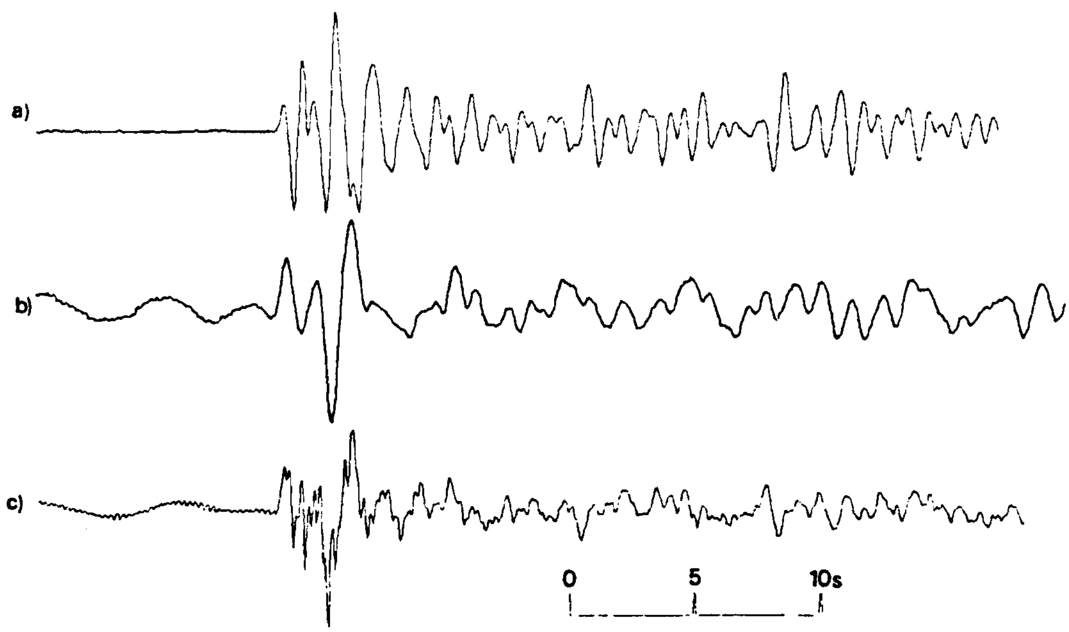

Figure 105. P seismograms recorded at Yellowknife, Canada from N.T.S. explosion BOUSCHET.

(a) Short-period array-sum seismogram.
(b) Wiener filtered phaseless broad-band seismogram.
(c) Seismogram (b) corrected for anelastic attenuation assuming t*=0.5s.

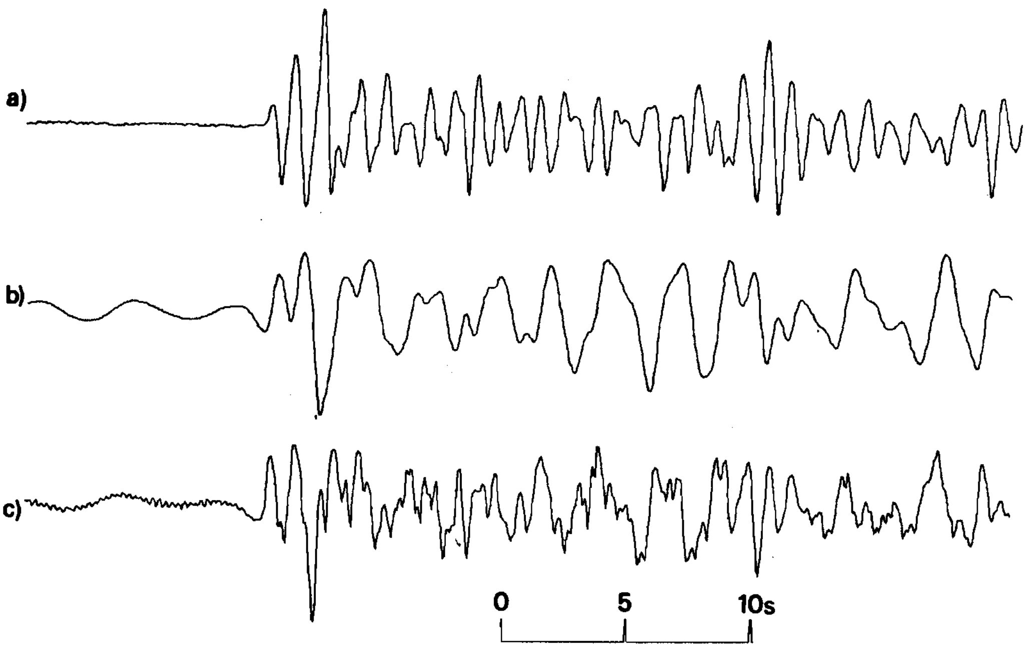

Figure 106. P seismograms recorded at Yellowknife, Canada from N.T.S. explosion NEBBIOLO.

(a) Short-period array-sum seismogram.
(b) Wiener filtered phaseless broad-band seismogram.
(c) Seismogram (b) corrected for anelastic attenuation assuming t*=0.5s.

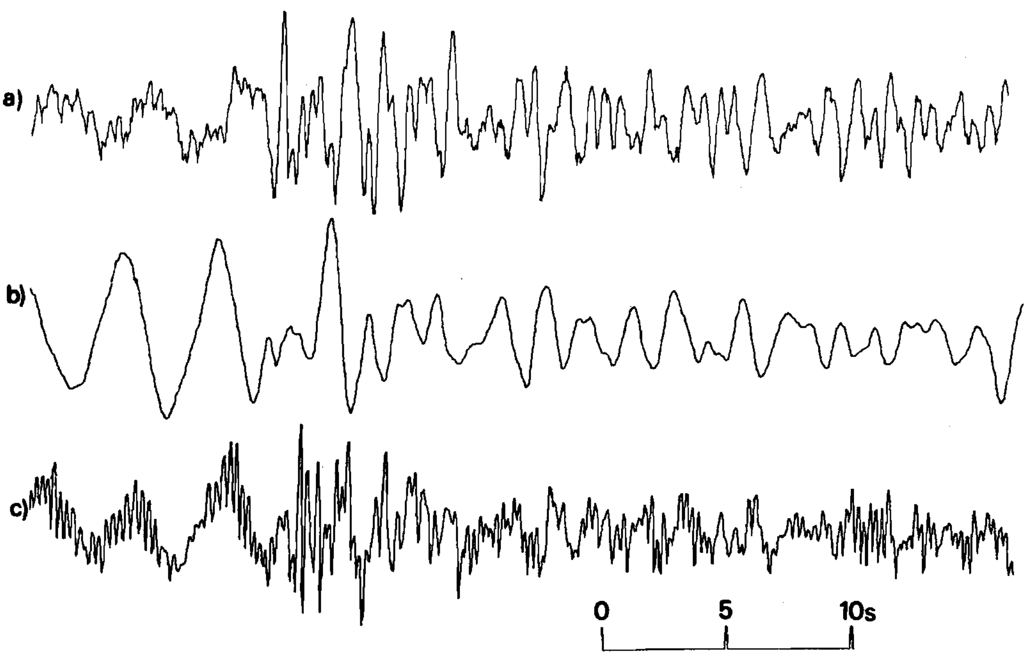

Figure 107. P seismograms recorded at Yellowknife, Canada from N.T.S. explosion MONTEREY.

(a) Short-period array-sum seismogram.
(b) Wiener filtered phaseless broad-band seismogram.
(c) Seismogram (b) corrected for anelastic attenuation assuming t*=0.5s.

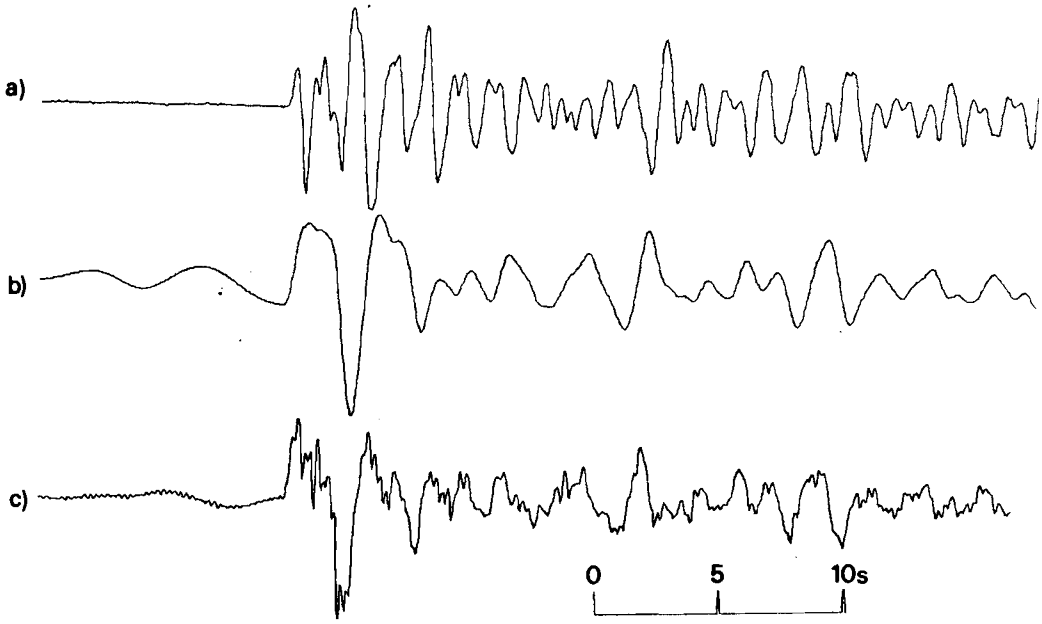

Figure 108. P seismograms recorded at Yellowknife,Canada from N.T.S. explosion ATRISCO.

(a) Short-period array-sum seismogram.
(b) Wiener filtered phaseless broad-band seismogram.
(c) Seismogram (b) corrected for anelastic attenuation assuming t*=0.5s.

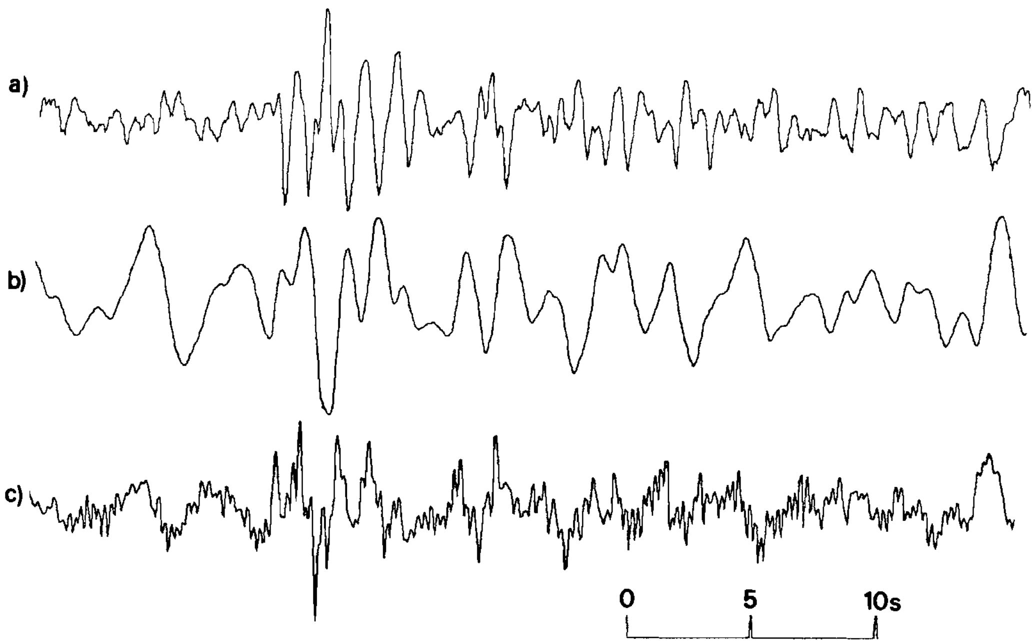

Figure 109. P seismograms recorded at Yellowknife,Canada from N.T.S. explosion DIAMOND ACE + HURON LANDING.

(a) Short-period array-sum seismogram.
(b) Wiener filtered phaseless broad-band seismogram.
(c) Seismogram (b) corrected for anelastic attenuation assuming t*=0.5s.

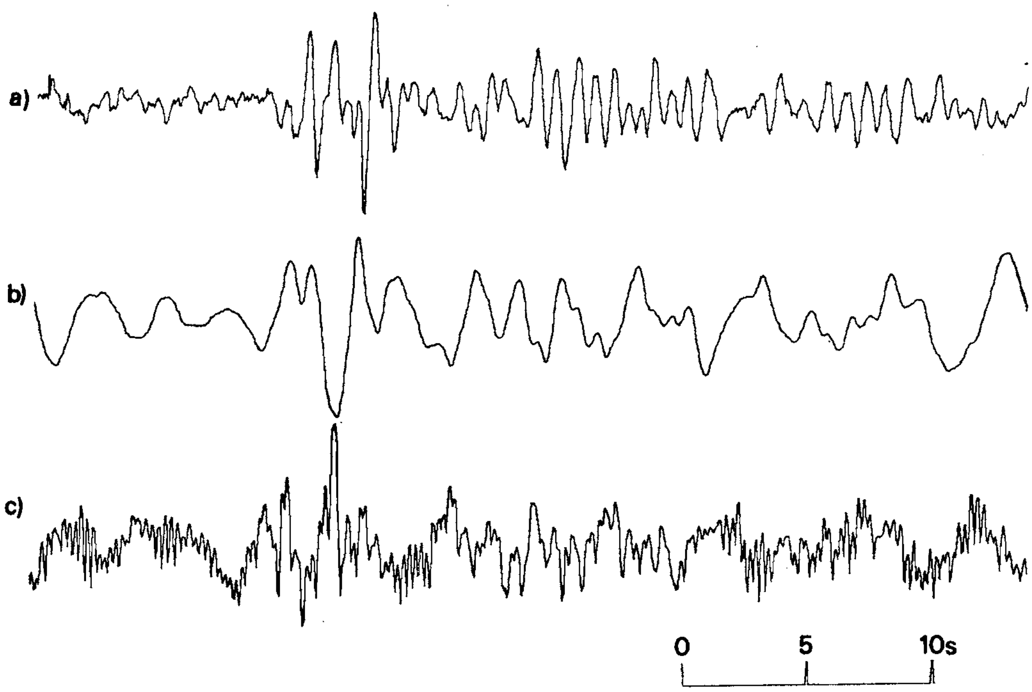

Figure 110. P seismograms recorded at Yellowknife,Canada from N.T.S. explosions FRISCO.

(a) Short-period array-sum seismogram.
(b) Wiener filtered phaseless broad-band seismogram.
(c) Seismogram (b) corrected for anelastic attenuation assuming t*=0.5s.

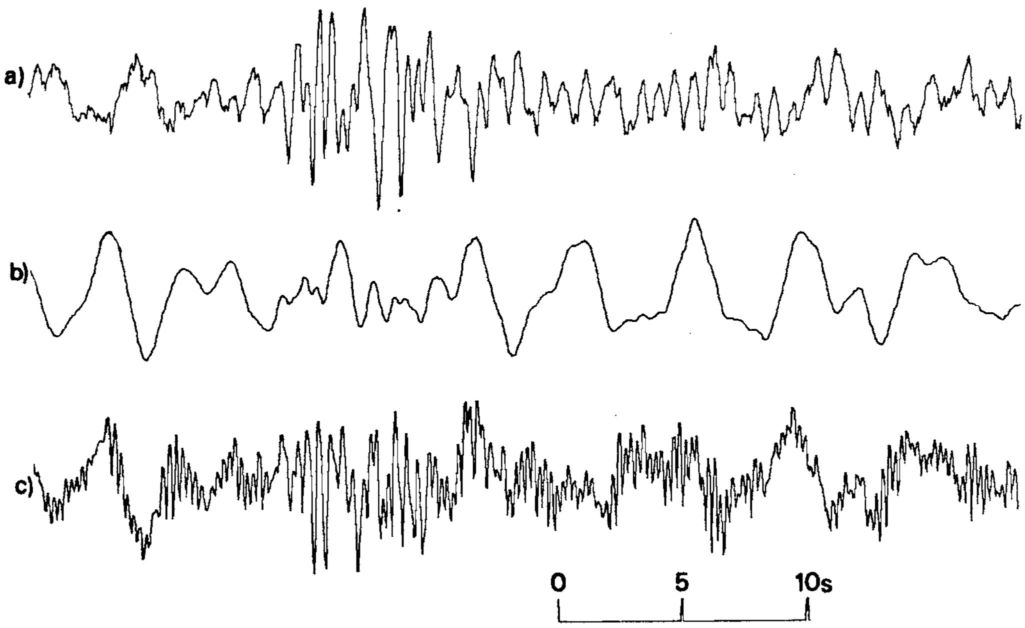

Figure 111. P seismograms recorded at Yellowknife,Canada from N.T.S. explosion SEYVAL.

(a) Short-period array-sum seismogram.
(b) Wiener filtered phaseless broad-band seismogram.
(c) Seismogram (b) corrected for anelastic attenuation assuming t*=0.5s.

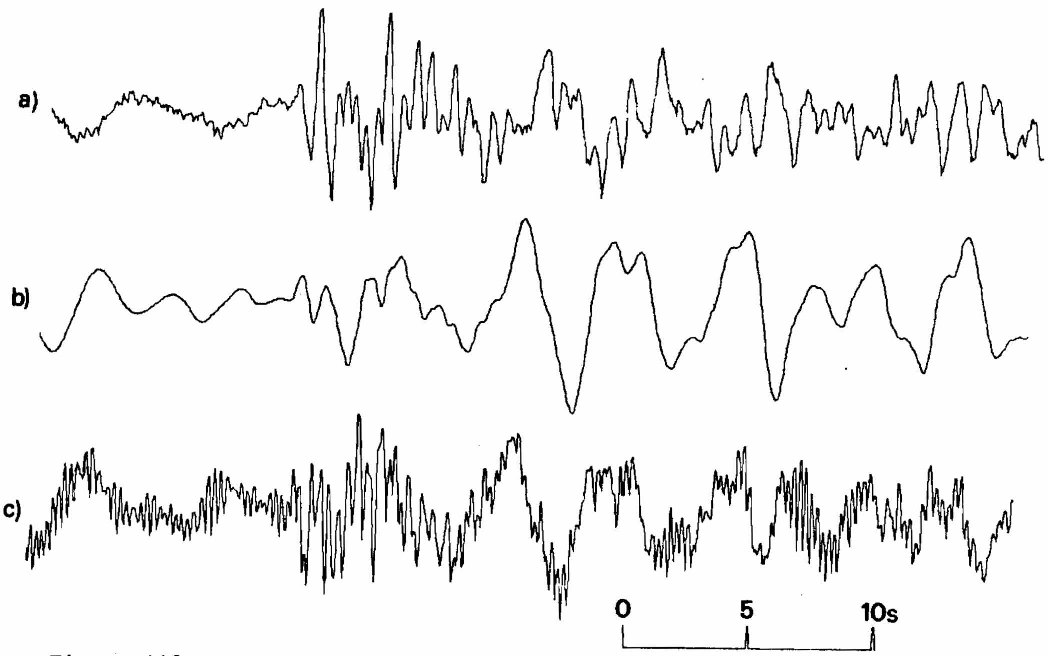

Figure 112. P seismograms recorded at Yellowknife, Canada from N.T.S. explosion MANTECA.

(a) Short-period array-sum seismogram.
(b) Wiener filtered phaseless broad-band seismogram.
(c) Seismogram (b) corrected for anelastic attenuation assuming $t^*=0.5s$.

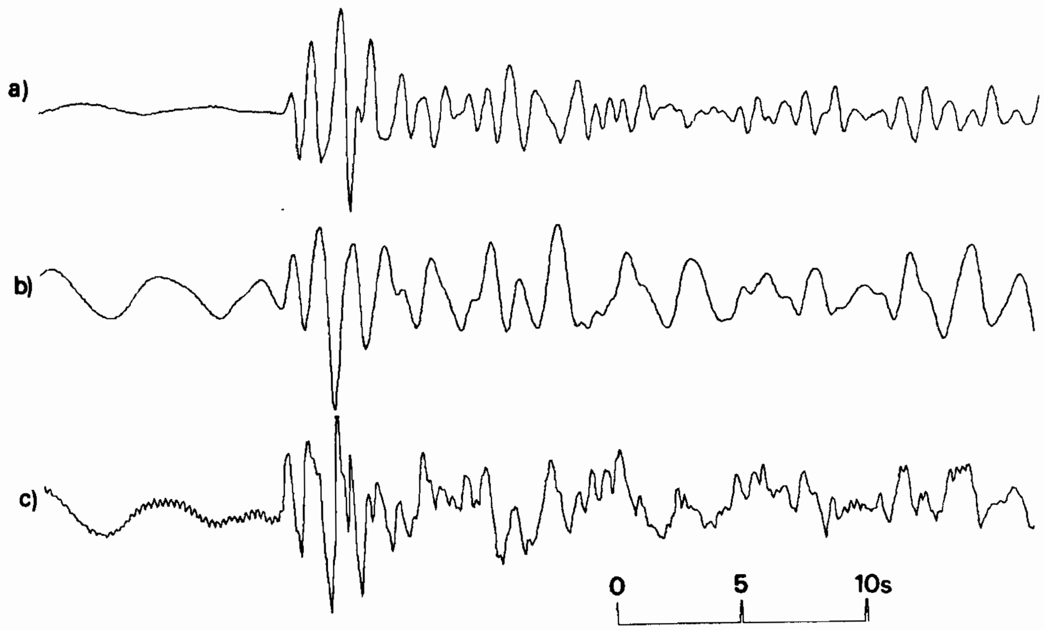

Figure 113. P seismograms recorded at Yellowknife, Canada from N.T.S. explosion CABRA.

(a) Short-period array-sum seismogram.
(b) Wiener filtered phaseless broad-band seismogram.
(c) Seismogram (b) corrected for anelastic attenuation assuming $t^*=0.5s$.

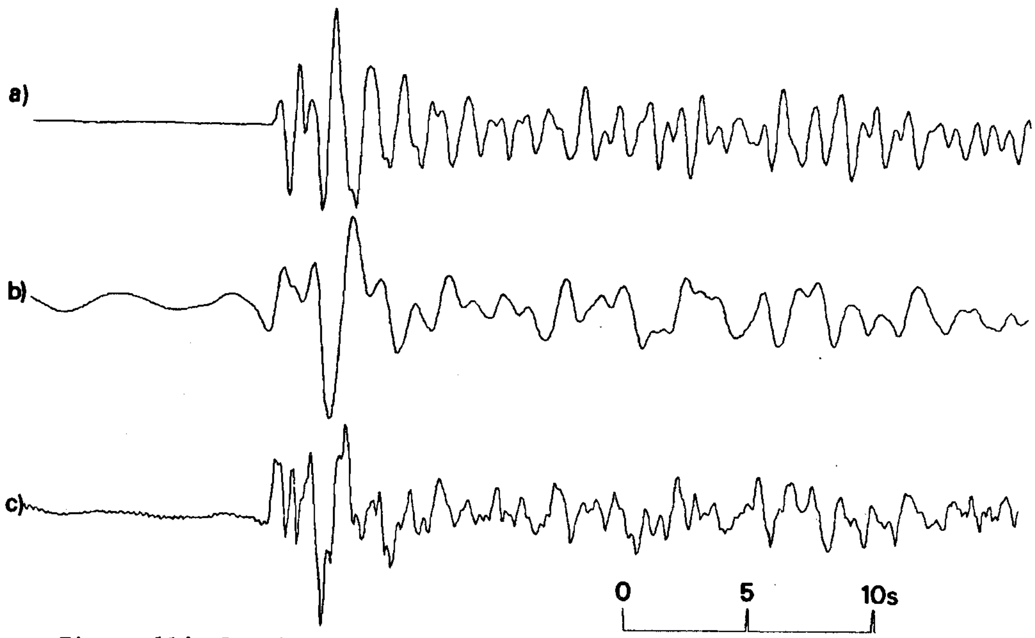

Figure 114. P seismograms recorded at Yellowknife,Canada from N.T.S. explosion TURQUOISE.

(a) Short-period array-sum seismogram.
(b) Wiener filtered phaseless broad-band seismogram.
(c) Seismogram (b) corrected for anelastic attenuation assuming t*=0.5s.

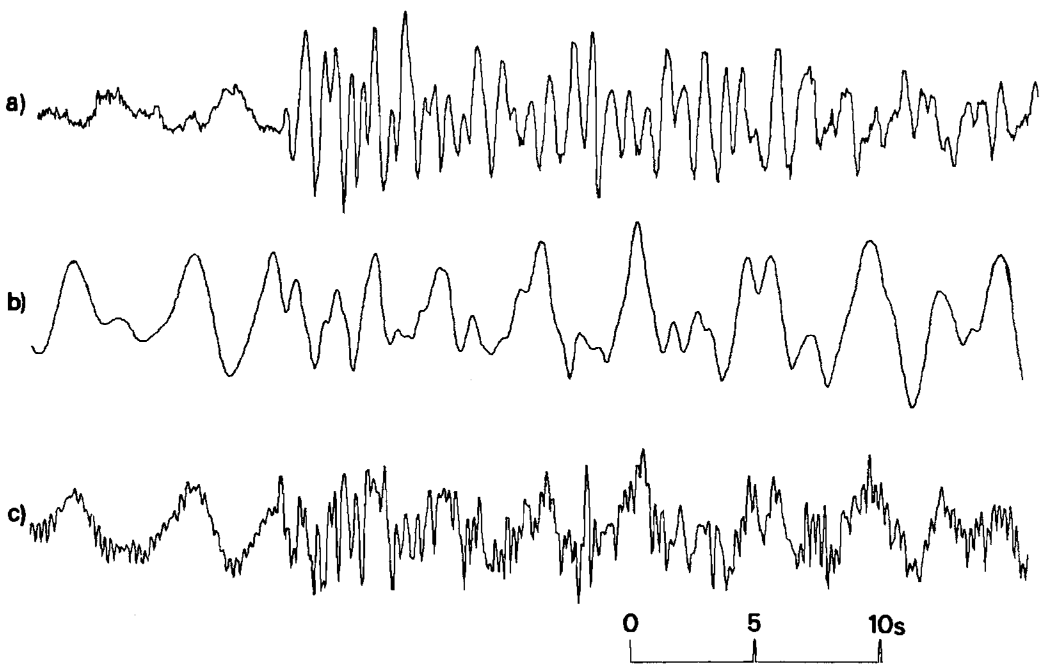

Figure 115. P seismograms recorded at Yellowknife,Canada from N.T.S. explosion CROWDIE.

(a) Short-period array-sum seismogram.
(b) Wiener filtered phaseless broad-band seismogram.
(c) Seismogram (b) corrected for anelastic attenuation assuming t*=0.5s.

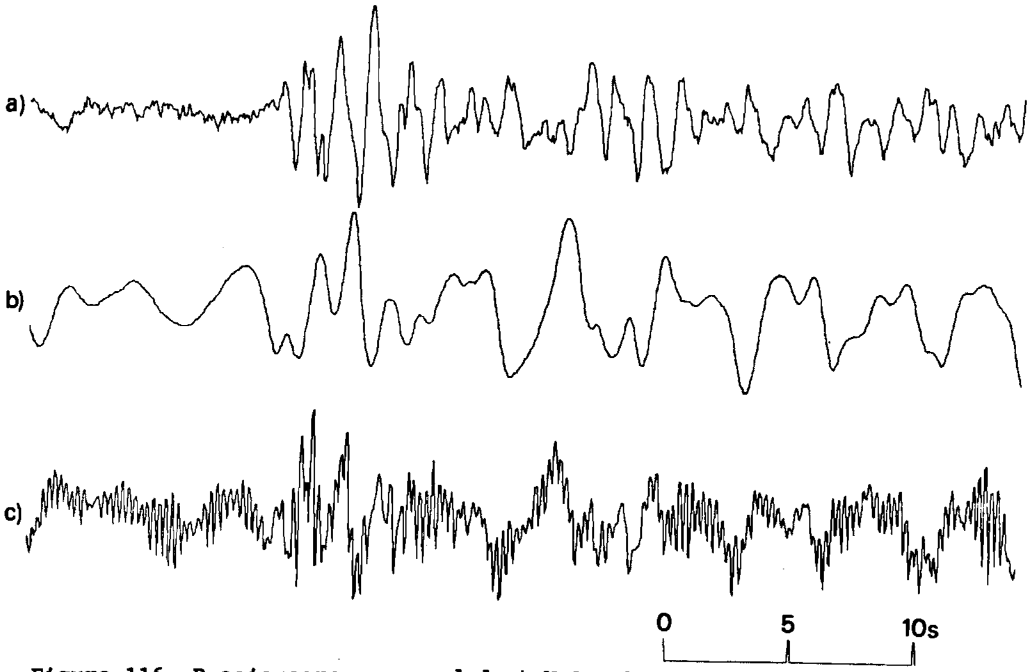

Figure 116. P seismograms recorded at Yellowknife, Canada from N.T.S. explosion FAHADA.

(a) Short-period array-sum seismogram.
(b) Wiener filtered phaseless broad-band seismogram.
(c) Seismogram (b) corrected for anelastic attenuation assuming t*=0.5s.

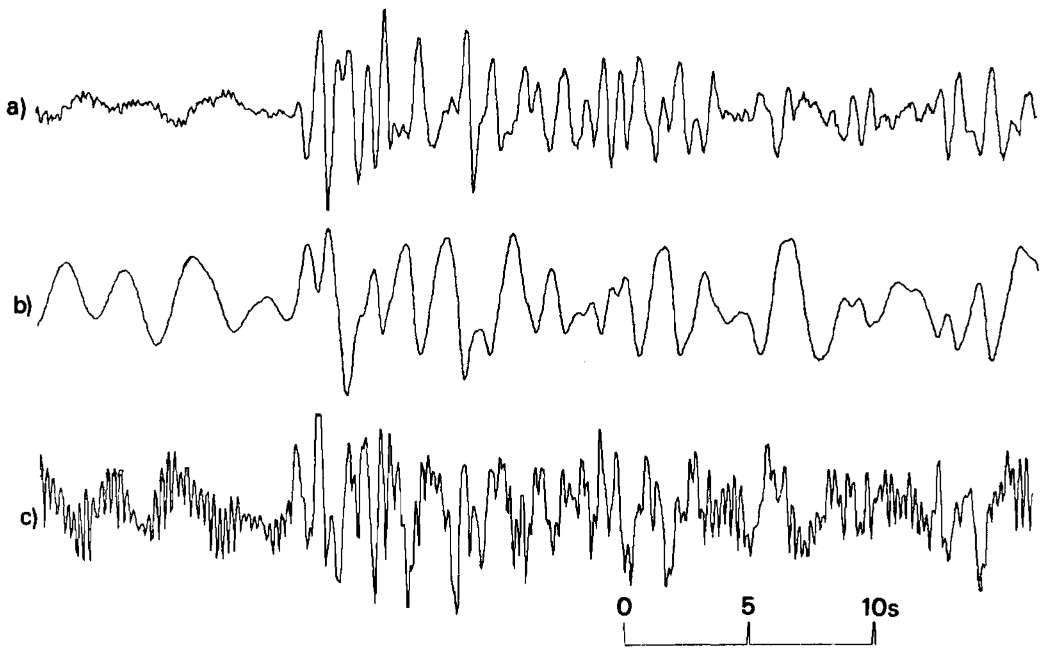

Figure 117. P seismograms recorded at Yellowknife, Canada from N.T.S. explosion DANABLU.

(a) Short-period array-sum seismogram.
(b) Wiener filtered phaseless broad-band seismogram.
(c) Seismogram (b) corrected for anelastic attenuation assuming t*=0.5s.

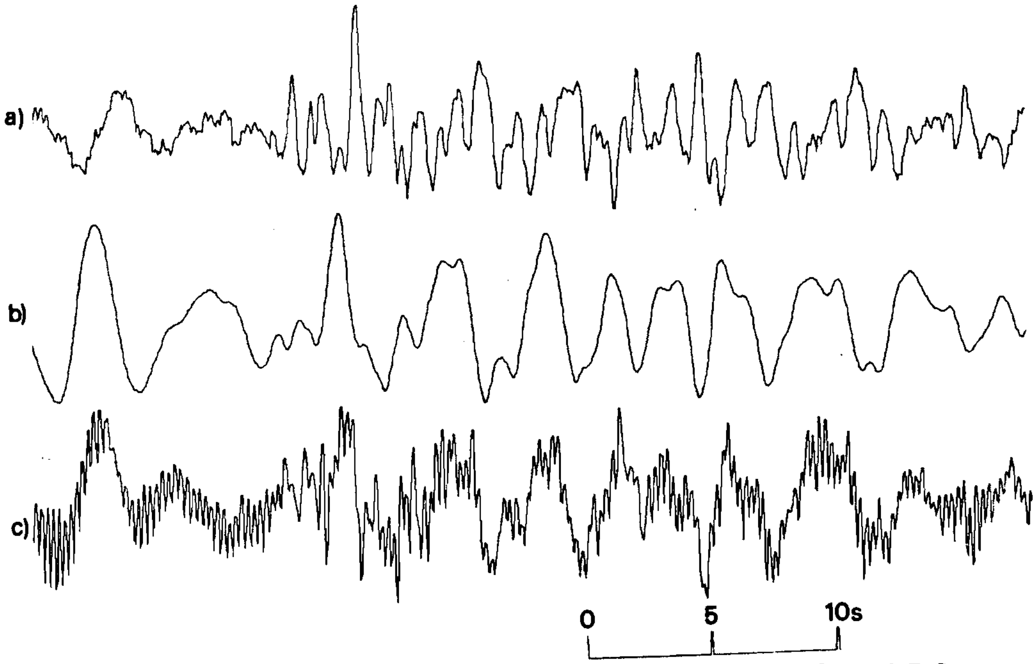

Figure 118. P seismograms recorded at Yellowknife,Canada from N.T.S. explosion LABAN.

(a) Short-period array-sum seismogram.
(b) Wiener filtered phaseless broad-band seismogram.
(c) Seismogram (b) corrected for anelastic attenuation assuming t*=0.5s.

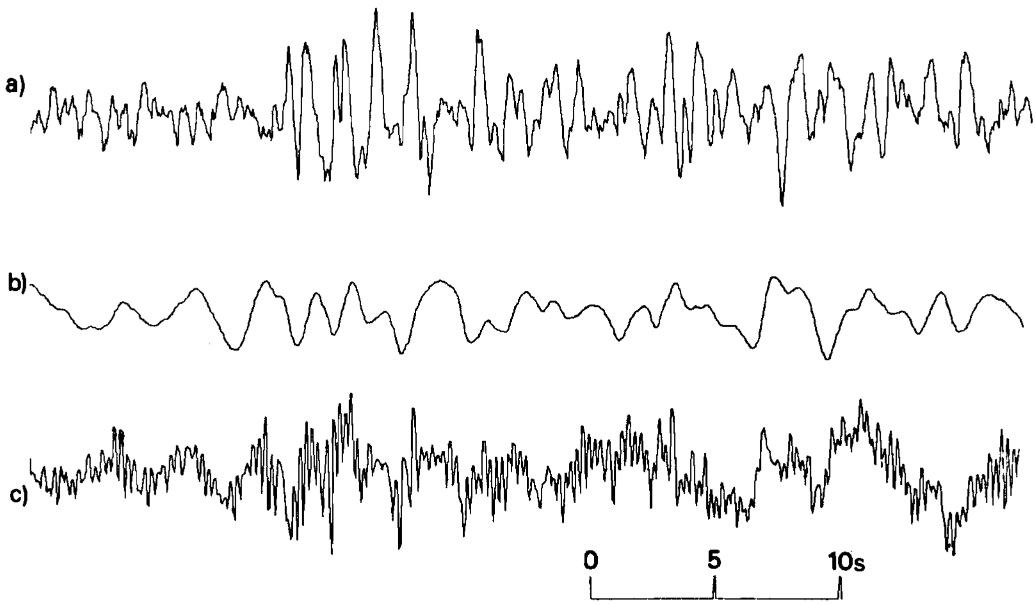

Figure 119. P seismograms recorded at Yellowknife,Canada from N.T.S. explosion SABADO.

(a) Short-period array-sum seismogram.
(b) Wiener filtered phaseless broad-band seismogram.
(c) Seismogram (b) corrected for anelastic attenuation assuming t*=0.5s.

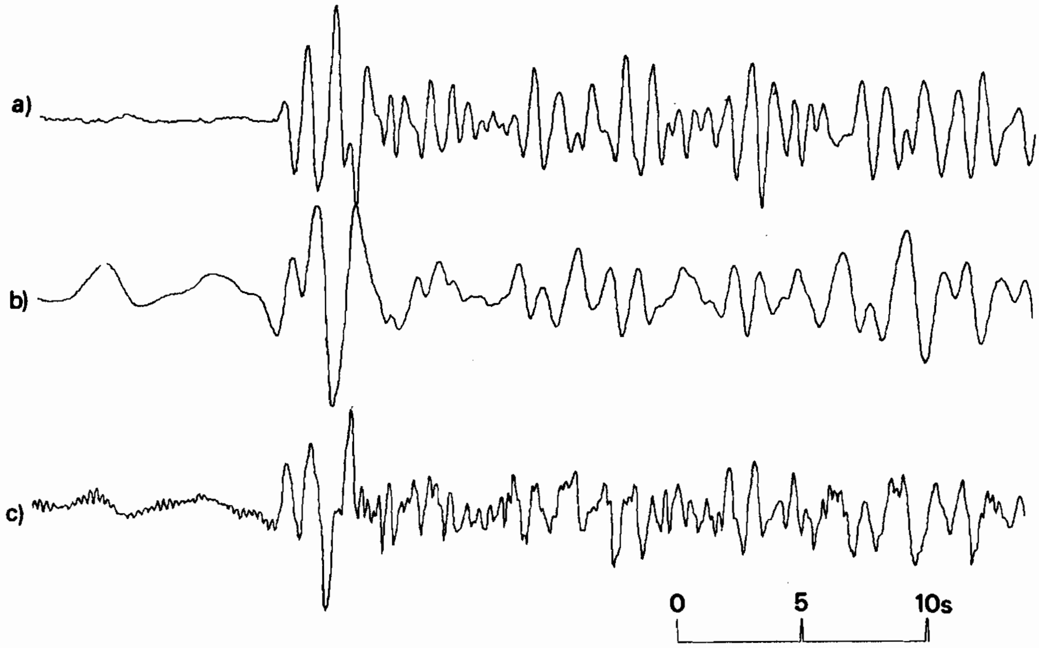

Figure 120. P seismograms recorded at Yellowknife, Canada from N.T.S. explosion CHANCELLOR.

(a) Short-period array-sum seismogram.
(b) Wiener filtered phaseless broad-band seismogram.
(c) Seismogram (b) corrected for anelastic attenuation assuming t*=0.5s.

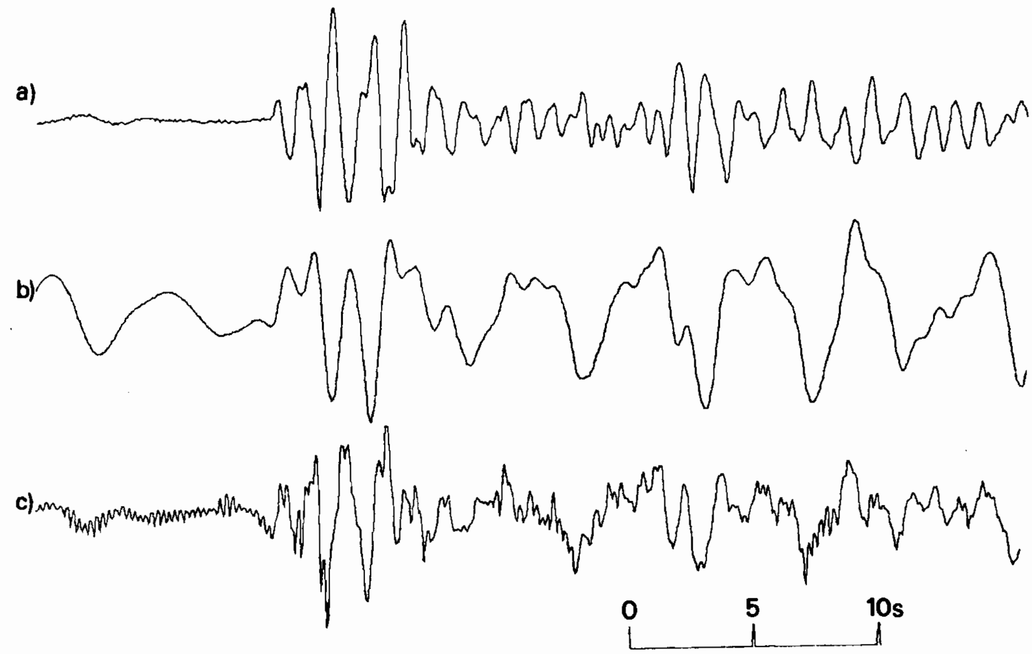

Figure 121. P seismograms recorded at Yellowknife, Canada from N.T.S. explosion ROMANO.

(a) Short-period array-sum seismogram.
(b) Wiener filtered phaseless broad-band seismogram.
(c) Seismogram (b) corrected for anelastic attenuation assuming t*=0.5s.

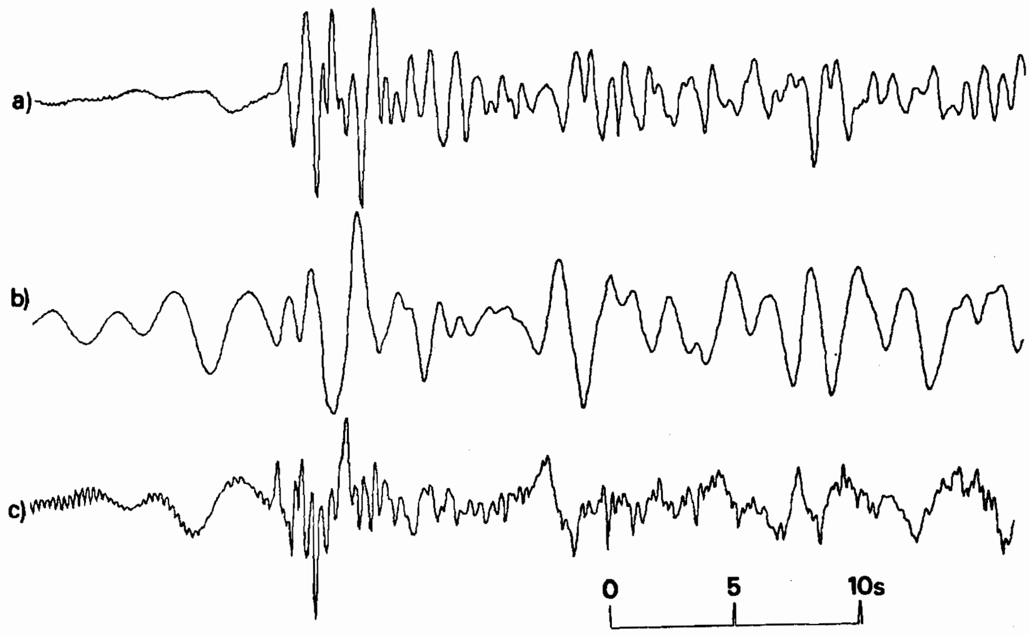

Figure 122. P seismograms recorded at Yellowknife,Canada from N.T.S. explosions MIDAS MYTH/MILAGRO.

(a) Short-period array-sum seismogram.
(b) Wiener filtered phaseless broad-band seismogram.
(c) Seismogram (b) corrected for anelastic attenuation assuming t*=0.5s.

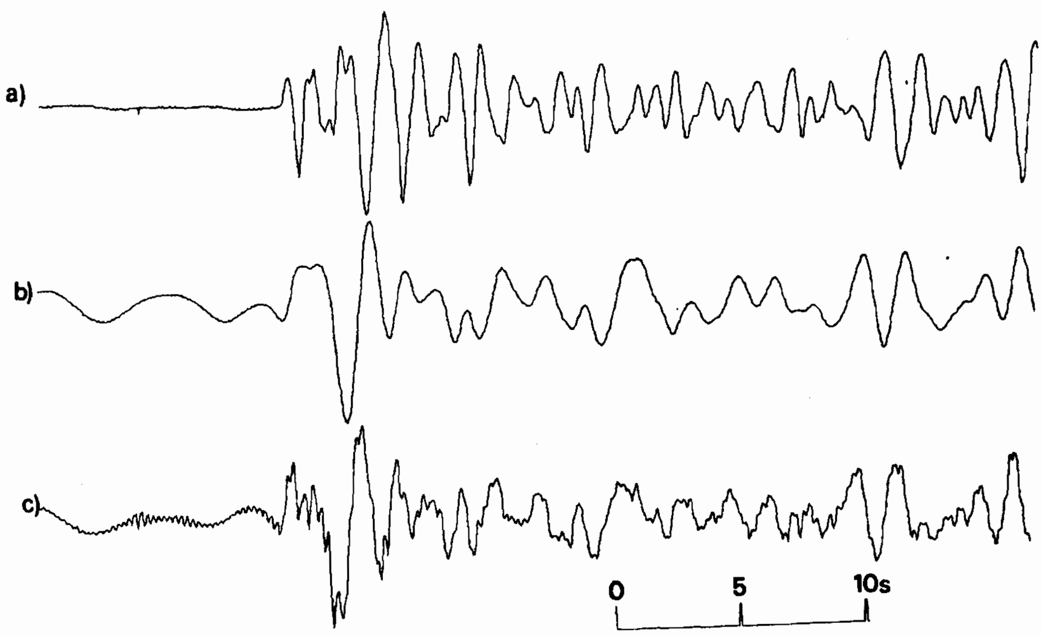

Figure 123. P seismograms recorded at Yellowknife,Canada from N.T.S. explosion MUNDO.

(a) Short-period array-sum seismogram.
(b) Wiener filtered phaseless broad-band seismogram.
(c) Seismogram (b) corrected for anelastic attenuation assuming t*=0.5s.

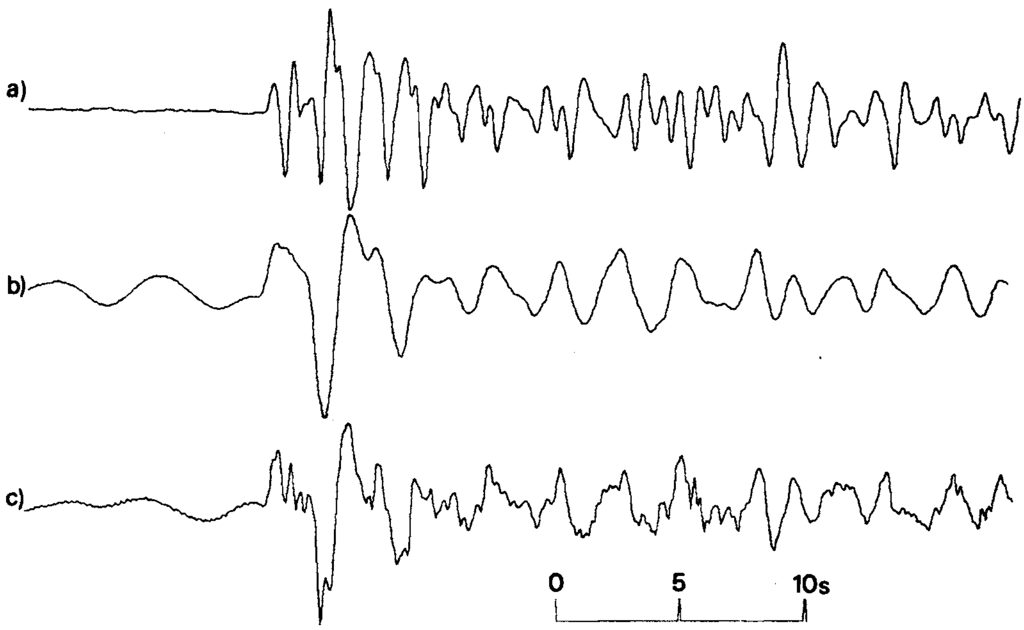

Figure 124. P seismograms recorded at Yellowknife,Canada from N.T.S. explosion CAPROCK.

(a) Short-period array-sum seismogram.
(b) Wiener filtered phaseless broad-band seismogram.
(c) Seismogram (b) corrected for anelastic attenuation assuming t*=0.5s.

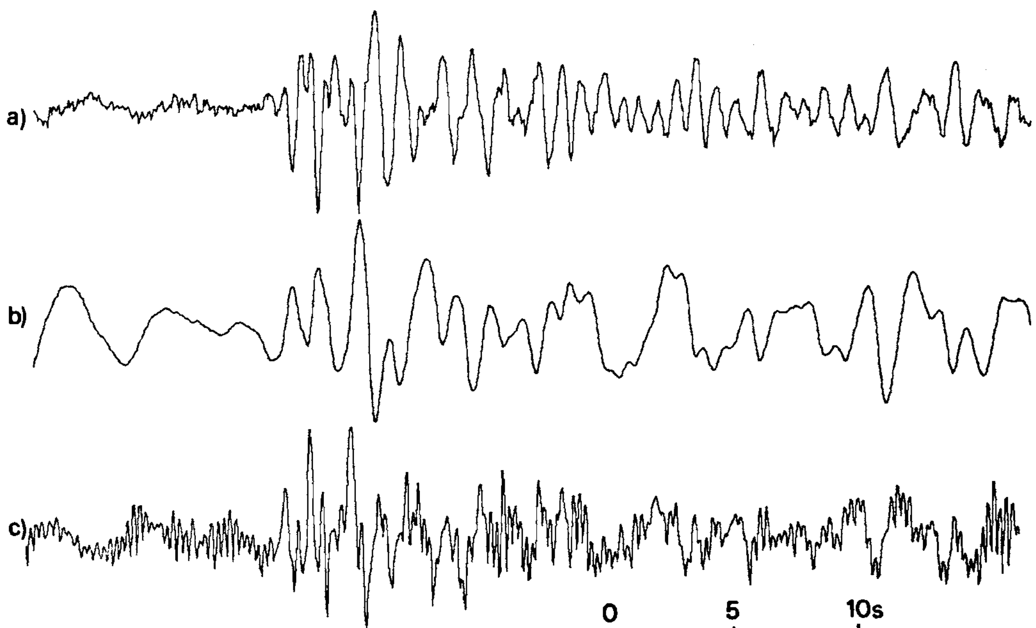

Figure 125. P seismograms recorded at Yellowknife,Canada from N.T.S. explosion DUORO.

(a) Short-period array-sum seismogram.
(b) Wiener filtered phaseless broad-band seismogram.
(c) Seismogram (b) corrected for anelastic attenuation assuming t*=0.5s.

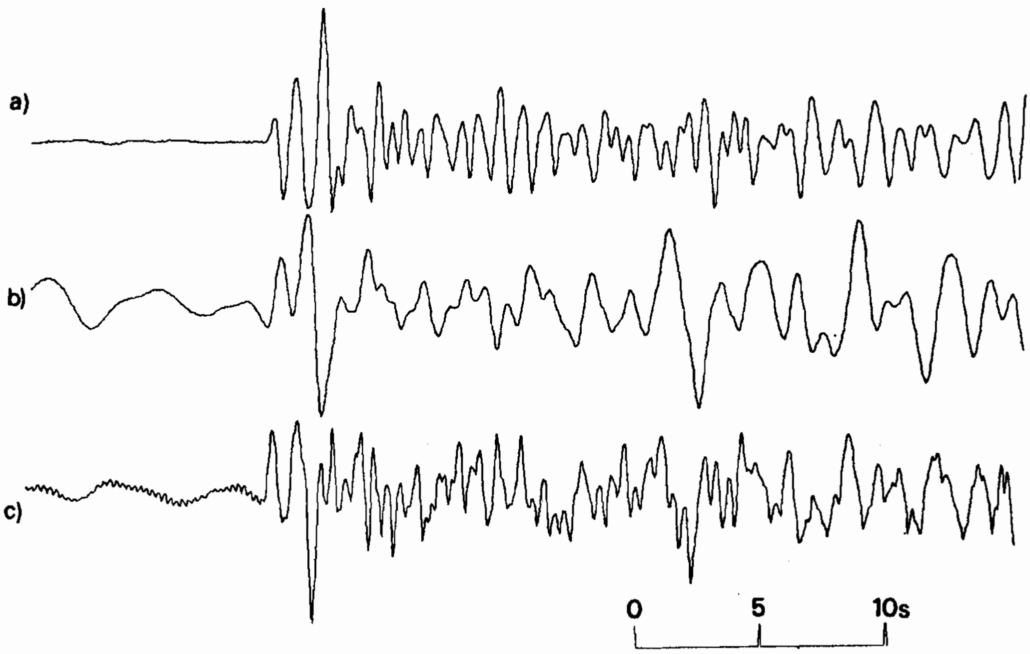

Figure 126. P seismograms recorded at Yellowknife,Canada from N.T.S. explosion KAPPELI.

(a) Short-period array-sum seismogram.
(b) Wiener filtered phaseless broad-band seismogram.
(c) Seismogram (b) corrected for anelastic attenuation assuming t*=0.5s.

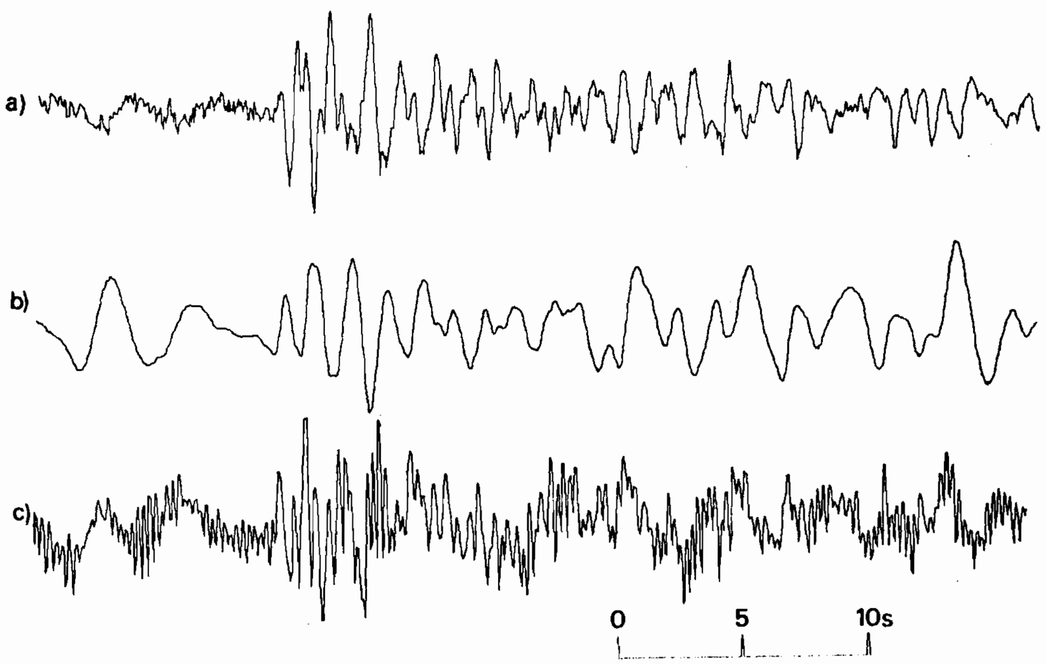

Figure 127. P seismograms recorded at Yellowknife,Canada from N.T.S. explosion CORREO.

(a) Short-period array-sum seismogram.
(b) Wiener filtered phaseless broad-band seismogram.
(c) Seismogram (b) corrected for anelastic attenuation assuming t*=0.5s.

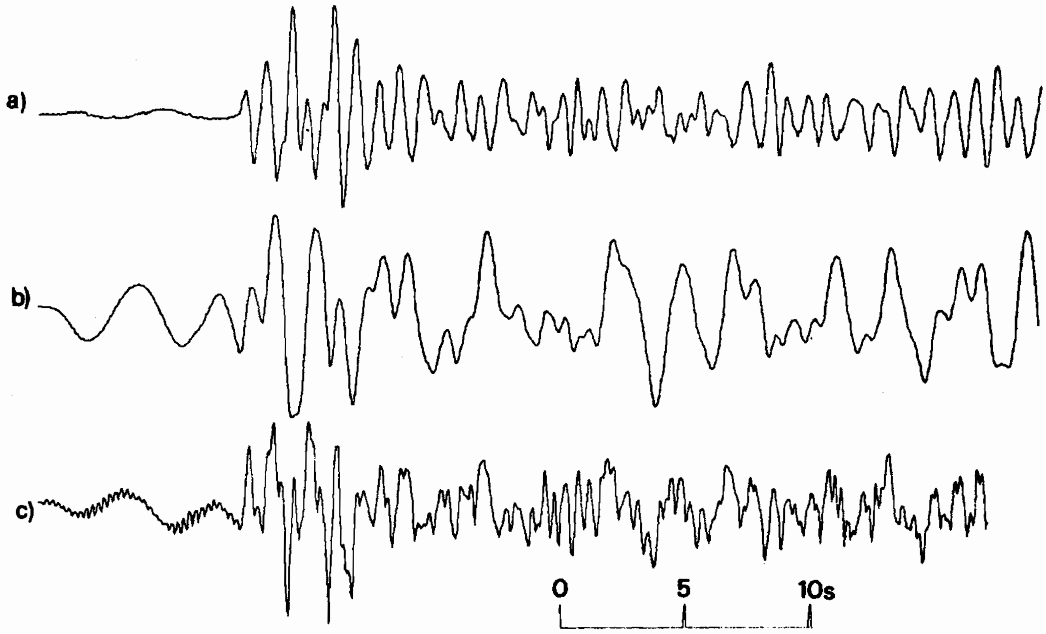

Figure 128. P seismograms recorded at Yellowknife, Canada from N.T.S. explosion TIERRA.

(a) Short-period array-sum seismogram.
(b) Wiener filtered phaseless broad-band seismogram.
(c) Seismogram (b) corrected for anelastic attenuation assuming t*=0.5s.

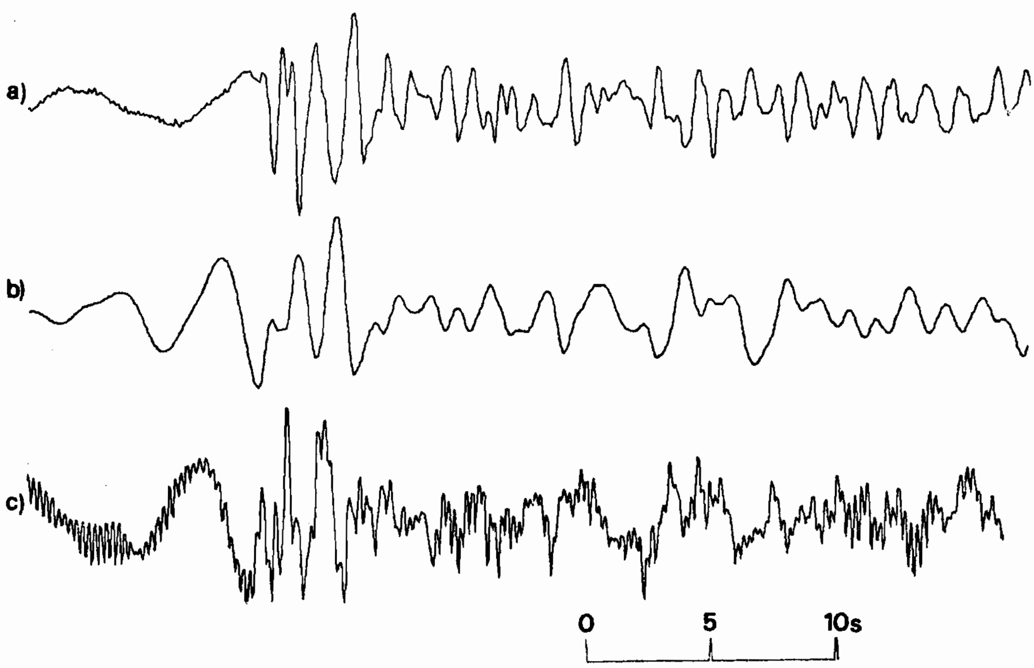

Figure 129. P seismograms recorded at Yellowknife, Canada from N.T.S. explosion VAUGHN.

(a) Short-period array-sum seismogram.
(b) Wiener filtered phaseless broad-band seismogram.
(c) Seismogram (b) corrected for anelastic attenuation assuming t*=0.5s.

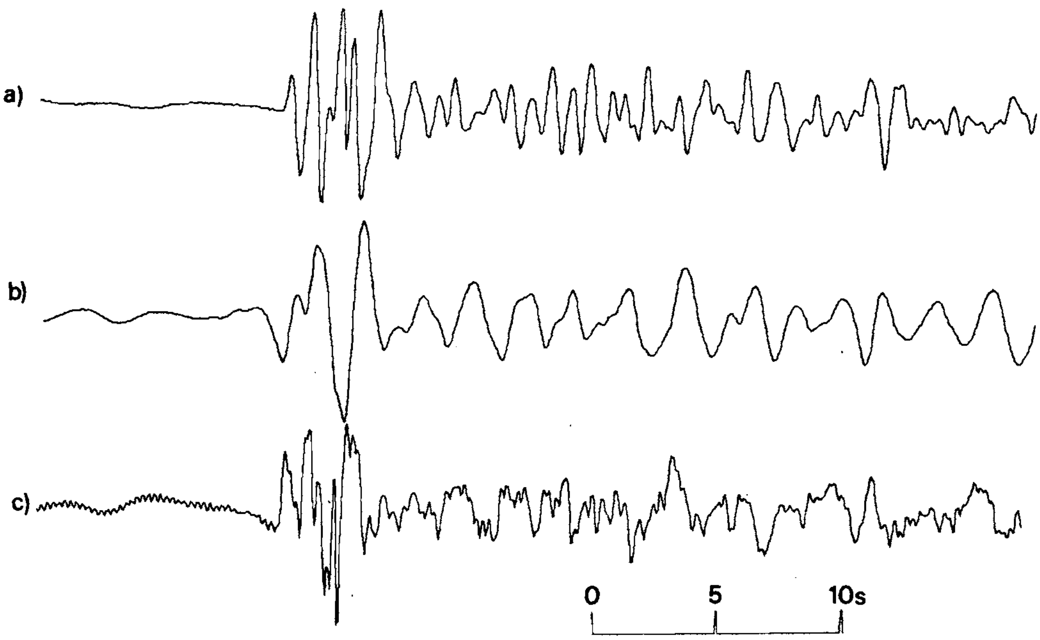

Figure 130. P seismograms recorded at Yellowknife,Canada from N.T.S. explosion COTTAGE.

(a) Short-period array-sum seismogram.
(b) Wiener filtered phaseless broad-band seismogram.
(c) Seismogram (b) corrected for anelastic attenuation assuming t*=0.5s.

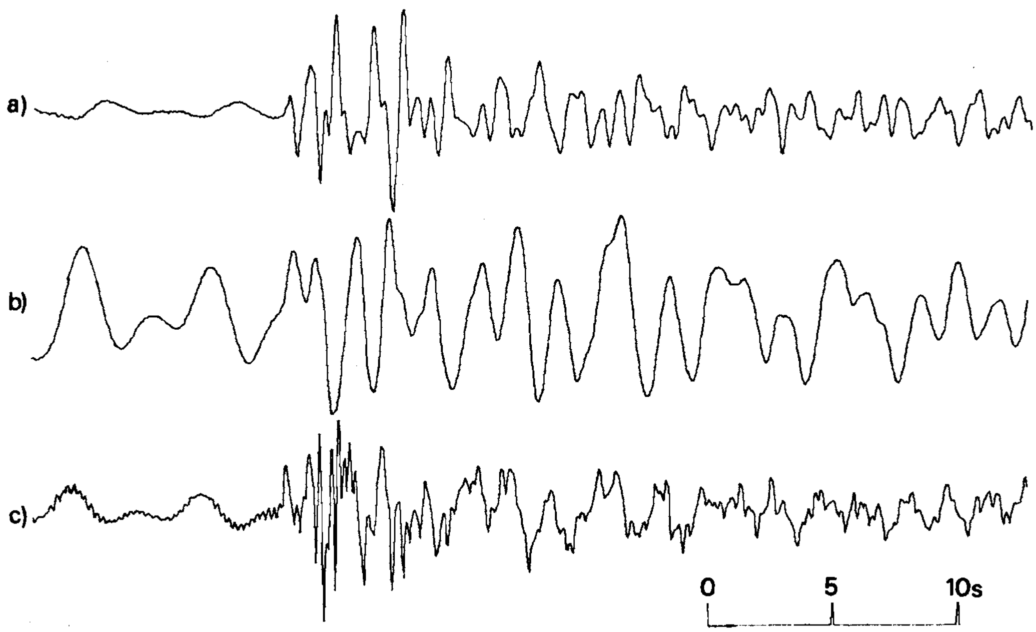

Figure 131. P seismograms recorded at Yellowknife,Canada from N.T.S. explosion MISTY RAIN.

(a) Short-period array-sum seismogram.
(b) Wiener filtered phaseless broad-band seismogram.
(c) Seismogram (b) corrected for anelastic attenuation assuming t*=0.5s.

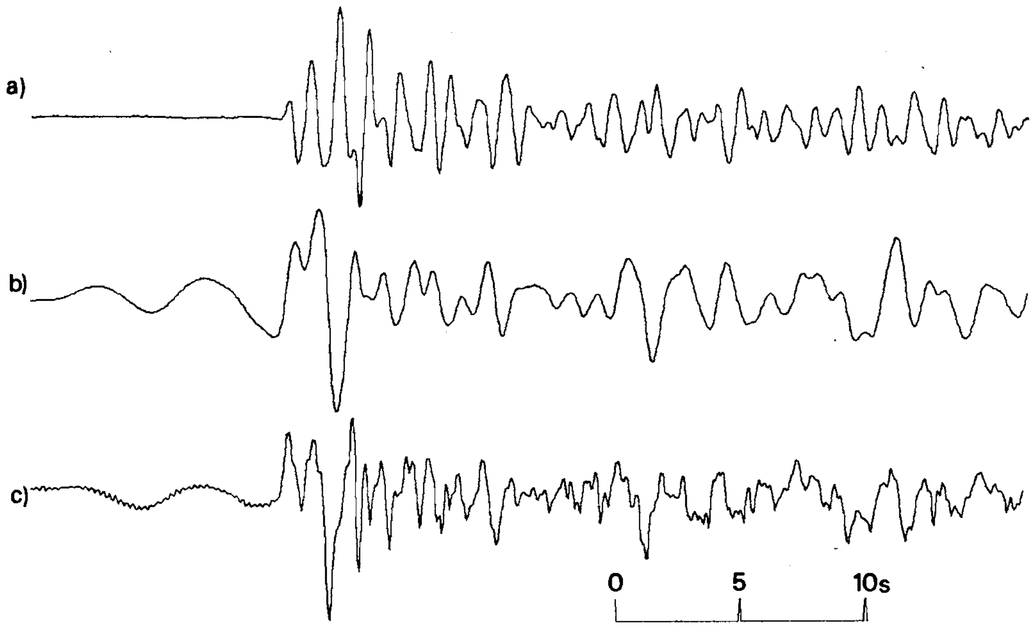

Figure 132. P seismograms recorded at Yellowknife,Canada from N.T.S. explosion TOWANDA.

(a) Short-period array-sum seismogram.
(b) Wiener filtered phaseless broad-band seismogram.
(c) Seismogram (b) corrected for anelastic attenuation assuming t*=0.5s.

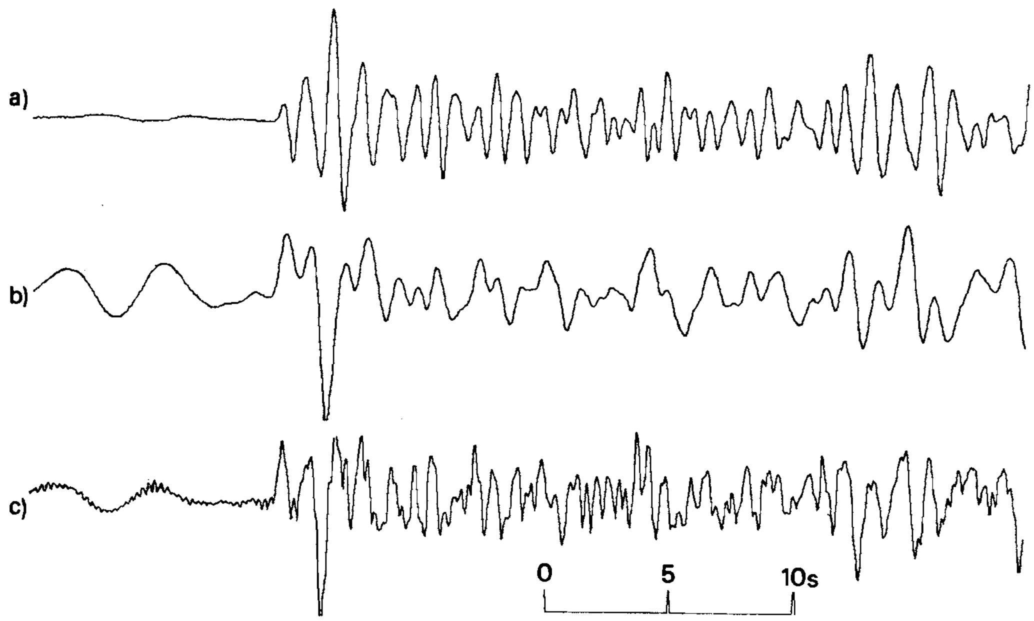

Figure 133. P seismograms recorded at Yellowknife,Canada from N.T.S. explosion SALUT.

(a) Short-period array-sum seismogram.
(b) Wiener filtered phaseless broad-band seismogram.
(c) Seismogram (b) corrected for anelastic attenuation assuming t*=0.5s.

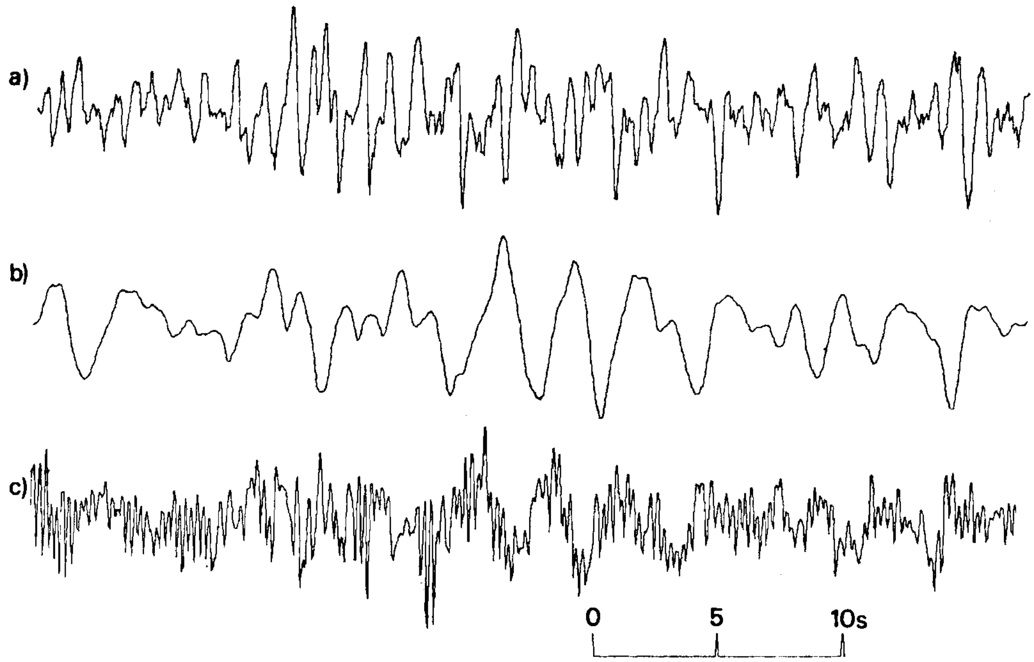

Figure 134. P seismograms recorded at Yellowknife,Canada from N.T.S. explosion MARIBO.

(a) Short-period array-sum seismogram.
(b) Wiener filtered phaseless broad-band seismogram.
(c) Seismogram (b) corrected for anelastic attenuation assuming t*=0.5s.

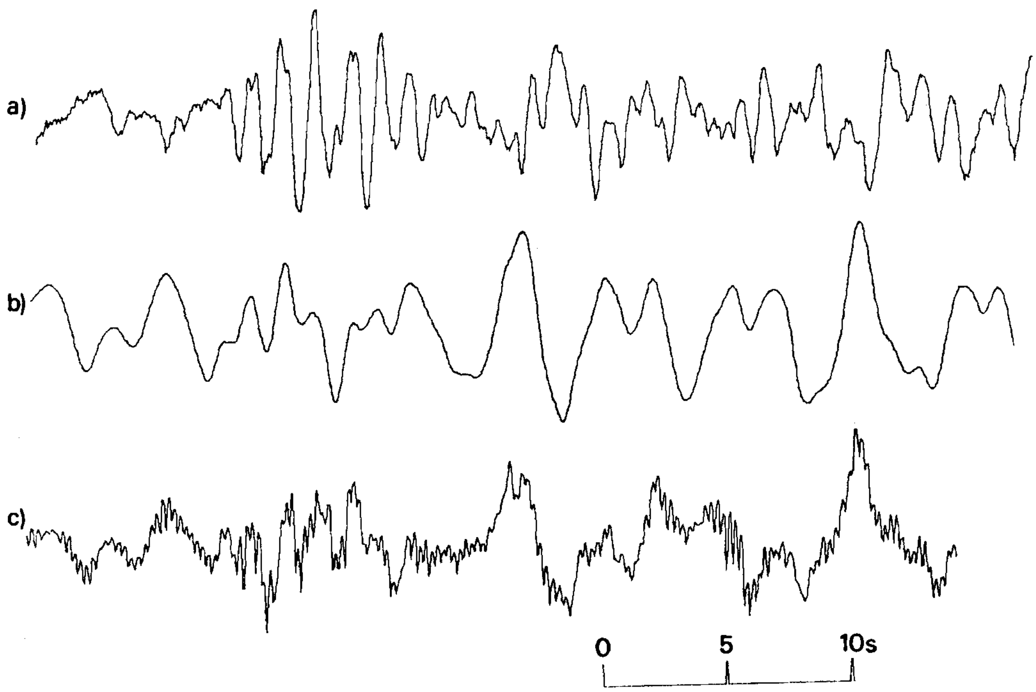

Figure 135. P seismograms recorded at Yellowknife,Canada from N.T.S. explosion PONIL.

(a) Short-period array-sum seismogram.
(b) Wiener filtered phaseless broad-band seismogram.
(c) Seismogram (b) corrected for anelastic attenuation assuming t*=0.5s.

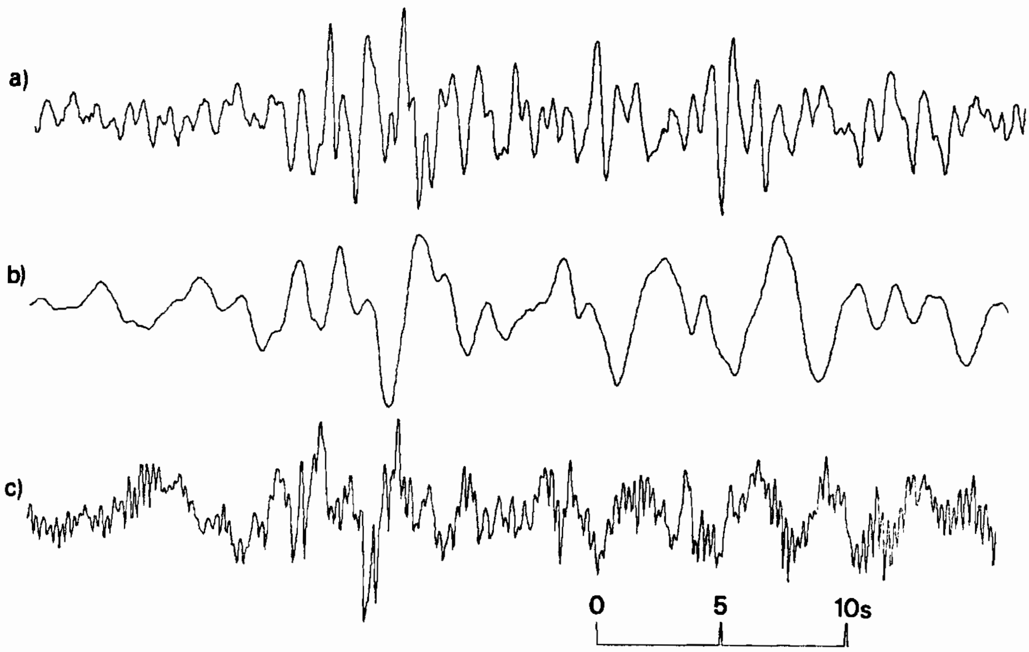

Figure 136. P seismograms recorded at Yellowknife,Canada from N.T.S. explosion ROQUEFORT.

(a) Short-period array-sum seismogram.
(b) Wiener filtered phaseless broad-band seismogram.
(c) Seismogram (b) corrected for anelastic attenuation assuming t*=0.5s.

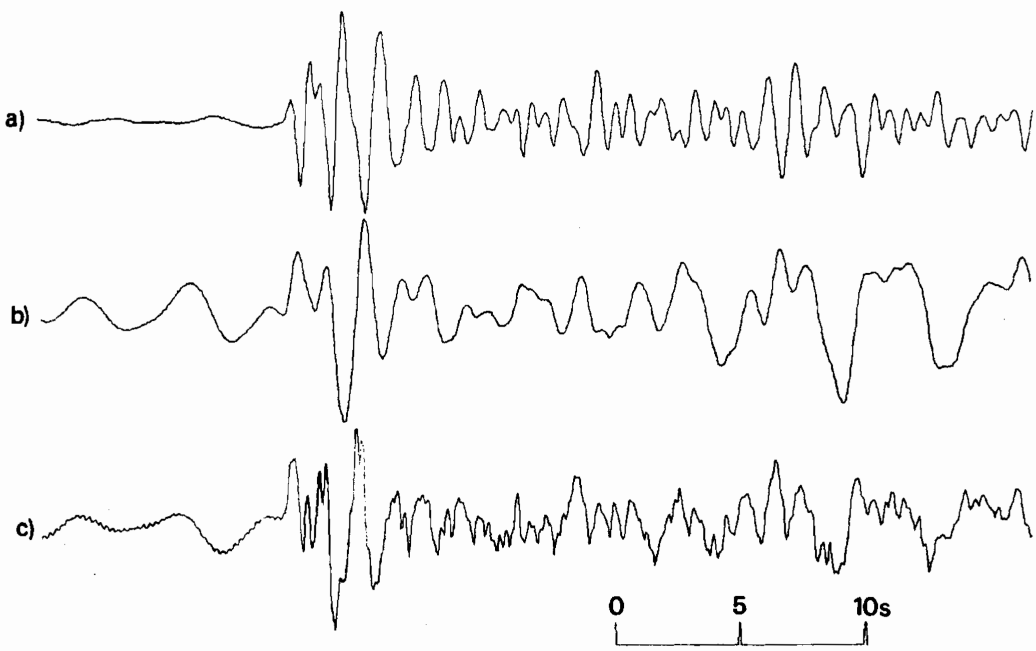

Figure 137. P seismograms recorded at Yellowknife,Canada from N.T.S. explosion KINIBITO.

(a) Short-period array-sum seismogram.
(b) Wiener filtered phaseless broad-band seismogram.
(c) Seismogram (b) corrected for anelastic attenuation assuming t*=0.5s.

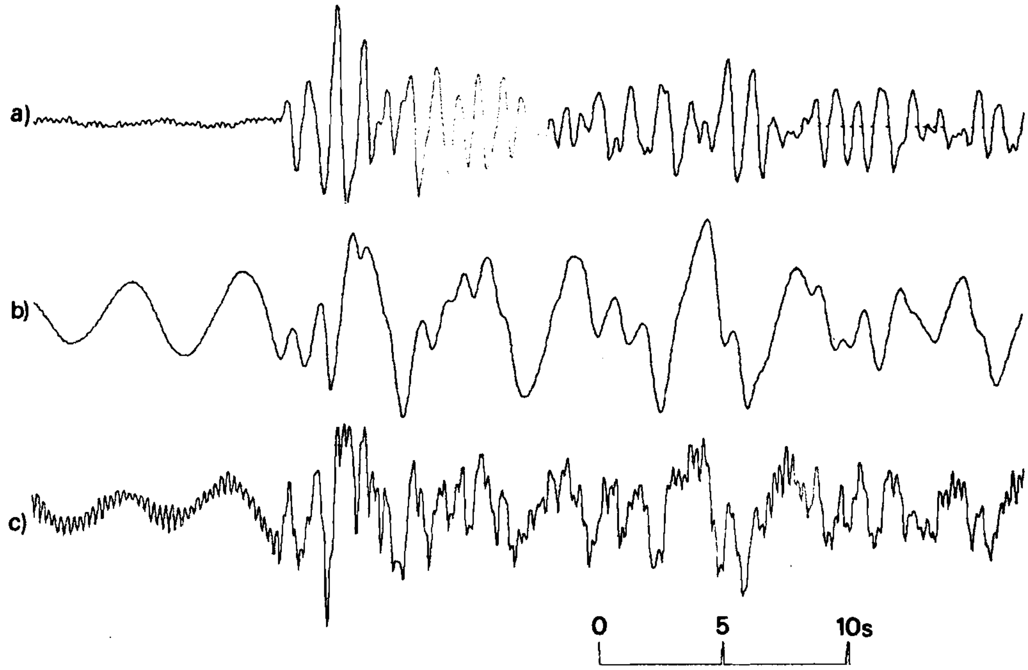

Figure 138. P seismograms recorded at Yellowknife, Canada from N.T.S. explosion GOLDSTONE.

(a) Short-period array-sum seismogram.
(b) Wiener filtered phaseless broad-band seismogram.
(c) Seismogram (b) corrected for anelastic attenuation assuming t*=0.5s.

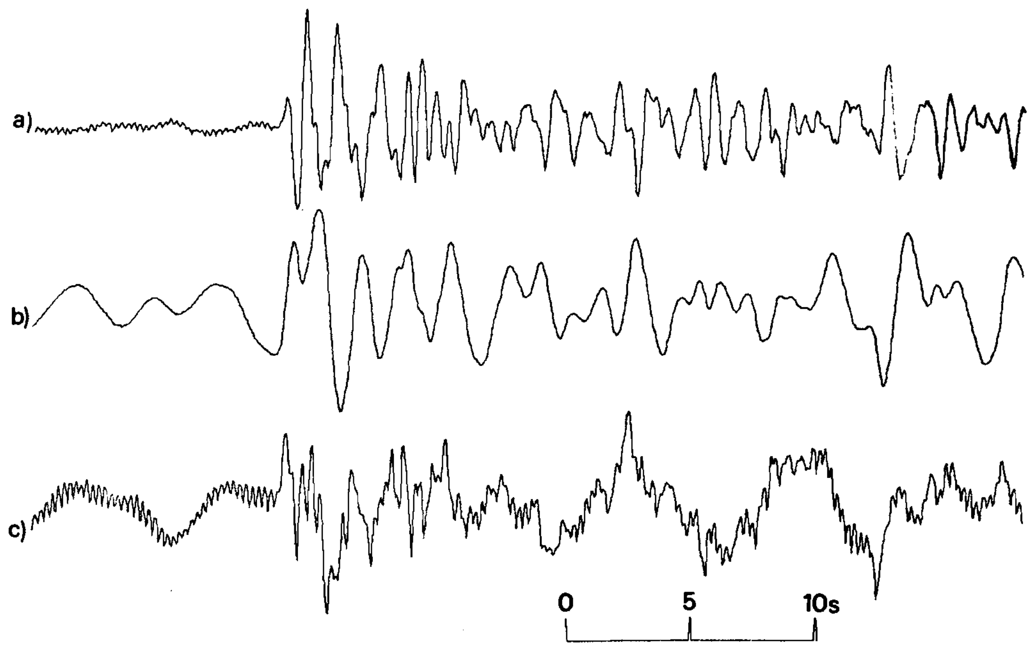

Figure 139. P seismograms recorded at Yellowknife, Canada from N.T.S. explosion GLENCOE.

(a) Short-period array-sum seismogram.
(b) Wiener filtered phaseless broad-band seismogram.
(c) Seismogram (b) corrected for anelastic attenuation assuming t*=0.5s.

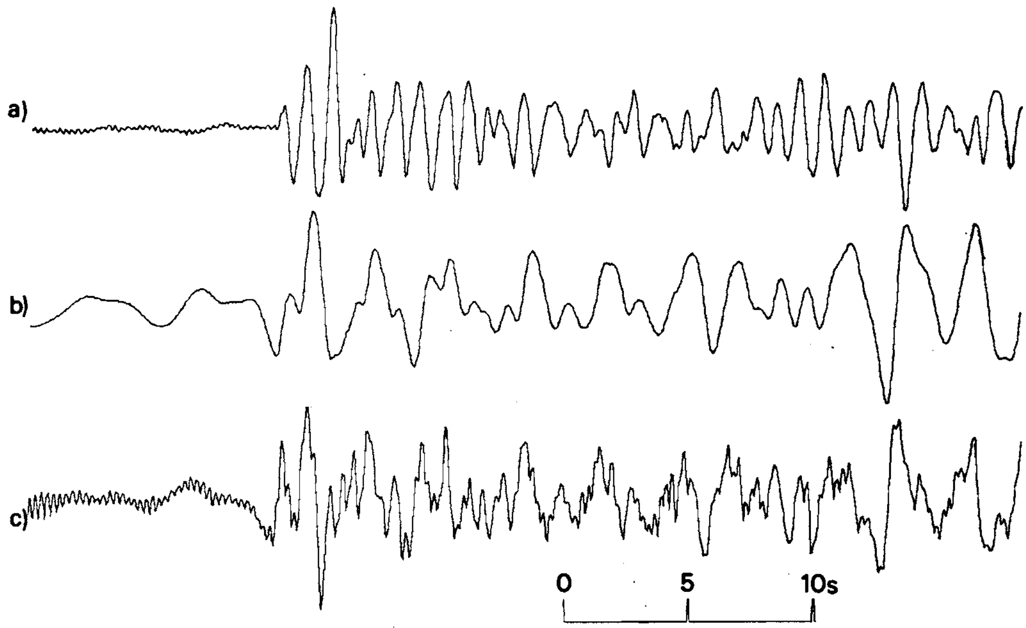

Figure 140. P seismograms recorded at Yellowknife,Canada from N.T.S. explosion MIGHTY OAK.

(a) Short-period array-sum seismogram.
(b) Wiener filtered phaseless broad-band seismogram.
(c) Seismogram (b) corrected for anelastic attenuation assuming t*=0.5s.

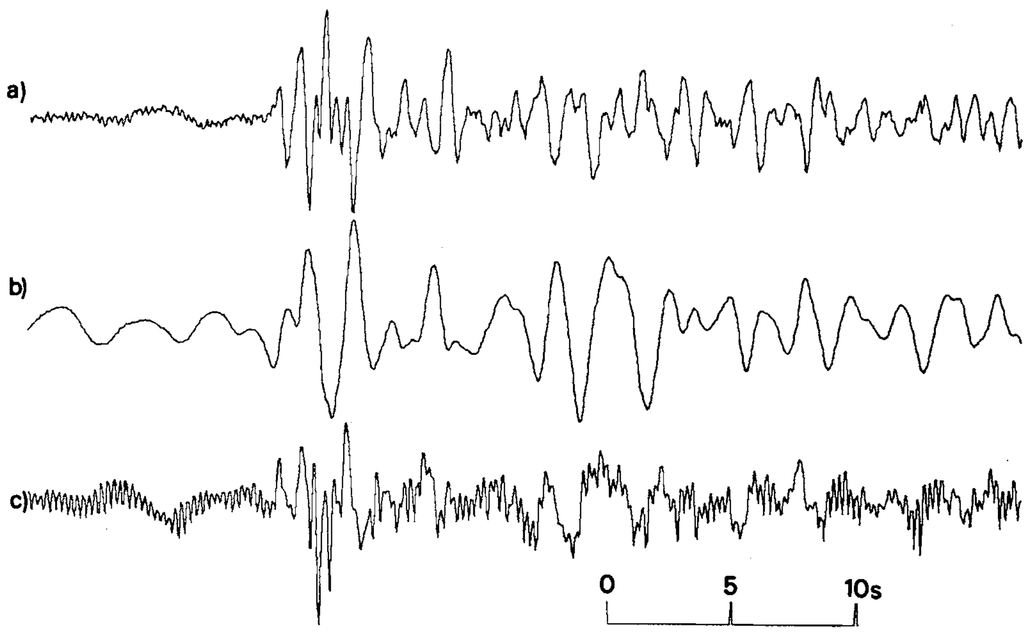

Figure 141. P seismograms recorded at Yellowknife,Canada from N.T.S. explosion JEFFERSON.

(a) Short-period array-sum seismogram.
(b) Wiener filtered phaseless broad-band seismogram.
(c) Seismogram (b) corrected for anelastic attenuation assuming t*=0.5s.

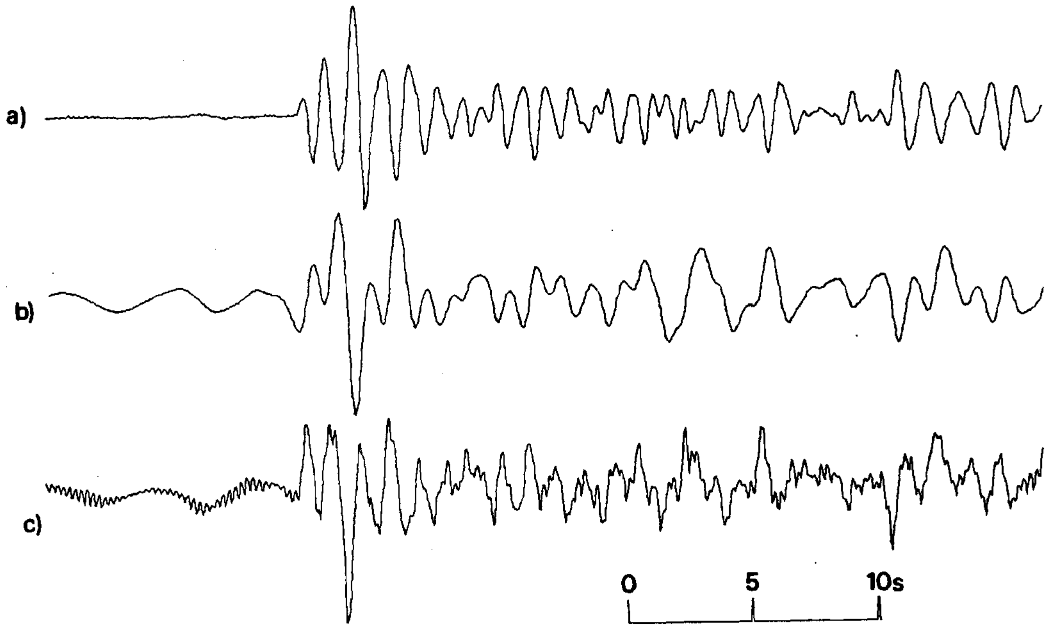

Figure 142. P seismograms recorded at Yellowknife,Canada from N.T.S. explosion DARWIN.

(a) Short-period array-sum seismogram.
(b) Wiener filtered phaseless broad-band seismogram.
(c) Seismogram (b) corrected for anelastic attenuation assuming t*=0.5s.

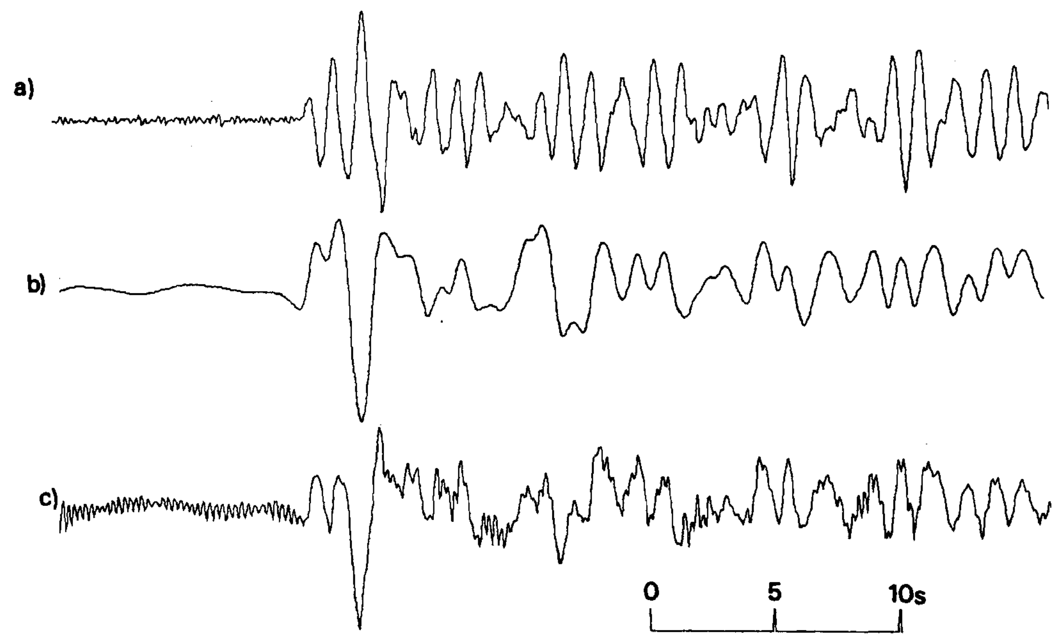

Figure 143. P seismograms recorded at Yellowknife,Canada from N.T.S. explosion CYBAR.

(a) Short-period array-sum seismogram.
(b) Wiener filtered phaseless broad-band seismogram.
(c) Seismogram (b) corrected for anelastic attenuation assuming t*=0.5s.

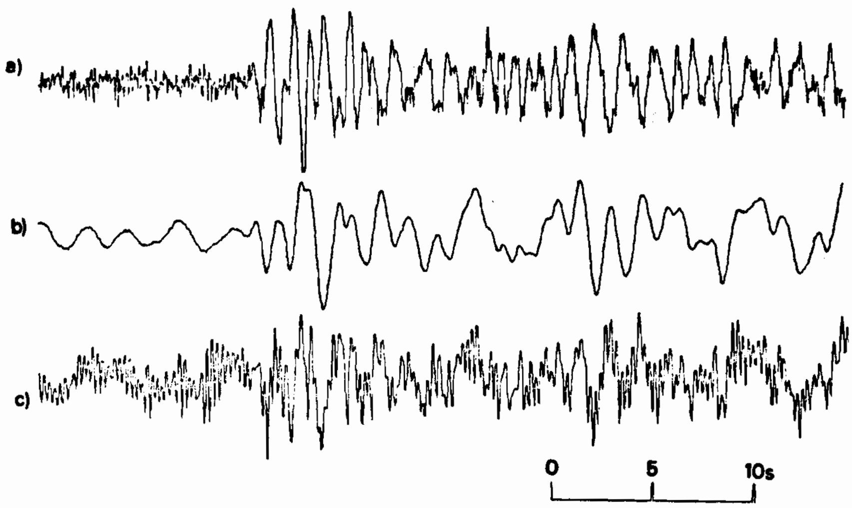

Figure 144. P seismograms recorded at Yellowknife,Canada from N.T.S. explosion CORNUCOPIA.

(a) Short-period array-sum seismogram.
(b) Wiener filtered phaseless broad-band seismogram.
(c) Seismogram (b) corrected for anelastic attenuation assuming t*=0.5s.

UK UNLIMITED

Available from
HER MAJESTY'S STATIONERY OFFICE
49 High Holborn, London W.C.1
71 Lothian Road, Edinburgh EH3 9AZ
9-12 Princess Street, Manchester M60 8AS
Southey House, Wine Street, Bristol BS1 2BQ
258 Broad Street, Birmingham B1 2HE
80 Chichester Street, Belfast BT1 4JY
or through any bookseller.

Printed in England

ISBN 0 85518189 3

UK UNLIMITED